Detecting Critical Defects: Towards Standards for Conducting NDE on Cast Iron Trunk Mains

Alexander Rainer

Department of Mechanical Engineering Sciences
University of Surrey

A thesis submitted in fulfilment of the degree of Doctor of Engineering

2017

Declaration of Originality

This thesis and the work to which it refers are the results of my own efforts. Any ideas, data, images or text resulting from the work of others (whether published or unpublished) are fully identified as such within the work and attributed to their originator in the text, bibliography or in footnotes. This thesis has not been submitted in whole or in part for any other academic degree or professional qualification. I agree that the University has the right to submit my work to the plagiarism detection service TurnitinUK for originality checks. Whether or not drafts have been so-assessed, the University reserves the right to require an electronic version of the final document (as submitted) for assessment as above.

Dedicated to the friends and family who believed in, supported and helped me through this long, long journey.

Abstract

Every day, water networks across the developed world are relied on by billions of people to provide them with a fresh supply of water. Many of these networks are comprised of pipes made from grey cast iron and may have been in service for up to 150 years. Despite their age, some parts of these networks continue to operate with little degradation, whereas in other areas they degrade rapidly: more recently laid pipes are being outlived by their forerunners. In such networks, it is the trunk mains (pipes between 12-60" [300 mm to 1500 mm] in diameter) that are of great concern, since they pose the greatest risk of failure and are already bursting more frequently.

Accurate NDE is required to enable the mains in poor health with the highest risk of failure to be identified and replaced before they burst. A review of the published literature has shown that whilst there are many NDE techniques to choose from, many are not practical for application to the mains. The review process also highlighted the kinds of defects present in grey cast iron and an initial stress analysis using strength models and material data published in the literature has suggested defect sizes approaching 5 mm must be able to be detected to prevent catastrophic pipe failure.

Ultrasonic inspection has been investigated and shown to work effectively on uncorroded cast iron. Speed of sound values between 4100 – 4600 m s^{-1} have been observed across several pipes. A speed of sound of 2950 ± 80 m s^{-1} has been measured for graphitic corrosion, however, inspection on corroded main has not been possible.

A complementary magnetic technique, with the potential to scan pipe rapidly in order to identify mains in need of further investigation, as well as providing supplementary condition data, has been trialled and shown to detect corrosion layers up to 6 mm thick.

A methodology using a 3D scanner to accurately determine the "ground truth" pipe condition has been developed. This methodology proved to be successful and provided corrosion measurements that were in-keeping with those obtained through standard pit depth measurements. Further, the data showed that traditional pit depth measurements do not always find the deepest external corrosion pits, particularly where the surrounding geometry is complicated.

This methodology was used in a live comparison exercise of two, commercially available techniques. This comparison highlighted problems with the surface preparation required by some techniques, which can be quite damaging, and with some proprietary post-processing algorithms – the raw data can be more useful. From this assessment process, it has been possible to specify very detailed schedule for the testing of new NDE techniques in the future.

Acknowledgements

The completion of this thesis marks the culmination of five years of research work. I would be foolish to think that it was solely of my own doing without support from anyone. To quote John Donne, “No man is an island”. Never has this been as clear to me as it is now. Without the help of the people described below, the completion of this thesis would not have been possible. As such, it is only fitting that I acknowledge those people who have helped to me to get this far before venturing on to the work itself.

Firstly, I would like to thank my supervisors, both academic and industrial: Dr D. Jesson, Dr M. Mulheron, Prof. P. Smith, Dr L. Scudder and Dr T. Evans for their constant supervision to ensure that the project progressed in the right direction, and for continually stretching and developing my research skills.

I would also like to extend my thanks to my former Thames Water colleagues Mr. N. Clay-Michael, Mr. J. Farrow and Mr. M. Shepherd for sharing their extensive knowledge on the construction and operation of the TWUL clean water network with me.

My thanks also go to Mr. K Payne for carrying out the vast amount of cutting required to obtain sufficient samples of cast iron pipe, Mr J. Cruz for conducting the pit depth measurements on the shot-blasted pipe sections, and to Mr. A. Steele for the design and manufacture of the experimental rigs used in these experiments. Thanks also go to Mr. P. Thorne and Mr. A. Goldstraw for their help with 3D scanning and the post-processing of 3D models.

I must also thank Mr R. Hulley and Mr I. Doggett for their continued support when transporting such large sections of trunk main. Their help was invaluable and allowed samples to be exchanged quickly without delay to any experiments.

It would be remiss of me not to thank the EPSRC and TWUL as without them, there would be no facilities to experiment in. Thanks also to Mrs. N. Hartley and the other vital members of the MiNMaT CDT who ensure that the scheme is managed in such a smooth fashion.

Finally, and most importantly, I must acknowledge the help and support provided by my friends and family throughout the project. None of this would have been achievable without their tireless support and motivation. Special thanks must be given to my loving partner, Eleni, who has lived with me through this challenging project and supported me through it. I can safely say that that the success of this EngD will be the shared by more people than just me.

Contents

List of Figures

List of Tables

Nomenclature

AC	Alternating Current
AESL	Applied Engineering Solutions Limited
AMP	Asset Management Plan
BS	British Standard
CI	Cast Iron
DI	Ductile Iron
EPA	Environmental Protection Agency
MFL	Magnetic Flux Leakage
MRI	Magnetic Resonance Imaging
MWB	Metropolitan Water Board
N/A	Not Applicable
N/S	Not Specified
NDE	Non-Destructive Evaluation
NDT	Non-Destructive Testing
NRC	National Research Council
OfWat	Water Services Regulation Authority (formerly Office of Water Services)
PASTA	Pipe and Soil Technical Archive
PIG	Pipeline Inspection Gauge
PRF	Pulse Repetition Frequency
RFEC	Remote Field Eddy Current
SONAR	Sound Navigation and Ranging
TWUL	Thames Water Utilities Limited

1 Introduction

1.1 Context

Water is a precious resource and it is vital to sustaining life across the planet. Every day, water networks across the developed world are relied on by billions of people to provide them with a supply of potable water. Each network comprises sub-networks, providing either local distribution or bulk transportation. The smaller distribution mains, of the order up to 6" (150 mm) in diameter convey water stored in local service reservoirs, or water towers, to customers' homes, places of work or sites of recreation. Much larger diameter trunk mains, of the order of 12" to 60" (300 mm to 1500 mm) in diameter, transport significant volumes of water to key assets such as local service reservoirs or water towers. Very often this can be over significant distances (e.g. tens of kilometres) (Fahimi *et al.*, 2016). Many of the pipes in such networks are made of grey cast iron and may have been in service for up to 150 years (Jesson *et al.*, 2013). Despite their age, some parts of these networks continue to operate with little degradation, whereas in other areas they degrade rapidly and more recently laid pipes are found to be outlived by their forerunners (Rajani and Makar, 2000; Atkinson *et al.*, 2002). This problem has advanced as these mature networks are stretched further by the connection of new pipe networks constructed to meet the demands of growing populations.

Trunk main networks across the UK and other developed countries have come into focus as they are failing more frequently with a significant number of bursts occurring each year, a trend that is set to increase further (Johnston, 2016; Larter and Duffell, 2017). The consequences of a trunk main burst are significant, as a trunk main can easily transport many tonnes of pressurised water, and can lead to customers being off supply, significant quantities of treated water being lost and the surrounding area becoming flooded which has important implications for nearby assets and infrastructure (Walford, 2012). Consequently, a pipe burst can result in considerable damage to both the surrounding area and the reputation of the assets' operator alike. The consequences can vary in magnitude considerably depending on the location, as a burst in an isolated field would have relatively little impact compared to one occurring in a heavily populated area. A trunk main failure in central London typically impacts a significant number of people, both customers and members of the public, who will be inconvenienced by the loss of supply, flooding and disruption to travel. These consequences must be examined together with the probability of failure to determine the level of risk each main poses for the operator. Higher values for risk indicate pipes that must be attended to if these bursts are to be managed and their occurrence reduced. It is impossible to remove the risk completely but it is important to adopt suitable mitigation techniques that reduce the risk to an acceptable level.

Thames Water Utilities Limited (TWUL) are the UK's largest water and waste water operator and are responsible for running and managing the water network assets across London and the Thames Valley area. During each 5-year asset management plan (AMP) period, TWUL are allowed to spend an allocated amount

of money on pipe rehabilitation and replacement[1]. However, at a cost of £1 – 10 million per km of trunk main replacement (Scudder, 2013), the amount that can be replaced in any given period is limited. Indeed, at the current rate of replacement it will take some 800 years to replace the entire network; a period of time significantly greater than the average life of any individual pipe. Therefore, a targeted approach to pipe rehabilitation is required to ensure that the money is spent on pipes which present a significant risk of failure. Identification of trunk main assets that represent the greatest risk to the company finances, supply operations and damage to the surrounding areas is challenging and can only be done by understanding the true condition of the network. Consequently, accurate non-destructive evaluation (NDE) is vital for making informed replacement decisions.

1.2 Scope

Preventing trunk main bursts is of great importance if TWUL is to save water, reduce costs and maintain its reputation. However, the ability to pinpoint the location of the next burst before it happens is needed if there is any chance of preventing it. Sophisticated computer models can be developed to determine a pipe's likelihood of failing based on its environmental factors and its condition. However, the reliability of the output from these models is dependent on the quality of the environmental factors and condition data input into the model. If this data is not representative of the "ground truth" pipe condition, the recommendations it makes will be unrealistic and TWUL cannot place confidence in them.

NDE technology for the water sector is relatively immature compared to the sister techniques currently employed in the gas and oil sector and requires development to reach the point where the inspection data accurately reflect the pipes' condition. At this point, improved simulations of the mains with high risks are likely to be achieved and would aid the decision process when selecting mains to be replaced.

A large collaborative project between TWUL and the University of Surrey was undertaken entitled "Trunk Mains: Developing understanding, tools and models for characterisation, performance assessment and risk mitigation". This EngD project formed part of that project and focused on non-destructive methods of assessing the current condition of a trunk main.

The aims for this work are to:

- Identify the defects associated with the failure of cast iron trunk mains and determine the minimum size of defect NDE must be able to detect;
- Review the NDE tools currently available and understand their capabilities and limitations in order to identify those techniques that could be reliably deployed to inspect the 6,000 km of grey cast iron pipe within the TWUL network;

[1] The expenditure proportion for the AMP is decided by the regulator, Ofwat, during the price review prior to the AMP period starting.

- Develop, and test, a methodology to give an exposed trunk main an initial "health check" to determine if more detailed NDE is required.
- Develop a method of accurately capturing pipe geometry for comparison with results obtained by contractors.

1.3 Thesis Structure

The preceding sections have introduced the background to the problem and the need for accurate information on the condition of current water mains has been highlighted. The scope of the work presented in this report has also been discussed and the objectives for the work defined. As the literature presented pertains to several different topics, it has been kept with the relevant topic chapters to best present it. Thus, Chapter 2, reviews the structure of grey cast iron and its historical introduction into water pipes. It also examines the reasons why they experience failure and the defects that are instrumental in reducing the strength of the cast iron. Chapter 3 draws together the reasons for cast iron pipe failure and uses models documented in the literature to calculate the size of the defects which may lead to catastrophic pipe failure under normal service conditions. This underpins the requirements for any NDE tool to be deployed on cast iron trunk main. Chapter 4 discusses the various NDE methods that may be suitable to detect such defects. This includes a discussion on the commercial techniques that have potential to be applied to *in situ* cast iron trunk mains.

In Chapters 5 and 6, the experimental work undertaken to investigate ultrasonic and magnetic NDE methods suggested in Chapter 4 is described and the experimental methods are detailed and the results are presented. The findings from these two chapters are drawn together to provide a more informed view of their potential for NDE of a trunk main. They also describe the difficulties that can be faced by any contractor carrying out NDE on a cast iron main. Thus, whilst Chapters 5 and 6 focus on the tools and their capability to assess a main in a non-destructive manner, Chapter 7 considers the problem from a standards and calibration perspective and looks at a method of recording the pipe geometry to understand the actual condition of a main more fully. This is a significant advancement on the current industry standard of pit depth measurement sampling. The application of this developed methodology is further demonstrated in Chapter 8 where it is used to evaluate the accuracy of two current NDE contractors.

The findings from the results given in Chapters 2 – 8 are brought together in the final chapter, Chapter 9, in which the work conducted for each branch of experimentation is summarised and the key outcomes from these results are presented. A final section identifies the boundaries of this work and suggests where future research studies might usefully focus.

Appendix A contains a proof copy of a paper (based on the work presented in Chapters 2 – 4) which has been accepted for publication in Infrastructure Asset Management.

2 Cast Iron Pipes and Their Failure Mechanisms

2.1 Context

In the previous chapter, the importance of the trunk main network was described, together with the risks that TWUL face in the event of a trunk main burst. Mitigation of these risks to an acceptable level is necessary and could be achieved through a complete network replacement program. However, in practice this is not a realistic option due to: the prohibitive cost; significant engineering challenge; the location; and size of many of these mains. Therefore, a targeted approach to high risk trunk mains in high consequence areas must be adopted: identification of these assets which present such risks can only be achieved with tools that can non-destructively assess the condition of in service pipes. This is not a trivial task as grey cast iron is a difficult material to assess even when it is not buried underground.

This chapter reviews the properties of grey cast iron, providing a brief history of cast iron in the water industry, describing typical pipe failure modes and summarising the reasons for such failures. With regard to the latter, failure can be due to underlying defects in the iron, and these defects will be described so that indicators of deterioration, that would be important to identify during inspection, can be determined.

2.2 Cast Iron and its Role in the Water Industry

Grey cast iron is formed of an alloy of iron and between 2.5 – 4 wt% carbon (Angus, 1976) with the saturated carbon forming graphite flakes. The size and shape of these flakes is dependent on the processing route, cooling rate and various alloying additives and impurities present in the melt. These flakes give the iron its good machining properties, but, the sharp tips of the flakes act as stress concentrators and also give the iron its brittle behaviour (Sun and Wang, 1990). As a result, the mechanical properties of the iron are dictated by the graphite flake size and distribution. The identification and classification of graphite flakes can be carried out using ASTM standard 247-16a (ASTM International, 2016). Examples of the graphite flake size and distribution seen in grey cast iron water pipes are given in Figure 2.1.

Although available for many centuries, cast iron came to prevalence in the early 18th century as developments to the iron smelting process made its production more economical. These improvements include: the introduction of coke to the blast furnace (rather than charcoal); the addition of a reversing engine to recirculate driving water for the bellows and, later, drive the air pumps directly; the re-melting of pig iron using a reverberating furnace; and the introduction of wider furnaces with a larger interior volume (Allen, 2009). Within years this new ‘wonder material’ was being used in many engineering projects driven by the Industrial Revolution, as it afforded better mechanical properties than many other available materials (Addis, 2016). Its widespread use is clear to see, even some 100 years, or more, later in bridges, buildings and canal aqueducts that still stand.

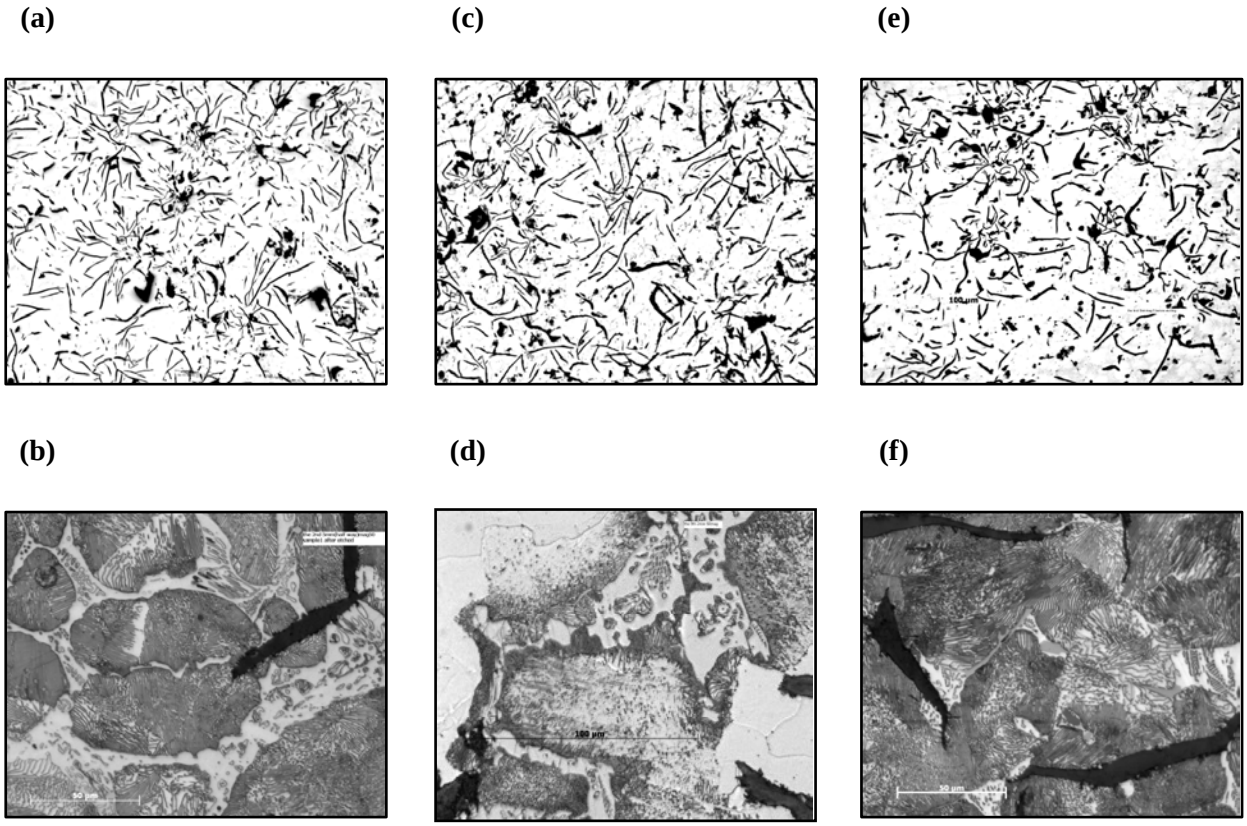

Figure 2.1 - Typical microstructure observed in cast iron mains: (a) an example of type B 'rosette' graphite flake morphology, (b) detail of (a), (c) an example of type A 'scythe/sickle' graphite morphology, (d) detail of (c), (e) an example of mixture of type A and type B graphite morphology and (f) detail of (e). After Mohebbi et al. (2009).

The earliest documented use of cast iron for water pipes can be traced to 1664 where it was used to supply water at Versailles (Sharp, 1914). Its use extended into the water industry and it soon became the material of choice for pipe manufacture as it leaked less and had a much greater design life than the 20 years afforded by wooden pipes made of elm (The Stanton Ironworks Company Limited, 1936). Cast iron pipes were commercially introduced in the late 18th century and continued to be used up until midway through the 20th century as they proved to be an effective option for water transportation (Cast Iron Pipe Research Association, 1952). In particular, Henry Stilgoe, appointed as the Chief Engineer for the Metropolitan Water Board in 1919, stated that: *'I can always say of the Cast-iron Water Main that it is a well-tried, faithful, and honest servant of the Water Engineer'* (Stilgoe as quoted by (The Stanton Ironworks Company Limited, 1936)). Even so, these were eventually superseded by ductile iron pipes in the late 1960s (Thomson and Wang, 2009) as they provided a greater cost benefit due to the reduced thickness of metal needed to withstand typical operational loadings.

At the introduction of cast iron for pipes, there were no standards in place to control the mixture of materials used in the casting melt or to stipulate the geometry of each pipe. Standards were only introduced in the UK in 1917 when BS 78 was released (British Standards Institute, 1917). Before this time, the pipes produced could vary in geometry and mechanical properties between foundries. As a result, it is possible to see significant variation in geometry in the joint. Unlike steel pipes which are usually welded together, cast iron

pipes are normally connected by a bell and spigot joint comprising a lead, or in some instances a leadite[2], and hemp seal pressed together to prevent water leaking out, Figure 2.2. Many different bell geometries have been observed across the network.

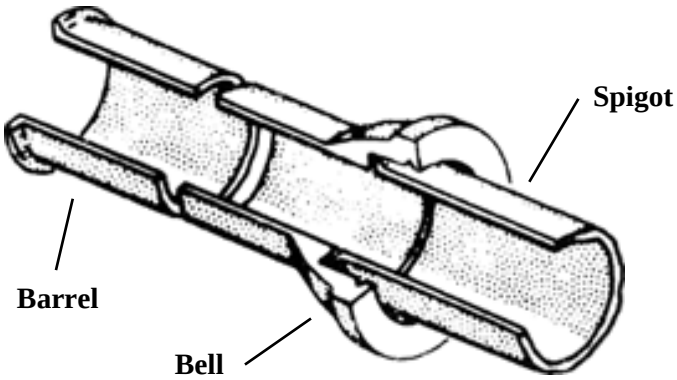

Figure 2.2 - A bell and spigot joint. After Harris (2005).

The methods of manufacture of cast iron pipes changed greatly over time. Early pipes were cast horizontally in a sand mould, however, this was gradually phased out and replaced by vertical casting in 1875 (Cast Iron Pipe Research Association, 1952). This improved the quality of the iron since more of the impurities could be removed from the casting. This method was itself gradually replaced in the 1930s by spin casting (Cast Iron Pipe Research Association, 1952). This further improved the strength as the porosity was reduced, since the air could escape the casting more easily. Further, this development led to both increasing uniformity of the wall thickness and a more refined microstructure with smaller graphite flakes, which ultimately improved the mechanical properties (The Stanton Ironworks Company Limited, 1936). As a result of the on-going development in pipe manufacture, it is possible to observe significant variation in material strength which can be seen across a range of studies (Talbot, 1926; Makar and Rajani, 2000; Seica and Packer, 2004; Jesson *et al.*, 2013). The on-going evolution of production standards and on-going metallurgical research has introduced great variation in the cast iron pipes produced. Consequently, it is not uncommon to find an assortment of pipes, each with different material grades, strengths, sizes and of varying bell geometry present in a water network.

2.3 Cast Iron Pipe Failure

Cast iron pipe failure can be split into two different categories, catastrophic and non-catastrophic failures, where catastrophic failure results in the pipe being replaced as it is no longer capable of performing its structural role. Catastrophic failures occur as circumferential or longitudinal cracking of the pipe or as a split or complete shear of the bell (Rajani *et al.*, 1996). Such failure modes can occur across all pipe diameters.

[2] *'Leadite is a plasticised sulphur cement compound that was used as an alternative to lead'* definition taken from EPA report on *"Condition Assessment of Ferrous Water Transmission and Distribution Systems" (Thomson and Wang, 2009).*

However, circumferential fractures are the dominant failure mode for pipes up to 8" in diameter and longitudinal fractures for all diameters greater than this value (Marshall, 2001). This diameter also marks the transition from bell splitting to shearing (Makar *et al.*, 2001).

Circumferential fractures propagate a crack around the pipe circumference as the axial stress exceeds the material's tensile strength. The increased axial stress can be attributed to poor bedding support or ground expansion, particularly in clay soils, which can increase the bending stress on the pipe, or to soil frictional forces which restrict pipe expansion (Rajani *et al.*, 1996). Axial stresses have also been found to be elevated by decreases in temperature. Such decreases result in tensile stresses as the pipe is restricted from contracting by the joint at each end. If the stress induced is not sufficient to cause catastrophic failure it can promote joint slippage and increased leakage (Jesson *et al.*, 2010).

Longitudinal fractures result in the propagation of an axial crack as the hoop stress exceeds the material's tensile strength due to a water pressure increase from a surge or through crushing forces applied to the pipe (Rajani *et al.*, 1996; Makar *et al.*, 2001). Bell splits and bell shearing are a result of increased stress within the bell and spigot joint. Bell splitting is most commonly associated with joints constructed using leadite. Here the thermal stresses created by the difference in thermal expansion coefficient between the metallic iron and the non-metal leadite can lead to the bell splitting as it tries to contract around the leadite seal (Makar, 2000; Thomson and Wang, 2009). Bell shearing is related to joint movement and the stress associated with joint rotation under load (Makar, 2000). One further failure to note is the "blow out" where a section of the pipe wall is driven out by the water pressure and often occurs as the result of a pressure surge. Such a failure is unlikely to happen in a pipe with uniform wall thickness. Instead it occurs where the pipe wall has thinned. The reasons for such wall thinning will be described in more detail in section 2.4. Examples of each of these failure modes can be seen in Figure 2.3.

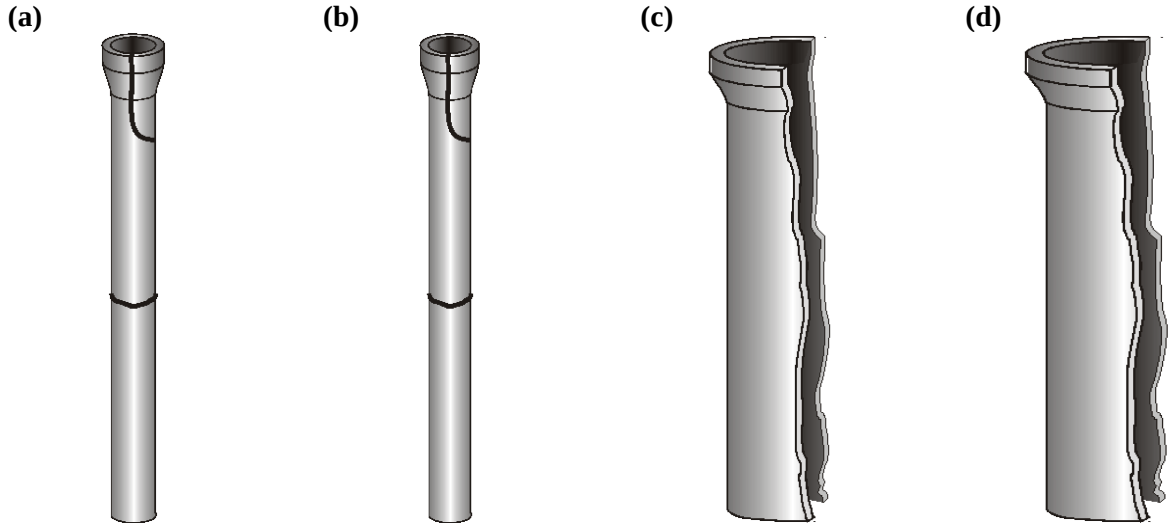

Figure 2.3 - Different failure modes seen in cast iron pipe: (a) bell split and circumferential failure, (b) blow out and through wall corrosion, (c) longitudinal failure and (d) bell shear. After Makar et al. (2001).

2.4 Failure Defects

2.4.1 Context

Section 2.3 introduced the failure modes observed in cast iron pipe. It was alluded to in the previous section by selective pipe blowouts that a deviation to the thickness of the pipe wall must be present to cause pipes to fail. Previous stress analysis suggests that increased stress alone does not necessarily cause failure, as the pipe walls are much thicker than needed to carry the working stress (Rajani and Abdel-Akher, 2012). The stress must be raised substantially by changes to the geometry or the presence of defects (Makar, 2000). Several different types of defects are present in cast iron which are created *ab initio* through manufacturing or installation as well as defects that develop with time. These defects can act to raise the stress experienced by the pipe.

2.4.2 Manufacturing Defects

It is well understood that the properties of cast iron are controlled by the graphite flake structure (Angus, 1976). Improvements in the manufacturing methods have led to smaller graphite flakes, which reduce the stress intensity around a flake, resulting in significant improvements to the mechanical properties of the cast iron. These improvements in manufacturing have also led to better uniformity of the pipe wall thickness. Despite such improvements, it is not unusual to see variations in the wall thickness of pipes. Figure 2.4 presents a contour map based on physical measurement of a vertically pit cast pipe dating from the 1920s and produced by the renowned Stanton Ironworks Company. The pipe, which can be considered to be of the highest quality available at the time, shows some ±10 % variation around a nominal average thickness.

Other possible casting defects, which also diminished as a result of advances in manufacturing techniques, include voids, porosity, slag inclusions, and so-called cold shuts, where two fronts of molten iron fail to fuse properly due to premature cooling.

2.4.3 Installation Defects

Following manufacture, the cast iron pipes were transported to site on trucks and trailers for installation, and would either be rolled down planks of wood from the edge of the truck or be lifted with a crane. It has been suggested that pipes handled in this way were susceptible to damage from collisions between the pipes and other external bodies (Rajani and Kleiner, 2011). Not all impacts would produce a visible crack: if a crack were internal in the bell or spigot, this would not necessarily have been detected by any on-site hammer testing that was employed at the time. Additionally, the use of chains for pipe handling, rather than canvas slings, is known to have damaged the protective outer coal tar or bitumen coating leaving areas of bare metal vulnerable to corrosion attack (Makar *et al.*, 2001).

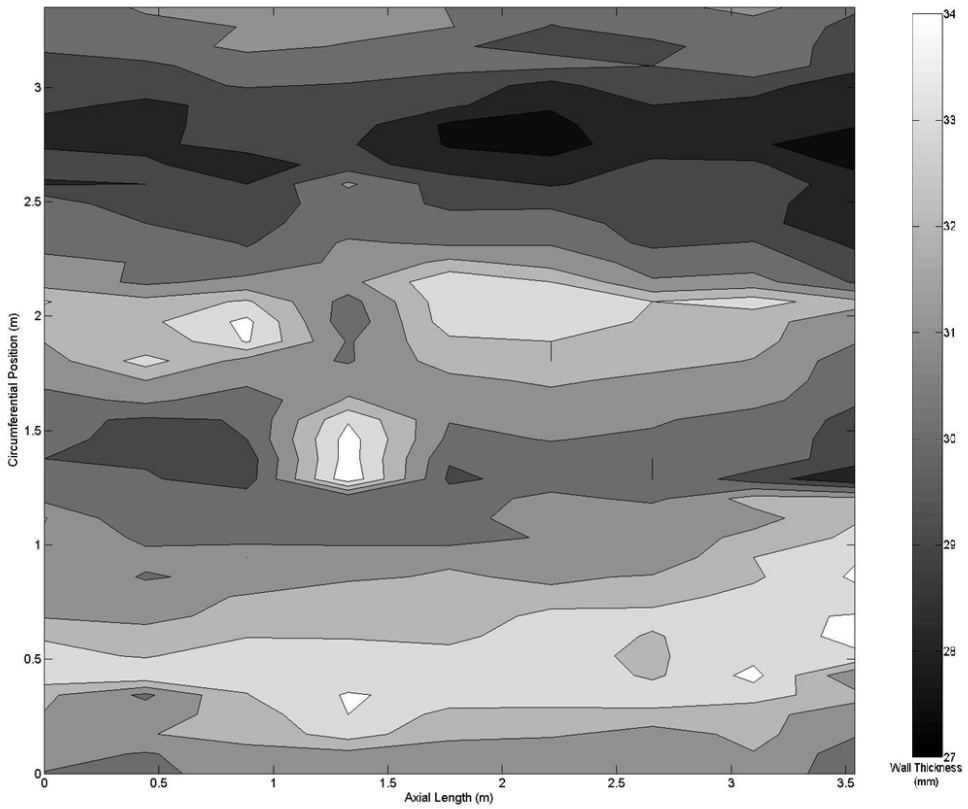

Figure 2.4 - A wall thickness map showing the variation in wall thickness in mm from manual point measurements, taken with a calliper, around the circumference of a 3.54 m length of 42" diameter vertical pit cast trunk main sectioned into rings and each ring into quarters. The darkest point represents the thinnest point and the lightest the thickest. The wall thickness varies by ± 4 mm around a mean of 31 mm. After Rainer et al. (2017).

Once the pipes were *in situ*, the joint would be packed with hemp to form a seal, filled with molten lead and finally caulked by hammering the solidified lead into the joint (The Stanton Ironworks Company Limited, 1936; Rajani and Abdel-Akher, 2013b). If the caulking was carried out incorrectly, the lead would be hammered too far into the joint, leading to an increase in stress around the joint, potentially causing a crack to initiate. A worst-case scenario would see poor caulking practice growing a crack created during the siting of the pipe. This could result in a pipe that is structurally flawed and hence has a reduced service life (Rajani and Abdel-Akher, 2013a).

2.4.4 In-Service Defects

Once in service, pipes are subject to further mechanisms which can cause defects to form and grow until they are too large for the pipe to sustain. Corrosion is one such defect. Early cast iron pipes would have been buried without any surface treatment. When bare cast iron is buried in soil, it outer surface is exposed to the water and oxygen present in the soil. This creates a corrosion cell where the iron is oxidised and can form different oxides of iron. Further, the interaction of the cast iron with the water it is conveying can lead to internal corrosion. Here tubercles are commonly seen as the most predominant internal corrosion (Sarin *et al.*, 2004),

Figure 2.5. Tubercles are the result of bacterial corrosion and produce a bubbles of iron oxide on the pipe wall which can vary in strength and structure dependent on the water flowing over them (Gerke *et al.*, 2008).

Figure 2.5 - A view of the inner surface of a water main showing significant tuberculation bubbles lining the whole inner surface of the pipe. After Świetlik et al. (2012).

To provide a further layer of protection against such corrosion mechanisms, many pipes were coated in a bitumen or tar coating[3] to protect them whilst buried (Shell Bitumen, 1995). However, in places where the coating has been broken (often as a result of the installation process as mentioned above), corrosion processes are initiated which can further undercut the coating, causing it to spall and expose bare metal which then continues to corrode.

Of greater concern is 'graphitisation', which is a far more damaging corrosion mechanism present mainly in cast iron. Once initiated, this corrosion can progress through the full thickness of a typical cast iron pipe wall. Technically, it should properly be termed 'graphitic corrosion' of cast iron (Logan *et al.*, 2014). Graphitic corrosion is identified by two distinct areas: a passive grey brittle corrosion product and an active transition zone, typically 2 – 4 mm in depth, bounded by the corrosion product on one side and the virgin iron on the other, where the corrosion process occurs (Logan *et al.*, 2014). Despite anecdotal assertion, it is not possible to identify graphitic corrosion reliably by visual inspection in exposed pipes, since the corroded region does not change in volume (although the density decreases) and so the surface of the pipe appears unaffected to the naked eye (Fitzgerald, 2007).

Examination of exhumed pipes has found that the graphitic corrosion product has been seen to occur in two broadly defined topologies: a uniform thickness over large areas, or more localised pits which can give variable condition along a pipe's length, Figure 2.6. In some places, it has been seen to extend through the full wall thickness resulting in a significant loss of strength. However, corrosion over 4 mm in thickness is noteworthy

[3] Bitumastic or coal-tar coatings were applied to the pipes at the time of manufacture to prevent corrosion and have proven to be effective at protecting the underlying metal, even after considerable time in the ground (Reid, 1934).

as this marks the transition in failure mechanism. Previous work has already shown that the iron possesses graphite flakes within its microstructure that are between 2 – 4 mm in size. These flakes dominate the failure mechanism. It is only when the defect size is larger than the flake size, at approximately 4 mm, that the failure mechanism transitions from a microstructural failure to a failure due to an external defect (Atkinson *et al.*, 2002).

(a) **(b)**

Figure 2.6 - Two different morphologies of graphitisation: (a) localised pitting and (b) uniform thickness. After Rainer et al. (2017).

Despite significant research into the corrosion experienced by cast iron, graphitic corrosion is not fully understood and no definitive reason for its initiation is given. A parallel workstream in the larger TWUL collaborative project has investigated the reasons for the initiation and progression of graphitic corrosion. Logan (2016) has found that graphitic corrosion occurs when a buried pipe is exposed to a favourable combination of the soil corrosivity, made up from the soils' water retention properties and its electrical resistance, oxygen content and the presence of salts in the surrounding soil. The exact combination of these conditions is not known, however, graphitic corrosion has been found to occur commonly in pipes buried in saturated soils, such as clay, where the soil corrosivity is high due to its water retention and low electrical resistance. These soil conditions can vary due to the pipe backfill. Such heterogeneity in the soil conditions around the pipe can result in variations in the corrosion behaviour seen across the pipe.

The study has also shown that the presence of chloride ions at the active transition zone are important for corrosion to progress. No, chloride ions were shown to be present in the uncorroded materials and few remain in the corrosion product. Hence it is likely that these ions have diffused into the pipe from the surrounding soil, where the conditions permit their migration and concentration, to congregate at the active corrosion interface. Their enhanced concentration in the soil is likely to stem from external actions such as road gritting. Once initiated, corrosion rates of between 0.1 – 0.7 mm per year would be expected (Mohebbi and Li, 2011; Logan, 2016). Consequently, corrosion with an average rate of 0.4 mm per year will progress through a 35 mm thick pipe in less than a century.

This corrosion product does not contribute to the mechanical strength of the pipe and can reduce the residual strength capacity of the pipe (Yamamoto *et al.*, 1983; Jesson *et al.*, 2013), Figure 2.7. Further, the difference in morphology can greatly affect the mechanical properties exhibited by the pipe as a uniform loss of material

may result in a slightly reduced loading strength, whereas a non-uniform loss can create points of stress concentration where it may be possible to form a crack, particularly if the pit has a very rough surface.

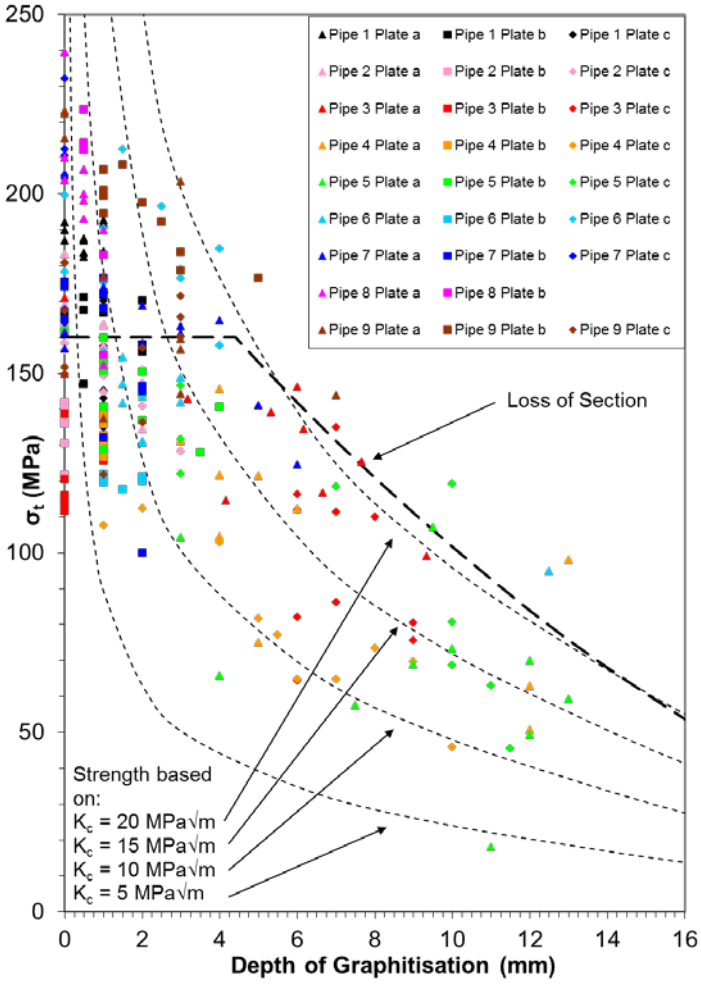

Figure 2.7 – Strength of cast iron samples versus the maximum depth of graphitic corrosion measured on the fracture surface of that sample. 10 samples were taken from a plate and three plates were taken cut from each of the nine pipes studied. The plates were taken from random locations along and around the barrel of the pipe. It is worth noting that in a number of cases the plates taken from a specific pipe exhibit very different properties. Models for strength based on loss of section and fracture mechanics (values of fracture toughness, K_c, ranging from 5 – 20 MPa$\sqrt{m}$) approaches have also been superimposed.

After Jesson et al. (2013).

In smaller diameter distribution mains, graphitic corrosion has been shown to have a significant impact on the strength of the pipe and to be in competition with defects that have originated during manufacture (*'a priori'*) and installation (*'ab initio'*). Further, because of the combination of the size of the pipe and its interaction with the local environment, it is possible to comment upon the behaviour of the main a significant distance (multiple casting lengths or 'sticks' of pipe, typically 3 – 5 m in length) either side of a sampling point (Belmonte *et al.*, 2007; 2008; 2009). The size and spread of graphitic corrosion in distribution mains can be seen in Figure 2.8.

(a)

(b)

Figure 2.8 - Split section of 4" diameter distribution main illustrating the spread of corrosion and the amount of metal that can be lost to the graphitic corrosion process: (a) before shot-blasting and (b) after shot blasting. After Rainer et al. (2017).

Finally, in terms of service induced defects, it is worth noting that fatigue has been cited as a problem, which can be induced by operational pressure variations and traffic loading, particularly in connection with the growth of installation defects (Rajani and Kleiner, 2011) . This assertion is predicated on the presence of a substantial initial crack (of the order of 20 mm) which needs to grow by only a small amount (1 - 2 mm) to cause catastrophic failure. Experimental work on the fatigue properties of cast iron presents a somewhat mixed view. It perhaps seems more likely that fatigue may be a contributory factor when taken in conjunction with corrosion: these two may combine to cause premature failure (Belmonte *et al.*, 2009). Cast iron is known to undergo mechanical fatigue (Angus, 1976; Belmonte *et al.*, 2009; Mohebbi *et al.*, 2010) although it should be noted that a specific mechanism which combines both fatigue and corrosion has not been established.

2.5 Summary of Cast Iron Pipe Failures

In this chapter, the on-going engineering developments that have led to great diversity of the materials and geometry seen in water networks have been discussed. It is clear to see that significant variation in strength and geometry is possible across any pipe network. Whilst significant variation has been shown, the failure mechanism for large diameter mains has been shown to remain constant and will be governed by the graphitic microstructure and the presence of defects. Many of the defects observed in cast iron pipes can be attributed to a lack of understanding of casting metallurgy and structural weaknesses that can be introduced with poor manufacturing practice. The defects induced *ab initio* can act in combination with other defects, such as corrosion, to concentrate the stress and cause pipe failure. However, it is worth noting that pipes do not necessarily fail where defects are present, as the defect may only raise the stress sufficiently to form a crack and it may take several stress cycles to grow a crack capable of catastrophically failing the pipe (Makar, 2000; Belmonte *et al.*, 2009; Mohebbi *et al.*, 2010).

Each of these defects could be responsible for the failure of a pipe. However, it is only when it has grown to a sufficient size that catastrophic failure ensues. Such values for these critical defect sizes are important if proactive NDE is to have a chance of detecting such defects while they are in a sub-critical state. In the next chapter, such critical defect sizes are investigated through the use of strength models given in the literature. These are brought together, along with extant material data, to provide guidelines on the defect sizes of interest.

3 Critical Defect Sizes for Cast Iron Pipe Failure

3.1 Context

The previous chapter has explained the pipe failures seen and has suggested what defects cause these failures. However, without an understanding of the size of a defect, the NDE will not be able to provide an informed view of the health of a pipe section. Further, determining a critical defect size provides boundaries for the sensitivity that any NDE technique must achieve.

In this chapter, two different approaches detailed in the literature for identifying the maximum tolerable defect size for a given stress level, and hence the critical defect size, are described. Both approaches have been developed to suggest values for the effect of corrosion on a pipe's strength: these two approaches are to calculate the remaining pipe strength given a uniform loss of section from corrosion or to calculate the stress intensity factor for a sharp defect, such as non-uniform graphitisation.

Other literature is gathered which provides guidance on the working stress that a pipe may experience under use. These sources of information are combined to identify the critical defect sizes tolerable for each suggested defect profile. Finally, this is brought together to give a map which suggests a red, yellow and green scale to indicate when a defect size may be bordering on, or likely to cause a pipe to fail. These values can be used to suggest the size of defects that any NDE technique will need to detect if the onset of premature pipe failure is to be detected early and prevented.

3.2 Loss of Section Approach

The loss of section approach determines the maximum stress that can be supported by a material with a reduced cross sectional area. Equations developed by Jesson *et al.* (2013) to determine working stress in the remaining sound metal, σ_{TB}, dependent upon the ratio of the uniform layer lost, *a*, and the original wall thickness, *d*, are given in Equation 3.1.

$$\sigma_{TB} = \begin{cases} 214.9\left(1-\frac{a}{d}\right)^2 & \text{if } \sigma < 160 \\ 160 & \text{if } \sigma \geq 160 \end{cases} \qquad \text{Equation 3.1}$$

A diagrammatic representation of this loss of section can be seen in Figure 3.1. In this approach, a yield stress of 160 MPa is assumed for cast iron as an upper boundary to the working stress that the cast iron can experience. Equation 3.1 has been plotted in Figure 3.2 and shows the maximum stress that can be supported for a given loss of section. It can be seen that a defect must grow to about 5 mm before any degradation in pipe strength with occur. From this graph it is also possible to determine the critical stresses for the loss of section approach for a given working stress. However, the working stress that the pipe is exposed to must be known. Each pipe in the network is different and it is very unlikely that any two pipes will experience the exact same working stress. To overcome this problem, two different values for the nominal operating stress have been

proposed. Marshall (2001) suggested that a value of 90 MPa should be used for all diameters. This value has been derived as the largest stress seen for any pipe in a network and is in agreement with values obtained from discussions with water companies. It suggests a worst-case scenario for the stress that any pipe may see and is applicable to water pipes of any diameter. However, Rajani and Abdel-Akher (2013b) have suggested a much lower stress of 30 MPa. This value has been inferred from the values for factor of safety presented by Rajani and Abdel-Akher (2013b) and the nominal strength of the cast iron described for many of the pipes currently in service.

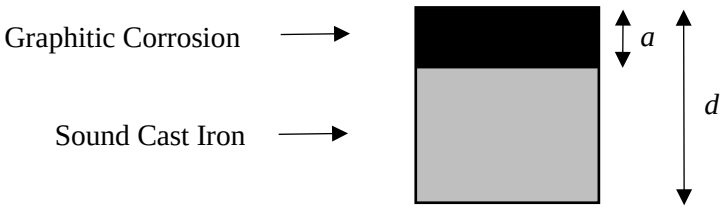

Figure 3.1 - Diagrammatic representation of the metal lost through a "Loss of Section" approach to graphitic corrosion.

The two working stresses of 30 and 90 MPa have also been plotted to determine the critical defect size at these stresses. These critical defect sizes are also given in Table 3.1 and it can be seen that a defect less than 12 mm or 22 mm can be supported at stresses of 30 MPa or 90 MPa respectively. Further material loss would result in failure.

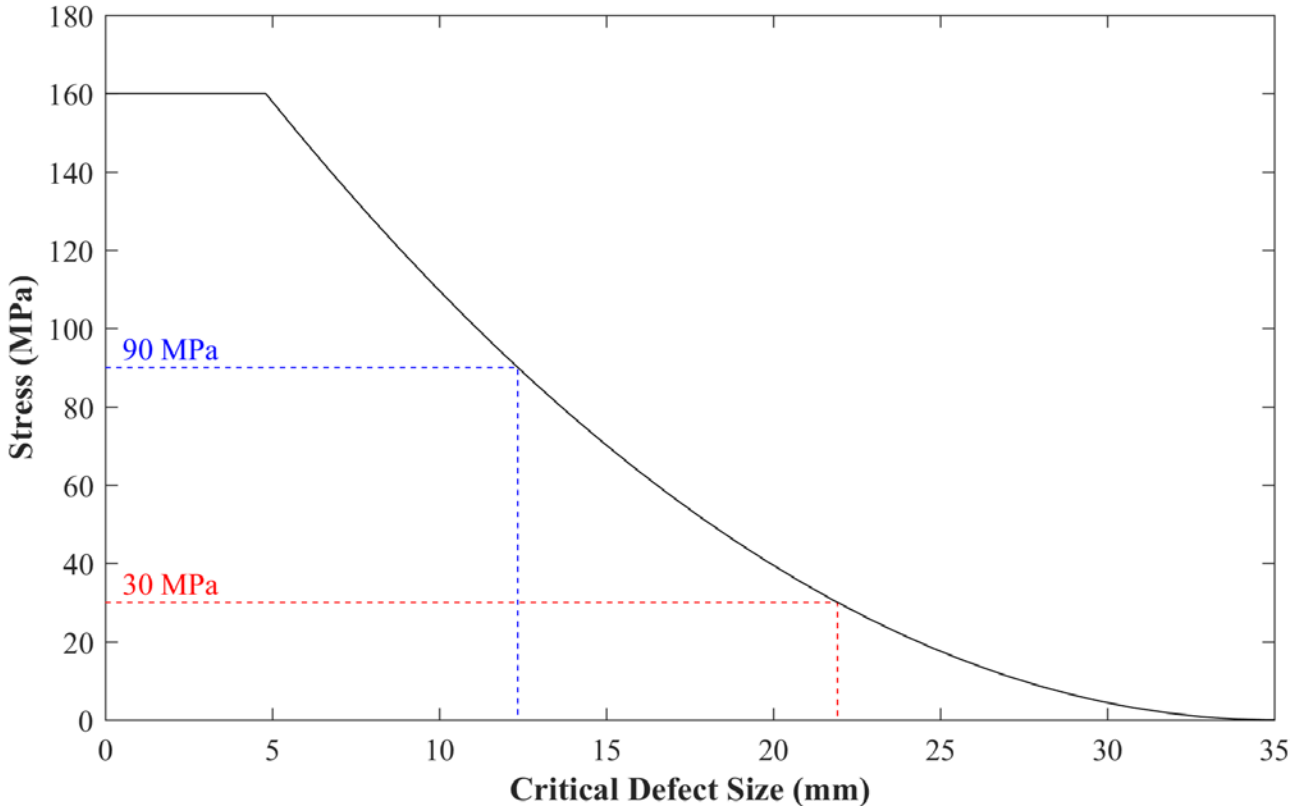

Figure 3.2 - A graph showing the critical defect size tolerable at the stress limits given by Marshal (2001) and Rajani and Abdel-Akher (2013b) for a pipe with an original wall thickness, d, of 35 mm as calculated by the "Loss of Section" approach.

3.3 Fracture Mechanics Approach

The loss of section approach provides a value of the critical defect size assuming that the corrosion has a uniform morphology. However, this is not always the case and the loss of section approach may give an overoptimistic defect size for cases of corrosion with non-uniform morphology. Conlin and Baker (1991) suggested that fracture mechanics may give a better approximation of the remaining strength where non-uniform corrosion, or other defects, create points of stress concentration. Grey cast iron exhibits brittle behaviour that can be characterised by linear elastic fracture mechanics. The fracture mechanics approach treats corrosion as a sharp crack with a stress intensity factor, K_1. This factor can be determined using Equation 3.2.

$$K_1 = Y\sigma\sqrt{\pi a} \qquad \text{Equation 3.2}$$

Where, Y is a geometrical correction factor, σ is the tensile stress applied to the pipe and a is the size of the defect (Hertzberg, 1996). Equation 3.2 can be re-arranged to give Equation 3.3 which relates the maximum critical stress, σ_c, tolerable for a set material fracture toughness, K_C, and critical defect size, a.

$$\sigma_c = \frac{K_c}{Y\sqrt{\pi a}} \qquad \text{Equation 3.3}$$

A simple fracture analysis, modelling the defects as a sharp crack, has been carried out to determine the size of defect that could be supported for a given working stress. Some of the defects exhibited in pipes may vary in geometry to a simple crack, but, this analysis serves to identify the size of defect which it would be desirable to detect in a worst-case scenario. Consequently, a geometric correction factor, Y, of 1 was chosen. This is consistent with other fracture mechanics analyses that have been carried out on cast iron water pipe (Conlin and Baker, 1991; Atkinson *et al.*, 2002; Mohebbi *et al.*, 2010)

From the literature it can be seen that cast irons have a fracture toughness that lies in the range of 6 - 20 MPa$\sqrt{\text{m}}$ (Ashby and Jones, 2005), and which is dependent upon the casting method (Makar, 2000). The critical stress has been plotted against a corrosion thickness of 0 to 35 mm for 4 different values of fracture toughness, ranging from 5 - 20 MPa$\sqrt{\text{m}}$ as seen in Figure 3.3. The two working stresses of 30 and 90 MPa have also been plotted to determine the critical defect size at these stresses. The critical defect sizes for each operating stress and fracture toughness are given in Table 3.1. It can be seen that the critical defect size can range from 1 mm up to 16 mm at a working stress of 90 MPa. However, a much larger defect can be supported, > 9 mm, if the working stress is 30 MPa or lower.

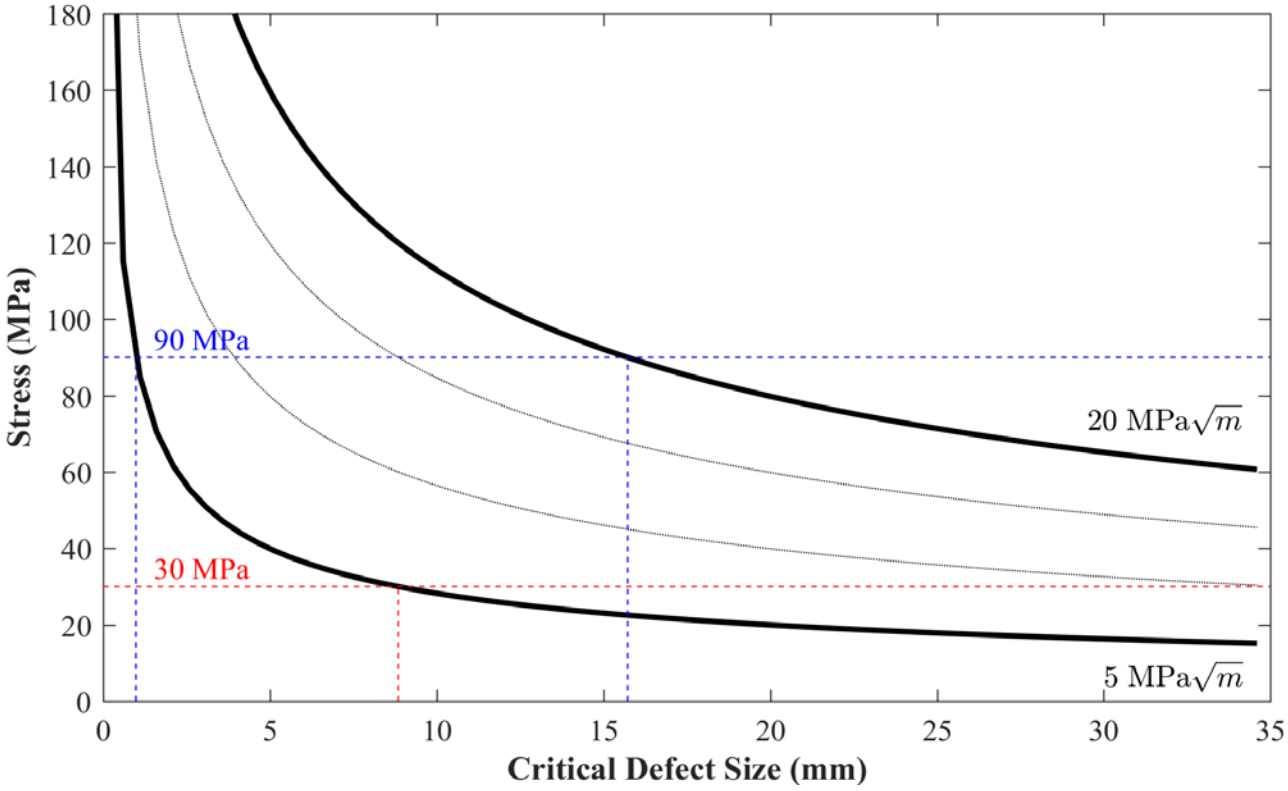

Figure 3.3 - Critical defect size tolerable at the stress limits given by Marshall (2001) and Rajani and Abdel-Akher (2013) as calculated by the "Fracture Mechanics" approach.

Table 3.1 - Critical defect sizes in mm determined by the "Fracture Mechanics" approach and "Loss of Section" approach for the given stress limits by Marshall (2001) and Rajani and Abdel-Akher (2013), for a pipe with an original wall thickness of 35 mm.

Pipe Operating Stress (MPa)	**Fracture Mechanics K_c (MPa$\sqrt{\text{m}}$)**				**Loss of Section**
	5	10	15	20	
30	9	Greater than wall thickness			22
90	1	4	9	16	12

3.4 Combined Analysis for an Overall Defect Envelope

The critical defect sizes obtained from both the fracture mechanics approach and the loss of section approach are given in Table 3.1. The analyses show a wide spread of sizes from as little as 1 mm to more than the pipe wall thickness, however, it is not possible for a pipe to sustain a defect of any geometry greater than 22 mm as it would fail from a loss of section. Also, it is unlikely that a defect of 1 mm or even 4 mm would be responsible for pipe failure. As mentioned previously, the external defect size must be greater than the graphite flake size before the external defect size becomes the reason for failure. Consequently, the critical defects are likely to be of the order of 9 to 22 mm in size dependent upon the working stress.

These approaches have been combined to generate an envelope which suggests the size of the critical defects tolerable and the method by which the pipe will fail, Figure 3.4. Here the green region indicates a combination of stress and defect size that is survivable by the pipe. The yellow region indicates a combination of stress and defect size that is likely to be survived by the pipe dependent on the fracture toughness of the pipe. Finally, the red region indicates combinations of stress and defect size that would lead to catastrophic failure of the pipe. In this region, the pipe is most likely to fail due to a loss of pipe section capable of supporting the stresses applied. However, the darker red region on the map indicates an area where the pipe is likely to fail from a fracture mechanics approach in preference to a loss of section.

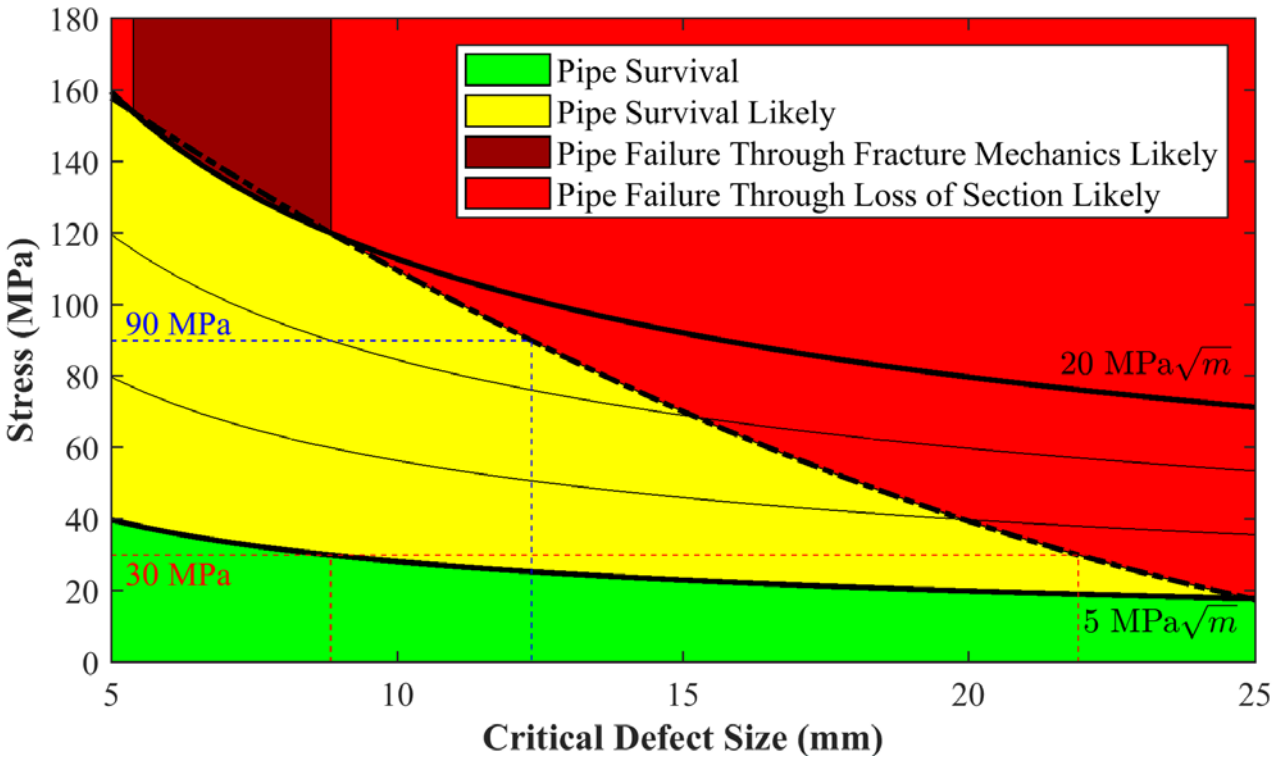

Figure 3.4 - A map showing the critical defects tolerable at the stress limits given by Marshall (2001) and Rajani and Abdel-Akher (2013b). The "Fracture Mechanics" (solid lines) and "Loss of Section" (variable dashed line) analyses, for a pipe with an original wall thickness of 35 mm, have been super imposed to create regions indicating the likelihood of pipe survival.

The fracture mechanics analysis shows that the tolerable defect size is considerably less than the loss of section approach. If the worst-case scenario is examined, the fracture mechanics analysis suggests that defects of the order of 9 mm thick could cause the failure of a pipe. This has been suggested as over pessimistic by Atkinson *et al* (2002) as it assumes the pitting behaves as a sharp crack. Consequently, thicker corrosion could be supported by the pipe than calculated. However, it is desirable to be able to detect these defects as they can be seen to represent the worst-case scenario. Cracking of this order may be possible as there have been examples of pipes that have failed without any prior warning and do not appear to be degraded (Rajani and Kleiner, 2011).

3.5 Summary of Cast Iron Pipe Critical Defect Sizes

In this chapter, two approaches that seek to identify the maximum stress tolerable for a defect of a given size in a pipe have been discussed. The working stresses that a pipe may be exposed to have been suggested and discussed. This information has been combined to give suggested defect sizes that may cause catastrophic pipe failure. The analysis has suggested that defects as small as 9 mm could cause the pipe to fail by fracture. Further, if the defect grows to 22 mm, the pipe will yield and fail due to insufficient cross section to support the loads applied. It should be remembered that these sizes indicate the defect size at which failure will occur. For proactive NDE and targeted pipe replacement, defects smaller than these sizes must be detected before they reach critical size. It is suggested that defects approximately half of the size of the critical size must be detected to ensure the pipe possesses sufficient remaining life to continue to operate in service without failure while rehabilitation actions for the main are planned and undertaken. As a consequence, a minimum defect size of 4.5 mm must be able to be detected in order to prevent catastrophic pipe failure.

4 Non-Destructive Evaluation of Cast Iron Pipes

4.1 Context

In Chapter 2, the legacy materials currently used in the water network were detailed. The main causes of pipe failure within this diverse network of materials were identified and the defects, or potential indicators of a pipe being in a state of poor condition, detailed. Ultimately pipe failure is the result of the load capacity of the pipe being reduced significantly through a combination of inherent material defects and defects induced through manufacture, installation and service use. In Chapter 3, approaches described in the literature were used to determine the critical defect sizes at which the pipe would fail catastrophically, under normal loading. It is clear that several defect types can undermine the structural condition of a pipe and it is important that these defects can be detected and sized. The need for an NDE technique to be able to detect these defects before they reach these critical sizes is clear, if the transition from reactive to pro-active pipe replacement is to be made.

NDE has been traditionally used in fields such as aerospace, nuclear, petrochemical and power generation, where failure can result in a loss of life, environmental disaster or similar intolerable costs (Roberge, 2007). Many of the current techniques available have been derived from these industries and are described in detail by (Halmshaw, 1991; Cartz, 1995). However, NDE is becoming more commonly used in applications where assurance that a system possesses sufficient structural integrity to operate over its design life with a low risk of failure is needed.

NDE in the water industry is a relatively new concept, although it has become more prevalent, driven by incentives to reduce the level of leakage from the network. Systems have been developed to identify possible leaks in water mains through noise correlation. Examples include “Sahara” which comprises a tethered hydrophone capable of travelling down the inside of a pipe (Bond *et al.*, 2004), or “Trunkminder”, which comprises a set of hydrophones fitted at specific locations along a pipe (Syrinix, 2017). Such systems have become fairly advanced and give a good indication of the location and size of leaks in a main, but tools available for assessing the condition of the pipe material remain limited.

In this section, the techniques for NDE that may be appropriate for the water industry will be considered. The requirements for NDE are defined together with barriers to application. Finally, the techniques which are most likely to meet the needs stated will be explained: any that can’t be applied to cast iron trunk mains in the field will be removed from further investigation. Any technique selected must be capable of being deployed in potentially busy city streets as well as locating and sizing the required defects. As such, any technique will be selected on its ability to be commercially deployed, not just its ability to identify defects.

4.2 Non-Destructive Evaluation – Uses and Limitations

4.2.1 Definition of NDE

In its simplest guise, NDE describes any form of inspection or investigation that provides results pertaining to the condition or construction of an object or objects under inspection without causing any permanent damage

to the object of inquiry. A simple example is knocking on a wall to see if it is hollow. Here a change in the sound properties provides a yes/no answer to the question and avoids visual inspection after the demolition of the wall. As stated, this is a simple example and NDE has moved on greatly to capture more detailed information on construction and condition, such as the thickness and composition of the wall in our earlier example. Perhaps the most noticeable area of growth and development is in the medical sector. Typical examples of NDE used in the medical industry would be X-Ray, ultrasonic or even magnetic resonance imaging (MRI) scanning. In this industry, the need for non-destructive tools is obvious, particularly where data needs to be collected on or around sensitive organs such as the heart or brain. These tools reduce the risk of tissue damage which may be incurred via traditional invasive techniques such as surgical exploration.

It is not only patients that require a periodic health check, but also many engineering structures to ensure that they are in a condition capable of surviving the design life, which can be lengthy particularly when the fixture may have been extremely costly or difficult to install. This is true of many civil engineering installations. Cast iron water pipes are no different. However, unlike their oil and gas relatives that are routinely inspected, and often designed with inspection in mind, they have experienced less care and attention due to the fact that they are buried underground where access to them is both disruptive and costly.

It should be clarified that non-destructive evaluation (NDE) and non-destructive testing (NDT) are often used interchangeably. However, they have similar but subtly different meanings. NDT refers purely to the acquisition of physical results from testing that identify the presence of a defect. NDE takes this definition one step further. Whilst NDE also refers to the testing of an object through non-destructive means, the evaluation provides data that is more quantitative in nature, such as the size and position of a defect (Raj, 2001). Such data is important for further processing to produce a decision outcome, such as acceptable or unacceptable defect sizes. The decision making process to determine the suitability of an item based on the outcome of NDE is a complex process and is influenced by many variables which are dependent on the structure being investigated. The judgement of and not the judgement of the potential of such defects for failure falls outside of the scope for this thesis. Further information on this decision making process can be found in Fahimi (2017). The focus for this thesis is on non-destructive methods that are capable of not only finding defects within a cast iron pipe, but also able to determine their size, shape and position to support the decision making process. Consequently, the term NDE is most relevant and is used throughout this thesis to describe any non-destructive measurements.

4.2.2 Mechanisms of NDE

As it has already been alluded to in the hospital environment, NDE can come in different variants in industry. This is driven by the data being sought from the inspection but also the ability to apply the technology. This can be broken down into many different areas and hence into different criteria for acceptance, depending on the evaluation being conducted. A simple form of NDE on cast iron pipes would be to undertake leak testing on a system of pipework to ensure that a system performs its function without losing fluid. However, when talking about material properties, it is more common to use NDE to evaluate the remaining strength within the

material to state whether or not the component can continue to perform its function. Both inspections are seeking indicators of a failure however, the two are very different and will require significantly different tools to detect them. To meet such requirements different methods of NDE are used: Acoustic, Visual, Electrical, Dye Based, Magnetic, Ultrasonic, Radiographic, Thermographic, Chemical, Electromagnetic or a combination of several methods. This list is by no means exhaustive. Many of the techniques can be broken down into further subsets and newer techniques are constantly being developed as applications demand enhanced assurance of their ability to function.

4.2.3 Continuous or Instantaneous Monitoring

When applying NDE to a pipeline, it is important that the method of application is carefully selected. Two different options exist which can provide different results:

Continuous Monitoring – The component is instrumented with sensors which continually record the changes over a set period of time. These systems look for changes that are exhibited over time, very often from passive emission by the material, that would be highly unlikely to be experienced during a planned inspection. Examples include: Acoustic emission testing on the Forth Bridge suspension cables or leak noise correlation. Ultimately it could be argued to be the most comprehensive method of conducting NDE as it can be configured to detect a problem at its onset and allow it to be resolved at a very early stage. However, in doing so, there is a significant setup cost and a considerable overhead to monitor the data being produced by the sensors. In many applications, this type of monitoring is not practical and it is reserved for mission critical components or components with a high likelihood of failure.

Instantaneous inspection – When continuous monitoring is considered an unnecessary expense, instantaneous inspection is opted for on a single one-off event or as part of a regular maintenance program. The component is inspected using the desired technique at a point in time to determine if any indicators are present which might indicate that it will not perform satisfactorily. This could be immediately after manufacture as a quality assurance inspection or later on in life to ensure that the component or system will continue to perform as expected, such as ultrasonic weld examination during manufacture for example.

It can be seen clearly that the choice of NDE used for inspection and their applications is vast. Each technique available is suited to particular applications and defects. The choice of NDE for application to cast iron water mains will be determined by the environment in which they are expected to operate and the indicators that are being sought.

4.2.4 Principles of Application of NDE in the Water Industry

In Chapter 2, the different ways in which a cast iron pipe section can fail were described and the underlying defects which can cause such failures were described. Whilst the defects mentioned previously could all contribute to failure, some are more likely to cause failure than others. Corrosion has been shown to reduce the structural performance of the cast iron severely and must be a priority for inspection. It is also important to establish the level of metal remaining in the pipe, especially as geometric disparities such as wall thickness,

variations not necessarily known about beforehand, can further concentrate the forces around the corrosion site and so further reduce the pipe's capacity. Following on from corrosion, cracks also present a significant risk to the structural performance of the pipe as they have the potential to grow until failure through fatigue loading (Rajani and Kleiner, 2011). It would be beneficial to be able to identify the location and dimensions of any cracks particularly if there is the potential for them to interact with another defect present. Finally, it would also be beneficial for asset management if the presence and location of porosity, inclusions, cold shuts and other such defects could be determined, to characterise the condition of a pipe fully. However, if the defect populations introduced at manufacture have not led to early failure, they are likely to be in a stable state and may not lead to failure in the near future, unless combined with newer defects. Hence, the detection of cracks and corrosion, both of which can worsen over time, are of much greater importance.

Finding these defects is challenging as there are several barriers which inhibit the use of NDE, not least, their buried nature. It is an aspiration that the condition of a buried asset could be assessed from above ground without the need to excavate the pipe, thus saving time and expense. Engineering and Physical Sciences Council (EPSRC) funded UK research programmes "Mapping the Underworld" and, more recently, "Assessing the Underworld", have been working to determine what underground assets can be successfully inspected without being exposed. Whilst progress on identifying the location of a buried asset has been made, no methods of NDE have shown the ability to detect the defects discussed here either from above ground or by using point assets, such as valves or hydrants, as access points (Hao *et al.*, 2012).

Where above ground inspection is not possible, the ideal deployment would be via an inspection system which can pass along the inside of an in-service main (such a tool often being referred to as an intelligent pig, smart pig, or inspection pig). In principle, this would allow large portions of the network to be inspected without disruption to supply. However, in practice, this is problematic as the physical contact of the sensor and/or the carrier with the pipe wall is likely to cause surface deposits to be dislodged or in the worst-case may damage corrosion prevention measures (e.g. bitumastic coatings). In a worst-case scenario protruding corrosion features (known as tubercles, Figure 4.1) can be damaged by internal NDE, leading to chronic water quality issues and potentially accelerate internal corrosion due to the removal of the passivated layer. Tubercles are the result of bacterial corrosion and produce bubbles of iron oxide on the pipe wall which can vary in strength and structure dependent upon the water flowing over them (Gerke *et al.*, 2008). Hence, the use of an inspection pig is likely to require the main to be taken out of service during inspection and subsequently flushed.

Figure 4.1 - Example of tuberculation build-up on the inner surface of a cast iron trunk main.

The use of this approach would also require a significant amount of network modification to enable a pig to be inserted and retrieved from the network, and a device or a collection of devices that could cope with the range of mains diameters in use (12" to 60"). Lastly, the pig must be capable of traversing a trunk main which may change direction or depth along its length, and could have off-takes. Given that many parts of the pipe network are not always easily accessible if the device should become stuck, this presents a significant challenge (Vickridge and Lau, 2000; Dingus *et al.*, 2002).

As a consequence, conducting NDE from the outer surface of the pipe is currently preferable, even if it means that the pipe must be excavated for NDE to be conducted. Very often mains are exposed for routine work, which may present sufficient opportunity to assess the main's condition whilst the excavation is still open. However, this is still not without challenge. An excavation creates a muddy trench and may only expose a small section of main, (approximately 1 m in length), which is not significantly wider than the pipe's diameter. This can leave limited access to the surface of the pipe, particularly underneath the pipe, Figure 4.2. Any NDE method will need to be capable of operating within the clearance around the pipe afforded by the excavation and the neighbouring utilities.

Any technique must be capable of dealing with an outer surface which is often hidden by a well adhered layer of surface encrustation which is formed from the soil and aggregates around the pipe and, in some circumstances, iron leached from the pipe may react with the soil and the aggregates to form a binder, increasing the tenacity of the encrustation to cling to the surface, Figure 4. 3(a). Whilst this encrustation can be removed, it must be done carefully so that the pipe is not compromised or the rate of degradation accelerated. Even once removed, the surface can be seen to be heavily pitted. This is a long way from the typically smooth surfaces seen in the aerospace industry where NDE techniques are routinely used. Finally, NDE must be capable of penetrating thick sections of cast iron, of the order of 30 - 40 mm. This is further complicated as cast iron pipes have a heterogeneous microstructure and so can be difficult to inspect with many established techniques. The graphitic corrosion product, that forms over time, can also be very difficult to inspect as it is also heterogeneous and can greatly attenuate any signals being put into it (Logan *et al.*, 2014). Not all of these

surfaces are of simple geometry. The pipe joints also limit the use of NDE as they can have varying geometry of which the inner profile is not always known, Figure 4. 3(b). Consequently, it may be difficult to distinguish between a geometrical variation and a genuine defect. It also makes accessing the spigot very complex as it is hidden by the pipe bell. Effective NDE will cover the whole pipe section including the pipe joint where the geometry can become significantly more complicated.

Figure 4.2 - Exposed 20" trunk main in situ at Regent Street in central London with several other pipes and services crossing it showing the restricted space available around a main.

(a) **(b)**

Figure 4. 3 - Barriers to NDE on cast iron trunk main: (a) surface encrustation and (b) variable geometry.

The water industry is subject to strict controls and measures for the prescribed concentrations and values for chemical and bacterial content in the treated water (UK Government, 2016). Any NDE technique deployed to the network, either internally or externally, must not have an adverse effect on the water quality. Further, any NDE technique must not affect the supply of water to the customers. Any change to either is likely to attract negative attention for the company, not least from the water regulator and so must be avoided.

4.3 NDE Currently Used in the Water Industry

Every NDE technique has strengths and weaknesses: there are several excellent reviews on such techniques and their specific capabilities (Jackson *et al.*, 1992; Dorn *et al.*, 1996; Dingus *et al.*, 2002; Costello *et al.*, 2007; Thomson and Wang, 2009; Prinsloo *et al.*, 2011; Hao *et al.*, 2012; Liu and Kleiner, 2013): the key features of these reviews are summarised in Table 4.1. All of these papers review the literature regarding NDE and explain the operation of each technique. In some cases, the results of field tests that evaluate each NDE technique's efficacy on cast iron main are given. However, such reviews, whilst providing an insight into potential NDE techniques that may be applicable to cast iron, rarely consider the different *types* of defect and the challenges in *finding* such defects in a buried pipe in-service ('live'), in the field. Where field results have been obtained, the results only consider inspection carried out internally on small diameter pipes. Little consideration has been shown for techniques that can be applied to the outside of the pipe, nor on the techniques that could be used to inspect much larger trunk main. Ultimately, many of the reviews identify very similar tools for potential use on cast iron pipes, rather than describing how their methodology may be applied to the pipe or locating specific defects.

Aside from studies in the literature, TWUL are not new to NDE and have trialled a number of different approaches including an in-house project which developed the "Super-pig" (Thomson and Wang, 2009). The Super-pig was a free-swimming PIG capable of inspecting 8 – 12" main with an array of ultrasonic transducers as it travelled along the main. The prototype was successfully trialled, but funding priorities changed before it could be developed further into a commercial tool for large diameter cast iron mains (Evans, 2017). Externally, many contractors currently offer NDE on trunk mains as a service. Companies such as JD7 and Hydrosave offer inspection using an ultrasonic tool. JD7 use a tethered probe that travels down the inside of small diameter cast iron mains and captures condition data using a rotating ultrasonic transducer (JD7, 2017). Hydrosave use a single transducer that is hand-scanned over the outer surface to capture condition data (Hydrosave, 2017). Other NDE companies are also known to use ultrasound to inspect cast iron, although TWUL have had little exposure to some of the other ultrasonic offerings. Ultrasound is suggested to be one of the most useful tools for inspecting cast iron, however it is not the only technique. One other company, Advanced Engineering Solutions Ltd (AESL), use magnetic flux leakage (MFL) to inspect cast iron main (Advanced Engineering Solutions Ltd, 2016). Their E-Cat tool is rastered over the surface of the pipe to assess the corrosion. Further thickness measurements are carried out using an ultrasonic probe.

Table 4.1 - A summary of the literature comparing NDE on cast iron water pipes in chronological order. Although each paper may describe NDE for more than one material, any technique which is not applicable to cast iron, or which is only used to evaluate the environment around a pipe, is not considered in the table. (N/S – not specified, N/A – not applicable)

Reference	Format	Pipe					NDE Techniques Discussed	Defects Considered	Comments
		Materials Considered	Diameter	Length	Wall Thickness	Field Conditions			
Jackson *et al*. (1992)	Physical Study (Laboratory Testing)	Cast Iron; Ductile Iron	4.5 - 6"	Up to 5.49 m	3.175 - 8.76 mm	Sections of jointed pipe	Acoustic Emission; Magnetic Phase Shift; Remote Field Eddy Current (RFEC); Ultrasonic;	Wall thinning; Man-made defects (10 - 40% of the wall thickness)	This review shows the start of NDE of cast iron pipes and comprises a literature review and a physical study split between the laboratory and the field. Potential NDE techniques were identified from the literature of well-established techniques present in the oil and gas industry. These techniques were then applied to laboratory pipe samples and buried pipelines. Here the RFEC test show potential for inspection, however this study is limited to internal inspection of small 4.5 - 7" diameter mains which is not reflective of the true sizes of pipe present.
	Physical Study (Field Testing)	Cast Iron	7"	80 m	~ 8 mm	Abandoned Pipeline	Magnetic Phase Shift; RFEC; Ultrasonic;	Wall thinning; Graphitic Corrosion	
			6"	65 m	N/S				
	Literature Study	Steel; Ductile Iron; Cast Iron	Up to 36"	N/S	N/S	N/A	Visual; Penetrant Flaw Detection; Radiology; Ultrasonic; Magnetic Flux Leakage (MFL); Eddy Current Testing; Potential Drop Inspection; Acoustic Emission; Thermography; Holography	Cracking; Breaks in Lining; Pitting; Wall thinning	
Dorn *et al*. (1996)	Literature Study	Ferrous Materials; Cementitious Materials	> 150 mm	N/S	N/S	N/A	Eddy Current; Radiographic; Ultrasonic; Visual;	Graphitic Corrosion; Wall Thickness	The paper reviews techniques for assessing a pipe's condition and then suggests methods of inspecting this condition using NDE. The review recognises the many defects that can cause pipe deterioration, but the size and importance of detection are not given. It then suggests which NDE techniques could work on cast iron. The paper goes on to suggest indirect identifiers that can be used to identify pipes that may be susceptible to failure based on other data that can be gathered non-destructively, such as soil corrosivity.
Dingus *et al*. (2002)	Literature Study	Metallic Pipes	N/S	N/S	N/S	N/A	Impact Echo; Remote Field Eddy Current (RFEC); Ultrasonic; Visual;	Cracking; Graphitic Corrosion; Pitting; Wall Thinning	This review is split into two parts and initially reviews the current literature to identify NDE that could be useful for cast iron mains. The paper continues by showing the results of field trials which used NDE selected based on the information provided in the literature review. All cast iron pipe inspection was conducted using internal inspection pigs. RFEC was shown to be the best at inspecting metallic pipe for thinning but could not find any cracks or voids. Whilst the results show potential for inspecting cast iron they are limited as only two different techniques were tested on cast iron pipes, covering only a small range in diameter when compared to the 60" cast iron mains that are present in the UK. Further the paper did not explain the sizes of defects that were important to detect.
	Physical Study (Field Testing)	Cast Iron	6"	50'	N/S	Abandoned Pipeline	RFEC	Cracking; Graphitic Corrosion; Man-made Grooves; Wall Thinning	
				800'					
			10"	1080'		In Supply Pipeline	Electromagnetic		
			16"	1000'					

Reference	Format	Pipe					NDE Techniques Discussed	Defects Considered	Comments
		Materials Considered	Diameter	Length	Wall Thickness	Field Conditions			
Costello *et al*. (2007)	Literature Study	N/S	N/S	N/S	N/S	N/A	Eddy Current; Impact Echo; Laser Profiling; MFL; RFEC; Sonar; Ultrasound; Visual;	Cracking; Pitting	The review covers methods of NDE that could be used to locate buried utilities or to conduct condition assessment of known utilities. The mode of operation is explained for each technique and some known potential problems with each technique are given. Many of the techniques listed are for use in sewers. However, as the focus of the paper is not specifically on buried cast iron water pipes but buried utilities in general, the review of each technique does not suggest how each technique would cope when being applied to an aging cast iron pipe and tasked with finding the specific deterioration mechanisms present in cast iron. Further, there is no mention of the size of the utilities these techniques are applied to.
Thomson *et al*. (2009)	Literature Study	Ferrous Pipes	<6 - >48"	N/S	N/S	N/A	Visual; Ultrasonic; Eddy Current; MFL; RFEC; Radiographic	Corrosion; Pitting; Cracking; Remaining Wall Thickness	This paper reviews the published literature on cast iron mains failures and methods of conducting condition assessment on them. It recognises the different types of cast iron manufacturing and the defects that each pipe suffers, before going on to describe the possible failure modes and detailing the indicators that should be detected to prevent a failure. The capabilities of some techniques are suggested but not for all. Further, the practicalities of conducting this inspection are not considered.
Prinsloo *et al*. (2011)	Literature Study	Metallic Pipes	> 100 mm	N/S	N/S	N/A	Acoustic Emission; Visual; MFL; RFEC	Corrosion	The paper reviews the current techniques available for internal inspection of large diameter mains but not specifically to water. The defects that cause deterioration to cast iron water mains, and the NDE ability to detect these types of defects, are not mentioned.
Hao *et al*. (2012)	Literature Study	N/S	N/S	N/S	N/S	N/A	Eddy Current; Impact Echo; MFL; Rapid Magnetic Permeability; RFEC; Sonar; Laser Profiling; Visual	Cracking; Pitting	This paper provides an updated review of the techniques mentioned in Costello *et al*. (2007). However, the focus of the paper is still on the tools that can be applied to the buried utilities in general and whilst some areas have been updated as new technologies have become available, the fundamental defects affecting deterioration in cast iron pipe and their chances of being detected are not discussed.
Liu and Kleiner (2013)	Literature Study	Metallic Pipes; Pre-stressed concrete pipes; Polymeric Pipes;	N/S	N/S	N/S	N/A	Eddy Current; Impact Echo; MFL; Laser Profilometry; Radiography; RFEC; Sonar; Thermography; Ultrasonic; Visual	Corrosion; Pitting	The paper reviews the latest NDE technologies that can be used to conduct NDE. It covers many more techniques than have been mentioned in previous papers. Whilst the paper covers the techniques that could be applied to all buried pipes, it does not suggest the specific defects of interest in cast iron and the capabilities of the NDE for assessing these. Further the paper does not consider the difficulties of implementing any of the methods suggested on a buried cast iron main.

4.4 Unsuitable Techniques

4.4.1 Context for Unsuitable Techniques

The literature reviews on the techniques have shown that a reasonably comprehensive list of NDE techniques might be expected to include: ultrasonic, magnetic flux leakage (MFL), eddy current, acoustic, radiographic, dye penetration, visual and pit depth measurements. Whilst it is vital that any NDE technique being deployed on the water network can detect the defects of interest, it is also paramount that they can be deployed to network given the space around an asset and operate in a safe fashion. The techniques mentioned above have been evaluated and some have been found to be inapplicable to the water network for such reasons. These techniques and their reasons for being unsuitable are given in this section.

4.4.2 Constrained by Safety

Dye penetration testing requires the use of a fluid dye which must not enter the water supply but could be drawn in through a through-wall crack. Radiographic inspection with gamma rays or X-rays carries immediate health risks and would require an extremely powerful source and lengthy exposure time to penetrate the thick cast iron. Given the small exposure area, this process would need to be repeated several times to build up a complete image of the pipe successively. Furthermore, the inspection would only have access to the outer surface of the pipe which would mean that the radiation source and detector would be sited either side of the pipe, effectively doubling the material that the rays would need to penetrate. Hence more powerful X-rays with longer exposure times would be needed, increasing the health & safety risks. Finally, there is a public perception issue regarding the deployment of radiographic equipment, and associated shielding, barriers and signage, in urban areas.

4.4.3 Constrained by Working Space

Remote field eddy current techniques have been shown to assess the level of corrosion on a main well but it would be impeded by the available space in the excavation (Dingus *et al.*, 2002). Hence, the technique is suited to an inspection pig application since it requires a substantial separation, of the order of two pipe diameters (Hao *et al.*, 2012), between the exciter and the detector. This is unlikely to be possible in an excavation where space may be limited.

4.4.4 Constrained by Damage to the Asset

It is feasible to gather visual condition data on the level of external corrosion by mechanically removing corrosion products and measuring with more or less accuracy the pits which are revealed. However, this is a partially destructive method which, whilst providing a useful measure of corrosion, could lead to problematic situations for an in-service main. If through-wall corrosion is present, disturbing it may lead to a leak or, worse, failure of the pipe.

4.4.5 Constrained for Other Reasons

Passive acoustics are used in water mains to detect leaks but can also be employed to listen for mechanical deterioration in a structure, such as the wires breaking inside a pre-stressed concrete pipe (Travers, 1997). This

method can only be applied to situations requiring continual monitoring and not inspection as it can only measure the deterioration since it was installed rather than providing a complete instantaneous picture of condition (Makar and Chagnon, 1999). It is questionable whether such an approach is relevant in the context of the subcritical growth of a crack. Pre-supposing that such a crack has been identified and a sensor placed at an appropriate location to monitor ongoing crack growth, such a detector would need to be capable of detecting the energies associated with crack growth of the scale of the order of 1 μm per cycle (Mohebbi *et al.*, 2010), whilst also subjected to a range of other events found in live main, particularly those under busy roads. Active acoustic methods such as modal analysis, where the frequencies at which an object resonates are monitored and compared to a known reference, as in the traditional tapping test of a train wheel to identify a flaw, have also been suggested. For a buried water pipe, the different volumes and types of earth which surround it, and the large volumes of water within it, can affect greatly the resonances of the pipe wall (Leinov *et al.*, 2015). Such environmental variations may be very difficult to factor into the reference and, hence, the results obtained may be negated. At higher acoustic frequencies, shorter range guided waves might be used to inspect trunk mains. This technique is often used to inspect long lengths of welded pipes where the waves can progress between lengths of pipes. However, the bell and spigot joint between pipes on trunk mains would limit the wave progression between adjacent sticks.

Non-contact strain measurements which use interference optical methods, such as holography and shearography, may be challenged by the environment when used to perform measurements on a large pipe. Preparing the surface sufficiently well to use precision optical equipment would be very demanding and it is doubtful that an excavation on trunk main could provide a suitable environment for such optical based NDE methods to function.

Visual inspection may not be sufficient on its own but would be a precursor to any other technique, allowing information, such as casting marks and the environment in which the pipe sits such as the presence of other utilities or traffic loadings to be assessed. All this information can contribute to a ‘health check’ of a pipe. If the pipe is badly deteriorated to the naked eye, then this may negate the need to proceed with further inspection.

4.5 Potentially Suitable Techniques

4.5.1 Context for Suitable Techniques

Several of the techniques detailed in these review papers have the potential to operate in the environment around a trunk main and have not been discounted. These techniques are detailed here and their applicability is discussed further.

4.5.2 Magnetic Flux Leakage

Magnetic Flux Leakage (MFL) shows some potential for the inspection of cast iron and is already commercially available as an inspection technique (Liu *et al.*, 2012). However, there are some questions over the efficacy of the method in characterising defects in the pipe wall. In particular, the often poor surface condition present on an exhumed trunk main can make it challenging to ensure that the tool is in full contact

with the pipe wall. Failure to maintain full wall contact does not ensure that the magnetic field generated by the magnets is coupled into the pipe wall consistently and can lead to difficulties with accurately determining the size and shape of the defect. This is as the tool's capacity to capture the flux leakage around a defect is linked to the spacing between the tool and the pipe wall. Further, the sensitivity of the tool is reduced for greater wall thicknesses as it becomes progressively harder to detect magnetic flux leaking from the distant wall with a system stationed at the proximate wall (De Silva *et al.*, 2002). Given its operating principles it seems very unlikely that narrow cracks will be detected because it is debateable whether the crack will provide a sufficient discontinuity for the flux to leak out of the pipe.

4.5.3 Eddy Current Testing

Eddy current technology, using low frequency alternating electromagnetic fields, is another possible method for corrosion detection in a trunk main. Conventionally, AC fields, in the 5 – 60 MHz range, are applied to find surface-breaking cracks in metallic objects with good surface finishes. However, the inspection of thick sections with this technique is limited by the depth to which the eddy currents can penetrate. This is dependent on the induced frequency (Rizzo, 2010), e.g. skin depth of 3 mm in a steel pipe exposed to a 50 Hz AC field (Hao *et al.*, 2012). Reducing the frequency to the order of 10 – 100 Hz can enable the skin depth penetration to be increased (Jackson *et al.*, 1992); however, full coverage of a 35 mm wall still may not be possible. The challenge for a field-deployable system will be to achieve the required resolution of cracks and other defects, although this will be aided by the technique's tolerance of a variety of surface conditions.

4.5.4 Ultrasonic Inspection

Finally, ultrasonic inspection may prove to be of great use as, in principle, it can be applied in different ways to search for different defect populations from one surface of the trunk main (Liu *et al.*, 2012). Configured in its simplest pulse-echo mode, with ultrasonic signals travelling normal to the pipe wall, it can measure the degree of corrosion thinning in a wall. It can also be arranged for the ultrasonic pulses to travel into the pipe wall at an angle to search for cracks in more remote locations within the bulk of the wall material. As with most NDE methods, raw waveforms from these tests must be post-processed to ascertain the condition of the pipe, and this requires a good understanding of the propagation of ultrasound within corroded iron to arrive at a robust determination of pipe condition. A key factor in accurately determining defect sizes is how fast the ultrasound travels in corroded and uncorroded areas of the pipe wall. In uncorroded cast iron the speed might range from 3500 m/s to 5600 m/s (Berens, 1989). This large velocity range covers all types of cast iron, but for the types of cast iron in trunk mains the range is likely to be narrower as a result of the relationship between velocity and modulus. For the trunk mains investigated by Jesson *et al.* (2013), the variation in modulus between the ten different pipes was less than a factor of two which would give a much narrower velocity range. Ideally the speed of sound should be determined for the particular pipe being inspected, but only having access to one surface of the pipe provides little opportunity to make speed measurements on a section of known thickness, unless a calibration coupon is available. There is then the added complication that the speed of sound may vary through the pipe wall due to *a priori* variations in microstructure. Improved accuracy could be achieved if the date and place at which the pipe was cast is known, thus allowing pipes of a similar provenance

with known properties to provide a closer estimate for use in an inspection. Also, the graphitic corrosion products of cast iron have been shown to be highly attenuative and so greatly impede the passage of ultrasonic wave (Dorn *et al.*, 1996) and there remain issues with respect to the compensation for this in the post-processing of field data. In principle, as with many techniques, a good surface finish is required for reliable contact between the sensors and the pipe and this may necessitate cleaning the pipe surface (Thomson and Wang, 2009). However, this may be mitigated through the use of ultrasonic immersion testing: in such systems, a thick layer or column of water is used between the sensor and the pipe wall to couple the ultrasound to the pipe.

Despite these potential issues, tools using ultrasound have been developed to inspect cast iron trunk main and it is commonly offered as a method of characterising a pipe's condition. Finally, ultrasound has the potential to detect the defects discussed previously and as progress on its performance is made, it may be capable of giving sufficient corrosion data for both internal and external corrosion. The possibility of operating NDE techniques in tandem, so that one may fill in the gaps where another technique struggled, could be beneficial in providing a better overview of a pipe's condition. However, it is worth noting that it is highly unlikely that truly non-destructive evaluation of a pipe can be carried out, as in most situations some surface cleaning to facilitate an inspection will be required, and this will inevitably have an impact on the remaining life of the pipe.

4.6 Summary of NDE on Cast Iron Pipes

NDE is regularly deployed in a number of industries for the purposes of quality control, inspection and lifetime assessment. The methods used to perform NDE on materials and engineered systems are diverse, relying on a wide range of physical techniques. NDE is a mature industry in its own right, but it is a long way from being able to field a handheld device capable of determining all critical defects in any material with significant partial accuracy from a distance: this remains the reserve of science fiction, such as Star Trek's tri-corder.

There are several very helpful reviews that consider NDE as a whole, specific branches of NDE, or NDE in a particular context. Many of these papers are based on desk studies comparing the application of such technologies. Where previous NDE reviews for water mains have been less helpful is in applying the filter of the field environment: otherwise ideal techniques are limited to the laboratory and are unlikely to be practical in the field.

Ultrasonic inspection, whilst its application is challenged by the poor surface condition present on the exterior of many mains, has been suggested to be the most applicable techniques for NDE on exhumed trunk mains. However, significant work is required to overcome the current barriers corrosion creates to the gathering and interpretation of informative condition data. NDE data collection can be further improved by conducting consecutive inspections using one or more complementary NDE techniques, who's operation is reliant on a different physical principle, such as MFL. The incomplete datasets gathered from each of these inspections

can then be fused together to give a fuller picture of a pipe's condition. Here the gaps in the condition data provided by one technique could be filled from data from another technique that captured data successfully.

Given the potential length of water networks and the range of soil environments in which they are situated, external NDE conducted in small excavations can only give a snapshot of the local pipe condition. Statistical analysis can allow these data to predict the condition of nearby sticks, and asset managers can use further analysis to consider cohorts of similar pipes using data from across the network to make a decision about a specific stick. However, ultimately, greater (contiguous) lengths of the pipe network must be inspected to understand its condition more fully. At present, a device capable of characterising the defects mentioned to the resolution suggested does not exist. Further developments in this area must be made if any certainty on the condition of the trunk main networks is to be obtained.

Building on this introduction to NDE the remainder of this thesis investigates two potential techniques in more detail (Ultrasonic inspection in Chapter 5 and Magnetic Force testing in Chapter 6) and presents a methodology for assessing and calibrating new developments and techniques (in Chapter 7 and 8).

5 Ultrasonic Inspection of Cast Iron Pipe

5.1 Introduction

In the previous chapters, the need for an NDE technique capable of evaluating cast iron mains for potential indicators of failure has been demonstrated. In Chapter 4, these needs were evaluated and the requirements of a tool, and the main barriers which it would have to overcome, were described. When compared against the NDE tools that are currently available commercially, ultrasonic inspection stood out as the most likely tool capable of capturing data on corrosion and cracking. The successful use of ultrasound on pipelines made from steel and ductile iron is described in the literature given in Chapter 4. However, further examination of the published literature showed that there was little convincing evidence that demonstrated the effectiveness of ultrasonic methods when used on cast iron pipelines. This is particularly true for its capabilities of inspecting graphitic corrosion.

Ultrasound has been shown to propagate through cast iron, however, the frequencies that can be used effectively are limited dependent on the grain size. There is a strong link to the degree of attenuation and the graphite flake size, and Kamigaki (1957) has suggested a transducer frequency for cast iron of 0.5 – 2 MHz. It is recognised that the presence of graphite flakes and porosity have a significant effect on the properties of the ultrasonic waves that propagate through the iron (Biswas *et al.*, 2015). Further, Viens *et al.* (1996) showed some progress in the inspection of cast iron water mains using ultrasonic inspection, however, the methodology used to conduct the inspection, and also the post-processing, was not fully documented. As such it shows potential for the use of ultrasonic inspection to cast iron pipes.

It is clear that cast iron trunk mains have NDE requirements, and obstacles to overcome, which are different from those applied in other pipelines. However, little literature exists for the direct application of ultrasonic inspection to cast iron for *in situ* defect detection. In this chapter, the capabilities of the ultrasonic inspection will be evaluated for use on cast iron against typical inspection scenarios. These will begin with the simplest requirements and progress to evaluate scenarios that are more complex. The aim is to understand whether ultrasonic inspection has the capability to gather the data of interest.

5.2 Principles of Ultrasonic Inspection

A standard approach to ultrasonic testing involves an electro-mechanical piezo-electric disc transducer, designed to produce a specific motion such as compression of the disc thickness or shear along a diameter at a specific frequency (typically in the 1 – 10 MHz band), being energised with a short high voltage pulse (100 - 200 V). An instrument called a flaw detector, specifically designed for this type of work, is used to receive and process data returning from the sample. The resulting mechanical pulse from the transducer, either in compression (longitudinal) or shear (transverse), is coupled to the surface of the object being inspected through a thin fluid layer, such as a water-based gel for compression waves or a highly viscous, honey-like, fluid for shear waves. Often the object will be placed in a bath of water so that coupling can be readily achieved

at all points over the surface. Other methods, such as laser excitation can also be used to conduct ultrasonic inspection, however, these are reserved for more specialist inspection (Monchalin *et al.*, 1998). On encountering an interface, such as that provided by a crack, within the body of the object, a portion of the ultrasonic waves are scattered from it and some travel back toward the transmitter, which now acts as a receiver. Hence the presence of the defect can be sensed. There are two key methods that can be used to conduct ultrasonic testing (Krautkramer and Krautkramer, 1977; Szilard, 1982). Further, each method can be applied in direct contact to the material under inspection or through immersion, as mentioned above. This results in four different configuration options that can be used when conducting ultrasonic inspection:

- Contact pulse-echo
- Contact through-transmission
- Immersion pulse-echo
- Immersion through-transmission

The two simplest methods of conducting ultrasonic inspection use one or two contact transducers in the pulse-echo or through-transmission configurations as illustrated in Figure 5.1. Pulse-echo testing is often used when it is difficult to access the opposite side of the material being examined. It uses a single ultrasonic transducer to emit the ultrasonic pulse and to detect the returned pulse. Through-transmission testing can be used when it is easy to access both sides of a material section. It uses two ultrasonic transducers to conduct inspection. One transducer introduces the ultrasound into the material and the other detects the ultrasound pulse on the other side of the material. For accurate results these transducers must be lined up and well coupled to the material surface.

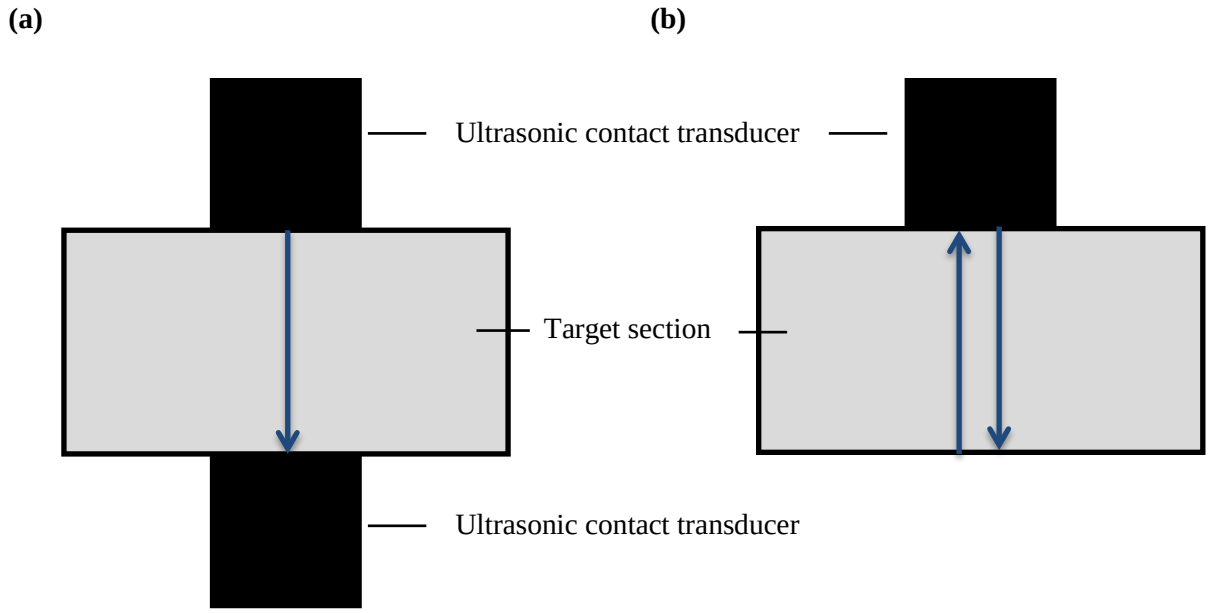

Figure 5.1 - Diagrammatic illustration of contact ultrasonic inspection: (a) through-transmission testing and (b) pulse-echo testing.

In both cases the elapsed time between the sound leaving the transmitter and arriving at the receiver can be related to material thickness by equation Equation 5.1, where *d* is the material thickness, *t* is the time between transmission and reception and *v* is the velocity of sound in the material.

$$d = vt \qquad \text{Equation 5.1}$$

In Equation 5.1, the thickness is calculated from the time taken for the pulse to travel through the object, provided that the speed of sound for the material is known. Examination of standard values of the speed of sound of many common materials shows that a range of possible speeds for each material (Berens, 1989; Kaye and Laby, 2015). Clearly for accurate measurements, the speed of sound in the material under inspection is needed. If the speed of sound in the material being inspected is not known, it is possible to re-arrange this equation and use it to calculate the speed of sound in the material provided that the material thickness is known. This enables the thickness readings to be calibrated from reference sample of the relevant material. This is important for cast iron, as the variation of the inhomogeneous graphite flake structure between different pipes can cause significant variation in the speed of sound in a pipe (Berens, 1989; Kaye and Laby, 2015). Visibly from Figure 5.1, for the case of the first arrival at the receiver, the pulse-echo arrangement requires double the time taken for the first arrival at the receiver to a through-transmission arrangement as the pulse must cover twice the distance.

In some cases, it is difficult to get a good contact to the material surface, particularly on rough surfaces such as those which are corroded. Immersion testing can be used to overcome this problem as the water can provide a good coupling layer between the ultrasonic transducers and the sample being investigated. This allows pulse-echo and through-transmission testing to be carried out. Figure 5.2 illustrates a typical set up for pulse-echo immersion testing. It illustrates the extra reflections displayed due to ultrasound reflection in the water gap. The separation of this gap may need to be adjusted to ensure that the reflected waves arrive at the transducer at the same time. If this happens, it will not be possible to determine the time of flight through the material and hence determine its thickness.

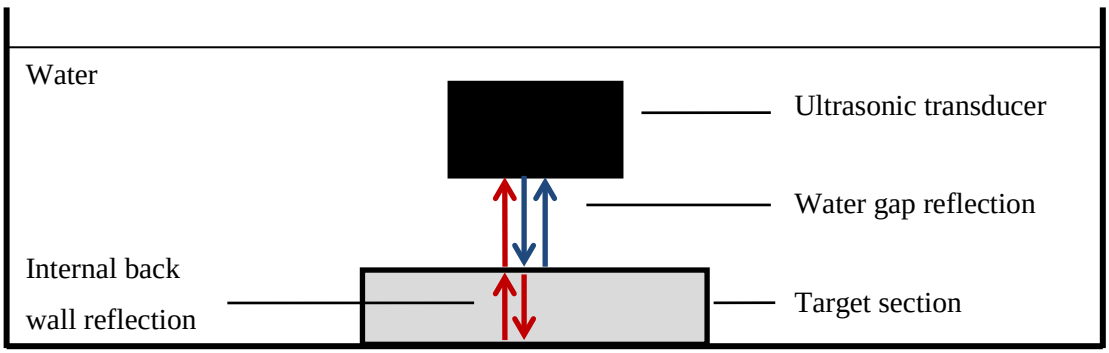

Figure 5.2 - Diagrammatic illustration of immersion ultrasonic testing showing a pulse-echo inspection configuration.

Through-transmission can be carried also out in immersion and can be very helpful when working on strongly attenuative materials, i.e. materials which tend to dampen the ultrasonic pulse, as the first arrival is less strongly attenuated as it passes only once through the material. Figure 5.3 illustrates the typical set up for a through-transmission test in immersion. In both of the immersion examples, Equation 5.1 can still be used to determine the thickness of the material under inspection, however, the extra journey time due to the pulse travelling through the water must be allowed for.

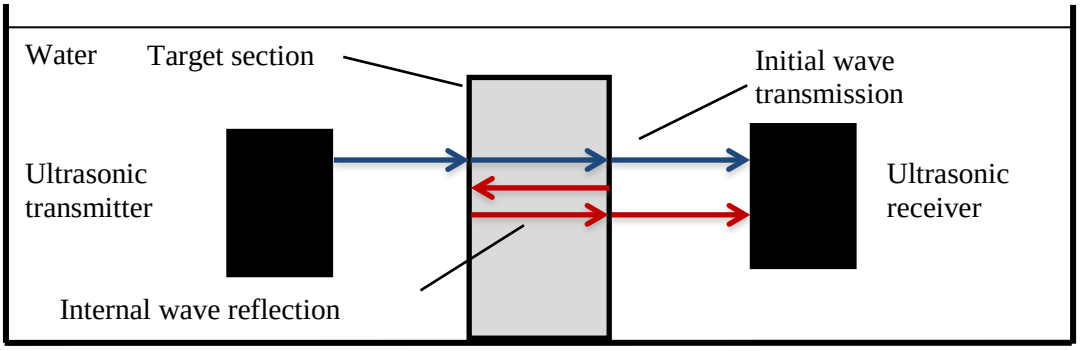

Figure 5.3 - Diagrammatic illustration of immersion ultrasonic testing showing a through-transmission inspection configuration.

5.3 Example Outputs using a Low Density Homogeneous Material

In order to understand the results observed for cast iron, it is important that waveforms from a less problematic material are observed for comparative purposes. Perspex is such a material. Whilst it is not perfect, since it is not fully crystalline, it is possible to propagate an ultrasonic wave through it with little loss of signal. As such, it provides useful service as a material on which to demonstrate the use of ultrasound.

An example of a waveform captured for pulse-echo contact ultrasonic inspection of a Perspex block, from henceforth referred to as the "Test Block", with a nominal thickness of 20 mm, is given in Figure 5.4. It illustrates when the internal reflections from the back wall are received. Further reflections are received as the sound wave continues to oscillate in the material. From Figure 5.4 it can be seen that the time taken for a wave to travel through the block and return is 14.4 ± 0.2 µs.

An example of a waveform captured for through-transmission testing of the Test Block is presented in Figure 5.5. In through-transmission, the first pulse received is the wave that travels through the material in a single pass. The wave then reflects internally and produces further internal reflections which make two passes each. The time between subsequent reflections can be used to determine material properties. In this example, the time between internal reflections can be seen to be 14.5 ± 0.2 µs which is similar to the value obtained through contact pulse-echo testing.

Figure 5.6 shows the waveform received for pulse-echo immersion testing of the Test Block. It illustrates the locations of the extra waveforms that were not present during contact testing. It also indicates the extra features detected due to reflections inside the tank and other water gap reflections interfering. The time taken for an

internal reflection from the Perspex to be produced is 14.8 ± 0.2 µs. This is still consistent with the previous value for time obtained.

Finally, Figure 5.7 illustrates the waveform received when carrying out through-transmission testing in immersion for the Test Block. It can be seen that the wave shape changes and, in some instances, can be seen to have a long pulse width. These changes in shape are thought to be due to constructive and destructive interference in the reflections arriving at the transducer at each interval. Here the time taken for the wave to travel through the Perspex block is 14.4 ± 0.2 µs which remains consistent with other measurements taken previously. This waveform indicates the extra signals that can be detected when carrying out immersion testing. It emphasises the point that it may be difficult to identify succinct reflections after the first reflection as the further reflections in the material and the water gap can overlap and cause destructive interference.

The Perspex block was measured to be 20 mm thick. Equation 5.1 has been re-arranged to calculate the speed of sound for the material. Speeds of the range 2700 - 2780 m s^{-1} were obtained based on the times of flight measured by each testing configuration. These values are consistent with those quoted in the literature (Berens, 1989; Kaye and Laby, 2015). Further, these values can now be used during an inspection to determine the thickness for an object made from the same material but with unknown geometry.

These simple experimental examples illustrate the typical modes of ultrasonic inspection and the potential areas of interest that would appear on an oscilloscope. The examples have shown how the time of flight through a material of known geometry can be used to determine the speed of sound in that material. This, in turn, can then be used to determine the material's thickness using measurements of the time of flight of ultrasound between two points.

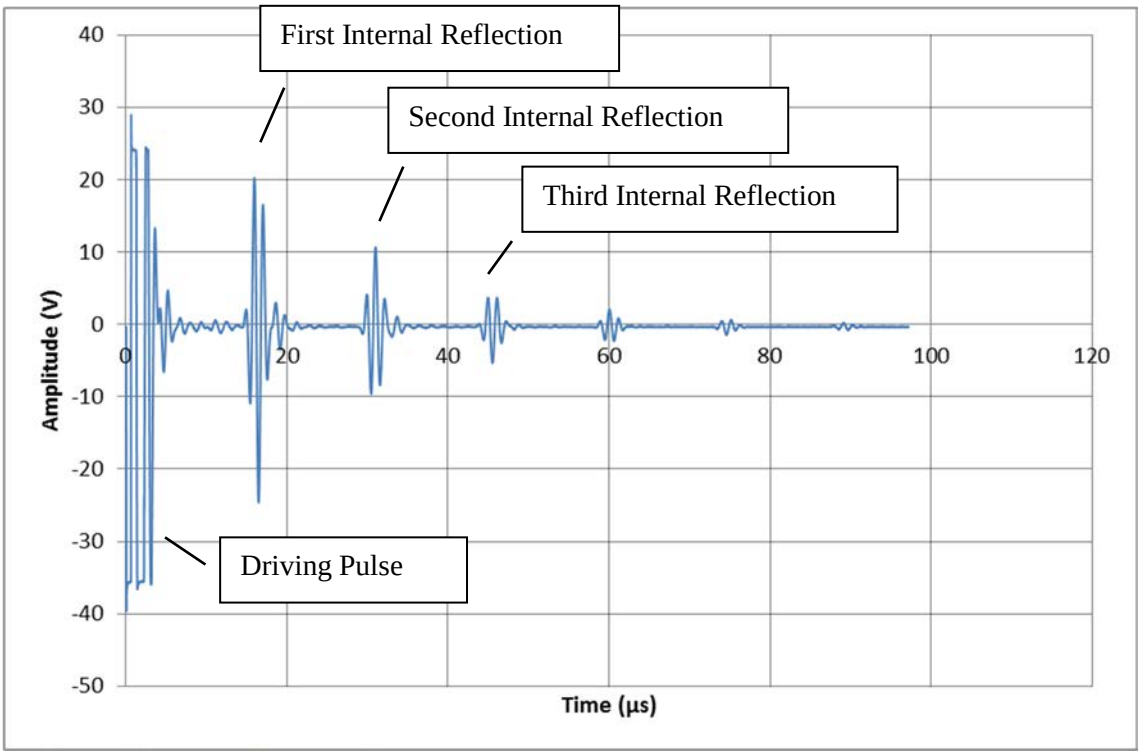

Figure 5.4 - An example contact pulse-echo ultrasonic waveform for the Test Block.

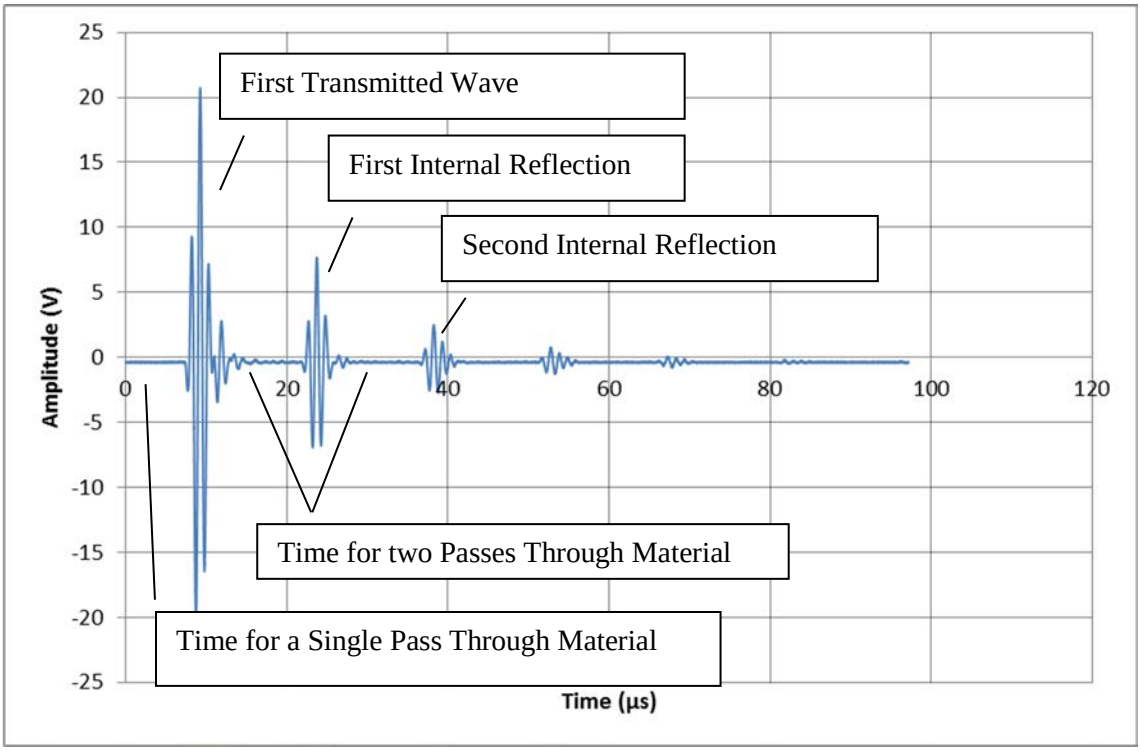

Figure 5.5 - An example contact through-transmission ultrasonic waveform for the Test Block.

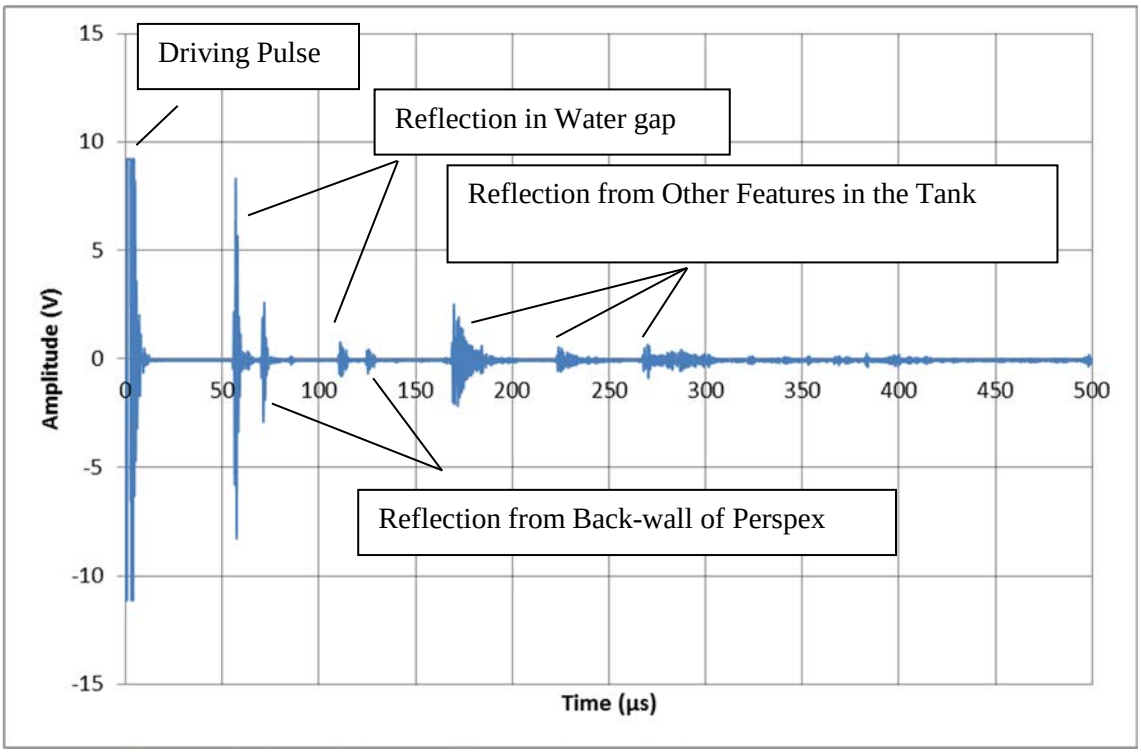

Figure 5.6 - An example immersion pulse-echo ultrasonic waveform for the Test Block.

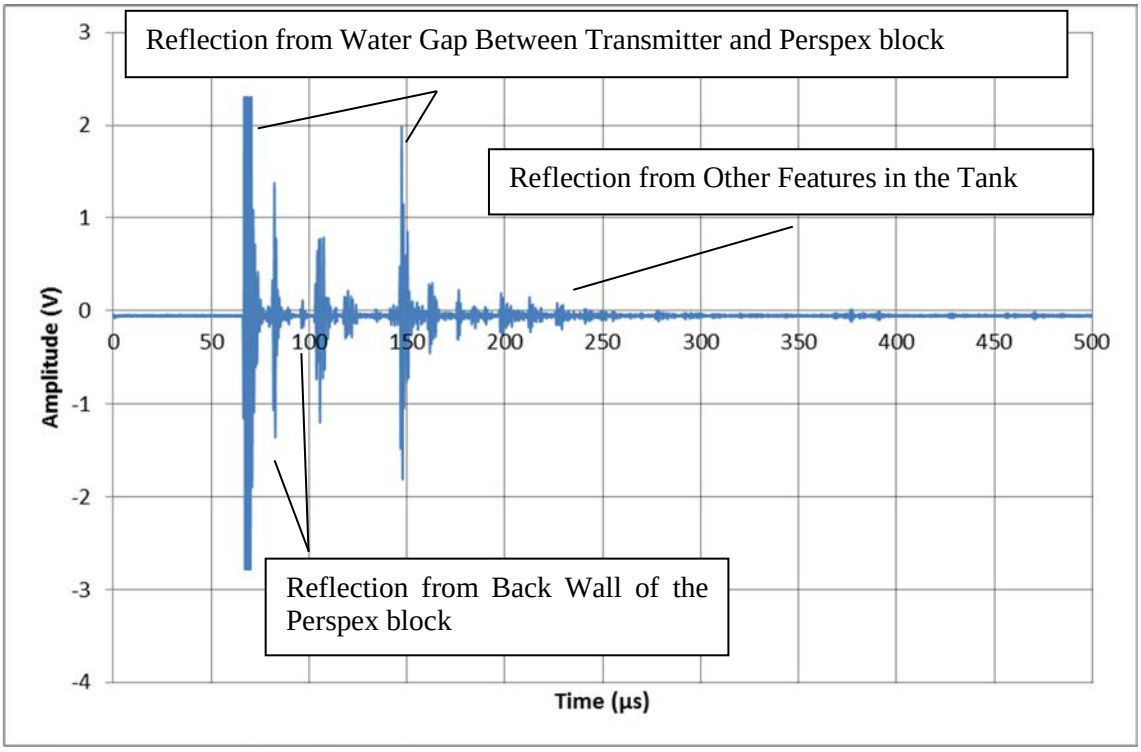

Figure 5.7 - An example immersion through-transmission ultrasonic waveform for the Test Block.

These examples assume that the back wall of the material is creating a simple reflection. Thickness measurements are only one practical use of ultrasonic testing. If a sizable defect was present, further reflections would be visible which would not match up with the known locations of the water gap or back wall, Figure 5.8. Further, by altering the angle and configuration of the transducers, it is possible to examine a material for defects at other angles.

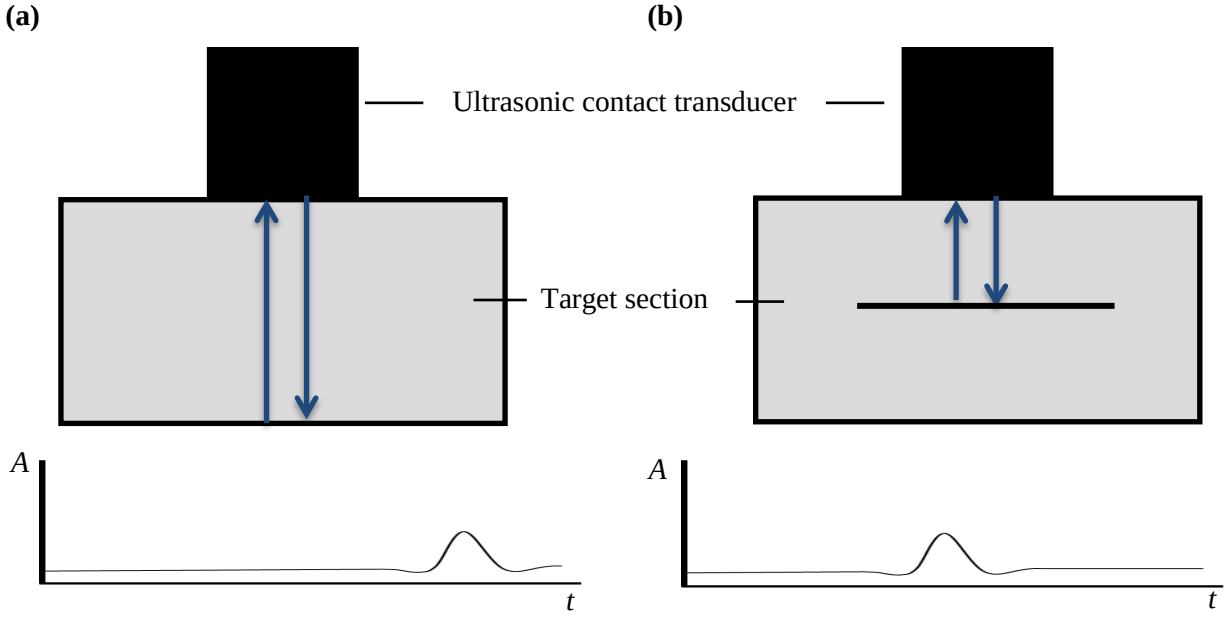

Figure 5.8 - Diagrammatic illustration of contact pulse-echo ultrasonic inspection of being used to identify the presence of a defect and the typical variation in waveforms that would be expected on an oscilloscope: (a) defect free material and (b) material with a defect present.

5.4 Materials and Methodology

5.4.1 Materials

In order to obtain cast iron samples with known geometry, a selection of blocks were cut from the pipe flange of a trunk main as it contained the largest amount of material. Samples of cast iron of nominal thickness 20 mm, were cut from the flanges of 4 different cast iron pipes of different ages. Initial cutting was trialled using a water-jet cutter to ensure that there was minimal heat transferred to the material as a result of the cutting. However, the water jet cutter proved to be too slow with a cutting speed of approximately 4 mm min^{-1} for large sections. It also did not give a smooth enough cut finish which would allow a transducer to be coupled to it. The striations created in this fashion can be seen in Figure 5.9(a). Further samples were cut using a reciprocating saw which proved to be quicker at cutting whilst giving a slightly smoother surface. These blocks were machined to set thicknesses to ensure that they were parallel and had a good surface finish. An example of a finished block can also be seen in Figure 5.9(b).

Graphitisation is also a key material to investigate, although, it is difficult to obtain as it is brittle and breaks when being removed from iron sections. However, a thick section of graphitisation was removed successfully from a corroded pipe as shown in Figure 5.10. The sample was gently sanded on both surfaces to give parallel flat sides to enhance the chances of allowing ultrasound to pass through the material. It was not possible to sand both sides to a perfectly smooth layer as one side was heavily pitted and would result in large amounts of graphitisation being removed. The final sample had an approximate nominal thickness of 13 mm.

(a) **(b)**

Figure 5.9 - Samples taken from cast iron flange: (a) water-jet cutting finish and (b) as machined surface

Aside from clean samples, a selection of other samples with layers of graphitisation and tubercles were cut from the barrel of the available cast iron trunk main stock. Figure 5.11 shows an example of a section of iron with a layer of surface graphitisation that was used for testing.

Figure 5.10 - Sample of graphitisation removed from a corroded main

Figure 5.11 - Sample of cast iron trunk main with graphitised layer

5.4.2 Equipment

A selection of ultrasonic testing equipment comprising a Sonotron ultrasonic flaw detector and 3 different ultrasonic transducers had been acquired previously by TWUL. However, after initial experimentation it became clear that these transducers were not well matched with the flaw detector and could not provide low noise signals. A selection of higher quality high and low damped Olympus ultrasonic contact and immersion probes were acquired to replace the initial probes, however, these also showed a degree of electrical “ringing” when coupled to the Sonotron, albeit much reduced. The ultrasonic signals captured must contain as little noise as possible if high quality results are to be obtained, as a degree of noise can hide any small signals that may be present.

As a consequence of the need for high quality signal generation and accuracy, a new Tektronix MSO 2014 oscilloscope and two Olympus ultrasonic pulser/receiver boxes, a PR 5072 and PR5077, capable of inducing a square wave or spike driving pulse, were acquired to match the transducers better.

5.4.3 Contact Testing

Contact testing was used whenever the surface permitted it as it minimised the energy losses through coupling and also simplified the analysis of the signals. However, the machined surfaces were the only surfaces suitable for contact testing. Low frequency[4] large diameter 1" transducers were used to maximise the ultrasonic signal transmitted to the iron and were arranged in a single-sided pulse-echo configuration or through-transmission configuration as required. A range of Olympus transducers were used in these configurations, however, a single Olympus A102s 1 MHz 1" Accuscan contact transducer in a pulse-echo configuration gave adequate results. This was driven by an Olympus PR 5077 square wave pulser/receiver and Tektronix MSO2014 oscilloscope. The devices were connected together to achieve a pulse-echo format. The pulser/receiver was set to 100 V transducer voltage, 100 Hz pulse repetition frequency (PRF) and pulse-echo mode with minimal damping. Ultrasonic couplant was applied to the surface of the iron and the transducer was pressed down in the centre of the sample, ensuring that it was sufficient distance away from the edges to minimise edge effects as seen in Figure 5.12. The pulser/receiver was switched on and the pulser gain was adjusted such that the signal shown on the oscilloscope was not being clipped by the internal pulser amplifier. The signal was then adjusted on the oscilloscope such that the first back-wall echo was vertically spread across the screen to ensure that there was sufficient level for digitisation. The signal was recorded by a computer linked to the oscilloscope running National Instruments Signal Express v3.0. The raw waveform was captured using a time averaging method of 32 samples to remove any shot noise from the signal.

In order to measure ultrasonic velocity, multiple back-wall echoes are needed. The oscilloscope was then adjusted to ensure that the second back-wall reflection was spread vertically across the screen to ensure that it was well digitised. The waveform was recorded using the time averaging method of 32 samples, to remove any shot noise from the signal, and repeated for each echo.

5.4.4 Immersion Testing

Because contact transducers can only be used on relatively smooth surfaces, immersion testing was used where surfaces were much rougher and could not support a contact transducer. This arrangement was used for inspecting the sample of corrosion products and when investigating the effects of surface geometry. The sample being inspected was placed in an ultrasonic immersion tank (41 x 25 x 25 cm) and stood upright on its side to allow the probe to inspect the surface in question whilst ensuring there was sufficient water cover. The probe was arranged in a pulse-echo format shown in Figure 5.13. An Olympus A303S 1 MHz 0.5" Accuscan immersion transducer was used to inspect the iron in combination with an Olympus PR 5077 square wave pulser/receiver and Tektronix MSO2014 oscilloscope. The devices were connected together to achieve a pulse-echo format. The pulser/receiver was set to 100 V transducer voltage, 100 Hz PRF and pulse-echo mode

[4] Low frequency transducers operate at a frequency of the order of 1 – 2 MHz

with minimal damping. The transducer was positioned over the site of interest and held in position by a stand, ensuring that it was not close to an edge of the sample. The pulser/receiver was switched on and the pulser gain was adjusted such that the signal shown on the oscilloscope was not being clipped by the internal amplifier. The signal was then adjusted on the oscilloscope such that the first back-wall echo was vertically spread across the screen to ensure that there was a sufficient level for digitisation. The signal was recorded by a computer linked to the oscilloscope running National Instruments Signal Express v3.0. The raw waveform was captured using a time averaging method of 32 samples to remove any shot noise from the signal.

Figure 5.12 - Contact ultrasonic transducer being used to measure the velocity of sound in a machined section of cast iron

Figure 5.13 - Ultrasonic pulse-echo testing carried out in immersion on a section of graphitised cast iron.

5.5 Results and Discussion

5.5.1 Clean Cast Iron

Figure 5.14 illustrates a typical waveform captured from pulse-echo testing of a section of clean cast iron. The waveform shows that the two strong reflections can be seen from the back wall of the iron. The time difference between these reflections is 9.5 ± 0.2 µs and indicates the time taken for a wave to reflect from the opposite side. Given that the material had a nominal thickness of 20 mm, this suggests a velocity of sound in the cast iron of approximately 4210 ± 90 $m.s^{-1}$.

When compared to a similar wave captured on a Perspex Test Block of similar thickness, Figure 5.4, the signal can be seen to attenuate strongly after the first two reflections. Further, the noise in the signal, between the reflections is significantly greater. It is possible to see locations where a reflection would be expected, albeit that the signal is less clear than the previous reflection. These waves are likely to have been attenuated by the microstructure, in particular the graphite flake structure, and other defects within the iron. The pulse distortion seen on the later reflections is also due to the waves being scattered within the iron and causing destructive interference.

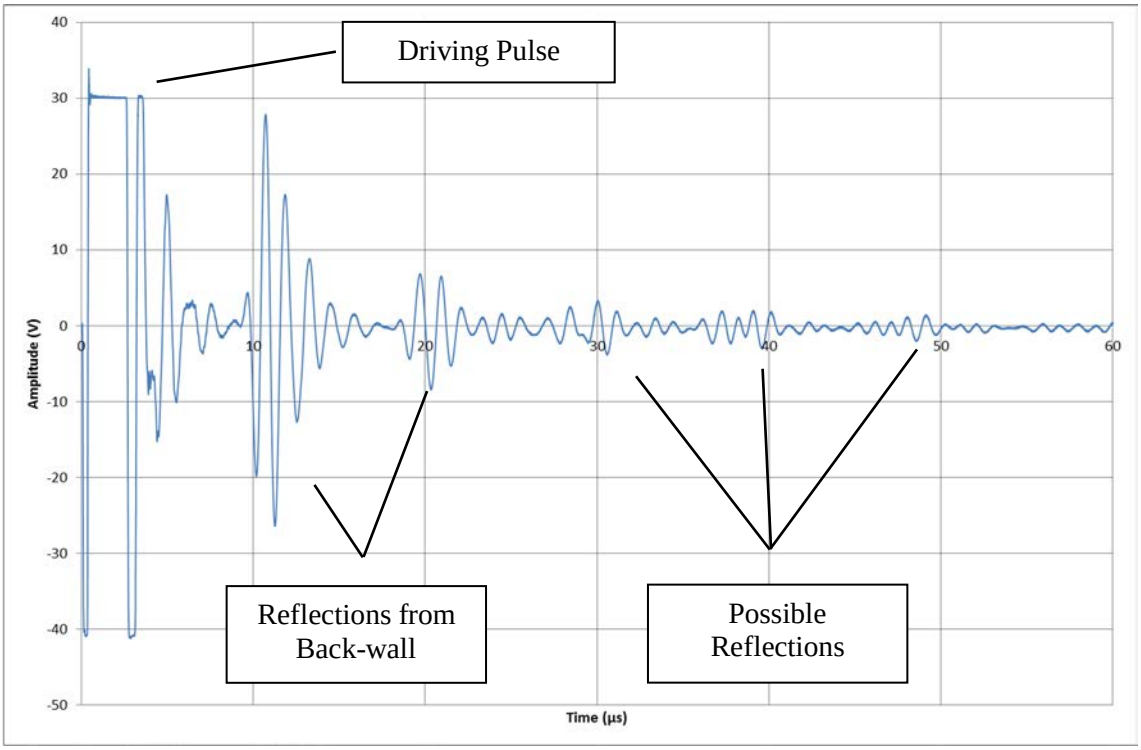

Figure 5.14 - An ultrasonic waveform captured from a clean piece of cast iron

5.5.2 Ultrasonic Velocity Measurements

Figure 5.14 showed a wave trace of ultrasound being passed through a machined sample of cast iron. This allowed a simple velocity measurement to be taken based on the time for the wave to travel and the material thickness. When carrying out ultrasonic inspection, it is crucial to have accurate material constants as these will affect the results when post-processing the raw data. Current literature shows that the speed of sound in

cast iron can vary by as much as 2100 $m.s^{-1}$, with a lower limit at 3500 $m\ s^{-1}$ and an upper limit of 5600 ms^{-1}, dependent upon the grade of cast iron (Berens, 1989; Olympus Corporation, 2013; Kaye and Laby, 2015).

Table 5.1 shows the results for the velocity of ultrasound determined for four different trunk main samples. The results show that there is a degree of variance in velocity between pipes; as much as 480 $m.s^{-1}$ can be seen between the upper and lower speeds measured. A pipeline inspection company who have been inspecting cast iron main for TWUL, have advised that they use an ultrasonic velocity of 4800 $m.s^{-1}$ for cast iron. It is important that the correct velocity is used for the pipe being examined otherwise any post-processing carried out on the raw data will produce incorrect results.

For example, a 20 mm thick cast iron section may have an ultrasonic velocity of 4100 $m\ s^{-1}$ for a wave reflection time of approximately 10 µs. However, if the data was processed with a different velocity, such as 4800 $m.s^{-1}$, then a thickness of 24 mm would be obtained. This is clearly wrong and would lead to false belief of increased wall thickness by approximately 20%. Consequently, it is very important that the right velocity is used. This will become even more important when sizing a defect as it could influence whether or not the defect meets the critical defect size.

Table 5.1 - Ultrasonic velocities measured for different trunk mains.

Pipe Origin	**Approximate Year of Installation**	**Velocity of Ultrasound ($m\ s^{-1}$)**
Devonshire Road	1924	4270
Original Bench Sample (Origin Unknown)	Unknown	4580
Olympic Park Finsbury Main	1890	4180
Olympic Park Woodford Main	1920	4100

5.5.3 Uneven Pipe Surface

The initial testing carried out on small machined sections showed that ultrasound will travel through cast iron, however, it was not truly representative of the real geometry that must be encountered when carrying out inspection in the field. Here the ultrasound must travel through a curved surface which is often covered in a corrosion product. A section of cast iron pipe was investigated using pulse-echo immersion testing to see whether it was possible to introduce ultrasound into a real piece of cast iron. The internal tuberculation was removed and the surfaces were lightly sanded to remove any flaking corrosion products. No graphitisation was present in the section that was investigated.

An example waveform from this test is shown in Figure 5.15 and shows that reflections from the back wall of the iron can be seen. The iron had a nominal thickness of 20 mm and the time for the back-wall reflection can be seen to be 9.5 ± 0.2 µs which means that the speed of ultrasound in the materials is approximately

4210 ± 90 m.s^{-1}. This is consistent with the other values obtained for cast iron shown in Table 5.1 and confirms that the reflection is being obtained from the back wall of the iron.

The reflections seen are greatly reduced in amplitude compared to the initial waves seen in the water gap. Part of this reduction is due to the attenuation processes in the cast iron. The majority of this may be due to the graphite flake structure. However, the curved geometry of the pipe sample adds further complications. This curved back wall increases the ultrasonic beam spreading and reduces the amplitude of the wave returning to the transducer. Also, the phase of the wave may change and result in a delayed arrival at the transducer. This shows why the pulses become less clean and have a ringing[5] nature.

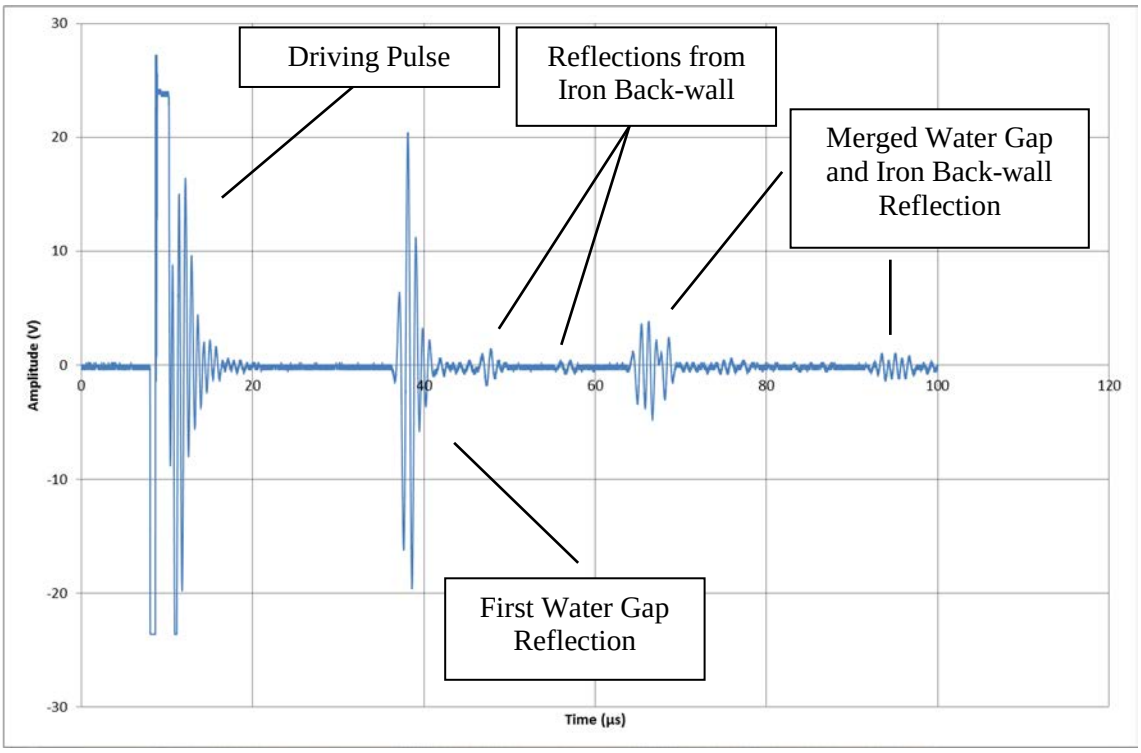

Figure 5.15 - An ultrasonic waveform captured from a pulse-echo test of a non-graphitised piece of cast iron trunk main

5.5.4 Graphitisation Interaction

Graphitisation has been a large concern as the published literature has not demonstrated clear results when inspecting areas of graphitisation. Consequently, it is important to understand the effect of graphitisation on ultrasonic signals. In the first instance, a section of graphitisation was investigated to determine the speed of sound in the material. The results show that a reflection from the back wall of the graphitisation is visible, however, it is greatly attenuated in comparison to the initial reflection seen from the water gap, Figure 5.16. Further the graphitic corrosion pulse reflections are considerably noisier that those obtained for cast iron pipe, Figure 5.15. The time taken for the ultrasound to pass through the 13 mm thick graphitisation is 8.8 ± 0.2 µs. Hence, the velocity of ultrasound through graphitisation is approximately 2950 ± 80 m s^{-1}. This value is significantly less than the lowest speed of sound in cast iron in the literature. Despite its nominally similar

[5] Ringing is the overlapping of ultrasound pulses such that they produce a longer wave that gradually attenuates.

speed of sound to Perspex, graphitic corrosion can be seen to attenuate the pulse reflections significantly more than Perspex, Figure 5.6.

These experiments have shown that it is possible for an ultrasound signal to travel through cast iron or graphitisation. In order to carry out effective non-destructive examination, the ultrasonic signal must be able to pass through a piece of cast iron, which may have graphitised layers, and produce a thickness value for both the iron and the graphitisation layers.

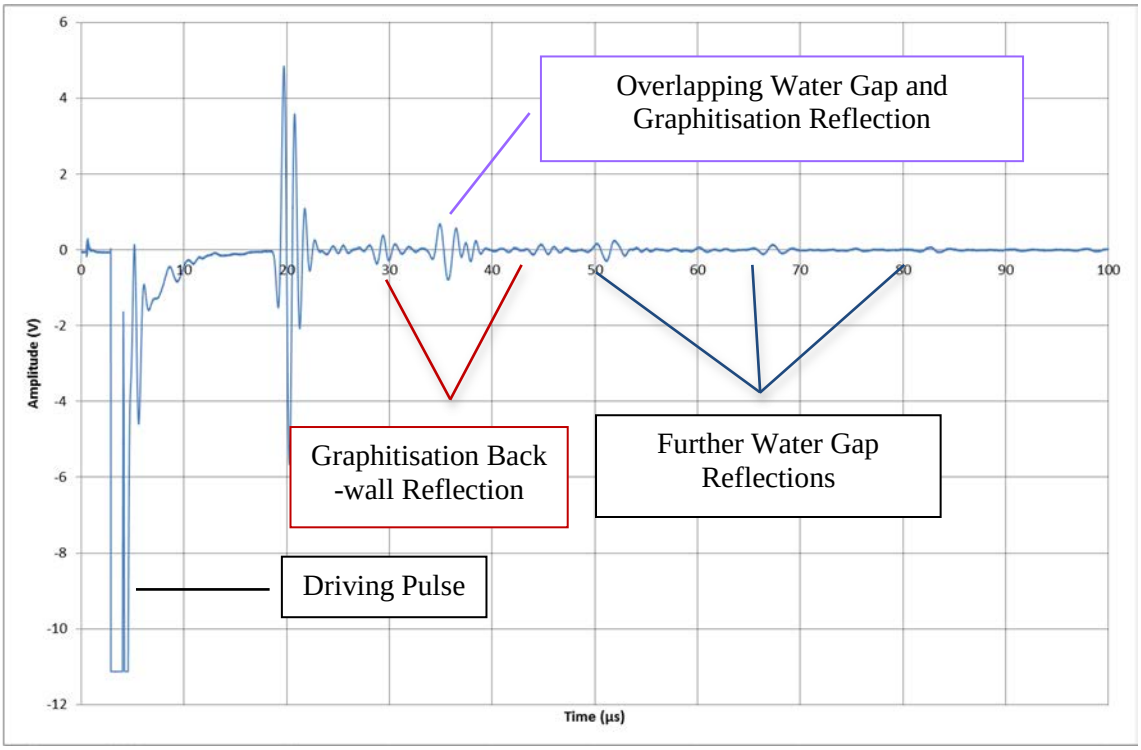

Figure 5.16 - An ultrasonic waveform showing the interaction with a sample of graphitisation, taken in pulse-echo immersion mode

A section of iron with a graphitised layer was inspected using pulse-echo ultrasonic inspection in immersion to see whether the interface between the graphitisation and iron could be seen (from the external face) in addition to the reflection from the back wall of the sample. Figure 5.17 shows the reflections expected from a graphitised section of iron being inspected from the external surface. If the ultrasound is capable of investigating the graphitisation thickness and the iron thickness, three distinct reflections will be seen in the wave signal.

The graphitised layer had a nominal thickness of 8 mm and the remaining iron had a nominal thickness of 13 mm. This would result in the graphitised layer producing a reflection at a time of approximately 5 µs and the iron would produce a reflection time of approximately 6 µs. Consequently, a reflection should be seen 5 µs after the first arrival of the water gap reflection and then a reflection for the iron should be seen 11 µs after the first arrival of the water gap reflection. The wave form captured during this testing is given in Figure 5.18 and it shows a clear first reflection for the water gap. However, the signal for the graphitisation and cast iron are not clear. A distortion to the signal train could indicate the presence of the graphitisation, however, it is not

sufficiently distinct to allow an acceptable assessment. Here the reflection from the iron cannot be seen. It is likely that the attenuation of the graphitisation attenuates the signal sufficiently that any signal becomes too weak to be seen.

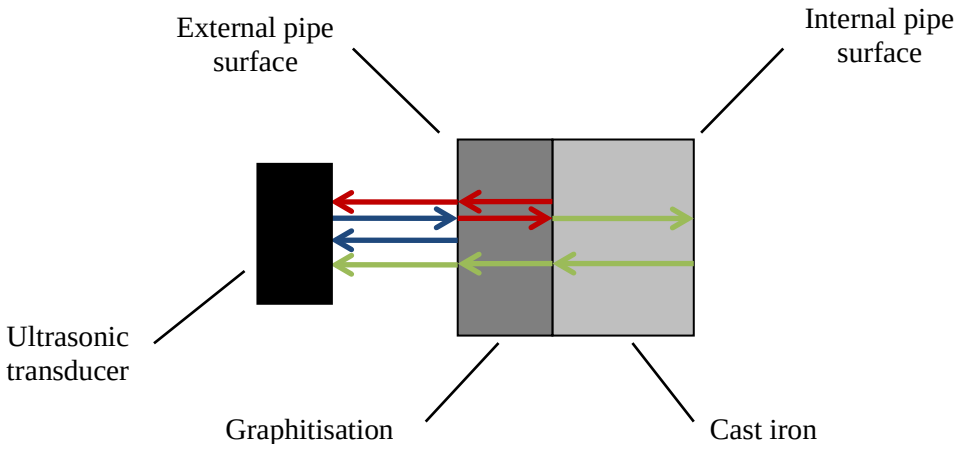

Figure 5.17 - Diagrammatic representation of the reflections expected from a graphitised section of iron when inspected from its outer surface.

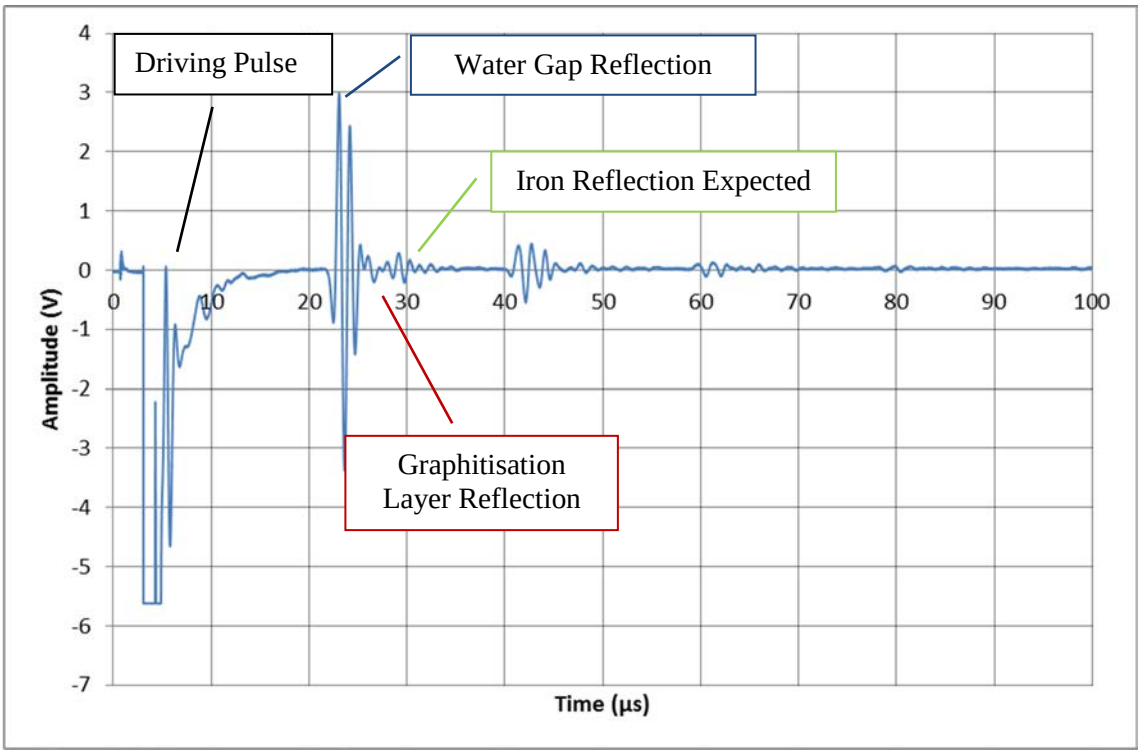

Figure 5.18 - An ultrasonic waveform showing the interaction with a graphitised section from the outside of cast iron trunk main in pulse-echo immersion

This test allowed the graphitisation thickness to be seen, however, it did not show the residual iron thickness to be seen. This test was repeated from the internal side of the pipe to see whether a better signal could be obtained. The order of the reflections seen would be slightly different from before, as illustrated in Figure 5.19, whilst an example waveform for this test is given in Figure 5.20. It shows a strong water gap reflection and one further, less distinct reflection that overlaps. It is now possible to establish the thickness the iron from the

inside, provided there are no corrosion products that would inhibit the progress of the ultrasound. However, a third reflection was not visible and as a result it is not possible to detect the graphitisation that is present.

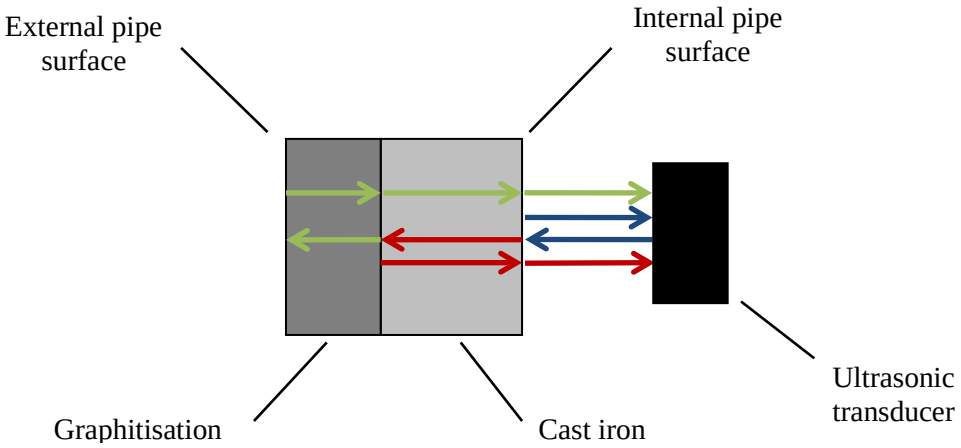

Figure 5.19 - Diagrammatic representation of the reflections expected from a graphitised section of iron when inspected from its inner surface.

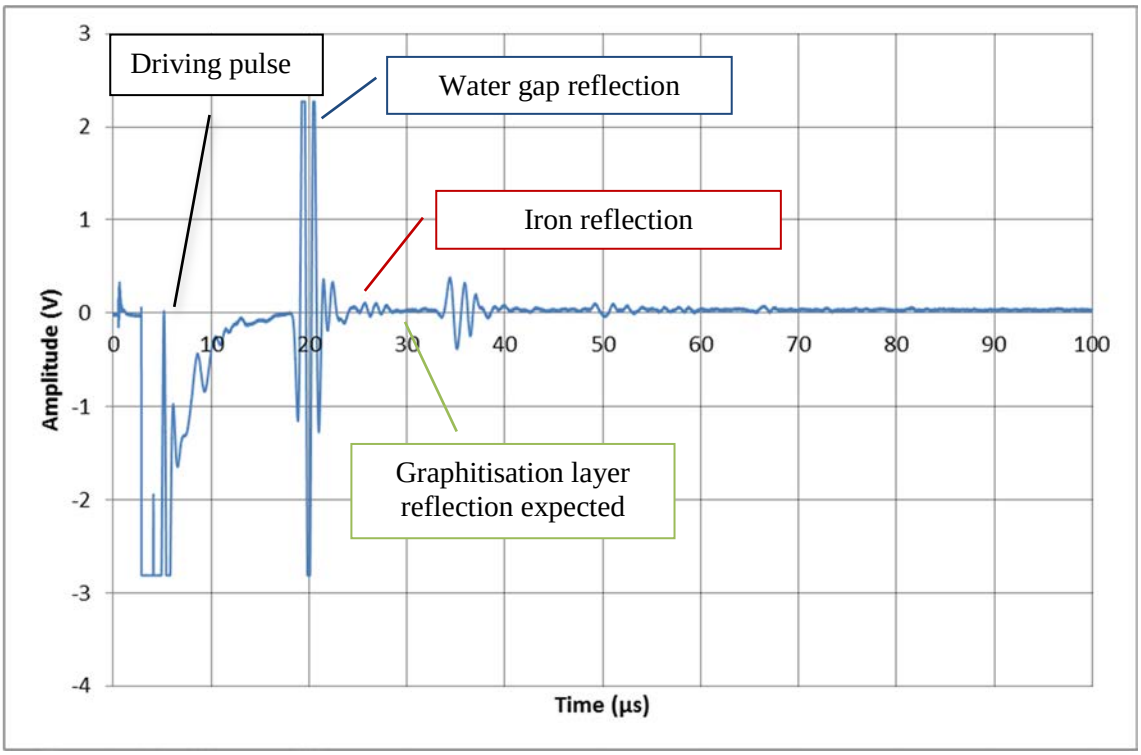

Figure 5.20 - An ultrasonic waveform showing the interaction with a graphitised section from the inside of a cast iron trunk main in pulse-echo immersion

5.5.5 Tubercle Interaction

Tubercles present a further challenge to inspection, particularly if any inspection is being conducted from the inside of the pipe. Current ultrasonic inspection systems have reported difficulty when encountering tubercles as they may not allow a signal to penetrate. An initial investigation into the effect of tubercles on an ultrasonic signal has been carried out. Figure 5.21 shows a waveform captured from the pulse-echo test carried out on a tubercle. Initial experiments have shown that the ultrasound pulses reflected from a tubercle are not distinct

and are very noisy. It is possible to see the reflection from the front of the tubercle in the water gap, however, it is not possible to see any further reflections inside the tubercle as these reflections are not sufficiently separated and overlap with the first reflection. The geometry of the tubercle is also likely to cause problems as the rounded shape of the tubercle will cause the ultrasonic beam to spread resulting in many staggered reflection arrivals at the transducer. Consequently, these effects cause an overlap of signals and a distinct reflection cannot be identified. The presence of tubercles on the internal surface of a cast iron pipe would make internal ultrasonic inspection difficult and further work is needed to better understand their effects and if they can be overcome.

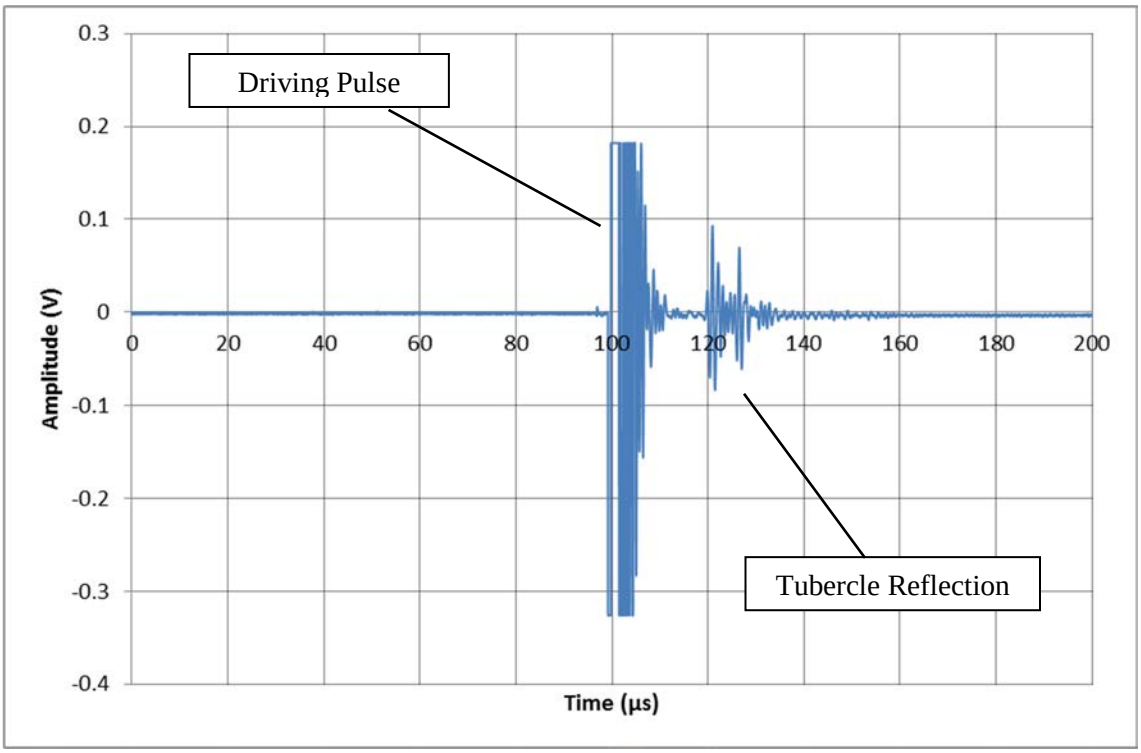

Figure 5.21 - An ultrasonic waveform captured from a pulse-echo test of a tubercle in immersion

5.6 Summary

This chapter has presented test results for experiments carried out on cast iron trunk main using off the shelf ultrasonic equipment. Cast iron is not an ideal material to apply NDE to, especially ultrasonic inspection, as the inhomogeneous graphite flake structure tends to attenuate the signal. The surface of the pipe further complicates inspection due to surface irregularity as well as the corrosion products that attenuate the ultrasonic signal, in particular, graphitisation. A further issue is that since there is a range of potential flake structures, there is a range of speeds of ultrasound that must be considered. This range is usually accepted to be between 3500 and 5500 m s^{-1}. In the current work, the range of speeds was found to be of the order of 4100 to 4600 m s^{-1}. Whilst this does indicate a need to be cautious, it does show that the technique has potential.

One aspect in particular that is worth noting is that at a recent demonstration of an ultrasonic technique, a default figure of 4800 m s^{-1} was used for cast iron. This could lead to (commercial) assessments of uncorroded cast iron wall thicknesses which are more than 10% inaccurate and significant issues when attempting to assess

graphitisation thickness and conformation, and it is recommended that where ultrasonics are carried out by a third party, either a figure for the speed of ultrasound is supplied by TWUL or TWUL undertake its own post-processing calculations. Despite the issues surrounding the use of ultrasonics, these tests have been very positive and further investigations are certainly warranted.

6 Magnetic Force Testing Investigation on Cast Iron

6.1 Introduction

In Chapter 5, ultrasonic inspection was investigated as a non-destructive evaluation method for use on cast iron trunk mains as it is a mainstream technology that is currently available. It demonstrated an ability for measuring the thickness of uncorroded cast iron, however, the method failed to gather meaningful data when applied to cast iron with graphitic corrosion present. Ultrasonic inspection requires trained inspectors to carry out any meaningful inspection and relies on appropriate calibration and standards. Further, it takes time to deploy the technique, and requires suitable surface preparation of the pipe that will be inspected. Undertaking an inspection at an opportune excavation using ultrasonics can then add significant time to the excavation being open. This is undesirable as any excavation costs money to initiate and more money to keep open, particularly if the inspection does not provide further information on condition. A need was identified for a technique that can be applied quickly to identify pipes which are significantly corroded and need a more detailed inspection.

One idea that has often been put forward as a simple approach to determining the profile of the corrosion layer on a cast iron pipe is to measure the force on a permanent magnet as it is methodically scanned over the pipe. Simple hand scanning of a magnet over a corroded pipe is often used to find graphitised areas and, by extension, it may offer a useful tool to characterise the depth and extent of any surface corrosion. A similar technique has been used in the coating industry to measure the coating thickness of zinc on galvanised steel, however, the magnet is placed in direct contact with the surface and the force required to detach it is recorded (ASTM International, 2014).

As well as identifying mains that need an in-depth health check, a tool that provides condition data for a pipe and which can then be used to validate data captured by other techniques is of benefit. The ability to inspect a trunk main with more than one technology is particularly important, especially if the main technique fails to inspect areas of a trunk main reliably, for example highly graphitised layers. The availability of a complementary technique, or techniques, may be able to suggest why this is and fill in the possible gaps in the data, if brought together successfully.

In this section, the development of a technique that uses a permanent magnet to identify sites of corrosion is presented. The graphitisation product is generally considered to be non-magnetic and so should appear transparent to the magnetic lines of flux produced by a magnet. It was not possible to obtain samples of cast iron with a well-defined and characteristic shape detail of graphitisation to conduct testing. Instead air has been used as a substitute. Based on work by Atkinson *et al.* (2002), to be of maximum use, a tool that can identify graphitic corrosion layers greater than 4 mm would be particularly useful as it would identify the point at which the failure mode transitions to graphitic corrosion.

6.2 Principles of Magnetic Force Testing

The technique relies on the difference in magnetic properties exhibited by the iron and its corrosion product. Iron displays strongly ferromagnetic behaviour. The magnetic properties of the corrosion product have not been characterised in the literature, however, given that corrosion can be identified using a simple magnet with little if any magnetic force felt, it can be thought of as being transparent to magnetic flux and has little or no residual magnetic properties.

When a magnet is brought close to the surface of the iron, the lines of flux interact with the magnetic domains within the iron and align them to produce a force of attraction between the magnet and the iron. If the spacing is reduced and the magnet is moved into closer proximity to the iron surface, the lines of flux can interact with more domains to align them and produce a greater force of attraction. However, at sites where graphitic corrosion is present, the lines of flux have few if any magnetic domains to interact with, and consequently no force of attraction is created.

As with atomic force microscopy there are then three modes in which such a system could operate, but of most relevance to the current context is contact mode i.e. where constant deflection is maintained and the subsequent change in force is measured. Here, instead of the change in the forces of attraction and repulsion between an atomically sharp 'tip' and the surface, the force of attraction between a magnet and an iron object within the magnetic field is dependent on how many ferromagnetic domains within the iron can be pulled into alignment. Clearly with a magnet at a set position, the uncorroded surface would represent a baseline and the reduction of magnetic domains due to the dissipation of iron and its transformation to other phases (i.e. oxides) caused by corrosion, should reduce the force on the magnet. Figure 6.1 illustrates the concept. One factor that will need to be assessed during calibration is the effect of variability in the wall thickness, which has been seen to vary by several millimetres from a nominal average. However, such variations should give a very different kind of response to even a limited amount.

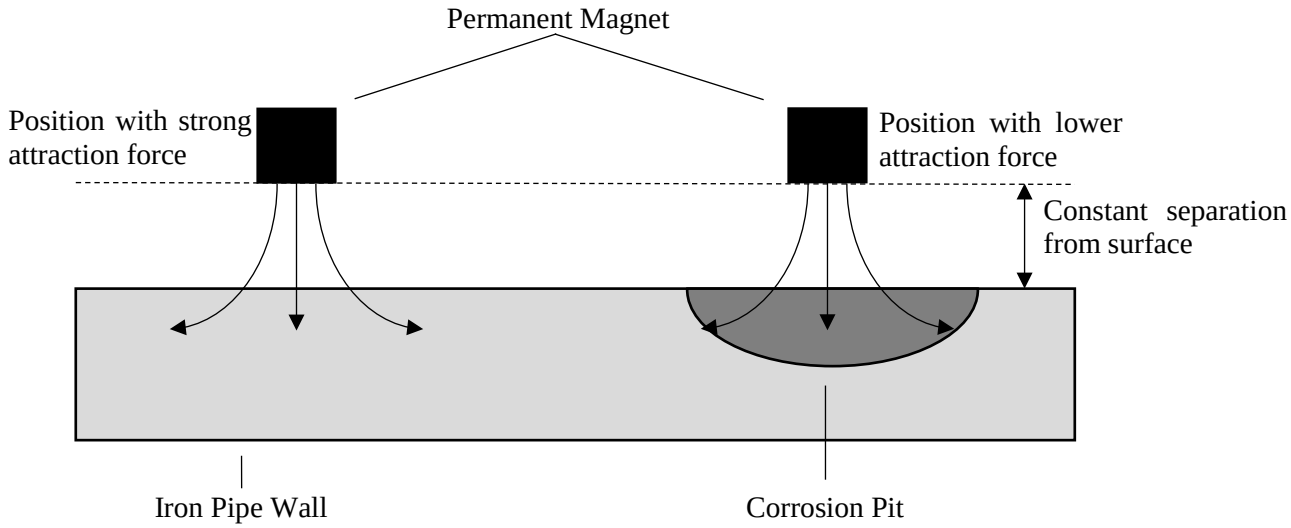

Figure 6.1 - A diagrammatic representation of the magnetic force testing concept.

6.3 Materials and Methodology

6.3.1 Materials

Samples of cast iron were obtained from two different cast iron pipes. Sample A is a section of cast iron trunk main with a uniform layer of external graphitic corrosion that could be seen to vary in thickness between 0 - 12 mm. The origin of this sample is unknown, Figure 6.2.

Figure 6.2 - Sample A, which was used for feasibility testing the magnetic force testing principle.

Two further samples were taken from a of cast iron distribution main obtained from the TWUL pipe and soil technical archive (PASTA). This pipe was chosen as it displayed minimal corrosion, twist and eccentricity. This main had previously been split into two halves longitudinally. Each half was prepared differently, Figure 6.3:

- Sample B had two different sets of mechanical defects machined into it. On one side, a selection of five equally spaced external 20 mm flat-bottomed holes of various depths, ranging from 2 mm deep to through wall in 2 mm increments, were machined into it. On the other side, four holes of various diameters, ranging from 5 mm to 20 mm in 5 mm increments, were drilled into it.

- Sample C had a selection of equally spaced internal 20 mm flat-bottomed holes of various depths, ranging from 2 mm deep to through wall in 2 mm increments, machined into it

Figure 6.3 - Samples B and C after preparation for magnetic inspection showing internal and external machined defects.

6.3.2 Equipment

A custom rig was designed and built in order to test the magnetic attraction principle scientifically, Figure 6.4. In order to minimise the rig size, it was designed to take cast iron distribution main sections. The rig allowed a magnet to be scanned longitudinally across a section of distribution main at a set height above the surface. The pipe can also be rotated to change the circumferential position inspected.

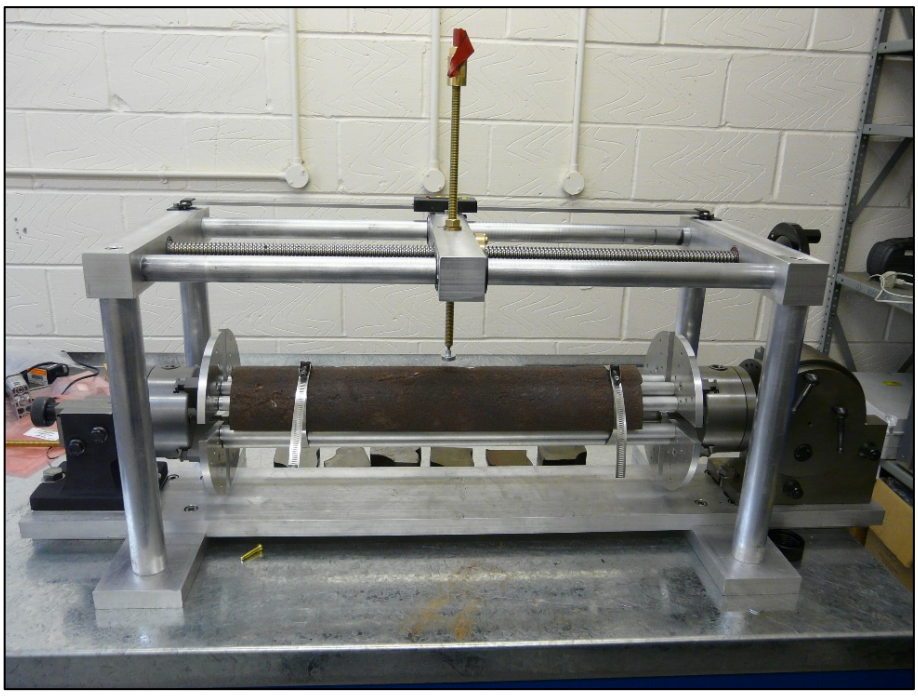

Figure 6.4 - Test rig used to investigate the magnetic attraction principle.

Three high strength neodymium pot magnets, of different diameters (5 mm, 13 mm and 20 mm), were used to investigate spatial resolution. The magnets were mounted onto a 50 N DBCR load cell from Applied Measurements (Aldermaston) which was used to monitor the force of attraction between the magnet and the cast iron section. The load cell has an accuracy of ± 0.025 N. The DBCR load cell was connected to a matching amplifier and digital display also supplied and calibrated by Applied Measurements. An analogue voltage output from the amplifier was connected via a National instruments DAQ breakout box, and matching input card, to a PC running National Instruments Signal Express. This ensured that the maximum force measured could be recorded as a function of position.

To ensure that a minimum spacing between the magnet and the pipe could be achieved, a 1 mm plastic spacer was bonded onto the bottom of each magnet to provide a set thickness whilst not affecting the magnetic field around the magnet. The separation could be adjusted at each point to ensure that a 1 mm separation was observed.

6.3.3 Feasibility Testing

Initially the technique's feasibility was tested by inspecting Sample A. The 20 mm magnet was mounted on the end of the load cell and an initial force reading was taken from the load cell to record the load cell force reading when no magnetic force is being applied. The edges of Sample A were inspected to identify sites of varying graphitic corrosion thickness. These sites were marked and their thickness was measured using a ruler. The section of graphitised iron was mounted in the rig such that the magnet could be positioned over the sites of varying graphitic corrosion thickness identified. The magnet was lowered into contact with the sample until the load cell began to decrease due to the contact force with the magnet compressing the load cell. The magnet was then moved away from the surface very slowly, until the force reading peaked. At that point, the magnet was no longer in direct contact with the sample and the peak load reading was recorded. The iron was then repositioned such that another reading could be taken from another site of interest. The thickness of the graphitisation at these sites was then measured and recorded.

6.3.4 Separation Testing

Sample B was clamped in the rig and positioned such that the 20 mm magnet was directly above an area of un-machined smooth iron in the centre of the section. A vertical separation of 20 mm between the pipe surface and the magnet was then set and the initial reading on the load cell was taken as the zero reading. The magnet was moved progressively closer to the surface by a millimetre each time and a recording of the force measured by the load cell was taken at each point. This was carried out until the magnet touched the iron surface. The iron was then repositioned such that another point of similar condition could be investigated and the testing procedure was repeated.

6.3.5 Magnetic Interaction Volume

Experiments to determine the depth of penetration of the magnetic field were carried out to determine the level of graphitic corrosion that might potentially to be detected. Further experiments were conducted to determine the area of inspection that the magnetic force interacted with. The 20 mm magnet was mounted on the end of

the load cell and an initial force reading was taken from the load cell to mark the zero reading. Sample B was positioned such that the magnet was directly over the centre of a site of interest. The magnet was then moved longitudinally 30 mm away from the defect centre. The magnet was lowered into contact with the sample until the force read by the load cell began to decrease due to the contact force with the magnet compressing the load cell. The magnet was then moved away from the surface very slowly, until the force reading peaked. At that point, the magnet was no longer in direct contact with the sample and the peak load reading was recorded. After the recording was captured, the magnet was moved longitudinally 1 mm closer to the defect centre. This process was repeated until the magnet was 30 mm past the defect centre to create a linescan over a machined defect, Figure 6.5. Once the linescan was complete, the magnet could be changed and the process repeated to determine the effect of each magnet. This testing process was repeated for each of the machined defects in Sample B. When Sample B was complete, it was removed from the rig and replaced with Sample C. The measurement process was then repeated for that pipe section.

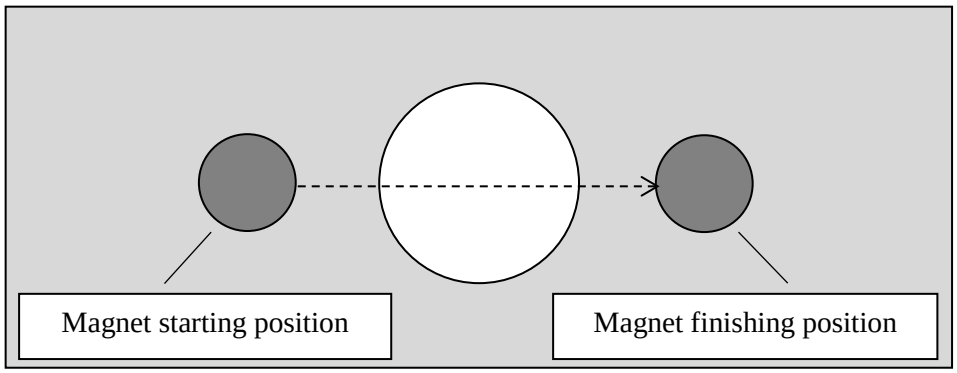

Figure 6.5 - Diagrammatic representation of a linescan conducted across a machined hole

6.4 Results and Discussion

6.4.1 Feasibility Testing

Anecdotal evidence suggests that magnets have been used for some time to locate patches of graphitisation on the external surface of metallic pipes. However, they do not appear to have been used to characterise the thickness of the corroded layer. This is likely to be due to the need for a calibrated system rather than a simple "good judgment". A sample of graphitised cast iron was examined at various locations of differing graphitic corrosion thickness to determine the simple variation in magnetic force compared to graphitic corrosion thickness. The results obtained from this testing show a correlation between reducing corrosion thickness and increasing magnetic force, Figure 6.6. It can be observed that there is a sharp change in the magnetic force of attraction between 2 and 4 mm of graphitic corrosion. Corrosion of a thickness between these values was not available for testing. Consequently, further testing would be beneficial to provide further data points that reduce the spacing between such data points. However, the initial feasibility testing suggests that this concept could possibly provide a useful NDE technique.

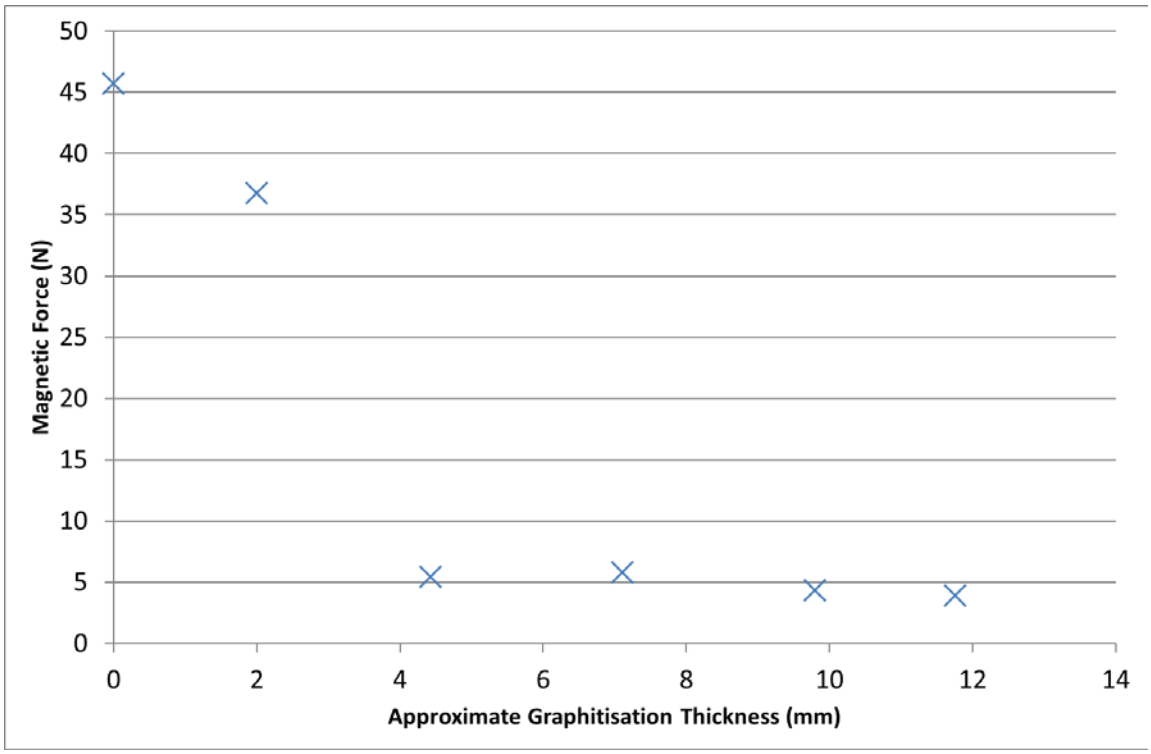

Figure 6.6 - Strength of the magnetic force for the 20 mm magnet compared to the thickness of the graphitisation layer captured during the initial feasibility testing.

6.4.2 Separation Testing

It has been suggested that regions of graphitisation have no magnetic properties and should be transparent to magnetic lines of flux. However, it proved difficult to find suitable sections of graphitisation or customise the thickness. Consequently, it was necessary to use a substitute material. Air was used as a substitute as it also possesses no magnetic properties.

Initially the effect of an air gap between the magnet and a smooth iron surface was investigated. This testing was initially carried out to determine the effect of a change in separation and its effect upon the magnetic force of attraction. A graph showing the magnetic force measured at each separation for each point can be seen in Figure 6.7. It shows that, as expected, there is a non-linear relationship between force of attraction and separation. It indicates that the technique may be able to detect graphitisation layers up to 7 – 8 mm in depth, provided that the magnet could be sufficiently close to the surface of the pipe. The change in force beyond 10 mm deep appears to be very small and may not be significant enough to measure confidently. In order to achieve the highest range of magnetic force, the magnet would need to be able to get within a millimetre of the pipe surface. Good surface preparation would therefore be needed to allow this to happen.

Figure 6.7 shows two trends similar in shape, although offset in the distance from the surface. This change is unlikely to be a variation in material as the pipe was of approximately uniform dimensions throughout. This offset is likely to be due to inaccuracy in the method of measuring the distance above the surface of the pipe. If improved, it is likely that the offset would disappear and the curves would be in closer agreement.

When comparing the results given in Figure 6.7 with those given in Figure 6.6, similar trends regarding separation thickness or corrosion thickness and the magnetic force measured can be observed. The results indicate that air would make a suitable substitution material in place of graphitic corrosion.

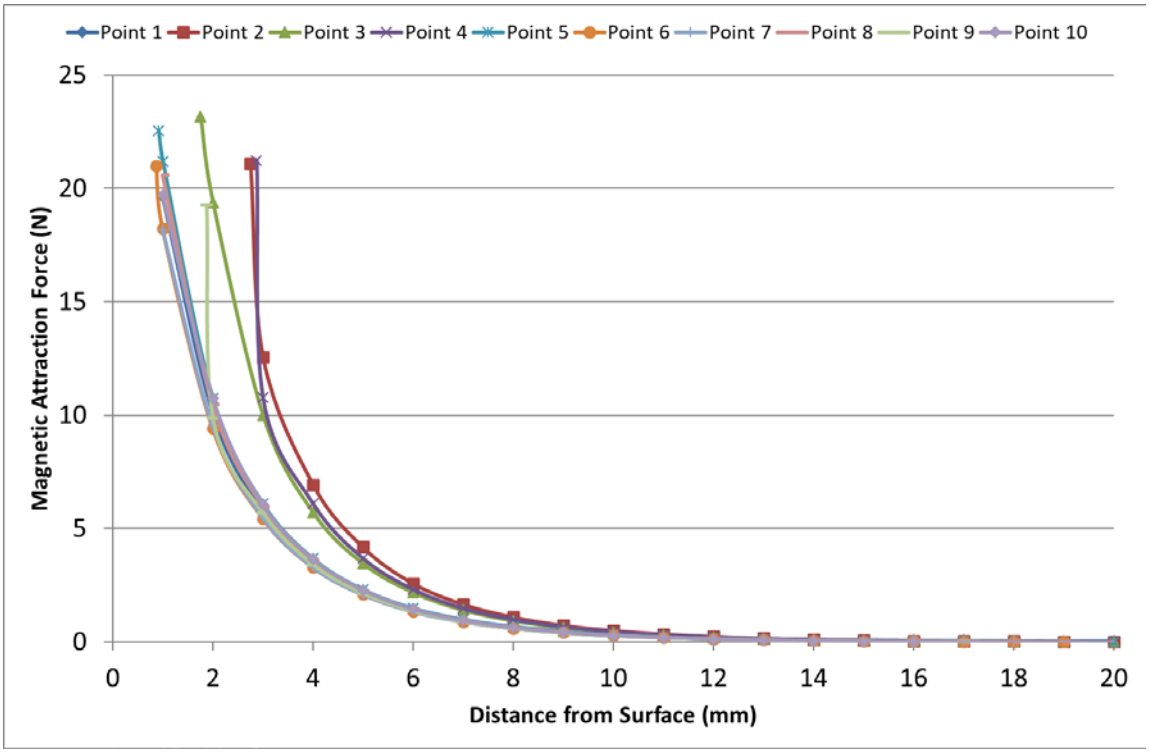

Figure 6.7 - Results of the separation testing carried out with 20 mm magnet

6.4.3 Depth of Interaction

The initial separation testing showed that the maximum corrosion thickness that could be investigated was 7 - 8 mm; beyond this the magnetic force of attraction becomes too small to measure and accurately distinguish. Further testing was carried out to see whether defects in a cast iron pipe could be detected as deep. In this test, a sample of cast iron distribution main with flat-bottomed holes machined in to the outside of it was used. Here the air gap in the hole represented the graphitisation. Figure 6.8 - Figure 6.10 illustrate the results obtained when performing a longitudinal linescan over the flat-bottomed holes of varying depths. In each figure, it can be seen that the magnetic force of attraction drops off dramatically for each magnet as it passes over the hole. The force of attraction levels out once the magnet is at the centre of the hole. It then rises sharply as the magnet begins to move away from the hole. This is in agreement with the results in Section 6.4.2 which show a sharp decay as the distance between the magnet and the iron is increased.

On further comparison of the graphs, it can be seen that the shape of the curves is different. It is suggested that the magnetic field around the 5 mm and 13 mm magnets has a smaller diameter than the 20 mm holes. Consequently, the field lines do not expand enough radially to cut through any iron when it is over the centre of the flat bottomed holes, whereas the magnetic field of the 20 mm magnet is likely to have a larger diameter than the 20 mm holes. Consequently, the magnetic field lines for such a magnet expand enough radially and

still cut some cast iron when it moves over the flat-bottomed holes and provides a force of attraction, even if the hole is deep enough to be outside of the axial magnetic field.

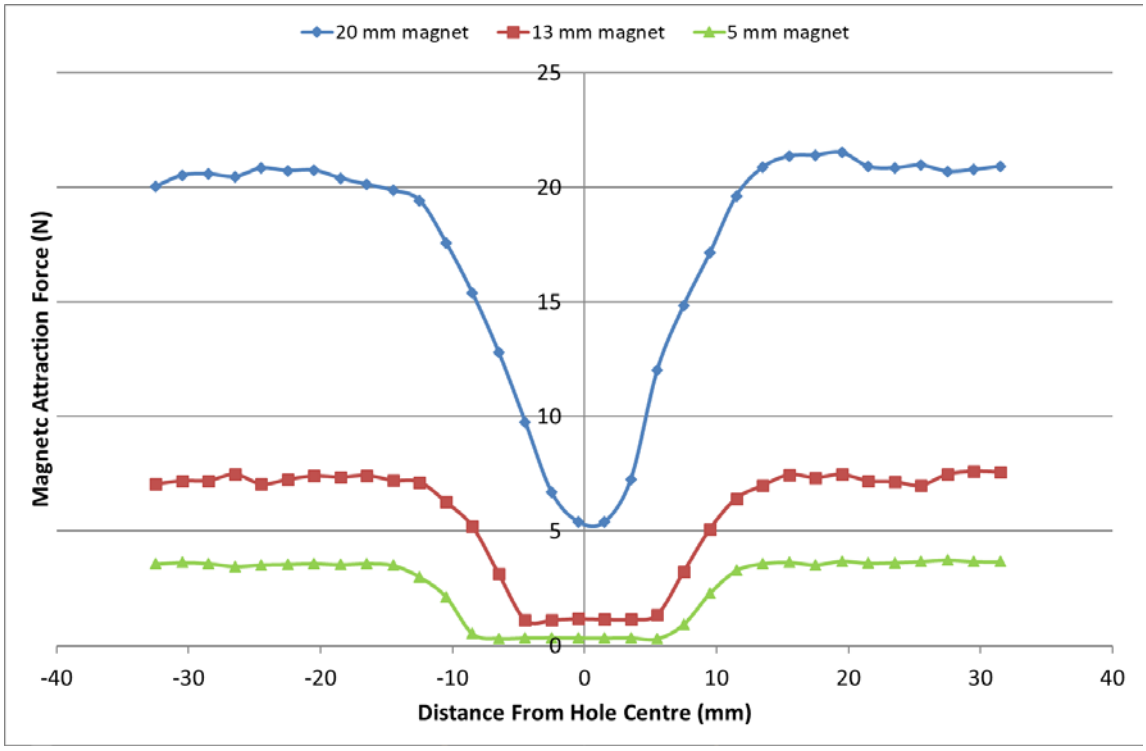

Figure 6.8 - Linescans showing the magnetic force of attraction against the distance of magnet centre from hole centre for the three magnet diameters for a 20 mm diameter flat bottom hole 2 mm deep

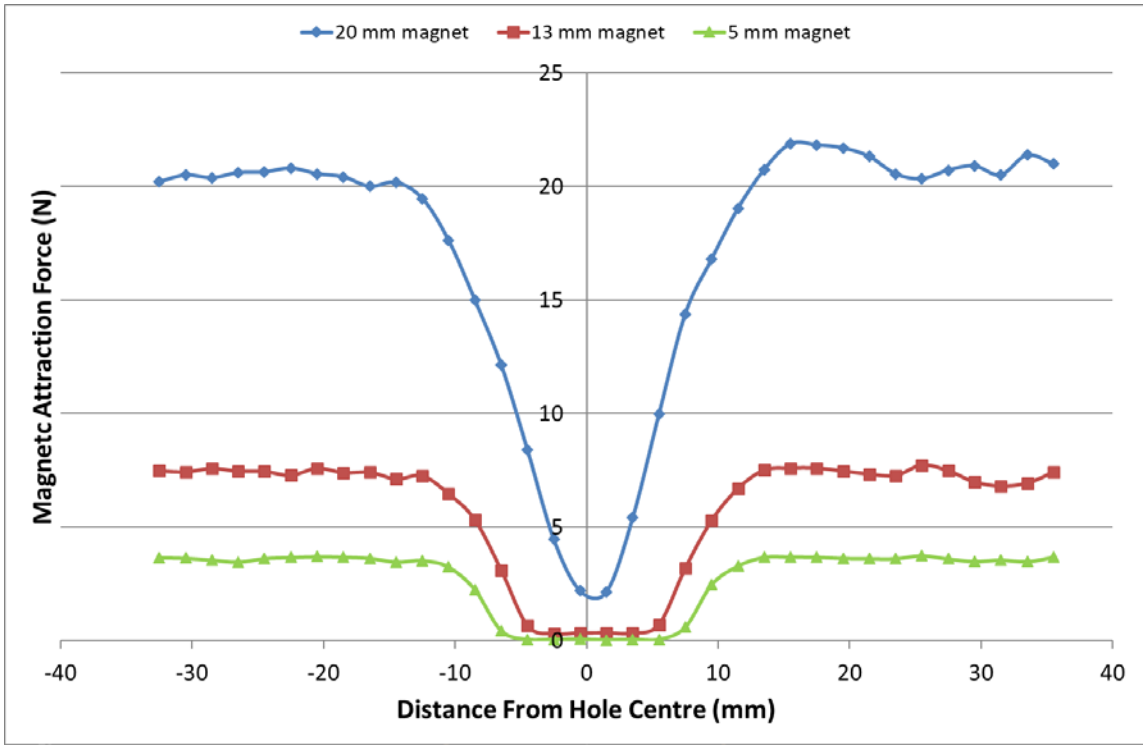

Figure 6.9 - Linescans showing the magnetic force of attraction against the distance of magnet centre from hole centre for the three magnet diameters for a 20 mm diameter flat bottom hole 4 mm deep

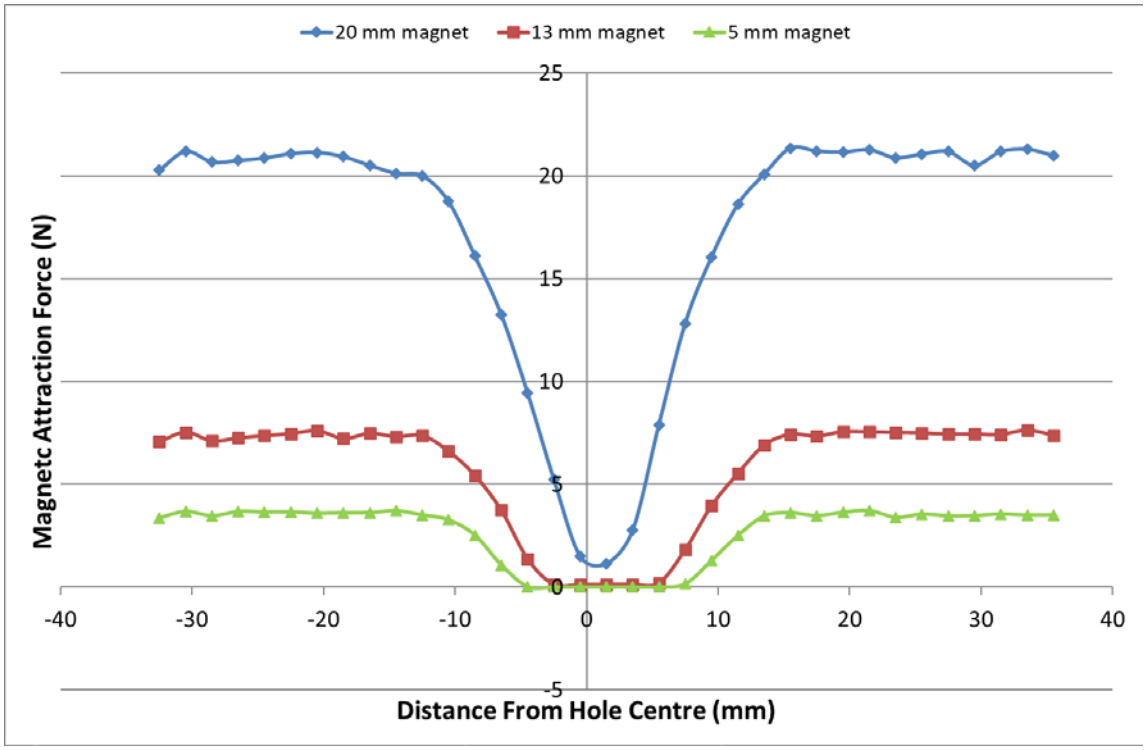

Figure 6.10: Linescans showing the magnetic force of attraction against the distance of magnet centre from hole centre for the three magnet diameters for a 20 mm diameter flat bottom hole 6 mm deep.

The results show that the magnetic force of attraction for the 5 mm, 13 mm and 20 mm magnet is greatly reduced by an air gap of 2 mm, 4 mm and 6 mm respectively. It is unlikely that significant magnetic force, capable of distinguishing further layer thickness, would be produced for larger air gaps. Hence, the maximum thickness that would be able to be classified with the current magnets would be 6 mm.

6.4.4 Hole Diameter

In section 6.4.3 the depth of magnetic penetration was investigated and three depths were suggested as the limit for each magnet. It was also noted that residual magnetic force was present even if the hole depth was deeper than the magnet could detect. It was suggested that this was due to the diameter of the magnetic field around the magnet being larger than the hole. As a consequence, experiments were conducted to determine the approximate diameter of the magnetic field around the magnets. This is important to know as a larger magnetic field will reduce the spatial resolution of the technique. The three magnets were scanned across four through-wall drilled holes ranging in size from 5 mm to 20 mm in 5 mm increments. The results are given in Figure 6.11 - Figure 6.14. It can be seen that the magnets produce a very narrow field whilst maintaining a strong force of attraction. Figure 6.11 shows that the 5 mm hole does not have a significant effect on the magnetic force of attraction. A more noticeable effect can be seen in Figure 6.12 which depicts the results for the 10 mm hole. Here all three magnets showed a drop in magnetic force of attraction. Most importantly, the 5 mm magnet shows no magnetic force when it is at the centre of the hole. Consequently, the magnetic field around the 5 mm magnet is likely to be less than 10 mm in diameter. Figure 6.13 shows a further drop in magnetic attraction force for each of the magnets. Here the 13 mm magnet has also lost all magnetic force and must have a magnetic field no larger than 15 mm in diameter.

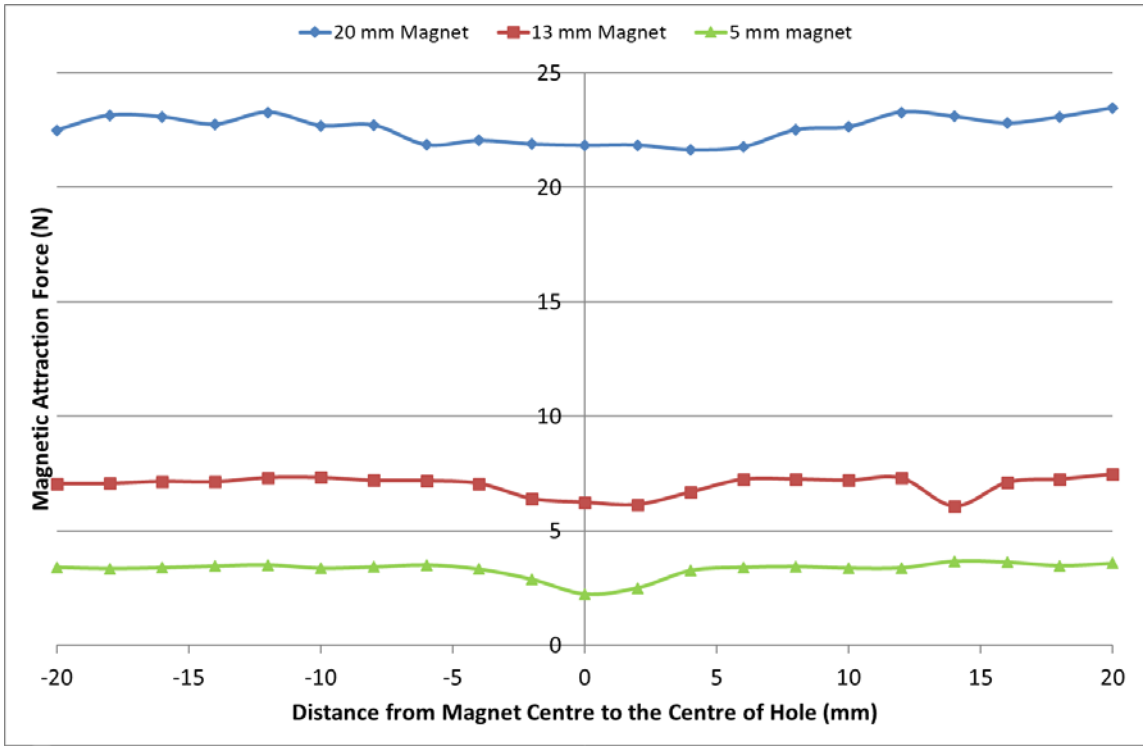

Figure 6.11 - Linescans showing the magnetic force of attraction against the distance of magnet centre from hole centre for the three magnet diameters for a 5 mm diameter through-wall hole.

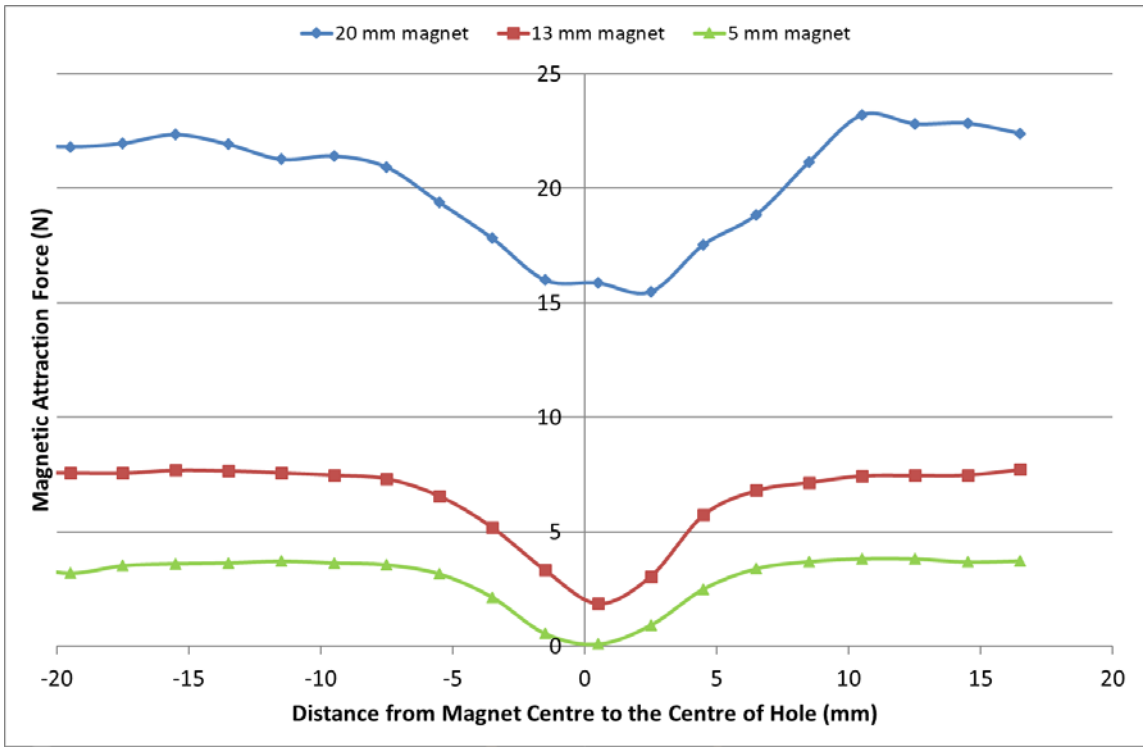

Figure 6.12 - Linescans showing the magnetic force of attraction against the distance of magnet centre from hole centre for the three magnet diameters for a 10 mm diameter through-wall hole.

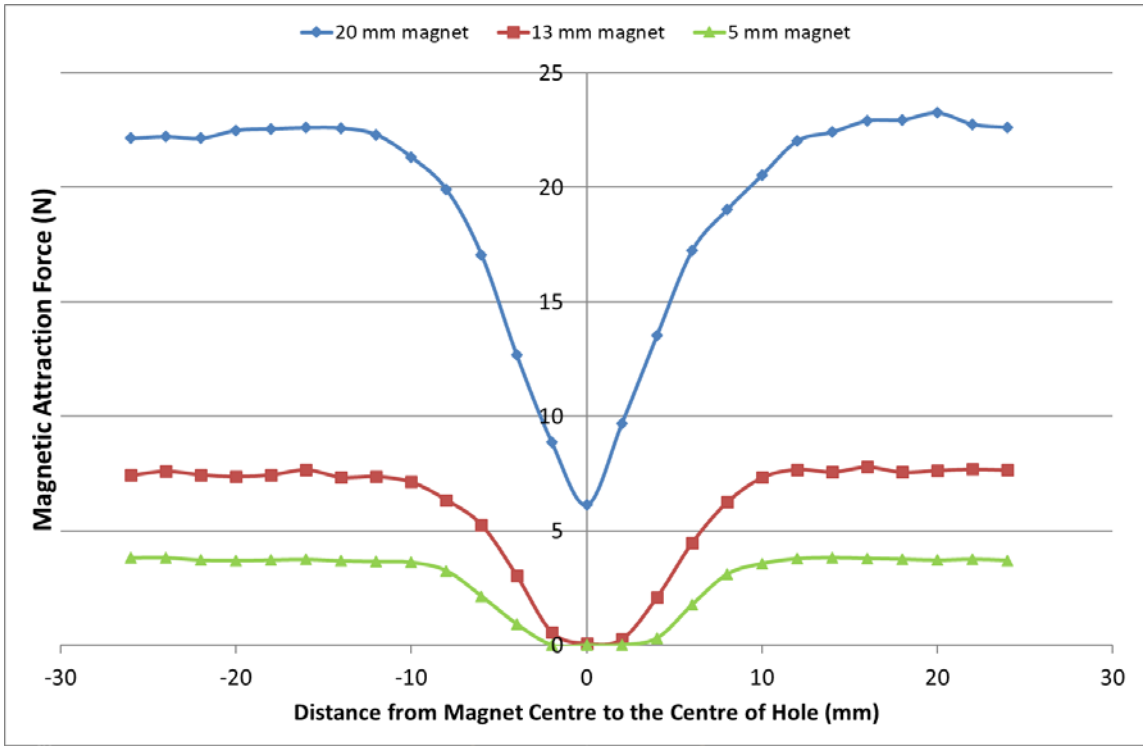

Figure 6.13 - Linescans showing the magnetic force of attraction against the distance of magnet centre from hole centre for the three magnet diameters for a 15 mm diameter through-wall hole.

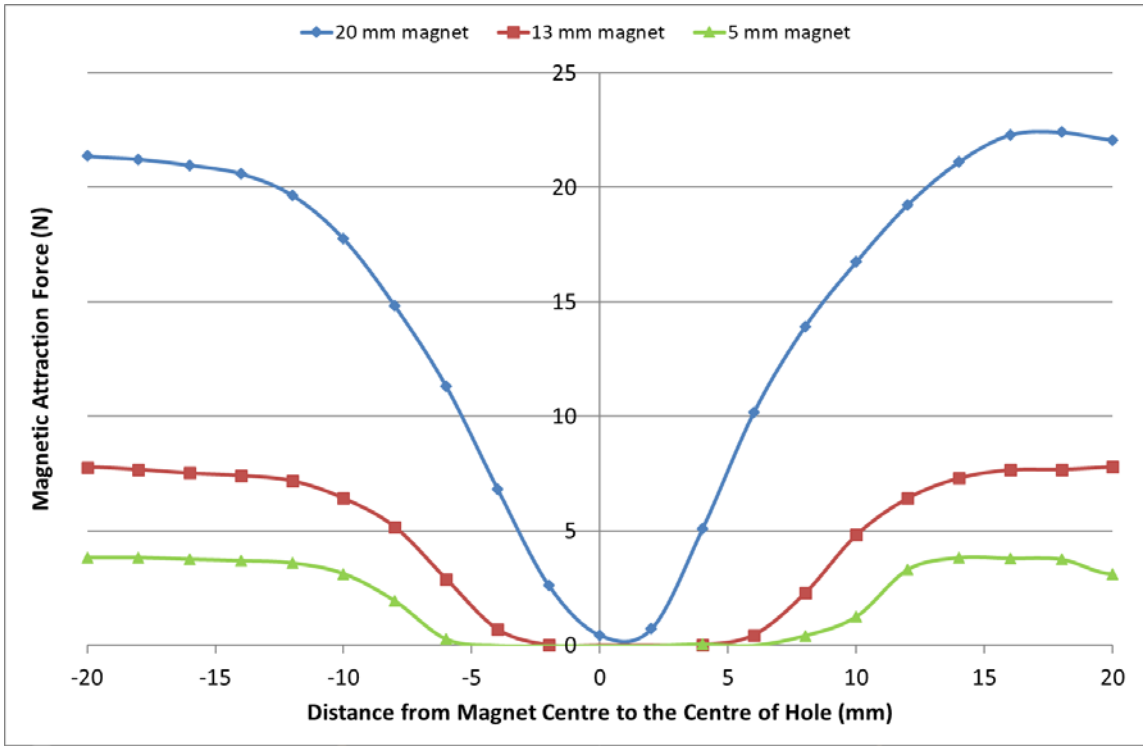

Figure 6.14 – Linescans showing the magnetic force of attraction against the distance of magnet centre from hole centre for the three magnet diameters for a 20 mm diameter through-wall hole

In the last linescan, Figure 6.14, both the 13 mm and 5 mm magnet have lost all magnetic force when they are over the hole. However, the 20 mm magnet has a small amount of residual force left. Given that the 13 mm

and 5 mm magnets had a magnetic field that only extended to a few millimetres greater in diameter than the magnet diameter, it is likely that the magnetic field for this magnet extends to 23 - 24 mm in diameter. These results have shown that the magnets have a narrow magnetic field and so would provide a spatial resolution not much greater than the diameter of the magnet.

6.4.5 Maximum Volume of Interaction

The experiments carried out in sections 6.4.3 and 6.4.4 have provided approximate areas and depths for magnetic interaction with graphitised layers, represented by air, with each of the magnets. These values have been used to give a theoretical maximum cylindrical volume of interaction beneath the magnet. These values are given in Table 6.1.

Table 6.1 - Volumes of interaction for each of the magnets with a layer of graphitisation

Magnet Diameter (mm)	Depth of Penetration (mm)	Area of Influence (mm^2)	Volume of Interaction (mm^3)
5	2	79	158
13	4	177	708
20	6	314	1884

It can be seen that the maximum values for volume of interaction increase cubically (and the area squarely) as the magnet diameter is increased. However, the depth of penetration also increases as the magnet size and strength is increased. It is undesirable to increase the volume of interaction as it results in a lower spatial resolution. However, it is desirable to increase the depth of penetration to encompass thicker layers of graphitic corrosion. Hence, a balance must be struck for optimum inspection.

6.4.6 Internal Metal Loss

The previous tests have shown that there is a correlation between the theoretical graphitic corrosion thickness and the magnetic force of attraction. The testing suggested that each of the magnets could investigate corrosion layers up to 2 mm, 4 mm and 6 mm thick. This testing relied on the corrosion being on the external surface of the pipe. Testing carried out with flat-bottomed holes has proved that it is possible to approximate the theoretical corrosion layer based on the magnetic force of attraction.

Further testing was therefore carried out to see whether it is possible to detect metal loss or corrosion on the inner surface of the main. In order to do this, flat bottomed holes were drilled on the inside of a main sample (Sample C). The magnet was then scanned over the unaltered surface of the sample and the magnetic force measured to see whether it is possible to detect the change in wall thickness. Even though the thinnest part of the wall was 3 mm and the 20 mm magnet had proven that it could investigate graphitic corrosion layers up to 6 mm thick, it was not capable of detecting metal loss under cast iron. It is suggested that the magnetic

properties of iron are significantly different from that of air, and hence graphitic corrosion, and does not allow the magnetic lines of flux to penetrate as deeply. Consequently, it is unlikely that internal metal loss could be detected without increasing the size of the magnet further such that the iron is magnetically saturated locally.

6.4.7 Magnetic Properties of Graphitic Corrosion

Initial thoughts suggested that graphitic corrosion would be diamagnetic due to its inheriting the properties of the graphite flake structure. However, experimentation has proven this to be incorrect. Fragments of the corrosion product have been passed under each of the magnets. As they passed under the magnets they became attracted to the magnet surface. Simple pull off testing estimates the magnetic force of attraction to be much less in comparison to that of cast iron. However, the assumption that the corrosion is transparent to magnetic lines of flux is demonstrably not correct. Further investigation would need to be carried out to determine the effect of the air gap being replaced with a graphitic corrosion layer.

Other techniques that involved the use of magnetics to inspect cast iron may also be affected by the weak ferromagnetic behaviour of the graphitisation. In particular, MFL as the magnetic force will saturate the corrosion where possible and result in less flux leaking out of the pipe.

6.5 Magnetic Force Testing Investigation Summary

The literature indicated that whilst there are many NDE techniques to choose from, many are not practicable for commercial or other reasons. Ultrasonic inspection was chosen as a relatively mature technology for which off the shelf equipment is readily available. However, its application requires trained operators and can add significant extra time to an excavation. This is far from ideal and cannot be conducted on every pipe that is excavated. Further, it has shown difficulty inspecting areas of graphitic corrosion. An alternative technique was required to be used to triage pipes and identify the corroded ones that could need more in-depth testing. Magnetic force testing was chosen for further investigation since it has the potential to be applied by untrained operatives in a swift fashion to decide if a pipe requires greater investigation. Furthermore, the additional data gathered could help to fill in gaps in the data gathered by ultrasonic inspection.

The principle is very simple, in that where there is extensive graphitic corrosion, the force due to attraction between a magnet and a sample of cast iron will decrease. There is, however, no literature detailing the magnetic properties of graphitisation and so it has been necessary to start from first principles. Using a purpose-built test rig, experiments have been conducted to evaluate the feasibility of this technique for the characterisation of graphitic corrosion thickness. The experiments focussed on the force of attraction generated from various sizes of magnets, the effect of an air gap on the force generated (which is essential for a less complicated contactless methodology) and the resolution that can be achieved. This testing has been very successful and suggests that this technology could be used to identify graphitic corrosion over 4 mm in thickness and up to 6 mm. There remains potential for thicker corrosion to be identified. However, the use of larger magnets of the same type would result in degradation to the spatial resolution of the technique. It may be possible to increase the depth of penetration by using a magnet with a higher flux density. This may be achieved using as an electromagnet or an improved magnetic material and would remove the need for a larger

diameter magnet, thus maintaining the spatial resolution. The technique is limited to external corrosion only and has shown that any magnetic testing would struggle to measure internal defects without saturating the cast iron. Further, it has shown that the graphitic corrosion product possesses some, if only weak, magnetic properties which need to be considered by any NDE technique using magnetic principles on cast iron.

In the next chapter, the focus is shifted from understanding the fundamentals of pertinent NDE approaches to evaluating commercial NDE techniques. Here a methodology is proposed to improve the current industry methods of capturing the "ground truth" pipe condition data. This will aid the company in understanding the accuracy of the NDE currently being conducted but also in visualising the problems with any ultrasonic or magnetic methods that have been found in the research documented in Chapters 5 and 6.

7 NDE Inspection Verification by 3D Scanning

7.1 Introduction

Previous chapters have focused on detailing the causes of failure of large diameter cast iron trunk mains, such as defects created during manufacture and installation, or through in-service degradation, and identifying NDE techniques capable of being applied to such mains. Tests conducted under laboratory conditions have identified numerous problems that make it extremely challenging to carry out informative inspection of cast iron pipes with conventional NDE techniques. The rough surface finish and accreted material can make it very challenging to maintain a sensor position or, where necessary, to couple a sensor to a pipe physically without significant surface preparation. Where it has been possible to couple an ultrasonic transducer to a cast iron pipe, it can be difficult to measure the wall thickness accurately due to the considerable variation in microstructure and, consequently, speed of sound in the material. Even if this can be achieved and the wall thickness measured, the ability to use a tool can be inhibited by the strong attenuation of an ultrasonic signal at sites of graphitic corrosion. Even if such problems can be overcome, there remains the issue of standard calibration methods and samples which has not yet been addressed by any of the commercially available techniques for cast iron.

Despite such problems, TWUL uses commercial NDE to assess their cast iron trunk mains whenever an opportunity presents itself, such as through a planned excavation to install an asset or during emergency maintenance. These inspections have been carried out by NDE contractors using a MFL or ultrasonic tool. A significant number of surveys (of the order of 1400) have been conducted over the past two AMP periods[6]. Given the challenges mentioned previously, it is important that the capability of these techniques, and any future techniques employed, are understood so that confidence levels can be placed on data collected. In order to interpret NDE surveys appropriately, a baseline of the true condition of the pipe being used for calibration is needed. This baseline is often termed “ground truth” and details the remaining iron thickness compared to the original pipe surface. This chapter will discuss “ground truth”, why it is important and how it can be determined.

3D scanning has the potential to capture the geometry of a pipe accurately at any stage in an inspection or verification process. Hence, the pipe can be compared pre and post-assessment, or at intermediate stages, as required. This chapter presents the use of a 3D scanner as a tool for gathering “ground truth” condition data for a pipe section. The trial compares “ground truth” with corrosion measurements gathered by destructive means. Initial tests investigated the possibility of determining the “ground truth” baseline from a single scan of the pipe geometry captured after the pipe has been shot-blasted. The chapter then progresses to evaluate a different methodology which seeks to compare the recorded pipe condition before and after shot-blasting was

[6] Surveys were collected during AMP 4 and AMP 5.

conducted. In the first instance, this was trialled on a small pipe section before the trial progressed to a full-size section of trunk main. Finally, a robust methodology for use on a trunk main section is developed and tested.

7.2 Background and Literature

7.2.1 Industry Standard Method of Destructive Baseline Collection

As current NDE techniques for the assessment of cast iron pipes remain unproven with no agreed calibration standards available, many water companies continue to rely on destructive analysis of pipe samples exhumed across the network to identify the condition of the network. A procedure documented by Dempsey and Manook (1986) is commonly used to conduct any destructive condition assessment of pipes. The procedure describes the splitting and shot-blasting of pipe samples to allow internal and external corrosion pits to be made visible and accessible for manual measurement. Further, guidelines on measuring the depth of these pits successfully by hand using a depth micrometer are given. Conducting pit depth measurements by hand for each of the pits present on a section of shot-blasted pipe is time intensive and may not yield a complete picture of the pipe's condition. To combat this problem, the method detailed by Dempsey and Manook (1986) assumes a worst-case condition scenario where the largest internal and external pits coincide on the pipe, thus reducing the cross sectional area significantly and leading to a severely increased localised stress. Consequently, it is not necessary to measure the depth of all the pits present. Only the deepest internal and external pits require measurement. Typically, the 10 deepest pits on each surface, as judged by the inspector through unassisted visual inspection, are identified and their depth is measured using a pit gauge. Ten (10) pits are chosen to ensure that the depth of the deepest pit is captured whilst allowing for any error in the judgement of the inspector. This method of capturing the extent of the pipe condition has become the industry standard for assessing the real condition of an exhumed main in a destructive fashion.

7.2.2 TWUL Previous Comparison Exercises

Previous attempts by Thames Water to evaluate the efficacy of any NDE contractor have seen contractors conducting inspections on lengths of exhumed trunk mains under supervised conditions. An initial comparison exercise was conducted in 2012 on a selection of 42" diameter cast iron pipes. It was undertaken to select an NDE contractor to carry out routine external NDE inspections. The exercise focused on an NDE contractor's ability to detect defects, such as artificial notches and slots machined into the inner surface of the pipe (Evans, 2014). However, these are not necessarily representative of the defects that are responsible for pipe failure. In reality, the literature review on cast iron pipe deterioration presented in Chapter 2 has shown that in-service defects, namely graphitic corrosion on the external surface of the pipe, can intensify the stress effects of underlying manufacturing defects in the pipe, such as wall thinning due to eccentricity in the pipe bore, to cause failure. Consequently, it is important that these techniques must accurately identify and size these corrosion defects.

Further comparison exercises were conducted in 2014 on sections of 36" diameter cast iron pipe. These exercises focused on finding existing defects in each pipe. No additional defects were machined into the pipe wall and each contractor was tasked with identifying the existing defects within the pipe. The pipe condition

was subsequently ascertained by shot-blasting the pipe to remove the graphitic corrosion. The corrosion thicknesses were measured at the deepest points of the pits using a depth micrometer to give individual pit depths. This method of capturing the extent of the corrosion follows that described in Section 7.2.1. To gain a better understanding of the spatial alignment between results, the axial and circumferential position of each pit was also captured for spatial reference. The method described by Dempsey and Manook (1986) is most commonly applied to small sections of distribution main. Experience suggests that there are often many more than 10 pits present on the surface of deteriorated trunk main. Whilst it would be desirable that any NDE technique can find every pit present in a pipe, it is unlikely, particularly where the corrosion is very thick. This makes comparing NDE data to the baseline 10 pit depth measurements complicated and may result in little spatial agreement. Consequently, the number of pit depth measurements taken for the comparison exercise was increased to provide a better sample of the corrosion thickness. These manual pit depth measurements do not seek to measure all the corrosion present. Instead, they seek to identify a selection of the most damaging pits which would be of key importance and which any NDE contractor must be able to capture accurately. These points provide a sufficient number of reference pits which any contractor must be able to identify if the technique used is to be of use.

Despite the increase in the number of pit measurements, it was only possible to capture pit depths for the top few hundred pits (Cruz, 2014). This work was extremely time intensive and required a skilled individual consistently to identify the deepest corrosion pits through visual inspection. Also, whilst the axial and circumferential location of each pit depth measured is recorded, it does not provide any insight into the geometry of each pit. This is because a single pit depth measurement that is recorded could be representative of a large or small pit: for example, many of the larger corrosion patches present on trunk main appear to be the result of several individually nucleated pits growing together to form a larger agglomeration of pits. Hence, measurements do not always accurately represent the extent and distribution of corrosion and, when comparing these measured values to the condition reported by the contractors, it has been challenging to find agreement, Figure 7.1. This problem can be exacerbated by inconsistencies in each contractor's reporting of the position and thicknesses of measurements (Scudder, 2014).

In addition to the pit depth measurements, contractors were also asked to provide wall thickness measurements and internal corrosion measurements. Internal corrosion, whilst less damaging than external corrosion, is still important to record, particularly if the worst-case scenario detailed by Dempsey and Manook (1986) is assumed. The actual internal corrosion was also measured using a pit depth gauge and was prone to the same geometric and spatial issues as mentioned for external corrosion.

Aside from the corrosion thickness, the remaining metal thickness is also of key importance. In current comparison exercises, it is only possible to measure the wall thickness of the pipe directly near the cut ends. Consequently, many of the comparison exercises struggle to compare the wall thickness measurements provided by contractors with the actual value. Further work would be required to section each pipe into smaller rings where the wall thickness could then be measured across the whole section.

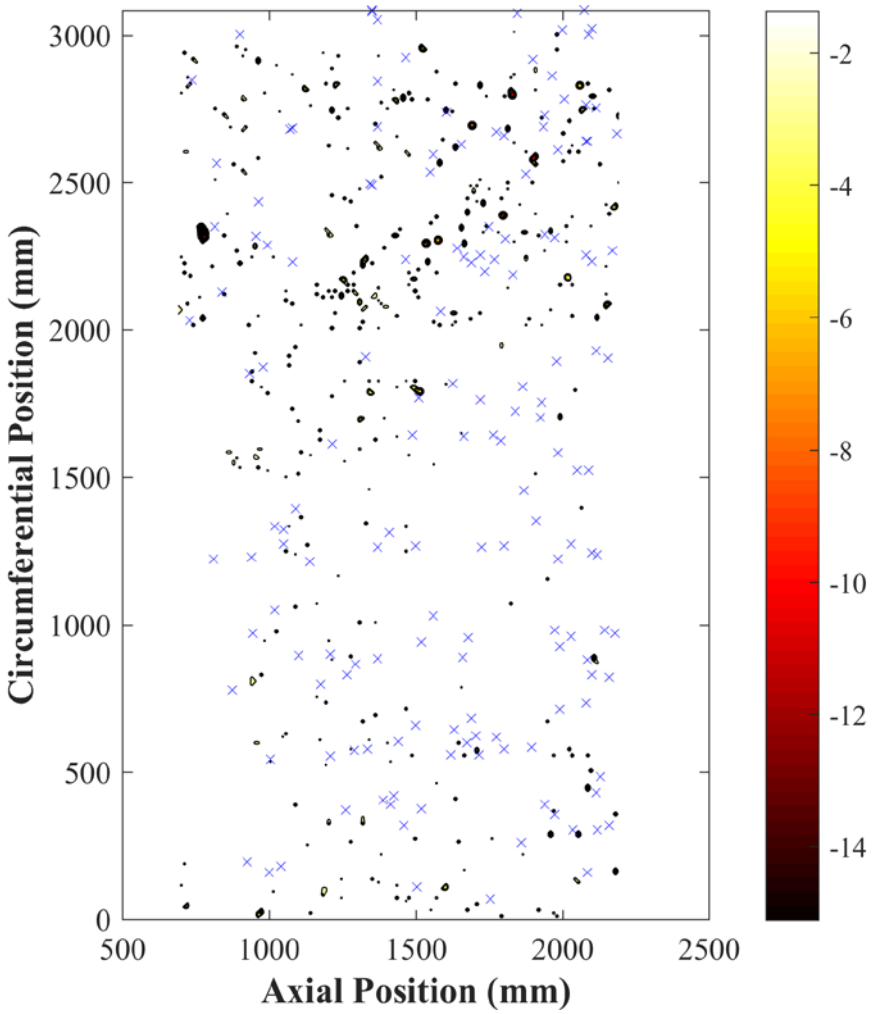

Figure 7.1 - Contour map detailing the external corrosion measured by an ultrasonic NDE contractor on a section of 36" cast iron pipe during an in-house comparison exercise run by TWUL. Each of the black contours highlights corrosion pits greater than 2 mm deep. The blue crosses indicate the sites of discrete pit depth measurements measured by hand.[7] The white bands at the edge of the plot indicate areas masked by the pipe supports where inspection was not conducted.

As a result, it has not been possible to judge a contractor's performance to any degree other than through statistical analysis comparing the spread of the corrosion depths measured by each contractor and the manual pit depth measurements, Figure 7.2. However, this is not without challenge. It is clear that the corrosion depths reported by each contractor do not mirror the results provided from the baseline pit depth measurements. In fact, the spread shows that one contractor appears to be over estimating the pit depths whereas the other is underestimating it. Further, the distribution of measurements appears to be different for each contractor. Given that the NDE data gathered from the network is used to inform the network rehabilitation strategy, an under or overestimation can lead to an inaccurate identification of the pipes in need of replacement, and hence, money will be spent replacing the wrong pipes. Meaningful conclusions for targeted replacement can only be made if the NDE data is accurate and represents the true network condition.

[7] Contour Map data supplied by TWUL but plotted by the author.

Finally, it is recognised that many of the NDE techniques employed require smooth surfaces to operate properly. All contractors are allowed to conduct surface preparation to enable effective NDE, however, it has been observed that the surface preparation of some contractors can be overly aggressive leading to graphitic corrosion being eroded from the pipe surface, Figure 7.3. This can lead to underestimation of the corrosion thickness measured. The current method of evaluating an NDE contractor can be seen to have problems which prevent information detailing their performance being gathered. Consequently, an improved method of destructive analysis is needed that can provide the internal and external corrosion thickness, and any loss during surface preparation, as well as the remaining wall thickness.

(a)

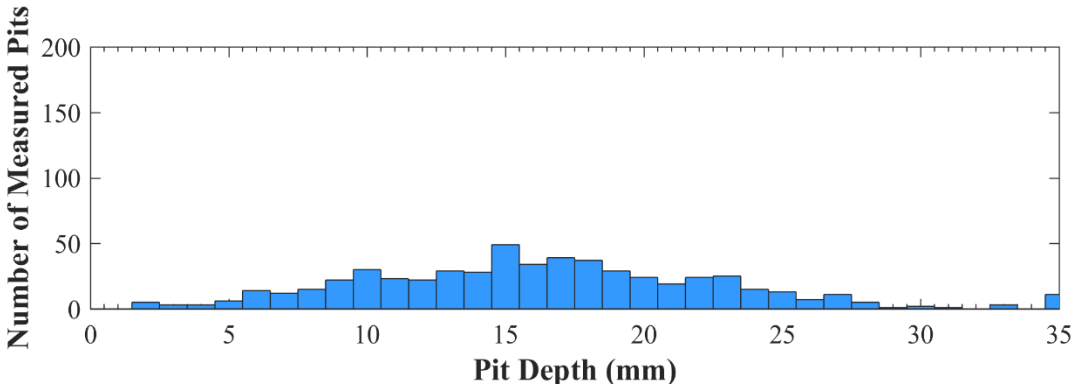

(b)

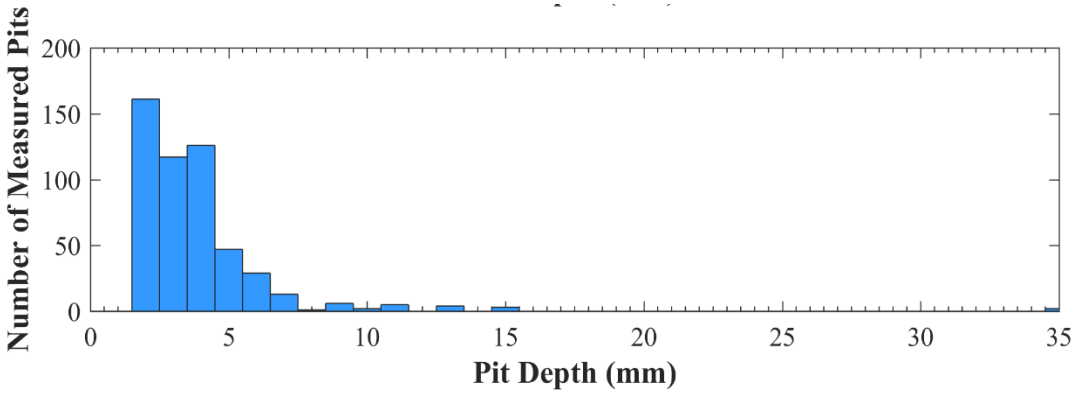

(c)

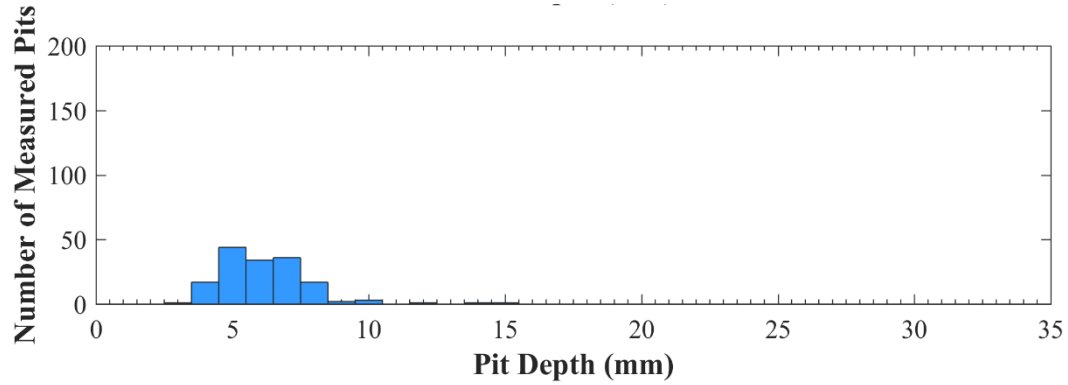

Figure 7.2 - Corrosion depth measurements taken from a trunk main section in a previous comparison exercise: (a) MFL Contractor, (b) Ultrasonic Contractor, and (c) Manual Pit Depth Measurements[8]

[8] Corrosion data supplied by TWUL but plotted by the author.

Figure 7.3 - Corrosion pit after the graphitic corrosion has been partially removed during surface preparation.

7.2.3 Use of 3D Scanners for Geometric Metrology

The problems of gathering accurate baseline pipe condition data have been experienced during previous comparison exercises (Scudder, 2014). Consequently, accurate and rapid methods of gathering more representative, "real" condition data through destructive analysis have been sought. For some considerable time, 3D scanners have been used to conduct verification exercises for quality assurance or for the purpose of reverse engineering. However, more recently, their capabilities have been directed at gathering condition data. Their ability to acquire geometry accurately over large surface areas rapidly and to record geometry from difficult to measure surfaces makes them the ideal tool to use when evaluating an object's condition. Examples of their use can be seen in the measurement of deformation of structural retaining walls (Oskouie *et al.*, 2016), in corrosion mapping of a pressure vessel (Allard and Fraser, 2013), or in the condition mapping of sewers (Kmpfer and Ziehl, 1996).

This technology has been transferred to the assessment of pipes and 3D scanning is available as a commercial tool for inspecting steel pipes in the oil & gas industry for corrosion defects or other geometric irregularities. In this application, the 3D scanner is being used directly as a tool for carrying out NDE, since the corrosion product spalls from the pipeline leaving corrosion pits visible and capable of being measured. Its application to these pipes has resulted in a significant reduction in the time taken to conduct a corrosion inspection compared to that conducted using manual methods. This reduction could be of the order of days, dependent on the size of the pipe being inspected. The technology also allows for more complete coverage of the surface (Prewitt, 2016).

Bruce et al. (1997) have demonstrated the use of a laser scanning tool to measure the loss of section due to outer surface corrosion on a section of deteriorated pipe. This approach relies on the pipe section having smooth ends to support the theory that the original pipe section is perfectly round. Further work, conducted by Reichert et al. (2001), has recognised that there are problems with assuming that a pipe was perfectly cylindrical and has described the use of an algorithm which can determine the external corrosion without assuming that the original pipe was perfectly circular. However, the details of this algorithm have not been published.

More recently, a manufacturer called Creaform has investigated the benefit of using their 3D scanners for inspecting corrosion. Allard (2012) demonstrated the use of a Creaform 3D scanner and Pipecheck software to map the corrosion on the outer surface of a pipe successfully. The methodology recognises that pipes can suffer from ovality as well as areas of flatness and suggests that a cylinder cannot be purely fitted around all of the scan model. Instead, a reference cylinder is generated from the unaffected areas of pipe model around the corroded areas. From this, "corrosion maps" can be generated for a pipe section. Examples of the application of the Creaform 3D scanner and software can be seen elsewhere (NACE International, 2013).

Modern steel pipelines have good quality assurance and it can be safely assumed that the pipe being inspected would have been almost perfectly cylindrical when first made. Hence, the 3D scan data of the pipe's outer surface can be compared to a perfect reference cylinder of the same diameter to ascertain the level of damage present. However, the same assumption cannot be applied to cast iron trunk mains, especially those that were made prior to the adoption of centrifugal casting. Here, significant ovality in the outer surface of the pipe can be present and would prohibit a suitable cylinder being fitted. As such, simply fitting a cylinder to the outside of a pipe section may yield inaccurate corrosion thickness measurements. Furthermore, the effect of removing the corrosion from a cast iron trunk main is unclear. However, it is not beneficial and as such it would not be possible to apply the scanner in this direct methodology. These issues limit the usefulness of a 3D scanner in the field for the determining the current condition of corroded cast iron main. However, the ability to measure the corrosion pits during a destructive analysis would greatly increase the coverage and speed of any validation exercise.

The National Research Council (NRC) in Canada have been investigating pipe failures for some time and have built an in-house scanning system capable of measuring the external corrosion on sections of cast iron distribution main. The system comprises a motor-driven chuck capable of holding and rotating a distribution main section in front of a laser line scanner. The laser scanner is able to traverse along the pipe and hence the outer surface of pipe section can be built up from scan strips. As part of this work, a set of algorithms were developed for the scanner which allowed the external pipe corrosion to be gathered. The use of this scanner can be seen in several of the papers published by the NRC (Liu *et al.*, 2008; Kleiner and Rajani, 2011; Kleiner *et al.*, 2012; Kleiner *et al.*, 2013; Kleiner and Rajani, 2013). In these papers, a scanner has been used to measure the geometry of the corrosion pits on a shot-blasted section of main. From this it has been possible to suggest the corrosion pit depths, corrosion areas and volumes. The literature does not explicitly state how the original pipe surface for comparison is generated, however, the cylindrical coordinate system applied to each strip scan

suggests that the system models the reference surface as a perfect cylinder fitted to the outer surface of the scan. On small diameter pipes, outer ovality may be less of a problem and the assumption that the pipe was originally a perfect cylinder may be acceptable provided that sufficient uncorroded area areas remain visible in the scan model to determine the original cylindrical geometry.

Due to the equipment size, this system is limited to sections of distribution main no longer than 1 m in length (Wu *et al.*, 2012). A much larger scanner would need to be built if sections of trunk main were to be inspected. Given that the current system can take of the order of 40 mins to conduct an inspection, it is likely to take many hours to complete an inspection on a full-size trunk main. Work to reduce the level of detail captured, without detriment to the system's resolution, has brought the scanning time down below 10 minutes for a distribution main (Wu *et al.*, 2012). Despite the potential to reduce the scan time, the results produced are based on the assumption that the pipe is perfectly cylindrical. However, a system such as this would be difficult to construct and operate for a much larger pipe section.

The Advanced Condition Assessment & Pipe Failure Prediction (aka Critical Pipes) Project is a research project operating in Australia, involving a number of water companies and universities (Advanced Condition Assessment and Pipe Failure Prediction Project, 2015). The project seeks to improve the way the pipe assets are managed for rehabilitation. To do this, several activities have been undertaken in order to gain an improved understanding of the reasons for pipe failure and associated deterioration mechanisms. The work also seeks to determine how to assess effectively the deterioration and current condition of a main and decide how to predict effectively a failure before it occurs using a decision support tool running on improved data gathered by the project. This work has been conducted on a number of trunk main including abandoned runs of pipe. The cast iron pipe found in Australia is similar to that used in the UK, however, there are two notable differences: the pipe walls are thinner, with many of the order of 20 – 25 compared to the 30 – 35 mm seen in the UK, and the inner surfaces are coated with a cement lining to minimise the internal corrosion. The literature produced by this project mentions the use of a 3D laser scanner to capture the "ground truth" condition of a pipe and its data is then used for assessing the onset of corrosion (Petersen and Melchers, 2012; Petersen *et al.*, 2013; Dafter and Petersen, 2013; Shannon *et al.*, 2016) or improving the sensors used to detect these defects (Miro *et al.*, 2013; Ulapane *et al.*, 2014; Falque *et al.*, 2014; Falque *et al.*, 2015). Part of the work undertaken by the critical pipes project has sought to compare the capabilities of current NDE contractors. Several of the papers make reference to examination of their capabilities, however, the results presented are focussed towards refinement of the techniques and associated data post-processing. Here, the data gathered by the contractors and the 3D scanner is fed into a machine learning algorithm which suggests improvements to the sensing algorithms. Few results have been provided, if any, that compare the contractor's predicted values against the "ground truth" condition.

Not all work has focused on assessing corrosion only. More recently Vidal-Calleja (2014), of the "Critical Pipes" project, has applied 3D scanning to cast iron pipelines to determine the remaining wall thickness. The inner and outer surfaces of a cast iron pipe were scanned to capture their geometry. It appears that each surface was scanned separately without any link. The surfaces were later concentrically aligned using reference values

for wall thickness of a standard pipe of such diameter. The work has shown that 3D scans captured on the outer surface have been used to create external corrosion maps and identify mechanical damage. Later developments in corrosion and wall thickness measurements have shown improvement due to the implementation of a ray tracing method (Skinner *et al.*, 2014). The paper does not confirm the analysis software used to generate these maps, however, it is known that Creaform Pipecheck was purchased to complement the Creaform 3D scanner bought to capture these surface profiles (Shepherd, 2014) before new algorithms were developed in-house.

One further example of optical metrology has been demonstrated by (Prewitt, 2016). Here the ability to measure the exposed corrosion seen on a bent pipe section has been demonstrated and shows that the 3D scanner provides more flexibility in inspecting complex geometry as opposed to current manual pit depth measurements. In that paper, the measurement of wall thickness is also mentioned as a possibility but no further mention of the methodology is given.

Much of the work described has focussed on determining the original pipe surface from the scan captured of the corrosion. In some heavily corroded iron pipelines, it may not be possible to construct a sensible original profile due to the deformation induced by heavy corrosion. A brief mention of capturing the starting pipe condition as a baseline is mentioned by Petersen and Melchers (2012). However, there is no written methodology explaining its application. This may be a further option to consider, to ensure that any measurements taken are reliable.

7.2.4 Baseline Pipe Condition Literature Summary

The literature has shown that there is a potential disparity between NDE data and the actual pipe condition which cannot be effectively compared due to the lack of a method capable of accurately mapping the real condition of a pipe. 3D scanning has shown that it is possible to evaluate corrosion, however, no utilisable method has been described in the literature. Several other methods have been described but their efficacy on cast iron is questionable. In the next section, the work to understand the capabilities of 3D scanning for "ground truth" measurement is described.

7.3 Equipment & Core Methodology

7.3.1 Equipment

All pipe scans were captured using an Artec Eva structured white light scanner supplied by Artec 3D, Figure 7.4(a). This scanner was connected to a Dell M6800 laptop, with Artec Studio v10 by Artec 3D installed, which drove the scanner and captured the scan files whilst in use. Whilst the scans were captured using a Dell laptop, all scans were processed using a custom built Intel i7 desktop computer. This computer was used as it provided greater system resources capable of meeting the demands of the intensive computational post-processing of the scans. All scan data was transferred to this machine after the data had been acquired. Verify, by Geomagic, was used to aid Artec Studio with 3D model manipulation.

The scanning of distribution main sections did not require any further equipment as they are light enough to be moved by hand and are small enough to be scanned on a laboratory worksurface. However, much larger

trunk main sections, of the order of 1 – 2 tonnes in mass, required much more careful handling and sufficient space in which to do it. A bespoke pipe rotator was manufactured by Spectrum Welding Supplies (Chesterfield) to allow large sections of pipe to be rotated safely for scanning. The rotator comprised a standard five tonne capacity motor driven rotator pair on a bespoke frame that could be repositioned using a forklift truck. This rig enabled sections of trunk main, up to one complete pipe 'stick' long, i.e. 5 m in length including the bell and spigot, to be safely positioned and manipulated for 3D scanning, Figure 7.4(b). This is believed to be a unique facility.

(a) **(b)**

Figure 7.4 - Equipment used to conduct the pipe scanning: (a) the Artec Eva structured white light scanner (Artec, 2016) and (b) the specialised pipe rotator used to manipulate the sections of trunk main loaded with a section of 42" main.

7.3.2 Data Acquisition

3D pipe models comprise one, or more, 3D scans which are aligned and fused together to leave one 3D mesh which represents the original object. All scans were captured utilising the same settings: the scanner was instructed to use texture and geometry to track its position. Scans were captured at the maximum frame rate possible. This was nominally 15 frames per second, however, the bandwidth available on the USB port of the associated laptop can reduce this to closer to 12 frames per second. Prior to recording the geometry, a trial scan was undertaken to ensure that the texture brightness setting was correct. Here, the scanner was moved to the minimum working distance from the pipe of approximately 0.4 m. It was then moved out to the maximum working distance of 1 m. The image on screen captured at these working distances was reviewed to ensure that the colours could be clearly defined and were not excessively bright. Where necessary, the texture brightness was increased or decreased and the test was run again until the optimum brightness setting was achieved. During scanning it was necessary to keep a working distance of ~ 0.7 m between the scanner and any pipe surface to ensure that the optimum scanning conditions were observed. Both scans of distribution mains and trunk mains were captured using this scanner with the acquisition settings mentioned above; the methods of hand scanning vary, dependent on the size of the pipe. The methodologies utilised to ensure full surface coverage of each of these pipe types are described later.

7.3.3 Data Post-Processing

In order for a full 3D model of a pipe section to be generated, the scans captured required cleaning and aligning with other scans to form a complete "rough" model before being fine-tuned and finally fused together to give a final pipe mesh. These operations were undertaken using Artec Studio v10 which was also used to drive the 3D scanner during data acquisition.

The following steps were carried out sequentially on the scans captured for a given pipe section to produce a complete 3D model of the pipe section. The steps highlighted in blue are not mandatory and only need to be used if the scan data requires further cleaning or editing.

1. **Rough Serial Registration**
   The default rough serial registration algorithm in Artec Studio v10 was run to ensure that each scan which had been captured was correctly assembled by the computer and adjusted where necessary.

2. **Scan Editing**
   It is not uncommon for unwanted background geometry, such as supporting surfaces, to be captured by the scanner. Each of the scans captured was individually edited to remove any traces of the floor or any other supporting geometry. This was carried out in Artec Studio v10 using the in-built editor. A combination of the manual selection tool and a cutting plane were used to select and then remove the unwanted geometry.

3. **Scan Alignment**
   All of the scans were aligned using common points to form an outline of the pipe scanned. The model was built up in the order that the scans were captured. Each scan was individually aligned to the previous scans and a completed model was built up in Artec Studio v10. A 3-point alignment was used to align common points on the overlapping geometry on concurrent scans.

4. **Global Registration**
   Once all of the scans had been aligned and a rough model had been created, the global alignment tool, built into Artec Studio v10, was run to fine-tune the position of each scan point until a complete model was created. The global registration tool was run using its default settings.

5. **Fast Fusion**
   Once a completed model made up of refined scans had been achieved, the scans were then fused together using the fast fusion tool to produce one geometric volume. The resolution for this model was set to the default value of 1 mm. All other settings were kept to the default settings.

6. **Hole Filling**
   It was common to find small holes in models where the scanner was unable to illuminate the geometry fully in order to capture the surface well. These points are no more than a few millimetres across. At these points, the in-built hole filling algorithm was used to construct mesh geometry between the edge points.

7. **Fused Model Cleaning**

   Once any holes on the model had been removed and the geometry was whole, a further algorithm was run to remove any hanging geometry that was not part of the model.

8. **Mesh Size Reduction**

   The final step in creating a reliable 3D model was to reduce the file size to make the model more manageable. Each model was reduced to a maximum number of 5 million triangles. This step was not necessary on sections of distribution main as their meshes did not exceed this threshold.

9. **Pipe Model Texturisation**

   For visual presentation, the coloured texture on the surface of the pipe was applied to the meshed model to provide a realistic looking pipe, Figure 7.5(a). This step is not strictly necessary since it is the geometric model that is interrogated to determine its health, Figure 7.5(b). However, it can aid with future pipe alignment operations if markings on the pipe are visible on the model as well.

During model processing, global registration and fast fusion were automated to run overnight when sufficient time was available for the computers to conduct the processing operation. Post-processing of data gathered for a distribution main was much quicker and did not need such periods of time.

a) **b)**

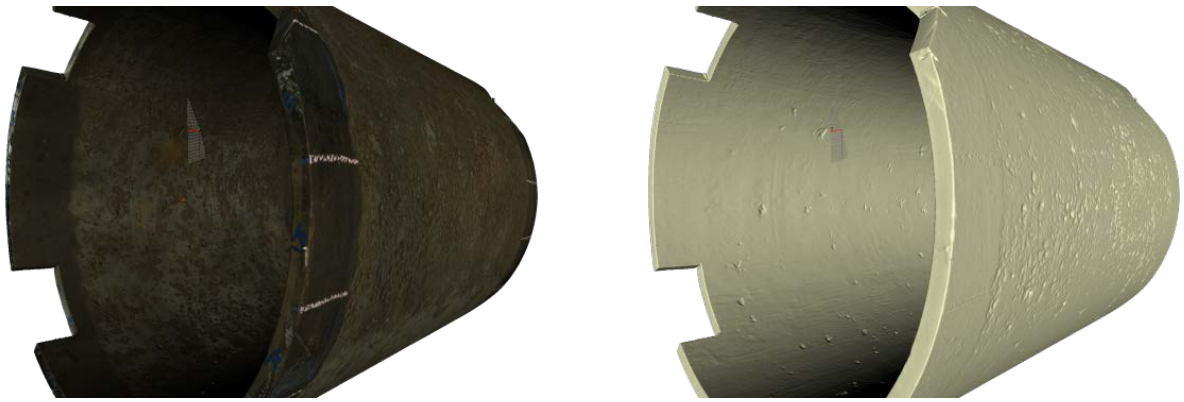

Figure 7.5 - Digital images showing the same 3D model: (a) with texture (b) without texture

7.3.4 Shot-blasting

Shot-blasting is an accepted method used by those in the water industry for removing any graphitic corrosion, as well as adhering encrustation or other oxides. The result of this process is a pitted cast iron pipe with several indicators of the position of any graphitic corrosion. Two different companies were used during experiments to abrade both pipes. Distribution main sections were sent to R D Cox and Son (Reading) who are the preferred shot-blaster for TWUL Innovation projects. However, they were unable to handle sections of trunk main due to their size and weight. The trunk main sections used in these experiments were sent to Hydrosave (Walsall). Both contractors are experienced in the shot-blasting of pipes and follow a similar procedure using chilled iron shot to clean the pipes of their corrosion without unnecessary abrasion of the underlying metal.

7.3.5 Pit Depth Measurement

Pit depth measurement is the current industry standard method of characterising the extent of the corrosion present on a trunk main. Pit depth measurements are conducted on shot-blasted sections of pipe where the corrosion has been removed to reveal the pit. All pit depth measurements were conducted in-house by the same inspector to ensure consistency in the method.

Prior to any measurements being conducted, the crownline of the pipe was marked on the outer pipe surface. Where the position of the crownline was not known, an arbitrary line was marked on the pipe for reference purposes. The pipe section was examined by the inspector and the deepest pits, as judged by eye, were identified. The positions of these pits were marked with a paint marker. The circumferential position of each pit was measured from the crownline using a tape measure. The measurement was taken in the same positive circumferential direction as that used by the algorithm that interprets the 3D pipe models to ensure that the results could be easily compared. The axial position of the pit was measured from a designated end of the pipe using a tape measure.

Once the circumferential and axial position of each pit had been recorded, the corrosion thickness was inferred by measuring the pit depth using a depth micrometer. The micrometer was placed over the pit and the probe was extended to measure the deepest part of the pit. The placement of the depth micrometer had to be carefully chosen to ensure that an accurate measurement was captured. A sensible corrosion thickness measurement can only be made using the depth micrometer where a consistent, flat surface around the periphery of a corrosion pit is present, Figure 7.6(a). At any sites where this criterion is not met, the corrosion measurement captured can be skewed by the angle that the depth micrometer forms as it conforms to the uneven surrounding surface, Figure 7.6(b). As a result, the measurement made is not representative of the original geometry and it is not captured. Measurements for pits of such geometry were not taken.

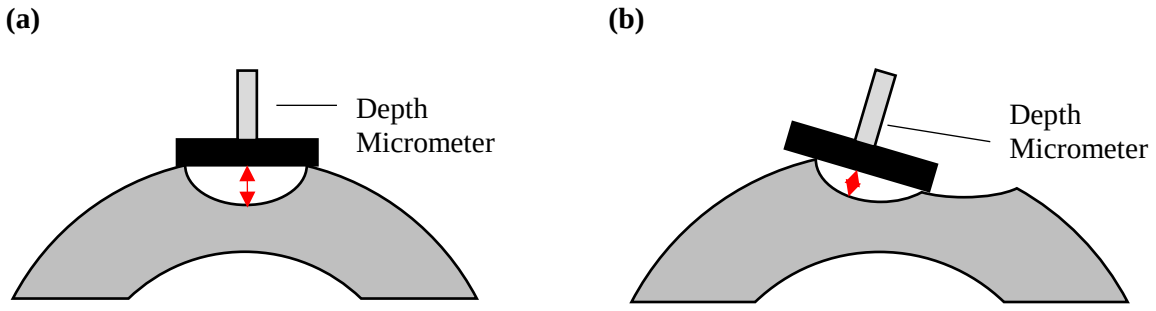

Figure 7.6 - Diagrammatic representation of two different surrounding geometries present when making pit depth measurements: (a) ideal and (b) impossible surrounding geometry. The red arrow indicates the corrosion thickness being measured.

This process can be used for distribution main sections or trunk main sections. Typically, an inspector will measure the top 10 pits on a distribution main pipe section, as this is considered sufficient to identify the deepest and most damaging pits. However, this number of measurements should be increased for a trunk main to account for the much larger surface area and the variety of corrosion formations observed (Jesson *et al.*, 2013).

This process can also be used to characterise the deepest internal pits, provided that the inspector has sufficient access. In the case of a large diameter trunk main this is not a problem. However, if the diameter is significantly reduced, access to the inner surface of a whole pipe is not possible and the pipe section must be split in half for successful measurements. It should be remembered that this process can only be used during a destructive analysis as mains in service offer poor accessibility, particularly to the inner surface, and may require the removal of significant, potentially damaging, volumes of material to make any pits visible for inspection.

7.4 Initial 3D Scanner Trial

7.4.1 Methodology

In this work, a section of shot-blasted 36" trunk main, nominally 1 m in length, was used. This is referred to as Specimen One. Specimen One had been shot-blasted for use in a previous comparison project and was selected as it did not require any further surface preparation before it could be scanned. As inspection was conducted before the pipe rotator had been procured, Specimen One was rested on chocks and sleepers to allow the pipe to be rolled by hand and repositioned as needed. The inner and outer surfaces of the specimen were marked up with an array of arbitrary symbols using yellow chalk to ensure the scanner could track its position across the smoother inner surface. The shape of these symbols is not important. However, it is advised that any markings should have lines that cross to provide points that cannot slide and can lock each frame captured together. Symbols such as # or + are good examples of such markings. Further, each shape must be unique and randomly placed to ensure that the scanner can accurately determine its position. Ideally, the shapes should be between 50 - 100 mm in size and there should be a spacing of 100 – 150 mm between them to ensure that more than one symbol is visible to the scanner at each time. Numbers were also drawn on each cut end of Specimen One to ensure there were common identifiable features that could be aligned between scans of the inner and outer surfaces.

The specimen was scanned using the Artec Eva, with the settings described in Section 7.3.2. A 3D model was built up in successive scans which sought to capture approximately one quarter of the specimen each time including the cut ends. After each scan, the specimen was rolled to allow successive sections of the specimen to be illuminated by the scanner. The inner and outer surfaces were captured independently as the scanner could not maintain tracking when moving from the outside to the inside of the specimen. The same procedure was repeated for the inner geometry. Once the scanning was complete, the scans were processed as described in Section 7.3.3 to give a 3D model of Specimen One. Geomagic Verify was used to fit a cylinder wall to the outer surface of the model to represent the original outer pipe surface prior to shot-blasting. Areas of the shot-blasted model that looked nominally uncorroded, Figure 7.7(a) and representative of the original pipe surface were highlighted and a "best-fit" cylinder was fitted through these areas. As many areas across the surface of the pipe as possible were chosen to ensure that the cylinder could achieve an optimum fit. The cylinder was set as the reference surface and the scanned model as the scan surface. Areas where the corrosion pitting was extensive, Figure 7.7(b) were not used during the fitting process. The minimum 3D deviation between these two surfaces was determined using the 3D deviation tool built into Geomagic Verify.

(a) **(b)**

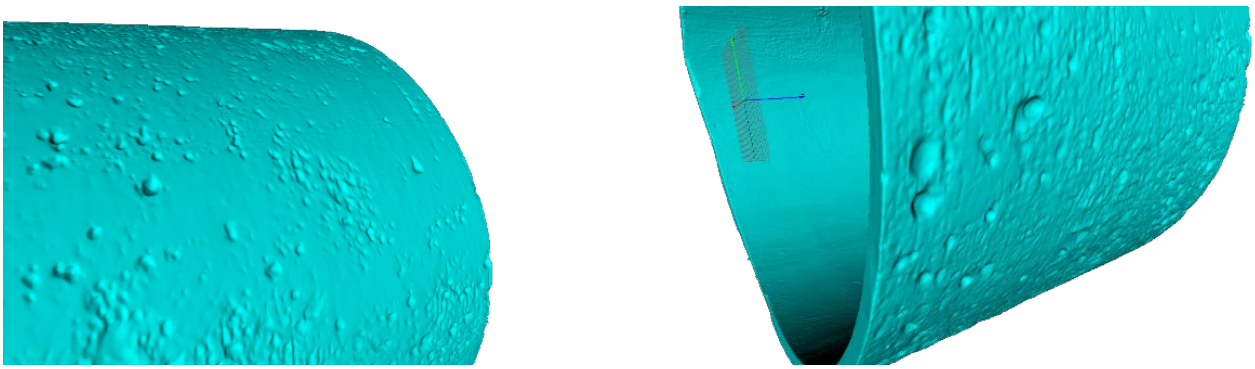

Figure 7.7 - Screen capture from Artec Studio showing the different surface morphologies present on the model: (a) Smooth Flat Areas Determined to be uncorroded and (b) Large Corrosion Pits

7.4.2 Complete 3D Pipe Section Models

Figure 7.8(a – d) show views from four angles around the pipe's central axis of the completed 3D scanned model of Specimen One as captured by the Artec3D Eva scanner. It can be seen that the graphitic corrosion pitting across the outer surface is extensive and is present around the whole outer surface. However, the level of pitting can vary greatly between angles. In Figure 7.8(b) and Figure 7.8(c), it is possible to see areas that are uniform and do not appear to contain any pitting. It is possible that these areas are uncorroded and represent the surface of the original pipe before the corrosion set in. The regions of the scan deemed nominally uncorroded were used as a guide to fit a reference cylinder over the pipe to represent the suggested original outer surface. Figure 7.8(e) shows the fitted cylinder in red over the scanned shot-blasted section in blue. Whilst the cylinder provides a good fit to the areas nominally selected as uncorroded, it can be seen that it does not fully encompass all parts of the model. There are other areas of the model which have a greater diameter and protrude through the fitted cylinder. Here, any corrosion measurements made are likely to underestimate the corrosion thickness. This is most prominent if the areas where the nominal uncorroded pipe sections lie at each end of the minor axis on a potentially elliptical pipe. Here, each end of the major arc has the potential to protrude through the fitted cylinder. Since the original external surface would have encompassed all of the geometry visible after shot-blasting, the cylindrical fit must be altered to encompass all of the scanned geometry.

A new cylinder was generated based on the requirement to encompass all of the scanned outer geometry. This cylinder has a larger diameter to incorporate these regions. Whilst encompassing all geometry, the fit is reduced and it is possible to see significant gaps, up to 10 mm, between the new fitted cylinder and the 3D model, Figure 7.8(f). As a result, any corrosion measurements made using this modified fit would contain a significant error. This is due to ovality and a fitted perfect cylinder is unable to account for this, and there will be significantly more error in the corrosion thickness measurement.

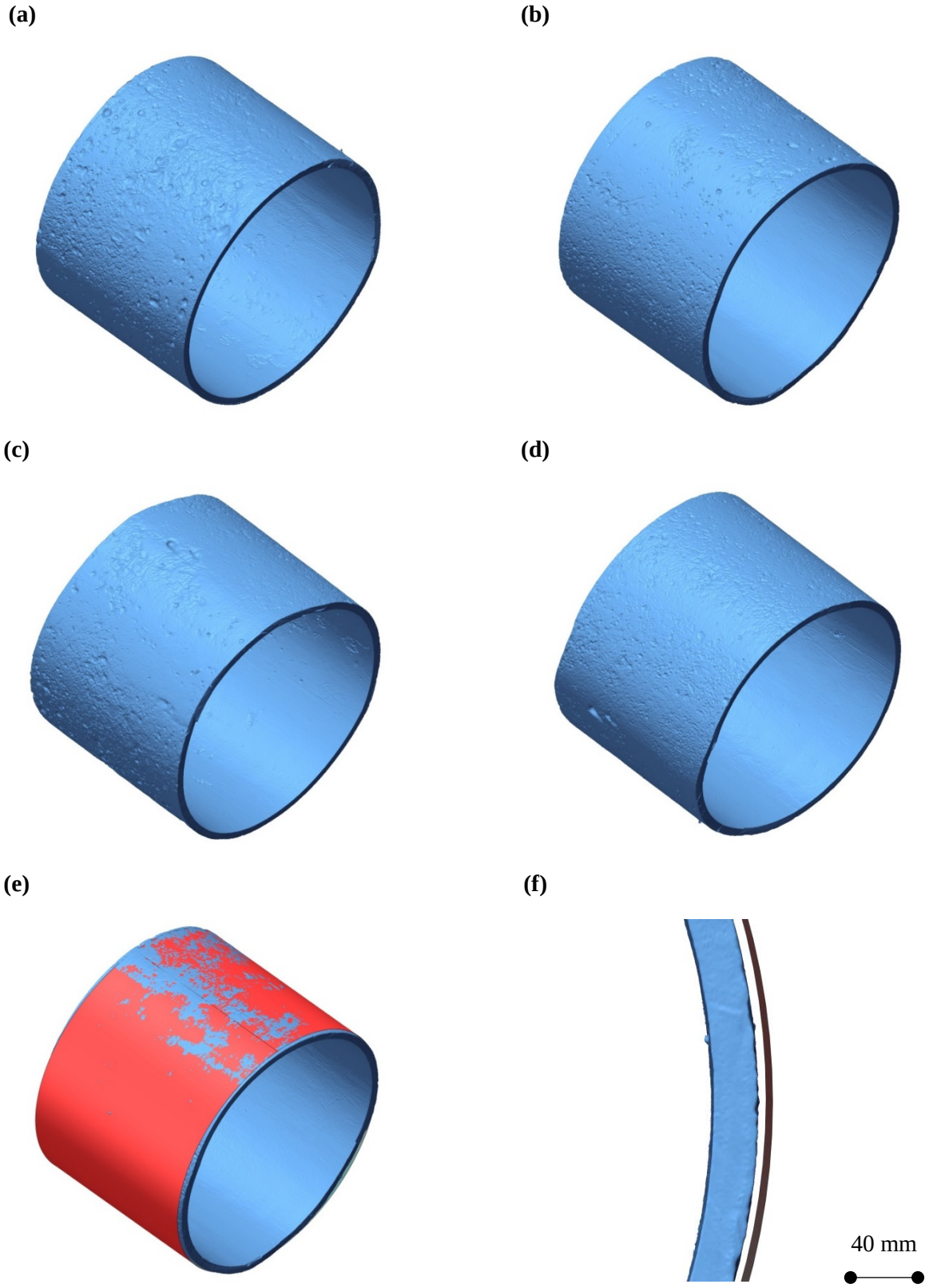

Figure 7.8 - a) – d) Digital models of Specimen One viewed from 90 degree angles about the central pipe axis. e) The shot-blasted section with a cylinder fitted to the possibly uncorroded sections of the main. f) A partial view along the length of the section showing the difference due to ovality between the 3D scan (blue) and the modified larger fitted cylinder (grey line).

7.4.3 Summary

A method has been trialled which uses a 3D scanner to build a model of a pipe after various inspections. It has significant potential, due to its ability to be applied to pre-existing pipe sections that would require little, if any, further preparation. Whilst the scanner has performed well and produced coherent models of a section of trunk main, the testing has shown several problems which mean that this method is impractical for use on sections of cast iron trunk main.

This method fails as it relies on a pipe being perfectly cylindrical, which is demonstrably not the case. Consequently, inferring corrosion thickness measurements from a single 3D model of the pipe after shot-blasting incurs significant error. To improve on the measurements captured here, a scan of the pipe must be captured before shot-blasting to provide a true representation of the original surface.

Such a model would not suffer from the error of approximating the original geometry and would allow for a more accurate comparison. A methodology trialling this assumption and the results obtained from it are detailed in Section 7.5.

7.5 Development of a new scanning method on a distribution main

7.5.1 Pipe Sample

Previous comparisons conducted by Thames Water have used exhumed 36” and 42” pipes as the test samples to be inspected by NDE. These pipe sections provide ample surface area for a contractor to evaluate, however, the logistics involved in the cutting, shot-blasting and transportation of a large section of trunk main are complex and can take a significant amount of time. Given these difficulties, it was decided that the first trial of a new method should be conducted on a more manageable distribution main before progressing to the more complicated trunk main section. A section of 4” distribution main, nominally 14” in length, was cut from a longer main that had been exhumed previously from Henshaw Street in South East London. This is referred to as Specimen Two. It was chosen as previous testing of the remainder of the pipes exhumed from this area had shown that the main was in poor condition and was very likely to have corrosion present around the wall. The main was cleaned of external encrustation during a previous exercise using a wire brush and did not require any further preparation.

7.5.2 Methodology

Reference markers were cut into Specimen Two to ensure that the scans could be aligned once the geometry had been altered by the shot-blasting. A v-notch was cut into one end of the specimen using a petrol disc cutter, Figure 7.9(a). Two slots, no wider than the cutting disc thickness (~ 4 mm), were cut at the opposite end of the specimen along the same axial line, Figure 7.9(b). Both marker geometries were chosen due to the ease of creation using a disc cutter. Other shapes could be used but they may be more complicated to machine into the sample. To ensure there were sufficient markers to allow the scans to be aligned during the post-processing stage, 10 mm holes were drilled into the specimen: Three holes diametrically opposite the v-notch, Figure 7.9(a), a further two holes were drilled approximately 120° around the circumference from the two slots and one further hole was 240° around the circumference from the two slots, Figure 7.9(b).

Once Specimen Two had been prepared, it was scanned using the Artec Eva following the settings described in Section 7.3.2. As Specimen Two was considerably smaller than Specimen One used in the previous experiment, the data scanning methodology was adapted.

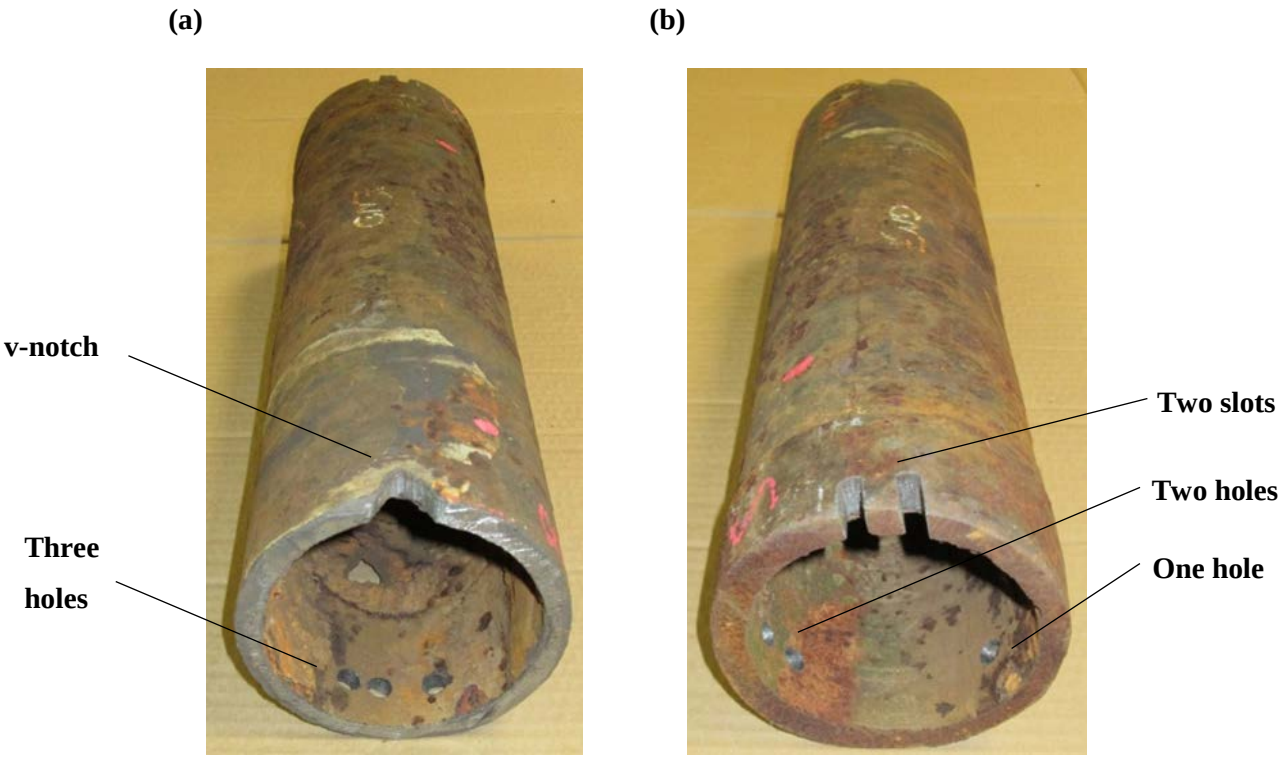

Figure 7.9 - Reference markers were cut into Specimen Two: (a) a v-notch at the bell end and (b) two slots at the spigot end.

Specimen Two was light enough to be moved by hand and small enough to be scanned on the work-surface in the laboratory. Here the specimen was positioned horizontally. The specimen was raised on two iron blocks, sufficient to lift it off the work-surface. The geometry of these blocks is arbitrary but, they must be narrow enough not to be visible during scanning. This ensures that any of the work surface captured by the scanner can be easily removed from the scans during post-processing.

The scans of Specimen Two were captured in several passes. Initially, a scan was captured of the specimen lying horizontally. Here the scanner was held normal to the pipe surface and moved around the specimen in a continuous fashion. The specimen was then rotated around its axis to reveal geometry that had not been visible previously. A sufficient overlap of visible geometry was maintained to allow the future scans to be stitched to the former scan during post-processing. The degree of overlap was typically 50% of the area. This process was repeated to capture a sufficient number of scans to cover the pipe barrel.

Once the barrel sections had been scanned, the specimen was stood vertically and the ends of the specimen were also individually scanned in the same fashion as the barrel to capture the cut edges and thus ensure that a complete model of the pipe could be generated. This allowed a small fraction of the inner surface to be captured. However, it was not possible to capture the full inner surface using this method. To enable full coverage of the inner surface, the specimen would need to be split in half and then each half scanned

individually following a similar process. Once the individual scans had been captured, they were processed to give a complete 3D model of Specimen Two as described in Section 7.3.3.

After producing the first 3D model, approximately 50 mm at each end of the specimen was protected using an adhesive cloth based tape, Figure 7.10(a). The protection was extended at the end of Specimen Two with two slots, as the pipe diameter increased due to a reinforcing band. The purpose of protecting these ends was to maintain a record of the original outer surface prior to shot-blasting, which is often used when capturing pit depth measurements. However, the reinforcing band does not represent the original barrel diameter. Extending this protection protected further pipe that was in keeping in diameter with the rest of the pipe. Once Specimen Two was fully protected by cloth tape, it was sent for shot-blasting, Figure 7.10(b).

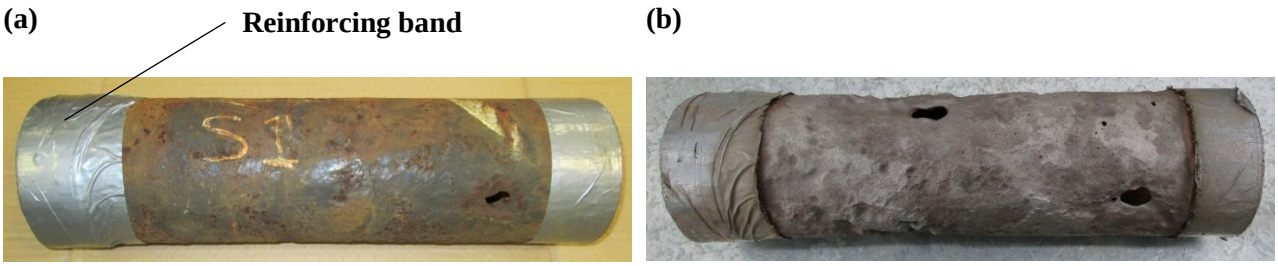

Figure 7.10 - Specimen Two protected with adhesive cloth based tape. (a) before shot-blasting and (b) after shot-blasting.

When Specimen Two arrived back in the laboratory, the cloth tape was removed and any tape residue removed. The specimen was scanned in the same way as described above and a 3D model of the specimen's geometry, after shot-blasting, was created. Finally, to determine how accurate the measurements taken using the 3D scanner were, the shot-blasted section was also evaluated using a pit depth micrometer, as described in Section 7.3.5. The axial and circumferential positions for each pit, relative to the v-notch, were also noted.

7.5.3 Completed 3D Models and Data Presentation

Figure 7.11(a) and (b) show 3D models created from 3D scans of the outer surface of Specimen Two before and after shot-blasting respectively. It can be seen that before shot-blasting, the specimen has a nominally smooth outer surface with minor undulation. However, once the graphitic corrosion is removed by the shot-blasting process, it becomes evident that there are significant corrosion pits present across the specimen. By aligning these scans and comparing them, it is possible to measure the changes in the specimen's geometry due to the shot-blasting. In Figure 7.11(c), the raw differences between each 3D model, as measured by Geomagic Verify, and hence the external corrosion removed during the shot-blasting process, is graphically represented as a colour-map conforming to the surface of the specimen. Here the red indicates no change in geometry whereas the yellow, green and blue indicate increasing changes to the geometry.

Whilst this format is desirable for graphics presentations, it is very difficult to work with in comparison exercises. A format that can be compared between scans is needed. It must be simple to understand and can represent a range of different pipe radii. Furthermore, inspection of the raw results produced by Geomagic Verify has shown that the minimum distance deviation measurement methodology employed by Geomagic

Verify does not provide a reliable representation of the corrosion, particularly around through wall corrosion. At these points, it has been found that the deviation vector is not being measured normal to the pipe surface, as a conventional radial pit depth measurement would be. An improved methodology that can make more representative measurements and present them in a format more conducive to comparison was developed and is described in Section 7.5.4.

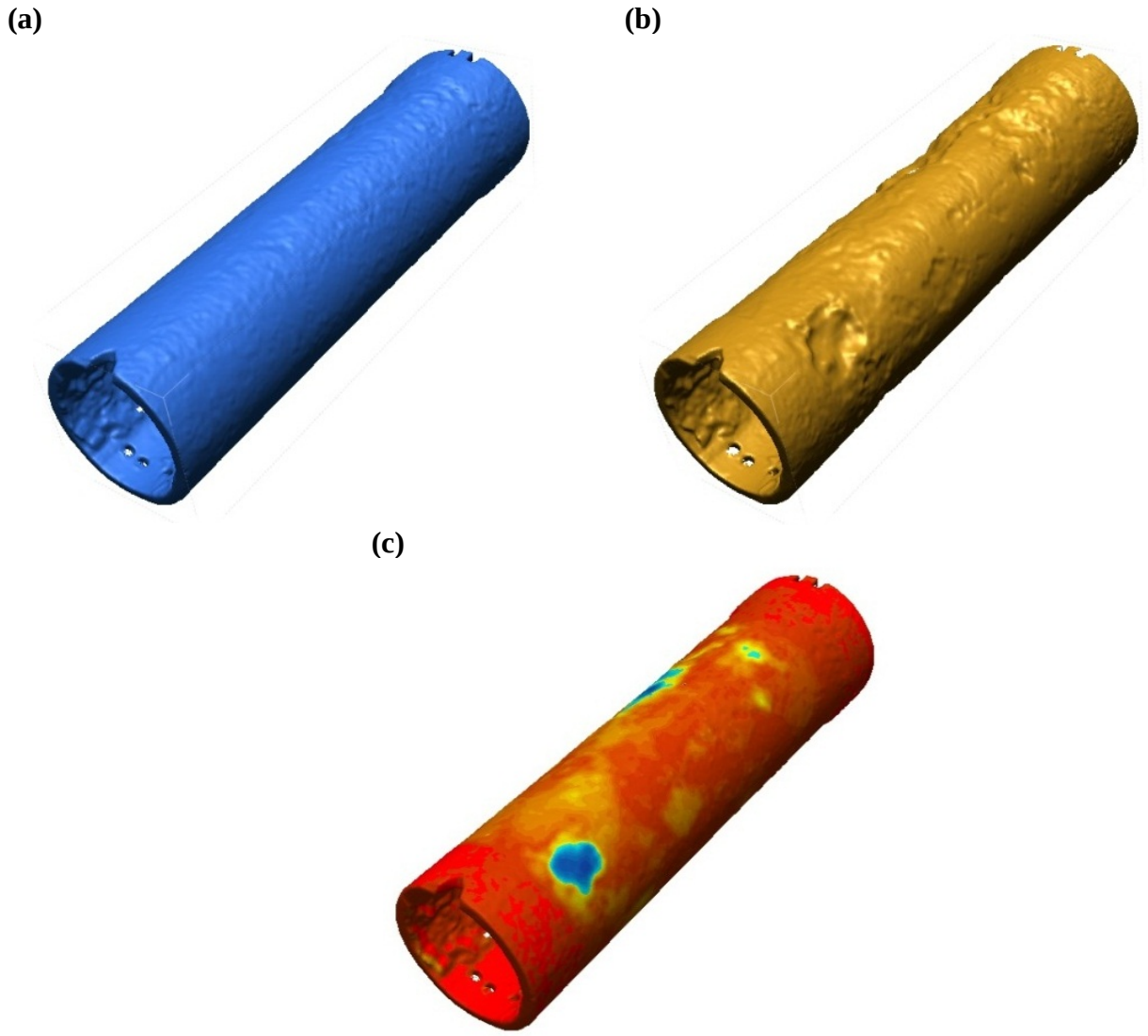

Figure 7.11 - 3D model of Specimen Two from Geomagic Verify at different stages of the processing: (a) Raw pre-shot-blasting, (b) Raw post-shot-blasting and (c) A deviation map showing the difference between the two models and hence, the external corrosion.

7.5.4 Revised Measurement Methodology

In order to manipulate and finally display the data collected by the 3D scanner in a more comparable way that could be interpolated and processed as necessary, the data was resolved to create a rectangular array that could be contour plotted with the circumferential position against the axial position whilst allowing numerical analysis to be conducted. To make the data easier to work with, and eradicate the need to translate complex coordinate geometry, the 3D models were given a complementary XYZ coordinate system. A reference cylinder was fitted to the outside of the smoother pre-shot-blasting scan. This was used to align both scans to

the origin such that the Z axis ran along the axis of the pipe and the X and Y axes sweep across the circular cross-section of the pipe. This is a more convenient polar coordinate system which allows direct comparison of similar angular points on a surface regardless of the radius. The coordinate system described can be seen in Figure 7.12. It has already been stated that a cylinder is unlikely to be able to make a fit to the outer surface sufficient for pit depth measurements to be made and the use of a further cylinder to align the scans could raise further questions. However, here the reference cylinder is not used as the original pipe surface, but rather it is used to align the imperfect scans to a perfect coordinate system as well as possible. It is important that this stage is carried out as it simplifies the coordinate geometry and makes it much easier to work with the data. Once the 3D model was adjusted to this position, any point on the 3D model, P, can be described by the angle, θ, and axial position, z, from the datum axis, Figure 7.12.

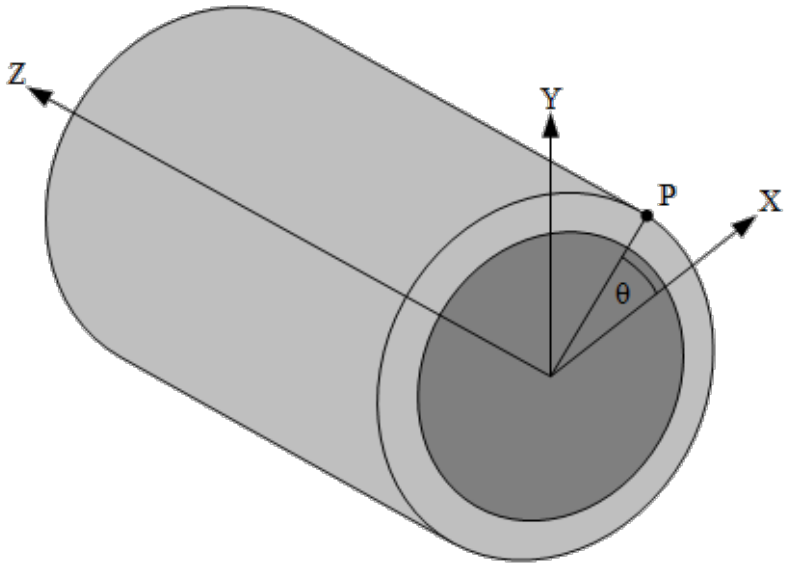

Figure 7.12 - Diagrammatic representation of a cylindrical coordinate system applied to a pipe section.

After all scans had been aligned to the new global coordinate system, each 3D model was trimmed to remove the cut ends and any internal geometry. Individual outer surfaces from the pre- and post-shot-blasting 3D models were compared, to determine a revised corrosion thickness measurement. However, the edited 3D scans were not compared directly. Instead each model was compared to an arbitrary cylinder which ensured that true radial measurements for the difference in thicknesses were made. This comparative process can be seen in Figure 7.13 where the distance to each point on the grey 3D model to the red arbitrary cylinder is calculated as D1 or D2, dependent on the models being compared. The distance *d*, which represents the thickness of the condition data being requested, which in this case is the external corrosion thickness, for a given angular and axial position can be found using Equation 7.1 for values of D1 and D2 with the same angular, θ, and axial, *z*, position.

The number of measurements made axially and circumferentially was controlled by the outer reference cylinder. This cylinder is formed of a cylindrical mesh with 720 facets around the cylinder by 465 along it. Here, each measurement compares the normal distance from each facet on the reference surface to the pipe 3D

model. This gives a spatial resolution of approximately 1 mm along the z axis and 0.5 mm around the circumference for this distribution main section. The radius of the reference cylinder is arbitrary, however, the cylinder must be sufficiently large that it encapsulates either 3D model without touching it at any point.

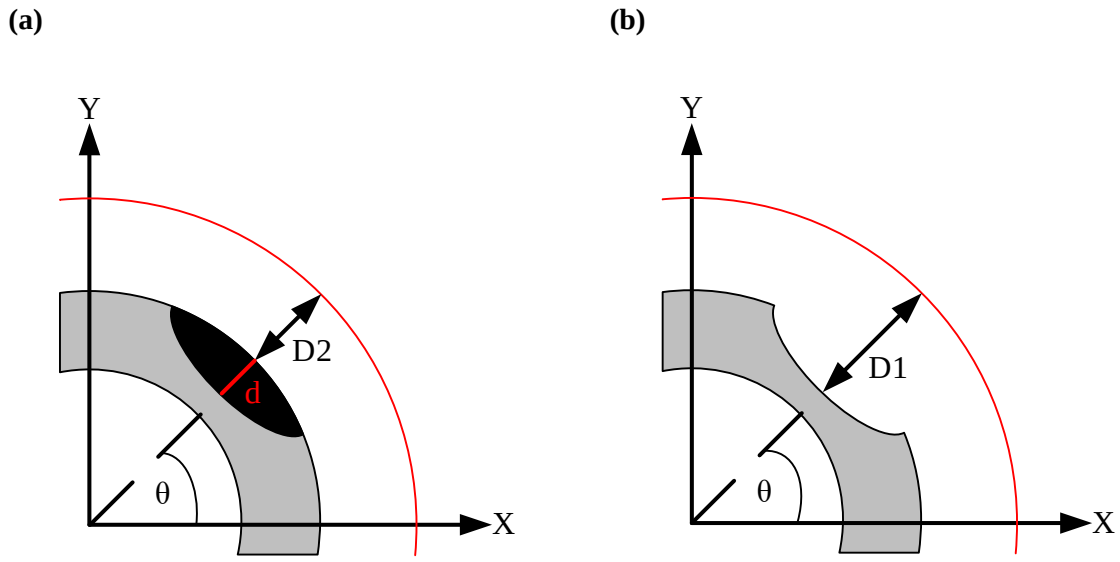

Figure 7.13 - Diagrammatic representation of the radial defect measurement: (a) outer 3D model before the corrosion been removed and (b) inner model captured after the corrosion has been removed. The red cylinder indicates the arbitrary cylinder used during processing.

$$d_{\theta,Z} = D_{1,\theta,Z} - D_{2,\theta,Z} \qquad \text{Equation 7.1}$$

The individual values for D1 and D2 for all angular and axial points was calculated using a custom plug-in for Artec Studio v10. The software measures the normal distance from the centre of each facet of the reference mesh to the point where it intersects the scan mesh. Unlike Geomagic Verify, Artec Studio v10 does not require the measurement to intersect a node on the scan mesh. Where the normal intersects a facet on the scan mesh, Artec Studio v10 will calculate the intersection coordinates from the surrounding nodes on the mesh to produce a distance measurement to that point exactly.

The two appropriate text files, detailing the XYZ position of each reference measurement, needed to compute the condition defect of interest were fed into a custom Matlab program. Provided that the reference cylinder has been aligned correctly, all measurements carried out with the same arbitrary cylinder will share a common set of XYZ coordinates over which measurements were made, thus allowing direct comparison to be made. The Matlab program calculated the difference between common axial and angular points between the text files to produce data on the condition defect of interest, Figure 7.13 and Equation 7.1. Furthermore, Matlab was used to produce contour maps of these condition defects as required. Given that the most extensive corrosion is often found at the invert of the pipe, it was decided that the contour plot should easily report the corrosion thickness across the invert and hence it was decided that the pipe data should be cut along the crownline such that the invert data is centred vertically on the contour plot.

7.5.5 External Corrosion Results

The data shown in the coarse colour-map in Figure 7.11(c) has been processed following the method detailed in the previous section to give a flattened contour plot which details the external corrosion across Specimen Two, Figure 7.14. The spread and depth of the graphitic corrosion is clear to see and several pits indicate significant corrosion thickness of greater than 5 mm. As well as corrosion pits, there are several points where the corrosion was so extensive that it progressed through the pipe wall and when removed, during the shot-blasting process, left a hole in the specimen.

In order to ensure that the external corrosion measurements gathered by the 3D scanner are accurate, and that the technique gives a representative corrosion thickness that is in keeping with the methods currently in use in the water industry, manual pit depths were measured using a depth micrometer. Here the top 10 deepest pits, as judged by the inspector, were measured using a depth micrometer. Their position can be seen overlaid on Figure 7.14. The corrosion thickness recorded at each position by the inspector is given in Table 7.1. The corresponding corrosion thickness at these reported positions on the 3D scanner's contour map, Figure 7.14, as measured by the 3D scanner, were also read off and are given in Table 7.1.

Each micrometer measurement refers to the deepest corrosion thickness of a pit, however, on closer examination it can be seen that the points measured with the depth micrometer do not align exactly to points on the 3D scanner's contour plot where the maximum pit thicknesses are shown, Figure 7.14. Further, the initial results show a difference between the corrosion thicknesses measured using a micrometer and the 3D scanner: these are up to 1.6 mm, i.e. one eighth of the nominal wall thickness. These inconsistencies are due to changes in the circumference of the pipe. Here, the positions captured by the depth micrometer measurements were made after the pipe was shot-blasted and would be subject to a reduction in the outer pipe circumference, whereas the 3D scanner position measurements are derived from the larger original circumference present pre-shot-blasting.

On closer examination of Figure 7.14, it can be seen that each depth micrometer measurement lies on the periphery of a corrosion pit reported by the 3D scanner. Hence, it is likely that these corrosion thickness measurements refer to the same corrosion pits measured by the 3D scanner, albeit the positions are offset due to errors induced when measuring their position. Consequently, the coordinates of each depth micrometer measurement have been adjusted to match the deepest corrosion thicknesses reported by the 3D scanner. This is indicated graphically in Figure 7.15. Here the circles close to each black dot indicate the site of the adjusted corrosion thickness measurement. The corrosion thicknesses at these corrected positions are displayed in the fourth column of Table 7.1. A final column shows the difference in corrosion thicknesses between the depth micrometer measurements and the 3D scanner measurements for the corrected positions. A much better fit between the corrosion thicknesses is observed with the majority of pit measurements showing deviations of 0.4 mm or less.

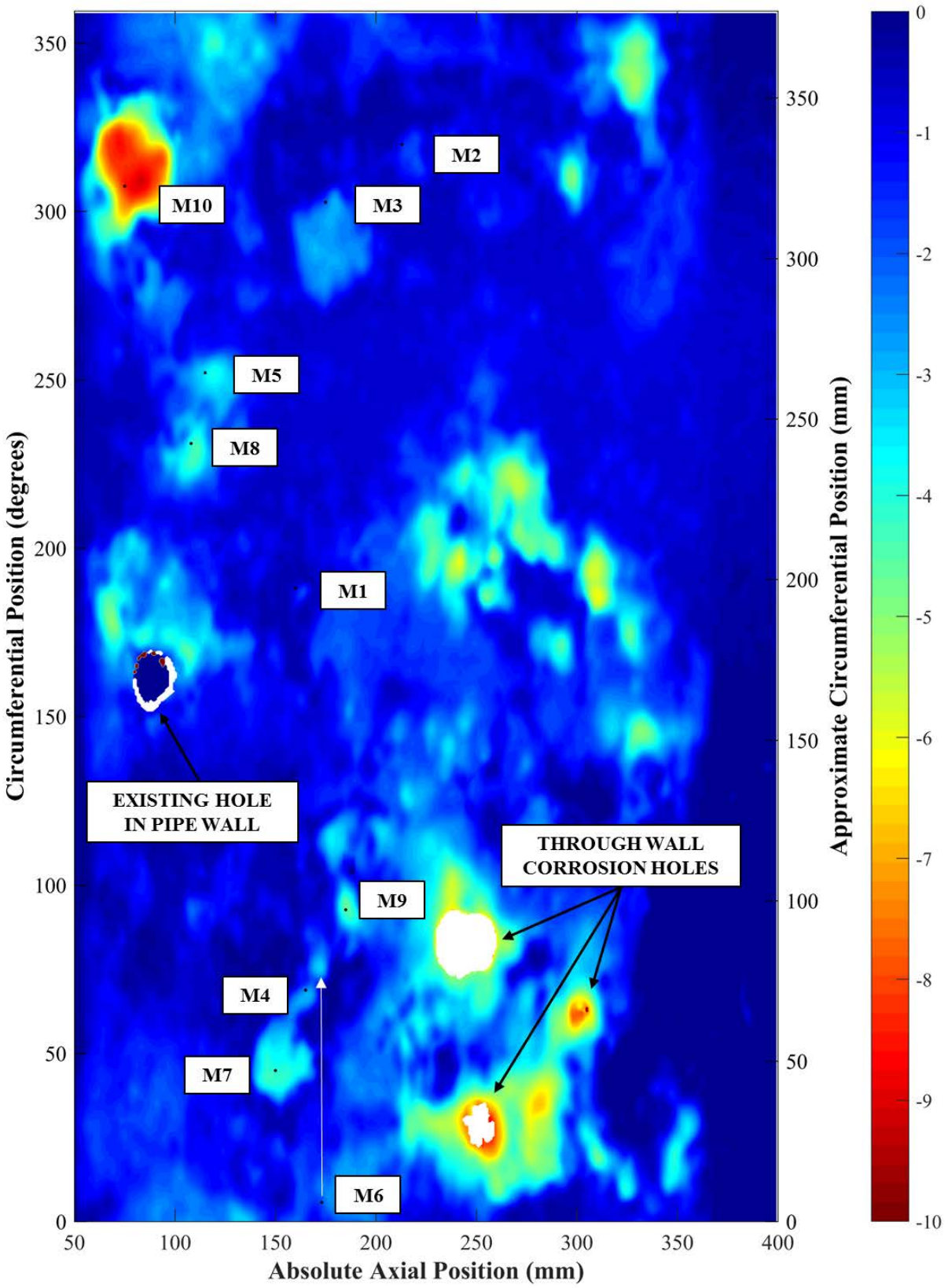

Figure 7.14 - Contour plot showing the external corrosion thickness for Specimen Two as measured by the Artec Eva 3D scanner. The black dots indicate the location of each numbered manual pit depth measurement. The numbers indicate the 10 deepest corrosion thicknesses, in ascending order, given in Table 7.1.

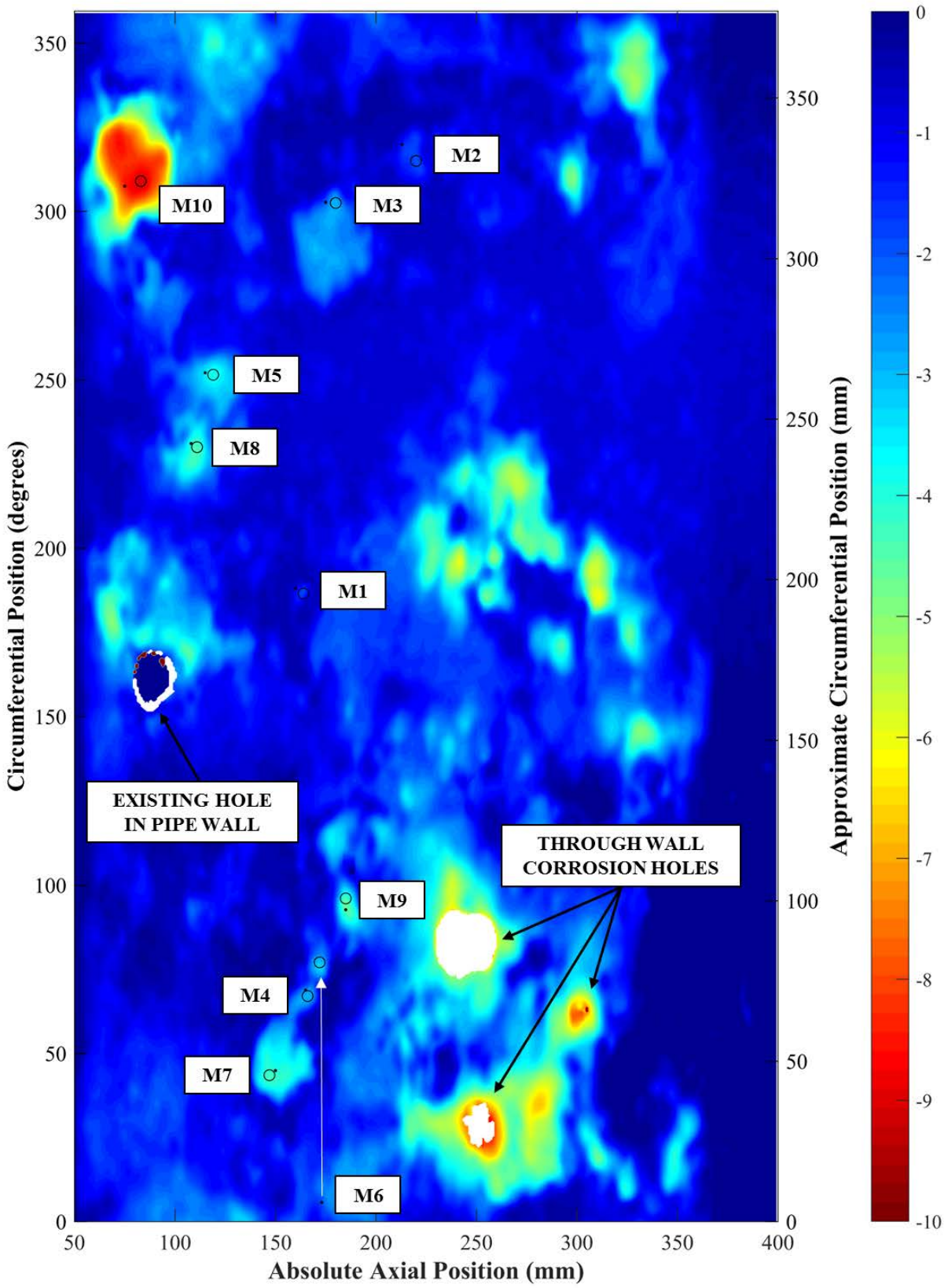

Figure 7.15 - Contour plot showing the external corrosion thickness for Specimen Two as measured by the Artec Eva 3D scanner. The black dots indicate the location of each numbered manual corrosion thickness measurement and the black circles indicate the location of the deepest external corrosion neighbouring the manual thickness measurement. The numbers indicate the 10 deepest pits, in ascending order, reported in Table 7.1 and the arrow indicate the position of the coordinate correction.

Table 7.1 - The ten (10) deepest external corrosion thickness measurements captured using a depth micrometer and the corresponding reported and corrected corrosion thickness measurements derived from the 3D scanner data for Specimen Two. The final column indicates the difference in corrosion thickness measurements made by the depth micrometer and the 3D scanner at corrected positions.

Pit Number	External Corrosion Thickness (mm)			
	Depth Micrometer	3D Scanner at Reported Position	3D Scanner at Corrected Position	Difference
M1	1.8	0.9	1.8	0.0
M2	2.0	1.4	2.0	0.1
M3	2.6	2.0	2.9	-0.3
M4	3.0	2.5	2.9	0.1
M5	3.4	3.5	3.8	-0.4
M6	3.4	1.9	3.1	0.4
M7	3.8	4.0	4.3	-0.5
M8	4.0	4.0	4.4	-0.4
M9	4.4	4.5	4.4	0.1
M10	9.3	8.3	9.1	0.2

It may be noted that the reported position of pit M6 was not close to the pit it measured. The location of each pit depth measurement was marked on the pipe sample as a permanent record, Figure 7.16. When compared to the 3D scanner contour map given in Figure 7.16, it can be seen that the position of pit M6 is wrong and hence its position has been corrected in line with the sites given in Figure 7.16.

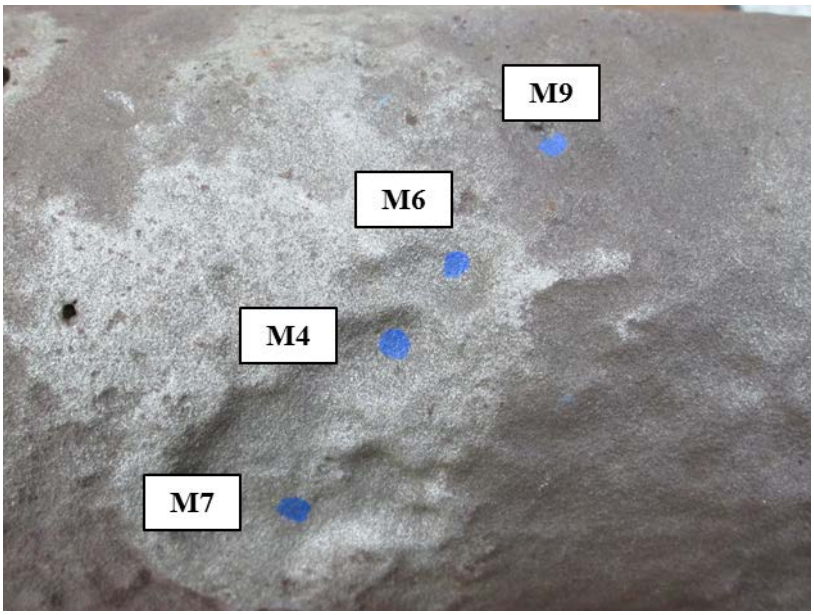

Figure 7.16 - Close-up view of the shot-blasted surface of the 4" distribution main where the corrosion depth measurements for pits M4, M6, M7 and M9 were measured using a depth micrometer. The blue dots indicate the exact location of each measurement.

The results suggest that the 3D scanner has successfully measured the corrosion thickness across the pipe section and produces corrosion depths that are in keeping with those measured using a depth micrometer, which is the industry standard.

Closer inspection of the external corrosion thicknesses measured by the 3D scanner suggests that the measurements measured manually using a depth micrometer do not represent the 10 deepest pits. Figure 7.17 shows an updated contour plot which shows the 10 deepest pits as determined by the 3D scanner. Here it is clear to see that pits chosen by the 3D scanner are different from those reported using the depth micrometer with only one pit, M10/S10 common between both. Table 7.2 details the corrosion thickness for each of the 10 deepest corrosion thicknesses measured by the 3D scanner. When compared to the values reported in Table 7.1 for the depth micrometer, it is clear to see that the corrosion thicknesses measured differ significantly. Apart from one reading, all of the corrosion thicknesses calculated by the 3D scanner are over 5 mm in depth. Even this reading is approaching 5 mm. Conversely, the manual depth micrometer only records one pit as being greater than 5 mm in depth, i.e. gathering all of the data can identify deeper pits than the traditional manual method.

Table 7.2 - The 10 deepest external corrosion thicknesses as measured using the 3D scanner

Pit Number	Pit Depth (mm)
S1	4.9
S2	5.0
S3	5.0
S4	5.0
S5	5.2
S6	5.5
S7	5.9
S8	6.1
S9	6.7
S10	9.1

Corrosion thicknesses of 4 mm or more are of potential interest as this value marks the transition from inherent material defects, such as the graphite flake size, to external defects, such as corrosion defects, as the dominant reason for failure (Atkinson *et al.*, 2002). Whilst there are many corrosion thicknesses greater than 4 mm present on the pipe, only a few of these corrosion thicknesses have been detected by the depth micrometer whereas all of the measurements made by the 3D scanner are over this threshold. This has significant implications as the depth micrometer measurements are used to characterise the severity of the corrosion present on an exhumed sample, which can infer the condition of the pipes adjacent to the exhumed sample. However, the severity may be underestimated as the depth micrometer measurements may be skewed due to the maximum corrosion thicknesses being ignored.

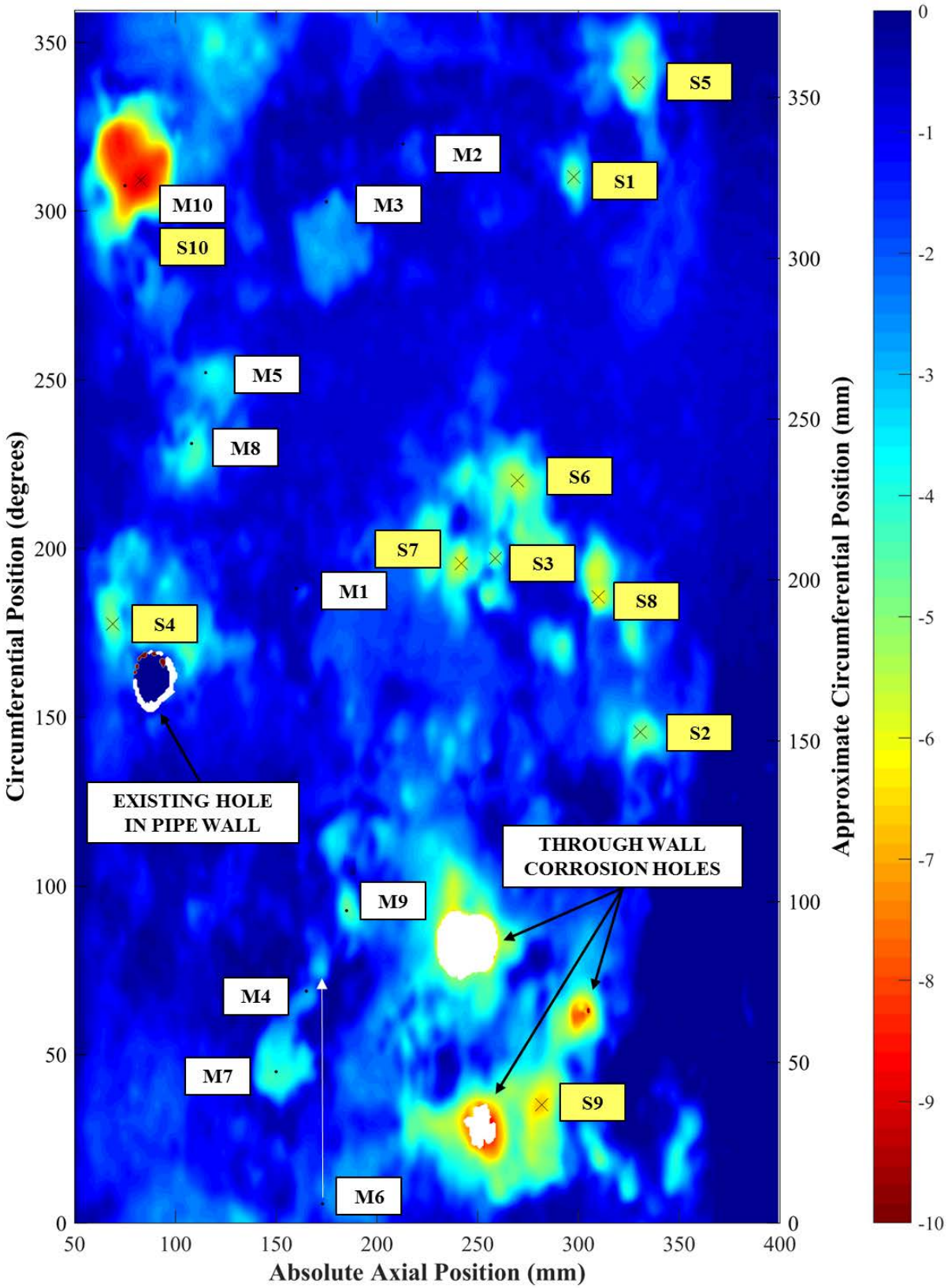

Figure 7.17 - Contour plot showing the external corrosion thickness from the 4" distribution main measured by the Artec Eva 3D scanner. The black dots indicate the location of the 10 deepest pits as measured using a depth micrometer. The black crosses indicate the location of the 10 deepest pits as measured by the 3D Scanner. The numbers indicate the relative pit location (white for depth micrometer and yellow for 3D scanner) and are ranked to show the deepest pits in ascending order.

These differences in distribution are likely to occur as the surface of the pipe where the depth micrometer can be used is limited. Figure 7.18(a) illustrates an example of a cluster of pits where a measurement using the depth micrometer was not possible. Conversely, there were no areas on the inspected pipe section that were unable to be measured by the 3D scanner. The corresponding corrosion thickness, as measured by the 3D scanner, for the pits shown in Figure 7.18(a) can be seen graphically in Figure 7.18(b). Here, the 3D scanner has demonstrated that it is capable of measuring the corrosion thickness in challenging areas where the traditional depth micrometer cannot. Further, several of the deepest corrosion pits were identified by the scanner in this range. These were not captured by the manual pit depth measurements, even if they were identified by the inspector. Consequently, the manual pit depth measurements obtained using the traditional method are likely to present a skewed picture of corrosion.

(a)

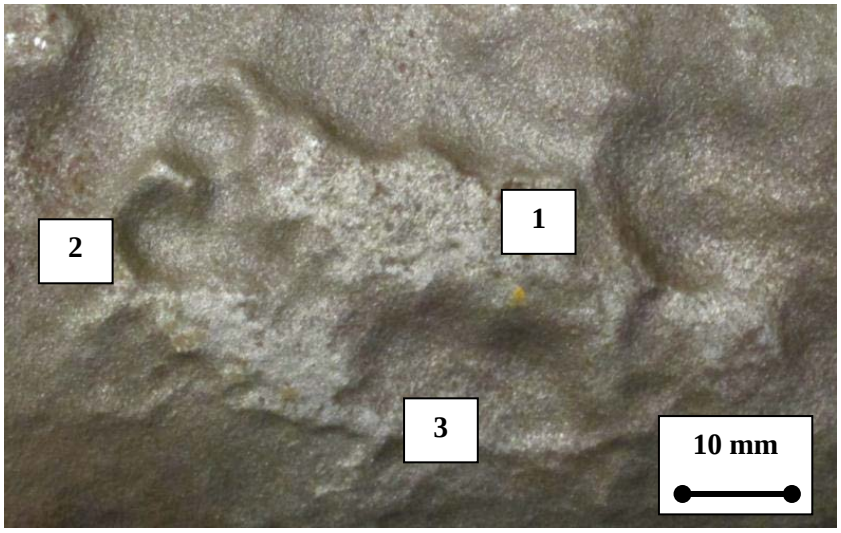

(b)

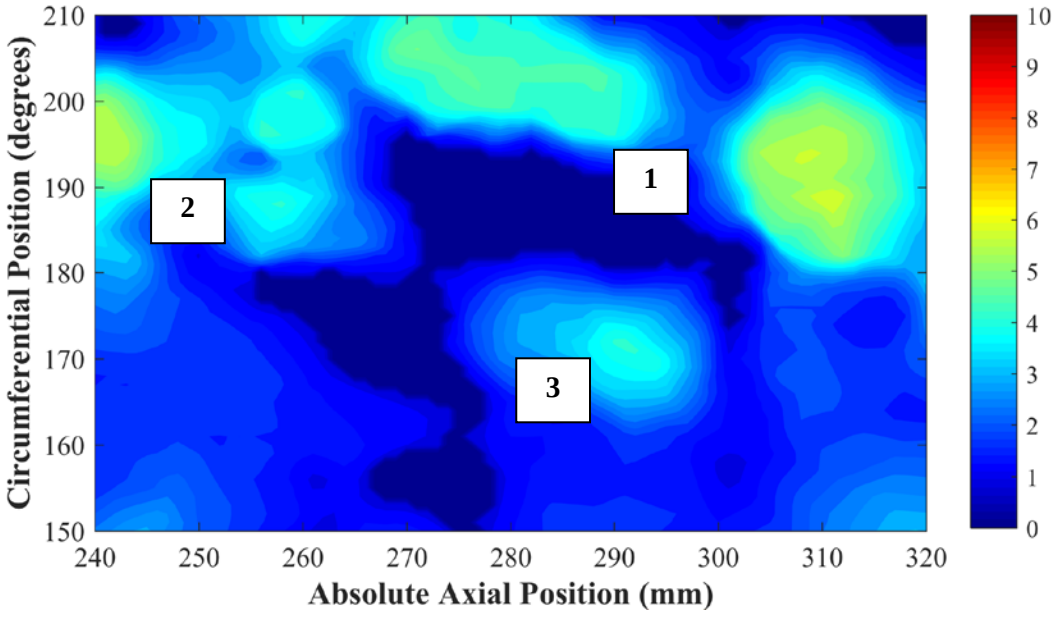

Figure 7.18 - Two images showing the same corrosion pits on the distribution main that cannot be measured using a depth micrometer. a) A digital image showing a close-up of the pits. b) The corresponding corrosion thickness as measured by the 3D scanner. The numbers indicate common features between each image.

Closer examination of these pits showed that the pits in question are greater in depth than all but one of the pits reported by the depth micrometer. Further, the 3D scanner shows that it is not hindered by difficult geometry and is capable of measuring any corrosion pits across the entire surface of the pipe. Consequently, a more representative estimate of the 10 deepest corrosion pits is obtained. Ultimately the 3D scanner provides a more complete view of the pipe condition as the corrosion thickness measurements made using the pit depth micrometer are not representative of the sample and, whilst certain areas may be identified by an inspector as an area of potentially deep corrosion, they cannot be quantified using a depth micrometer.

7.5.6 Summary

In this section, a method of scanning a pipe has been developed to record the geometry before and after shot-blasting to remove any error induced though deviation measurements made to the poor fitting of additional reference geometry. The initial results reported in Figure 7.14, Figure 7.15 and Figure 7.17 have shown the external corrosion thicknesses for a distribution main as measured by the 3D scanner. These measurements have shown good correlation with the current industry standard pit depth measurement. Further they have shown that pit depth measurements should not be relied on to give a full picture of the condition of a pipe as corrosion pit geometry may not lend itself to measurement with a depth micrometer. The 3D scanner has been able to characterise all of the external corrosion and has reported the top 10 corrosion thicknesses. Further, the results showed that more rigor is needed when analysing areas of through wall corrosion.

The in-built method of conducting deviation measurements in Geomagic Verify was not valid for the shape being inspected. Consequently, a custom plug-in was commissioned for Artec Studio v10 which allowed the measurements captured by the surface measurements in the program to be exported. The updated method allowed radial measurements from a datum cylinder around the pipe scan to be taken, before and after shot-blasting, and compared to infer the corrosion thickness. Whilst this methodology is more time consuming due to the increased number of scans required, and the downtime when the pipe is being shot-blasted, it has proved to be capable of successfully evaluating the external corrosion on the small test sample. As it was not possible to shot-blast the inner surface of the distribution main, the exercise was only able to test the scanners ability to measure external corrosion thickness and position. It was not possible to evaluate the scanner's capability to measure inner corrosion thickness and position or the remaining pipe wall thickness.

This work was conducted on a section of distribution main and, whilst useful, it is imperative that the technique is capable of functioning on a much larger trunk main section. With a surface area of almost 10 times that of a distribution main, the potential amount of external corrosion that could be measured would overload a contractor conducting pit depth measurements. Here the scanner has great potential to improve the real condition data gathered on the condition of a pipe. In the next section, the methodology evaluated previously is tested to see whether it is capable of working on a much larger section of trunk main. It is further refined to capture additional data, such as the internal wall thickness and the internal corrosion that could not be captured before.

7.6 Testing New Method on Full Size Trunk Main

7.6.1 Background Requirements

In moving from a small section of distribution main to a much larger (1 m long, or possibly more) section of trunk main, more constraints on the methodology are encountered. The methodology must also be capable of fitting around the needs imposed by the NDE contractors as well as the limitations of the 3D scanner. Further limitations imposed by the pipe shot-blasting contractor, the pipe stock available for testing and the capabilities for handling large sections of pipe on the Thames Water site were also taken into account. Consequently, a list of background requirements was generated before this technique was scaled up. The surface condition requirements for any NDE contractor can vary significantly and it is not possible to account for every requirement they may present at the very outset. Consequently, the guidelines were based on experience gathered from inspections conducted by NDE contractors which the company has used previously. When collated, the final methodology was left open, should any flexibility be needed to accommodate any requirements a new contractor may impose. These restrictions were:

- Testing was limited to the collection of 42” and 36” pipes stored at Kempton Park WTW in which the position of the corrosion was unknown.
- Pipe sections should be limited to being less than two tonnes to ensure that the mechanical lifting equipment on site can lift the pipe section and manoeuvre it into place.
- A minimum of 1.6 m long of section of pipe available to support their scanning frame which captures a 1 m section of NDE.
- Surface preparation would need to be carried out by the contractors, which in past experience can be extensive, and the changes made by this would need to be captured.
- Any pipes that would need to be cut (including for the purpose of introducing reference markers) must be capable of being cut by one man with a petrol disc cutter.
- The shot-blasters could not fully access the inside and outside of a pipe fully if it was no more than 1 m long for a diameter of 30” without splitting the pipe. Longer lengths were tolerable if the diameter could be increased.
- Scanning needs common geometry to be able to realign the models after any changes to the pipe sections.

These restrictions were taken into account and a process to map the corrosion from the pipe samples was created. During this testing, the methodology was fine-tuned to enable the 3D scans to be taken as needed given the constraints mentioned above and any further restrictions encountered during testing. Over the next sections the application of this methodology, and the 3D models created from it, are detailed. From these models, the external corrosion and other important condition data is inferred. The findings from this work have allowed a final methodology that can be used to conduct a live NDE contractor trial to be created. This is given at the end of this chapter.

7.6.2 Pipe Sample

A further section of trunk main was obtained to verify that the updated method, demonstrated on the section of distribution main, was capable of functioning on a full-sized trunk main section. This section was cut from a much longer section of 42" trunk main that had been exhumed from the Olympic Park during the pipe replacement project. This sample is referred to as Specimen Three. The specimen was cut to 1.8 m long using a petrol disc cutter, Figure 7.19. A crownline was marked along the specimen to give a reference vector from which measurements can be made.

In the case of a live comparison exercise, it is beneficial if this is the actual crownline, marked when the pipe is exhumed, as this can help to reference the position of the corrosion captured in the 3D scans. Two v-notches were cut into the Specimen Three: one at each end of the crown line. The geometry of these notches is not prescriptive, however, the notch must not encroach into the specimen more than 100 mm. It is also advised that the angle of this v-notch is greater than 90 degrees to ensure that the 3D scanner can fully illuminate the wall cross-section. Failure to do this can result in the notch geometry being poorly resolved in each 3D model and ultimately the alignment between each scan becomes poorer.

Figure 7.19 - Specimen Three.

7.6.3 Initial Methodology

The process to capture the "ground truth" pipe condition, and any pipe changes due to the NDE contractor, has several stages and requires the pipe specimen to be reduced in size after the NDE inspections have been carried out. This is to ensure that there is sufficient length available for an NDE contractor to be capable of conducting their investigation, but also to ensure that the specimen is short enough to remove the internal corrosion fully during the shot-blasting process. Unlike the initial comparison carried out on a distribution main, where only

two scans were needed, the methodology developed for use on a trunk main section requires several further steps. Whilst several of these steps provide further insight into specific pipe condition, such as the remaining wall thickness present across a pipe section, other steps have been added to allow any changes in geometry, due to the pipe reduction, to be recorded. This ensures that changes made to the pipe do not result in all of the common geometry between scans being removed such that 3D models created from consecutive stages of the exercise cannot be aligned to the common coordinate system. A diagrammatic representation of the main stages of the methodology are given in Figure 7.20.

Whilst this methodology is designed to capture the "ground truth" pipe condition, the 3D scanner has the potential to capture other information based on geometric data that could be difficult to collect by hand. For example, it has always been questionable whether adherent surface encrustation promotes the formation of external graphitic corrosion or if internal tuberculation performs a similar role internally. Prior to its use, this technique was evolved to allow the position and thickness of the internal tuberculation and external encrustation to be measured. Consequently, the pipe is scanned immediately after it is first cut to capture the adhering encrustation. The encrustation is then removed using an angle grinder fitted with a wire wheel leaving a nominally smooth surface that can be considered to be the original pipe surface.

To ensure that there is common reference geometry in each 3D model, to allow alignment of each of the 3D models, the surface within a 10 cm ring at each end of the pipe was left uncleaned. The pipe section was then scanned again to record this change. At this point the pipe is ready for NDE to be conducted. Once NDE was conducted, the pipe was scanned again, to capture any changes to the pipe surface that may have occurred during the surface preparation for the NDE. This approach ensures that the level of surface preparation conducted by a contractor can be recorded.

By using this approach, it is possible to compare more than one contractor. Here, the pipe should be scanned after each contractor has carried out their NDE to record any change between contractors. In this trial, no contractors were brought in to carry out any NDE. Instead, the surface preparation was imitated in-house using, the same methods employed by a contractor. A poly-abrasive wheel fitted to an angle grinder was used to prepare the pipe surface. Where possible, the abrasive wheel was used to excavate the graphitic corrosion in a similar fashion to that experienced in previous comparison exercises.

Following NDE, the pipe section was cut down to a manageable length before being sent for shot-blasting. In doing this, the original v-notch markers and external untouched end rings were removed leaving no common geometry which can be used to align further 3D models. As a consequence, further markers were cut into the pipe section which align axially with the original v-notches, Figure 7.21(a). A selection of diamonds, Figure 7.21(b), and squares, Figure 7.21(c), nominally 200 mm axially by 200 mm circumferentially in size, were cut into the pipe section with their centres 300 mm in from each end. A total of four markers were cut into the pipe at angles 0, 90, 180 and 270 degrees to the crownline at each end of the pipe.

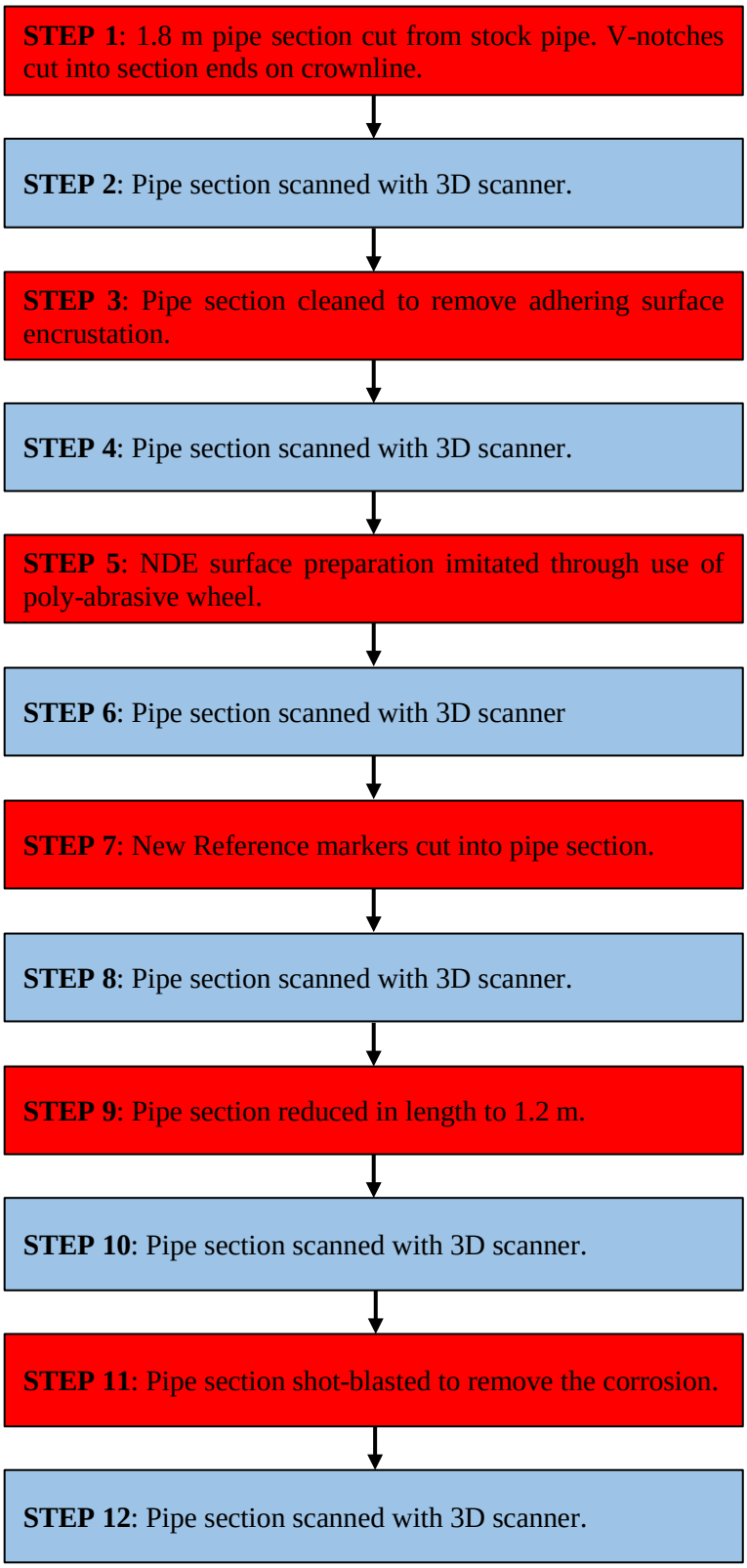

Figure 7.20 - Diagrammatic representation of the steps taken to conduct a trial of the initial methodology for capturing the real pipe condition on a large section of trunk main. The red boxes indicate steps where changes to the pipes geometry are made and the blue boxes indicate steps where the pipe section is scanned.

(a)

(b) **(c)**

Figure 7.21 - Additional reference markers cut into Specimen Three: (a) the complete pipe section with reference markers, (b) a close-up of a diamond marker and (c) a close-up of a square marker.

Once these markers were cut, the pipe was reduced in length to 1.2 m long leaving half of the reference marker geometry cut into the section, Figure 7.22(a). The pipe was scanned again, before being sent off for shot-blasting. Prior to shot-blasting the inner and outer end 100 mm rings are masked off, again to preserve the common pipe geometry using cloth tape, Figure 7.22(b). The pipe was scanned again once returned, and the models were compared to ascertain the “ground truth” condition.

(a) **(b)**

Figure 7.22 - Reduced length of Specimen Three being prepared for shot-blasting: (a) after length reduction following the reference markers being cut in and (b) with ends being preserved prior to shot-blasting.

7.6.4 3D Scanning Models

In Figure 7.23, six 3D models are displayed from each stage of the exercise. It can be seen that each model was successful and provides a representation of the pipe geometry present at that the stage. Initially a 3D model of the pipe as cut from the pipe was captured, Figure 7.23(a). This model provides a starting reference of the condition of the pipe after exhumation including the encrustation adhering to the outer surface. Here the pipe has had v-notches cut into each end to provide known reference geometry. The model shows that the surface encrustation is well resolved and can be easily identified. Further, the additional reference geometry is also visible and well resolved. It is also possible to see any tuberculation present across the inner surface of Specimen Three. A second 3D model of the pipe was created after the external encrustation had been cleaned off, Figure 7.23(b).

During the development of the methodology, no NDE contractors were used to conduct any surface preparation. Instead, the surface preparation was conducted in house to mimic that carried out by the current NDE contractors. A further 3D model was created to capture the geometric changes on the pipe section caused by the NDE surface preparation, Figure 7.23(c). Two large indentations can be clearly seen on the outer surface of the pipe where the surface preparation has been conducted.

Figure 7.23(d) shows a 3D model of the pipe after further reference markers were cut into it to replace the original v-notch markers that were lost after the pipe was reduced in length. The 3D model shows that the additional reference geometry is captured and well resolved. Figure 7.23(e) shows a 3D model of the pipe section after it was reduced in length to 1.2 m. The final scan after shot-blasting has been conducted is given in Figure 7.23(f). Here the pitting resulting from the removal of the graphitic corrosion can be clearly seen.

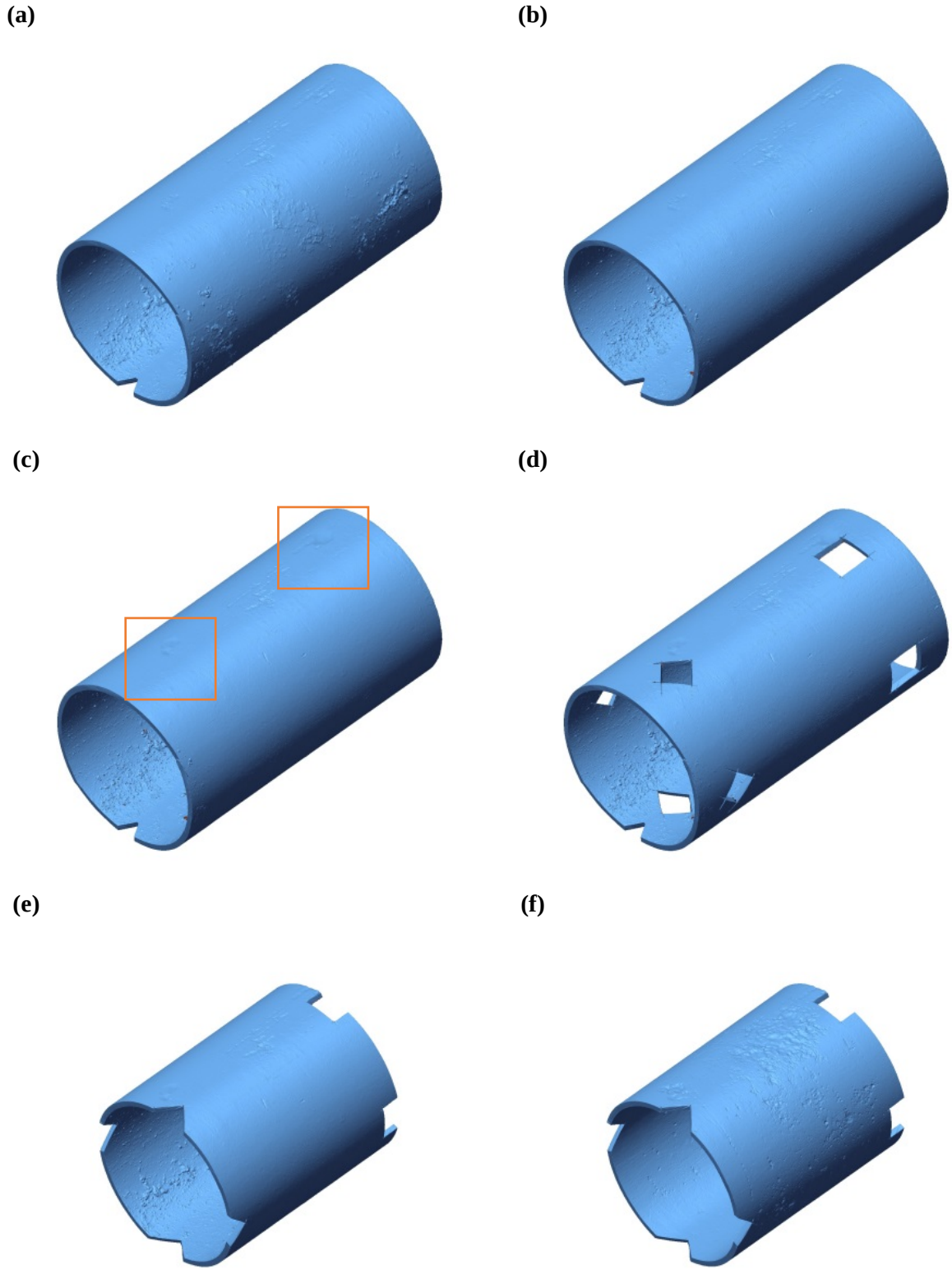

Figure 7.23 - 3D models of Specimen Three at 6 different stages of the process: (a) Stage 1 before cleaning with encrustation in tact, (b) Stage 2 after encrustation removal, (c) Stage 3 - After NDE has been conducted, (d) Stage 4 after the addition of reference markers. The red squares indicate the location of the surface preparation, (e) Stage 5 after pipe length reduction for shot-blasting and (f) Stage 6 after shot-blasting.

7.6.5 Data Post-Processing

Following the capture of the 3D models, each model was individually aligned to the global coordinate system as described in Section 7.5.4. The differences between the models were compared in the same fashion to that described for the distribution main to provide pipe condition data, such as the external corrosion. However, in this exercise it is no longer a case of comparing two models to obtain the condition data. Table 7.3 shows the two 3D models that were compared to determine the condition defect of interest.

Table 7.3 - The condition defect of interest and 3D models compared to determine it.

Condition Data	Outer 3D Model	Inner 3D Model
External Corrosion	Outer Trunk Main Surface After Encrustation Removal	Outer Trunk Main Surface After Shot-blasting
Remaining Wall Thickness	Outer Trunk Main Surface After Shot-blasting	Inner Trunk Main Surface After Shot-blasting
External Encrustation	Outer Trunk Main Surface Before Encrustation Removal	Outer Trunk Main Surface After Encrustation Removal
Surface Preparation	Outer Trunk Main Surface After Encrustation Removal	Outer Trunk Main Surface After NDE
Internal Corrosion (Could Not Be Separated in this analysis)	Inner Trunk Main Surface After Shot-blasting	Inner Trunk Main Surface After Tuberculation Removal
Tuberculation (Could Not Be Separated in this analysis)	Inner Trunk Main Surface After Tuberculation Removal	Inner Trunk Main Surface Before Tuberculation Removal

7.6.6 External Corrosion Results

Once the pipe had been shot-blasted, the results for the external corrosion were generated by comparing the 3D models captured once cleaned and after shot-blasting. The external corrosion present is plotted in Figure 7.24. The plot shows the methodology is capable of capturing external surface corrosion in a similar fashion to that conducted on a distribution main even when deployed to a trunk main. In particular, the 3D scanner has managed to capture certain corrosion features, such as the presence of a chain or band on one side.

To ensure that 3D scanning is still capable of capturing accurate corrosion thicknesses without being skewed by the increased size of the pipe section, manual pit depth measurements were again captured, as was done for the distribution main. However, due to the significant increase in external surface area in moving to a trunk main, the number of pit depth measurements taken was increased to provide a better corrosion pit depth sample to compare the 3D scanner results against.

The larger surface also made it more challenging to capture the manual pit depths. When operating on a distribution main section, it was possible for the inspector to observe the full outer surface and judge which were the top 10 deepest. However, when inspecting Specimen Three, it was not possible to observe the pits in the same manner. The greater surface area is too large for an inspector to focus on and accurately judge which pits were the deepest. To combat this problem, a method of subdividing the trunk main surface into smaller

more manageable areas, similar to that employed by many of the NDE contractors, was used to conduct a manual pit depth inspection. The pipe was split into 12 longitudinal strips nominally 30° in span. This is often described as a "clockface". These longitudinal strips provided the inspector with a smaller area to focus on and allowed 20 of the deepest pits in each strip to be recorded, thus giving a total of 240 pits. As per the pit depth analysis conducted on the distribution main, the axial and circumferential position of each pit was captured, as well as its depth. When attempting to plot the location of the pits against the results measured by the 3D scanner, it was not possible to find an agreement. There are two reasons for this: the axial measurements of the manual measurements have an associated positional error since the cut end of the pipe from which they were measured is not straight. Further the circumferential measurements change as the tape measure used by the inspector conforms directly to the shot-blasted geometry rather than the original pipe surface as the 3D scanner does. To combat this, the pit measurements were manually adjusted as described in the Section 7.5.4. The corrected position of each of these pits measured during the analysis have been plotted on Figure 7.25 as red circles. The boundaries of each strip are also given as horizontal white lines denoted by a letter from A - L.

The pit depths at each adjusted location were measured from the 3D data and compared against that provided by the pit depth inspector. The differences in measurement have been plotted as a histogram in Figure 7.26. The differences in pit depth measurement have been grouped to the nearest 0.1 mm. It can be seen that the distribution can be approximated to a normal distribution and has a mean difference of 0.57 mm and a standard deviation of 0.85 mm. Closer inspection shows that 75% of the difference measurements are within 1 standard deviation of the mean and 98% of the differences are within 2 standard deviations of the mean.

This provides good agreement that the 3D scanner produces corrosion measurements that are in keeping with the industry standard method of measuring pipe corrosion by pit depth measurement. Further, it should be remembered that pit depth measurements do not provide an exact value for the corrosion lost. In fact, they are only providing an indicative number based on the assumption that the periphery around the pit from which the depth measurement is made has itself not corroded and is not subject to misshapen geometry. On final inspection of this graph, it can be seen that there are two differences that stand out and away from the general population. At these points, the difference between the 3D scanner measurement and the manual pit depth measurement is greater as it was not possible to align satisfactorily the manual pit depth position to the 3D scanner data. This is the case if the pit depth is small and does not stand out on the corrosion maps.

In a similar fashion to that described for the distribution main, the deepest pits as measured by the 3D scanner have been identified and are drawn as black dots on, Figure 7.25. When comparing these positions, it can be seen that there is some agreement (38% of the points lie on the same position) between the position of the manual pit depth measurement and the points of maximum corrosion thickness measured by the 3D scanner. These results further show that the pit depth measurements made by the 3D scanner are in keeping with the manual method. In fact, several common deep pits are found by each technique. However, many other deep pits are missed by the manual measurement. Here the method of segregating the pipe into strips helps to focus on a smaller area but it can limit the selection of pits that can be made such that it is not representative of the corrosion pitting.

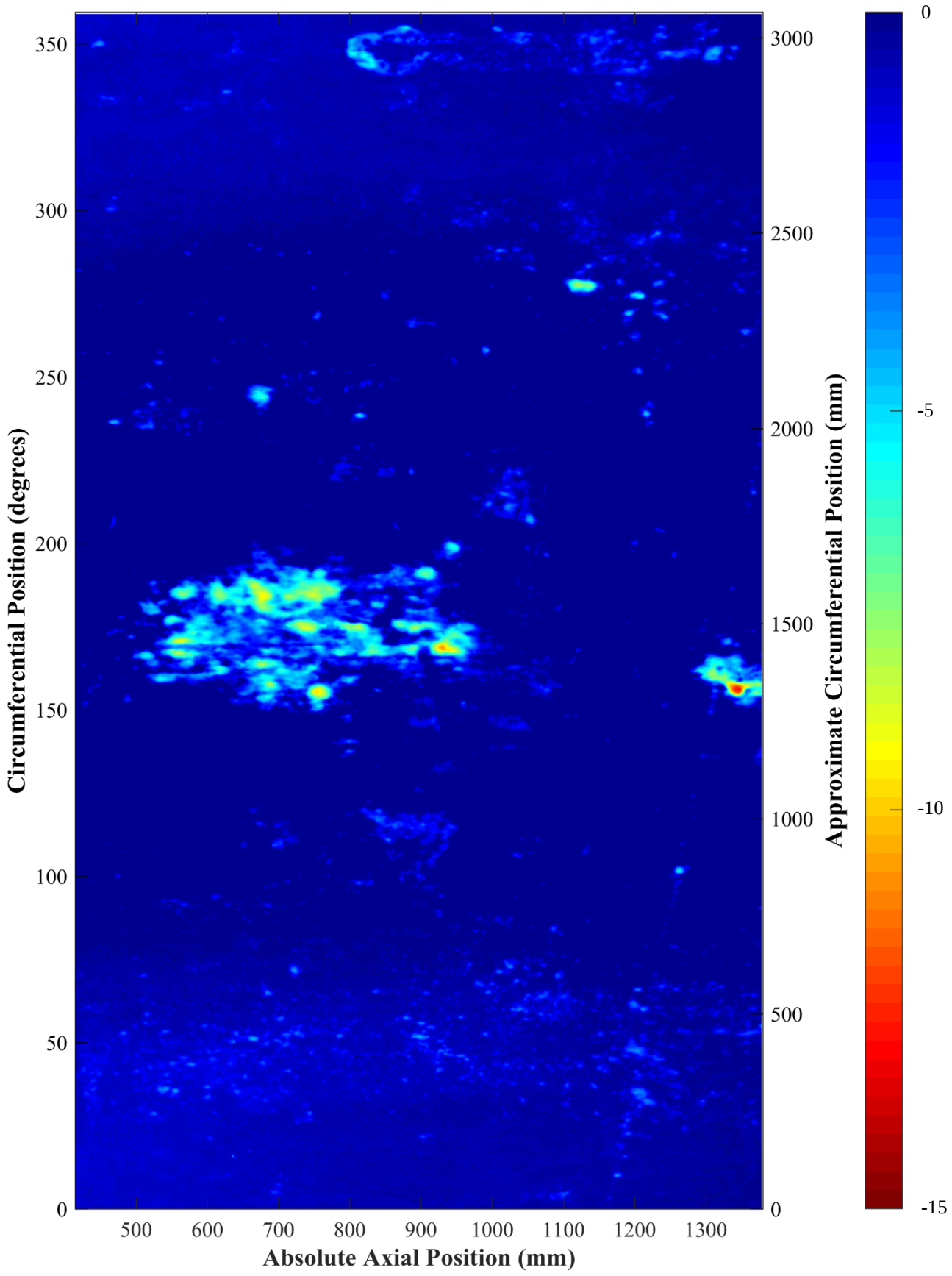

Figure 7.24 - Contour plot showing the external corrosion on Specimen Three as captured by the 3D scanner.

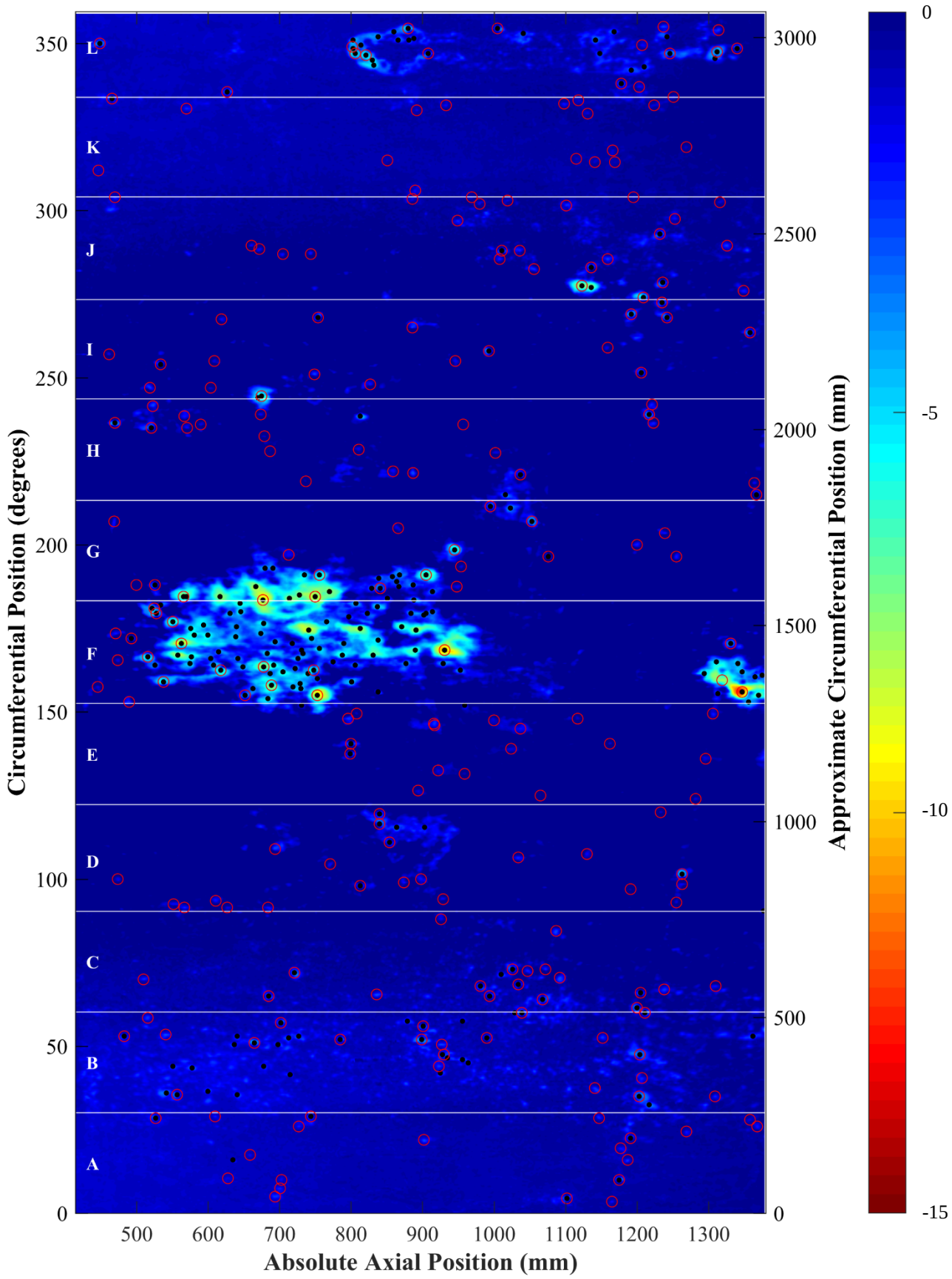

Figure 7.25 - Contour plot showing the external corrosion for Specimen Three as captured by the 3D scanner with the locations of the manual pit depth measurements as red circles. The black dots indicate the deepest pits as measured by the 3D scanner. The white lines mark the boundary of each section used during manual pit depth measurements.

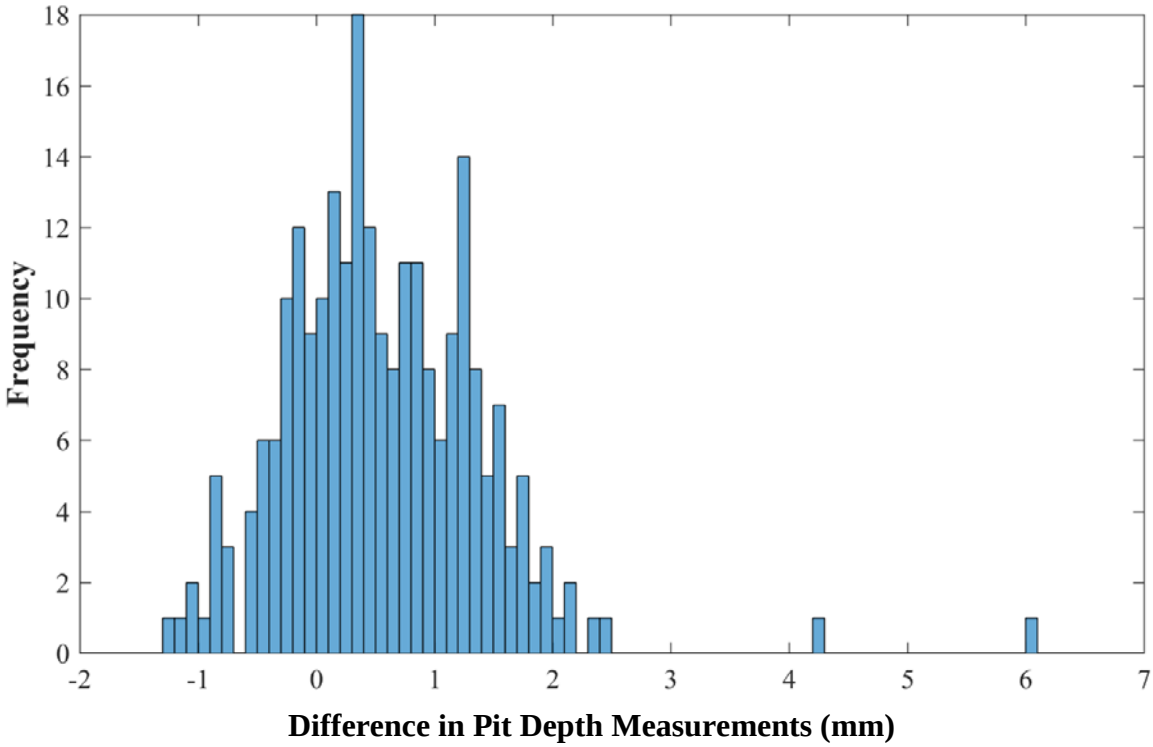

Figure 7.26 - Histogram showing the difference in pit depth measurements captured for the same pits by the manual pit depth micrometer and the 3D scanner. The difference is calculated as the pit depth as measured using the depth micrometer minus the pit depth captured by the 3D scanner.

Examination of the location of the 3D scanned deepest pits shows that approximately 50% lie in sections F and G, on the pipe crown. A further 26% of the measurements are spread over sections B and L. The other measurements are evenly spread across the remaining sections. Having said that, there are many small pits that were identified very close to the areas of deep corrosion pitting within each section that was not chosen. In sections F and G, the pitting may have been too complex to measure, particularly as it has a grooved profile where it was scraped by the excavator during exhumation. Further, the sampling window may still focus on an area too large to be fully appreciated by one inspector. Despite the pit depths not providing full agreement, the manual pit depth measurements did manage to identify the two deepest pits on the pipe successfully. Ultimately, the manual pit depth measurements are not truly representative of the spread of the corrosion thicknesses particularly when the geometry can be complex but they may be capable of providing sufficient information for a Dempsey and Manook (1986) style analysis.

7.6.7 Remaining Wall Thickness and Internal Corrosion

The key output from this work was the ability to be able to map the external corrosion and the surface preparation conducted on the pipe surface. This enables a better understanding of the accuracy of a contractor's results and the amount of cleaning that must be undertaken for a given technique to work. The 3D models have been further processed to enable further pipe condition data to be obtained. Here the pipe wall thickness has been measured after shot-blasting to determine the remaining cast iron thickness. The resulting contour plot showing this thickness is given in Figure 7.27. Here it can be seen that the remaining wall thickness is dominated by the external corrosion lost as many of the areas of reduced thickness are at points where external corrosion has been identified.

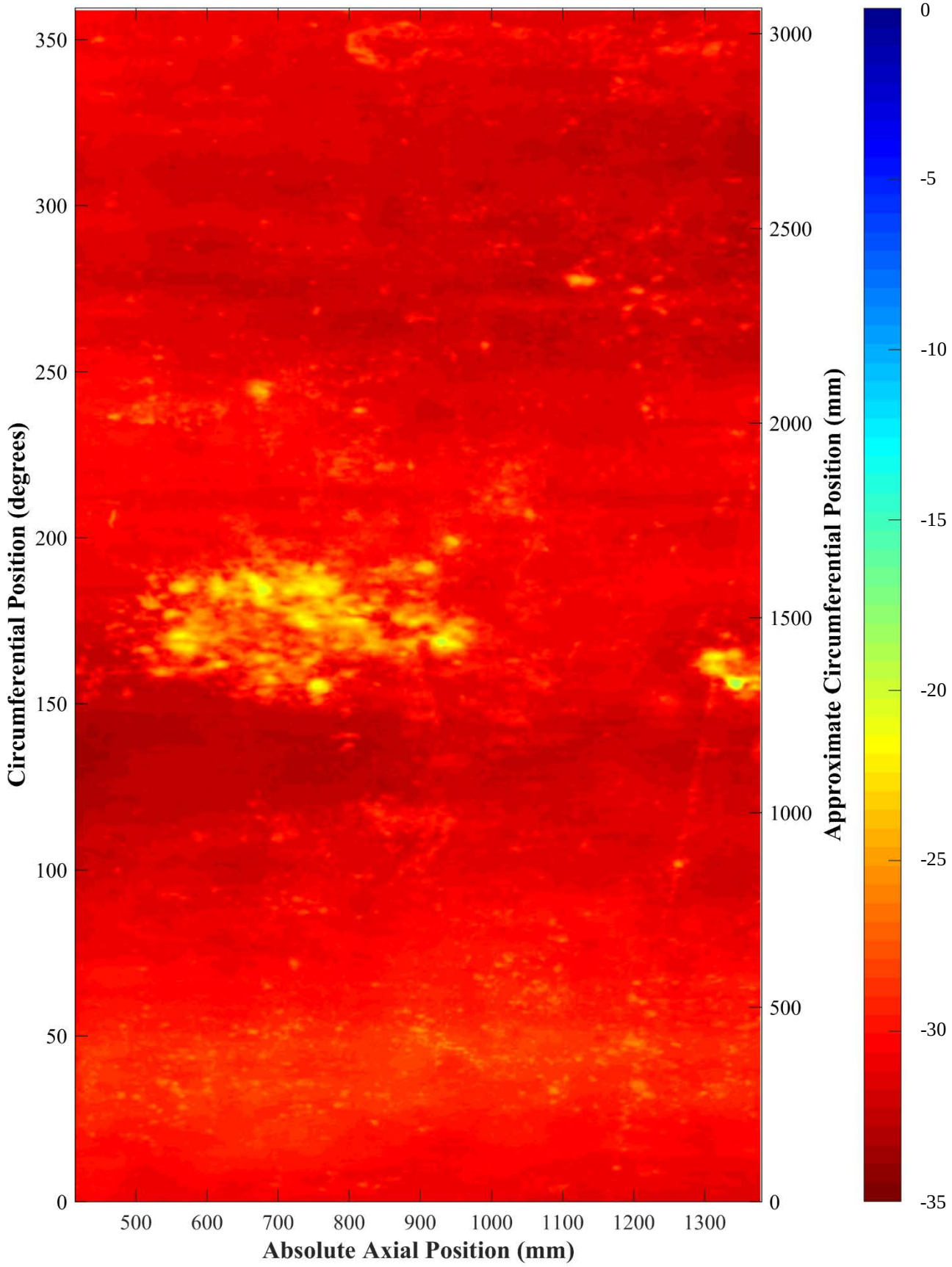

Figure 7.27 - Contour plot showing the remaining wall thickness for Specimen Three as measured by the 3D scanner.

In this test, it was not possible to measure the inner corrosion as the scans captured only recorded the geometry before and after both the tuberculation and internal corrosion was removed. As there was no scan detailing the geometry of the pipe with the internal corrosion but not the tuberculation, it was not possible to separate out the individual thicknesses. A further step which captures the geometry of the pipe with the internal corrosion in place without the tuberculation is needed to ensure this can be measured in future work.

7.6.8 Surface Preparation

As well as capturing the external corrosion, it is imperative that the technique is also capable of measuring the level of corrosion present. In previous comparison exercises, the level of surface preparation conducted has been shown to be aggressive and it has been unclear if the corrosion thicknesses reported are inclusive of the corrosion removed during the surface preparation. In this trial, no contractors were used and the surface preparation was conducted in-house. It was designed to imitate the "craters' that can often be seen after the surface has been abraded. An angle grinder fitted with a poly-abrasive wheel, similar to that used by the contractor in question, was used to prepare the pipe surface.

In this trial, the surface preparation focussed on cleaning distinct patches of graphitic corrosion and uncorroded iron to understand if the material was likely to be removed during the surface preparation and if the extent of material removed could be measured by the 3D scanner. Concerns were raised that the application of a poly-abrasive wheel could lead to areas of sound metal being removed on the surface of the pipe. However, during sustained use of the abrasive wheel over a constant area of sound metal, it was not possible to remove any of the metal. At worst, the poly-abrasive wheel was only capable of removing the bitumastic coating to reveal shiny metal underneath, Figure 7.28(a) and Figure 7.28(b). When the same abrasive wheel was used on an area of graphitic corrosion, it quickly removed it, leading to the "crater" structures mentioned above. In a very short time it was possible to quickly remove significant amounts of graphitic corrosion, Figure 7.28(c) and Figure 7.28(d). Previous experience has shown that these "craters" tend to have a significant diameter. During the testing, it was evident that the corrosion could only be removed where the pit was sufficiently large that the abrasive wheel could get into the pit to continue to excavate the corrosion product. When tested on small pits, it was not possible to excavate the corrosion product. The abrasion merely smoothed any rough edges whilst leaving the graphitic corrosion product in place, Figure 7.28(e) and Figure 7.28(f). As a result, the surface preparation focussed on creating several large pits.

The 3D models captured before and after the surface preparation has been conducted have been aligned and the differences compared, and hence the material lost during surface preparation has been calculated. Whilst a contour plot of the surface preparation for the whole pipe was created, the majority of this plot shows no change as the surface preparation conducted was localised as detailed above. Figure 7.29 focusses on the "crater" created from the surface preparation shown in Figure 7.28(c) and Figure 7.28(d). It can be seen that the scanner has measured a loss of material of up to 11 mm. Further the scanner has captured the shape of the bowl left behind and horizontal lines can be seen on the contour map, which represent the original ridges between each scratch that was lost during the surface preparation.

(a)

(b)

(c)

(d)

(e)

(f)

Figure 7.28 - Effect of the poly-abrasive wheel on sound metal and graphitic corrosion: (a) uncorroded iron before cleaning, (b) as (a) after cleaning, (c) graphitic corrosion before cleaning, (d) as (c) after cleaning, (e) small patch of graphitic corrosion before cleaning and (f) as (e) after cleaning.

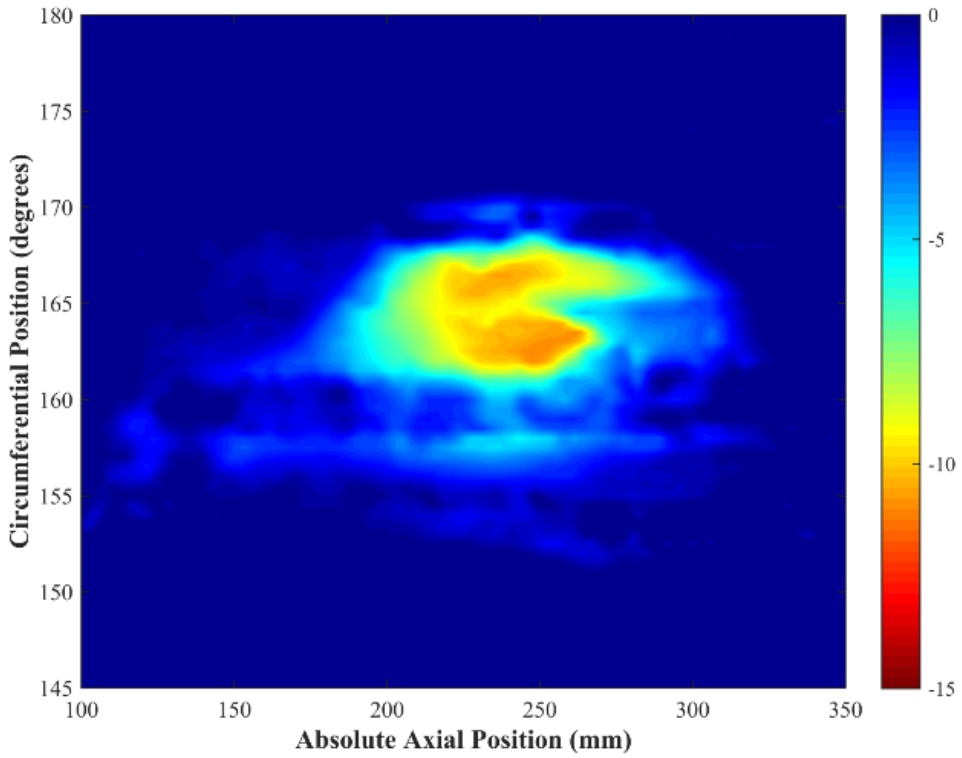

Figure 7.29 - Contour plot showing the level of surface preparation as measured by the 3D scanner for the corrosion patch excavated in Figure 7.28(c) and Figure 7.28(d).

The 3D scanning methodology has been shown to be capable of measuring the geometry of any surface preparation conducted by an NDE contractor. This technique could be further used to examine the surface preparation conducted over a whole section of trunk main.

7.6.9 Encrustation and Tuberculation

As well as being used for condition assessment, the ability to measure pipe geometry has opened up further avenues of inquiry. In particular, it has been questioned whether there is a link between the location of external encrustation or internal tuberculation and the underlying corrosion. The method adopted during this exercise was devised to include a record of the pipe before any surface preparation was conducted. A 3D model of the pipe was captured prior to any surface cleaning being undertaken and compared to the 3D model which detailed the pipe geometry after it has been cleaned. The resulting contour plot showing the external encrustation is presented in Figure 7.30. The graph shows that there are several areas where the surface encrustation was significant, however, a great deal of encrustation shown is the remnants of soil removed with the pipe rather than the concrete like encrustation sometimes experienced.

This encrustation was easily removed during the pipe preparation. Further, in this pipe section, the area around the deepest patch of corrosion appears to be devoid of any encrustation. This is not surprising as the top of the pipe was scraped clean by the excavator when it was being exhumed. Consequently, in this exercise, it is not possible to draw any links between the encrustation and the presence of corrosion. None the less, it has shown that the encrustation can be mapped if it is still adhering to the pipe surface. A similar process could be used to capture the internal tuberculation as well, however, as mentioned previously, it was not possible to separate the tuberculation or internal corrosion measurements in this exercise.

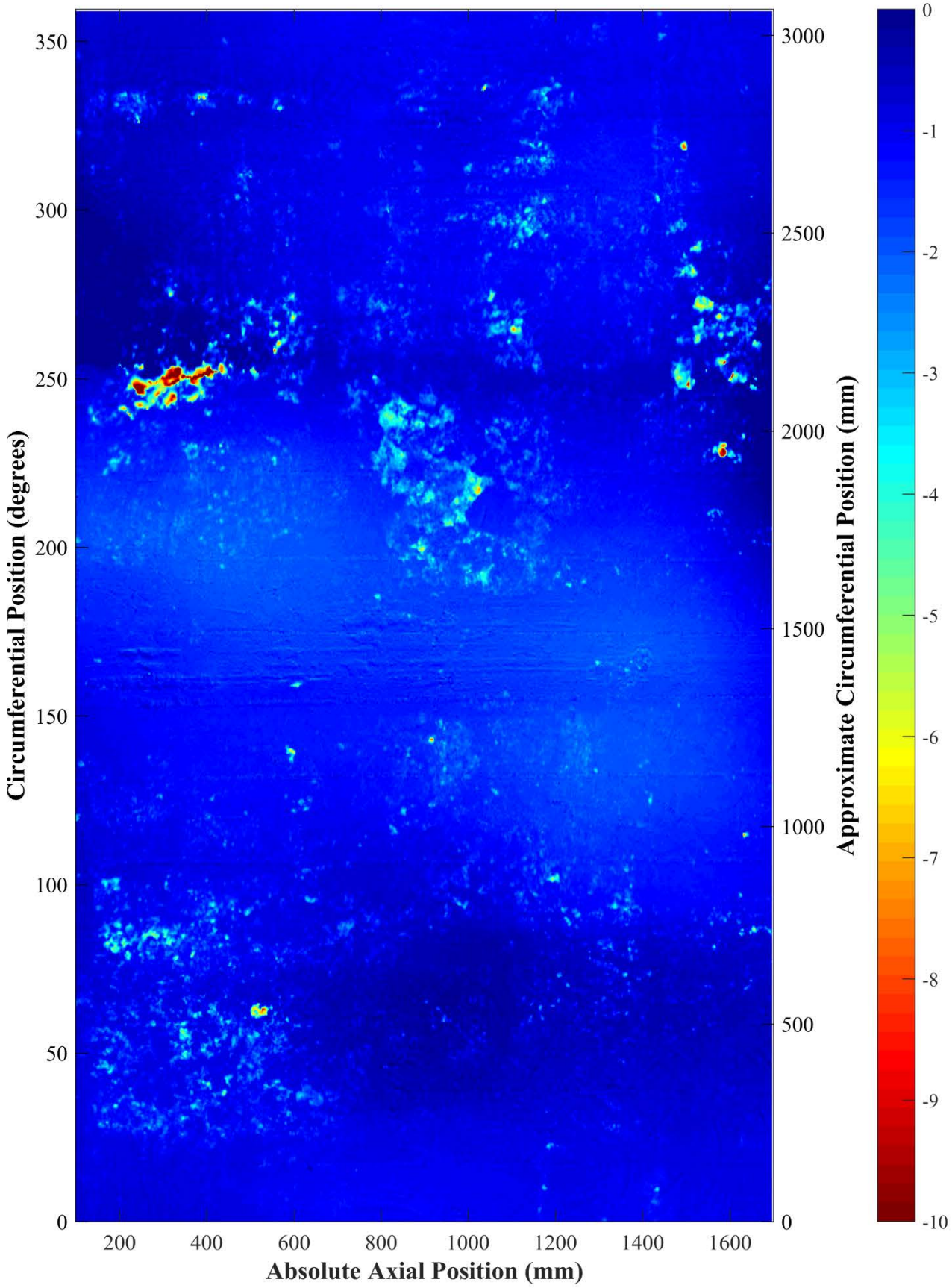

Figure 7.30 - Contour plot showing the external encrustation on Specimen Three as measured by the 3D scanner.

7.7 Resultant Developed Methodology

7.7.1 Revised Methodology

In the previous section, the progression from investigating the external corrosion on a distribution main to that of a trunk main using the 3D scanner was achieved. The developed method proved that it can successfully provide destructive condition data for corrosion on a trunk main section that remains in keeping with the current industry standard method of manual pit depth measurement. Further, the methodology was expanded to allow other items of condition data to be captured such as surface preparation. The methodology was also devised to allow internal tuberculation and corrosion to be measured, although, problems were encountered during the exercise that meant it was not possible to extract the tuberculation or internal corrosion data individually.

To combat this problem, the methodology was adjusted so that any future exercises will not experience the same problem. A further scanning step, which involves the tuberculation being cleaned away to leave behind the original inner pipe surface before the geometry was scanned, Figure 7.31, is added to ensure that each detail could be measured individually. This will not only allow the level of internal corrosion to be measured, but also the level of tuberculation to be individually measured. This resultant methodology will be used in any future comparison exercise.

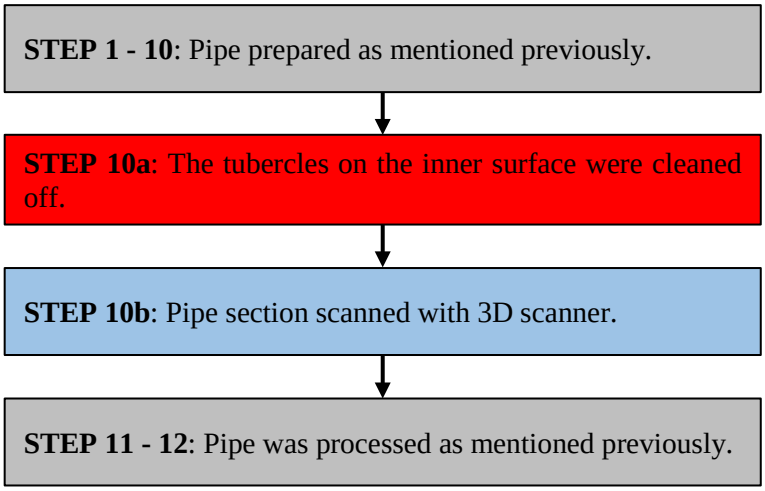

Figure 7.31 - Diagram showing the additional step incorporated into the initial methodology described in section 7.6.3 to allow the internal corrosion and tuberculation to be measured individually.

7.7.2 3D Scanning Procedure Observations

At each stage of the comparison exercise, it was important to remove any dust from the pipe as it has the potential to accumulate during the scanning process. Any dust and debris has the potential to be recorded during the scan as additional geometry that is not part of the pipe. This is most important on the inside surface since the rotation of the pipe can cause any loose dust and debris to gather around any protruding geometry such as a tubercle. The pipe was rotated for several minutes to ensure any material likely to become loose was loosened, collected and then removed. A soft brush was used to clean the inner surface of any remaining debris. The inner and outer surfaces of the pipe were brushed carefully to ensure that only loose material was removed

and no further corrosion products were removed. It became apparent that the most likely problem with debris was immediately after any cutting actions had been performed on the pipe. Here iron filings were found to accumulate inside the pipe, Figure 7.32.

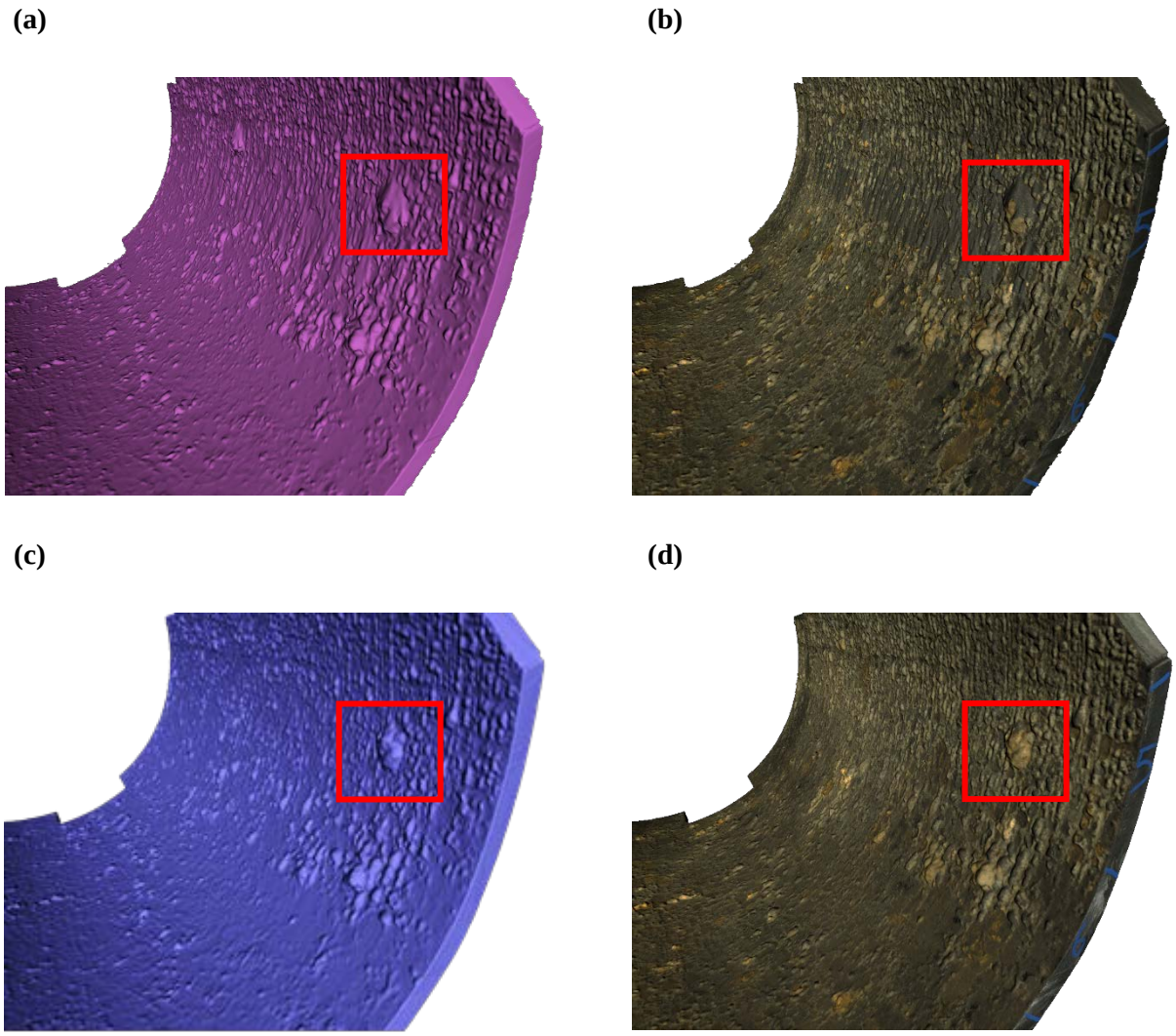

Figure 7.32 - 3D pipe models showing the effect of debris build up around tubercles: (a) 3D model with debris, (b) textured version of (a), (c) 3D model without debris, (d) textured version of (c). The red square highlights a common feature in all models.

7.8 Summary

In this chapter, the need for an improved method of collecting the "ground truth" data from a destructive analysis has been shown in detail from the previous NDE comparison exercises conducted by TWUL. 3D scanning was investigated to understand if it can be used on sections of trunk main to provide the information required. Initially, a trial sought to see whether the outer original surface of a pipe could be represented by a cylinder fitted to the nominally uncorroded areas of a trunk main. This proved to be wrong as the cylinder did not encompass all parts of the scan. An oversized cylinder, which encompassed all of the 3D scan's geometry, was tried but it proved that the fit became less realistic. Whilst suitable for steel mains that have been subject

to rigorous quality assurance, this option proved to be less useful for ageing trunk mains and induced significant error into the corrosion thickness measurements.

A revised methodology that determined the external corrosion thickness of a distribution main section by comparing the 3D geometry captured before and after shot-blasting was then tested. This methodology proved to be more successful and provided corrosion measurements that were in-keeping with those obtained through standard pit depth measurements. Further, analysis of the 3D scanned data showed that traditional pit depth measurements do not necessarily find the deepest external corrosion pits, particularly where the geometry is complicated, often rendering pit depth measurements impossible.

This improved methodology has been applied to a trunk main section and also achieved similar beneficial results to that demonstrated on the distribution main. Furthermore, this technique has also allowed the remaining wall thickness and external corrosion to be measured as well as potentially capturing the internal corrosion and tuberculation. Finally, the development work has resulted in a complete methodology that can be used when undertaking further comparison exercises.

In Chapter 8, this methodology is tried in a live comparison exercise. The methodology is used to evaluate the performance of two NDE contractors used by TWUL to provide guidance on their ability to accurately record internal and external corrosion, as well as the remaining wall thickness. The comparison also seeks to understand how dependent the results obtained are on the level of surface preparation conducted.

8 Trunk Main NDE Contractor Comparison Exercise

8.1 Introduction

In Chapter 7, a new technique developed in house which utilises a 3D scanner to record geometric changes to a pipe, and hence infer the condition (such as corrosion and residual wall thicknesses), was demonstrated. Following trials on a distribution main section, and later a trunk main section, the technique proved its competence for the collection of "ground truth" pipe data. Finally, a methodology for evaluating the efficacy of an NDE contractor using this approach was developed.

A NDE contractor comparison exercise was held using this new methodology. This exercise has been conducted in the past. However, it was only able to provide a statistical analysis showing the corrosion thicknesses captured by each contractor, and not the spatial positioning of corrosion. Hence a full comparison with the actual pipe condition has not been possible. However, this new methodology allows a more detailed comparison to be made which will allow the reported corrosion positions to be compared, rather than a pure statistical analysis. In this comparison, two sections of pipes taken from the same main were examined by two different NDE contractors. From here on in these contractors will be referred to as "Contractor A" and "Contractor B". At each stage of the comparison exercise, the geometry of each pipe was recorded using the 3D scanner to create a 3D model. This has ensured that any changes to the geometry of the pipe have been recorded, at every stage. These models have been compared to determine the real condition of the pipe. Whilst this technique has the potential to evaluate the capability of any NDE technique that is applied to the pipe, this comparison focusses on the two main NDE contractors that have been used by the business to evaluate their efficacy.

It has been anecdotally mentioned that one of the contractors compared adopts a relatively aggressive surface preparation, so much so that their inspection may be a little less than non-destructive. As the 3D scanner has proven its ability to measure the level of surface preparation carried out, the preparation carried out by the contractors is also recorded. Further, as the surface preparation has been so great it is important to understand how important it is to the capability of the NDE technique for gathering accurate condition data. As such, surface preparation was allowed on one pipe section but restricted on the other.

In this chapter, the equipment and methodology used to conduct this exercise will be detailed. The actual condition of the pipes, as measured by the 3D scanner, will be reported. The results reported by each contractor are then detailed in individual subsections along with the level of surface preparation that was measured after their NDE inspection along with the results gathered by each contractor.

8.2 Specific Methodology

8.2.1 Introduction

In section 7.7.1, a complete methodology for conducting an NDE contractor trial on a section of trunk main was described. This methodology was used as the basis of this comparison, however, due to two contractors

being evaluated a further scanning stage was added to allow the surface preparation from the Contractor A to be captured before the Contractor B conducted theirs. Also as this trial was conducted across two pipe sections to understand the NDE capability with and without surface preparation, the steps conducted were adjusted for each section. Any changes to the methodology can be seen graphically in Figure 8.1.

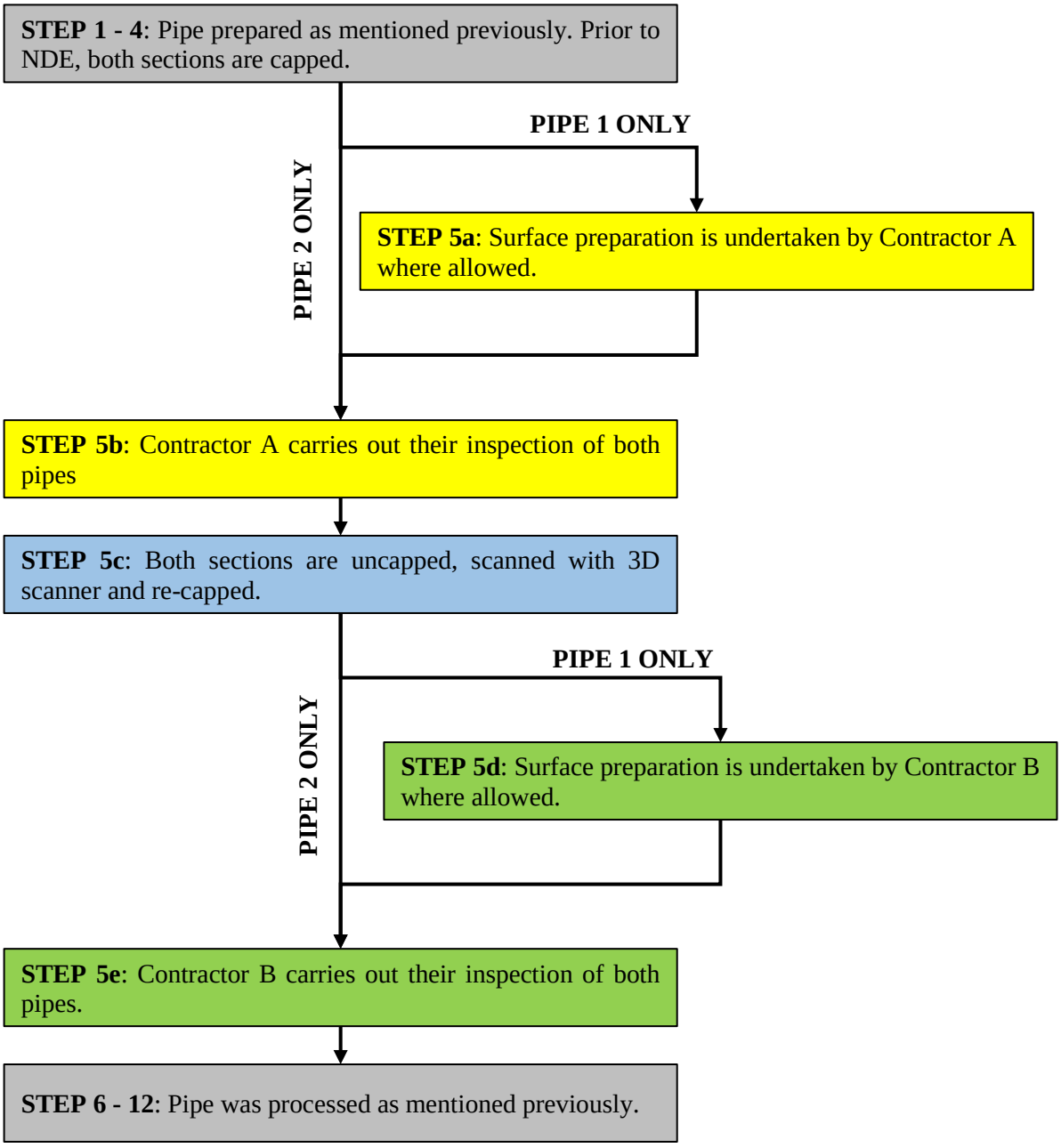

Figure 8.1 - Updated comparison methodology, based on section 7.7.1, with the addition of extra steps for each contractor.

8.2.2 Pipe Section Preparation

Two sections of cast iron trunk main, nominally 1.8 m long were cut from an intact jointed section of pipe that had been cut out as part of a repair job on a burst main at Hogsmill sewage treatment works in Surbiton, Figure 8.2(a). The two samples are referred to as “Pipe 1” and “Pipe 2”. Pipe 1 and 2 were cut and prepared according

to the methodology described in the previous section. Before this pipe was exhumed, the crownline was painted along the top. This enabled the original orientation of the pipe to be found.

In addition to the cuts described in the methodology given in the previous section, a further v-notch was cut into the pipe at the end approximately 90 degrees further round the pipe from the crownline to identify the spigot end, Figure 8.2(b) and Figure 8.2(c). This allows the original orientation of each section to be identified at a later date, if needed, but also provides a further point of geometry that does not change during the exercise and can be used to align the scans taken at each stage. Once the v-notches had been cut and the raw sections had been 3D scanned for the first time, the pipe sections underwent cleaning to remove the surface encrustation.

(a)

(b) **(c)**

Figure 8.2 - Jointed pipe cut-out before and after it was cut into smaller sections: (a) complete pipe cut out, (b) Pipe 1 and (c) Pipe 2

In the previous chapter, the trunk main examined and described was covered with a layer of minor surface encrustation. Removing this encrustation was a trivial task as it flaked off easily when abraded by an angle grinder fitted with a steel wire wheel. These wheels are typically used to remove loosely adhering rust when preparing metalwork. It is likely that, as the pipe had been out of the ground for several years, the encrustation had sufficient time to dry out and disbond from the pipe surface allowing it to be removed easily. However,

the encrustation present on Pipe 1 and Pipe 2 was significantly thicker and a great deal better bonded to the outer pipe surface, Figure 8.3(a) and Figure 8.3(b). The adhering encrustation was removed from the outer surface of both pipes using a hammer drill fitted with a wide chisel. In some places, the encrustation was extremely adherent and a chisel was not sufficient to remove it. Instead an angle grinder fitted with a tungsten carbide coated grinding disc was used to remove any further protrusions and leave the surface of the pipe nominally smooth. Care was taken to ensure that any corrosion penetrative into the wall was not removed or damaged.

(a) **(b)**

Figure 8.3 - Different types of surface encrustation found across the surface of both pipes: (a) a very hard pointed encrustation formation and (b) a softer encrustation formation including stones from the surrounding soil.

Once the surface preparation was completed, the pipe sections were prepared to be inspected. The perimeter of each end of each pipe section was traced on to 3 mm thick hardboard and then cut out using a jig-saw. These boards were fastened on to the ends using cloth tape to cap each pipe end, Figure 8.4(a). Further square caps were also cut to cover the v-notches that were cut into each pipe, Figure 8.4(b). The end caps prevented either contractor gaining an unfair advantage by seeing and being able to measure the wall thickness so as to influence their NDE results.

An origin was marked on the pipe for all the contractor measurements to be taken, including the positive directions around the circumference and along the length. This origin was positioned over the apex of the v-notch on the crownline at the spigot end of the pipe, Figure 8.4(b).

8.2.3 NDE Examination

Once the pipe sections were prepared, each NDE contractor was scheduled to conduct their NDE. The MFL contractor (Contractor A) conducted their inspection first as they have shown in previous examinations that they conduct little surface preparation. The ultrasonic contractor (Contractor B) carried out their NDE after Contractor A. Both pipe sections were inspected by each contractor. However, both contractors were restricted from conducting any surface preparation on Pipe 2. Pipe 1 and Pipe 2 were scanned using the 3D scanner after

each contractor had conducted their NDE to capture the geometry detailing the level of surface preparation conducted during each inspection.

(a) **(b)**

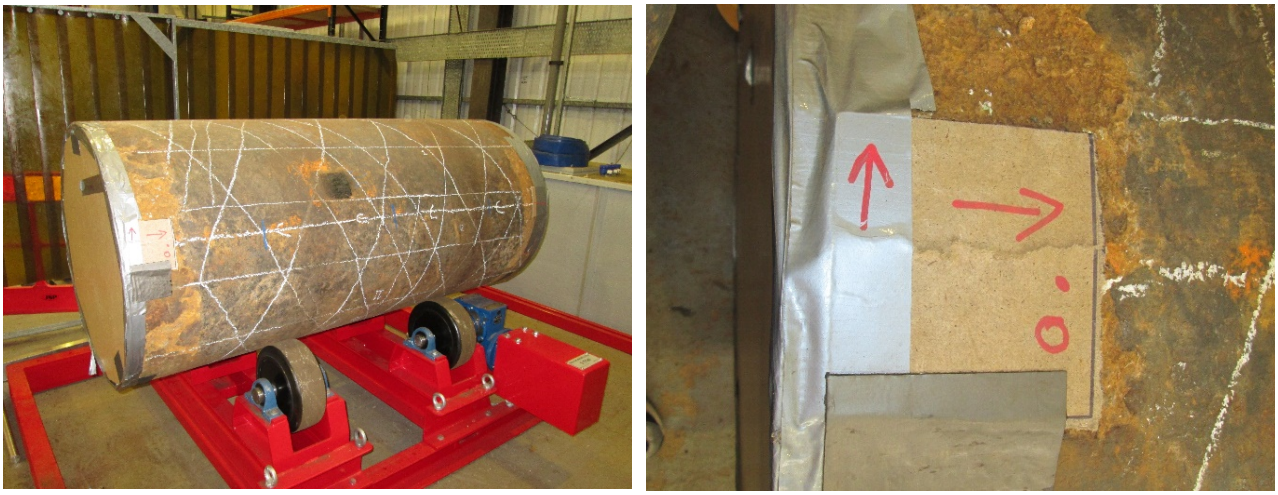

Figure 8.4 - Detail of the end caps that covered each end of the pipes and the caps covering each v-notch: (a) Pipe 2 with its end caps in place and (b) A cap covering a v-notch on Pipe 2 with the positive measurements directions and measurement origin drawn on.

8.2.4 Tuberculation Removal

In this comparison exercise, a further two steps were added prior to shot-blasting to allow the removal of the tubercles and the capture of a 3D scan of the pipe with the internal corrosion still *in situ*. The tubercles were removed using the same methods described above to remove the external encrustation. Here the upper layer of the tubercle could be removed using the chisel. The tungsten carbide coated abrasive disc was used to remove any remaining traces of the tuberculation to leave a smooth cylindrical surface. Care was taken to ensure that the internal corrosion was not removed with the tuberculation.

8.3 Contractor Methodology

8.3.1 Contractor A (MFL)

Contractor A used a combination of ultrasonic wall thickness measurements and corrosion measurements made using their MFL tool to profile the condition of the pipe sections. Initially the surface for inspection is prepared, when allowed to do so. Surface preparation was conducted using a metal scraper to remove any loosely adhering encrustation. A hammer and cold-chisel were used to remove any strongly adhering encrustation that protruded from the pipe surface.

The section undergoing inspection was divided into a grid with sections that are 90 mm tall x 100 mm long marked across the 1 m section of pipe being inspected. A 1.25 MHz twin crystal probe was used to measure the wall thickness for each square ultrasonically. Here the probe was moved over the area inside the square until a clean ultrasonic signal could be gathered. Following this the MFL tool, as shown in Figure 8.5, was axially scanned along each row of squares to measure the level of corrosion present on the internal and external

pipe walls. The MFL tool can only inspect 1 m of pipe per stroke, however, a total of 1.6 m of prepared space along the pipe is required to allow the tool to hold itself to the pipe.

Once the data was collected, it was post-processed at the contractors' offices and supplied in a written report. For a standard inspection, the contractor would only provide a statistical analysis of the corrosion across the pipe. However, for this comparison, more detail was asked for in terms of the corrosion depths and locations, and if possible, a contour map with a rastered dataset showing the results.

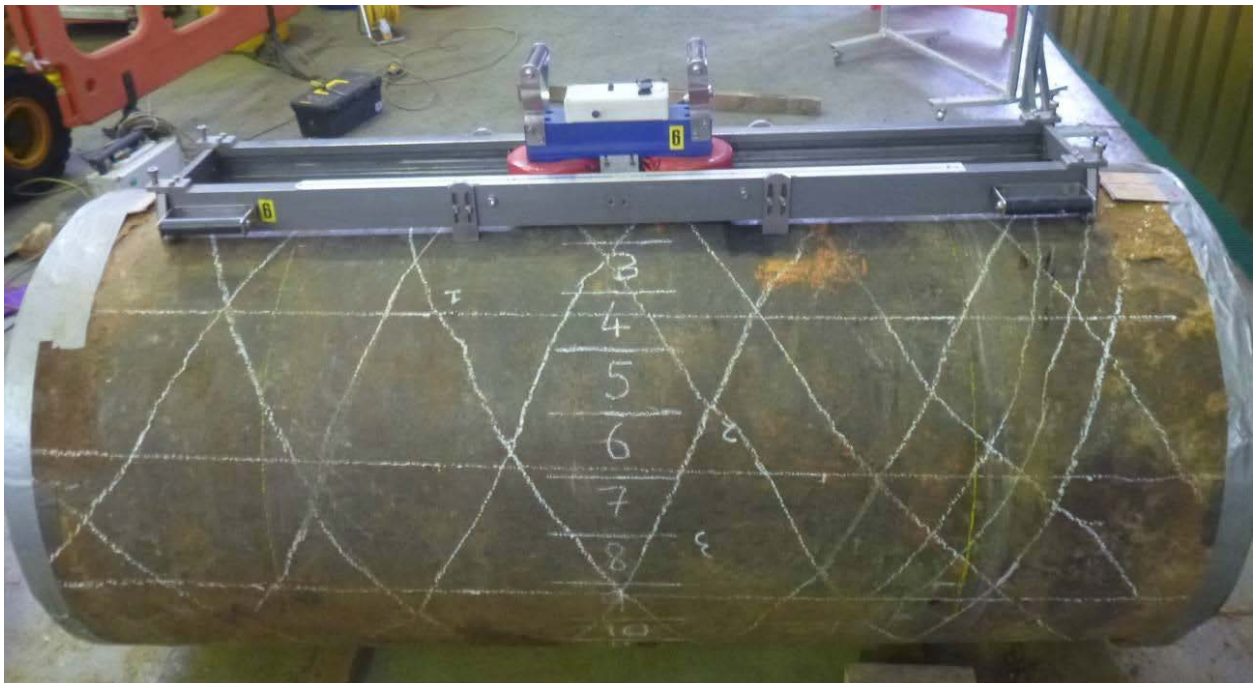

Figure 8.5 - Pipe 2 with the MFL tool in position. The yellow circumferential lines indicate the boundary of the 1 m inspection length and the numbered strips indicate the strips scanned by the MFL tool. (Image taken by contractor A).

8.3.2 Contractor B (Ultrasonics)

Contractor B used an ultrasonic inspection system to record the condition of the pipes being inspected. Initially the contractor conducted surface preparation using an angle grinder fitted with a poly-abrasive wheel. The contractor removed any surface encrustation and can abrade graphitic corrosion to produce a smooth outer surface which the ultrasonic transducer can glide over.

Once the surface preparation has been conducted, the contractor uses a twin crystal ultrasonic probe to inspect the pipe section. The contractor did not advise what frequency probe they use. A micromap system is used to conduct the inspection. This system utilises a camera to calculate the position of the probe on the pipe surface. As this system has a limited inspection area, the camera is repeatedly moved to allow patches of the surface to be inspected. These patches of data are then stitched together during the post-processing to give a complete picture of the whole condition of the pipe. The contractor also provides a statistical analysis of the pipe's condition. A further contour plot including rastered data was also requested.

8.4 Pipe Condition as Measured by 3D Scanning

Figure 8.6 and Figure 8.7 detail the pipe condition as measured by the 3D scanner for Pipe 1 and Pipe 2. In Figure 8.6(a) and Figure 8.7(a), it is possible to see the external corrosion measured for Pipe 1 and 2 respectively. Both sections are covered with extensive corrosion and have a maximum external corrosion thicknesses of 17.2 mm and 19.7 mm. Given that the nominal pipe wall thickness for these pipes was 25 mm thick, this equates to 68% and 76% of the pipe wall being lost to external corrosion only. Further, the corrosion appears to be located at similar circumferential positions on both pipe samples.

Pipe 2 is of particular interest, due to the shape of the corrosion, Figure 8.7(a). This corrosion geometry came as a great surprise. As Pipe 2 did not undergo any surface preparation, no clues were given as to the level of corrosion present during the trial. It is clear that this pipe section was in a very poor state of health and may have soon failed at this point if it had been left in service.

In Figure 8.6(b) and Figure 8.7(b), it is possible to see the internal corrosion present in each section. Both sections show significant coverage across the whole pipe surface and a maximum value of 6.6 mm and 3.8 mm for Pipes 1 and 2 respectively. However, in both sections, there appears to be an absence of corrosion along the pipe invert. It is likely that this pipe may have had sediment which flowed along the invert and ultimately settled on the surface to protect the inner surface of the invert. In order to calculate the internal corrosion measurements, the tuberculation was removed from the pipe surface to leave a smooth cylindrical surface that was representative of the original inner pipe surface at manufacture. Despite the use of a hard, abrasive wheel, the base of many of the tubercles proved to be significantly adherent and it was not always possible to create a smooth surface where the tubercles had been removed. In some cases, a rough surface several millimetres in height was left behind and without significantly more aggressive methods being used, it was not possible to eradicate all traces of tubercles. These surface undulations will be detected by the 3D scanner and will have a bearing on the results reported. Consequently, the results for the level of internal pipe corrosion presented should be treated accordingly and only the larger values for internal corrosion should be used.

Finally, the remaining wall thickness in each pipe section is given in Figure 8.6(c) and Figure 8.7(c). It can be seen that the remaining wall thickness is heavily controlled by the external corrosion. The minimum wall thicknesses were 6.6 mm and 5.9 mm for Pipes 1 and 2 respectively.

8.5 Contractor A (MFL) Analysis

8.5.1 Description of Their Experience

Contractor A used two people to carry out their inspection following the methodology described in section 8.3.1. The contractors were very happy to work with the guidelines that had been given to them and were happy to use the measurement directions that were provided. Initially Pipe 1 was inspected. Their surface preparation conducted was sparing and only removed a few protruding remains of surface encrustation. Further Contractor A seemed to have little concern operating the tool on the unprepared pipe surface.

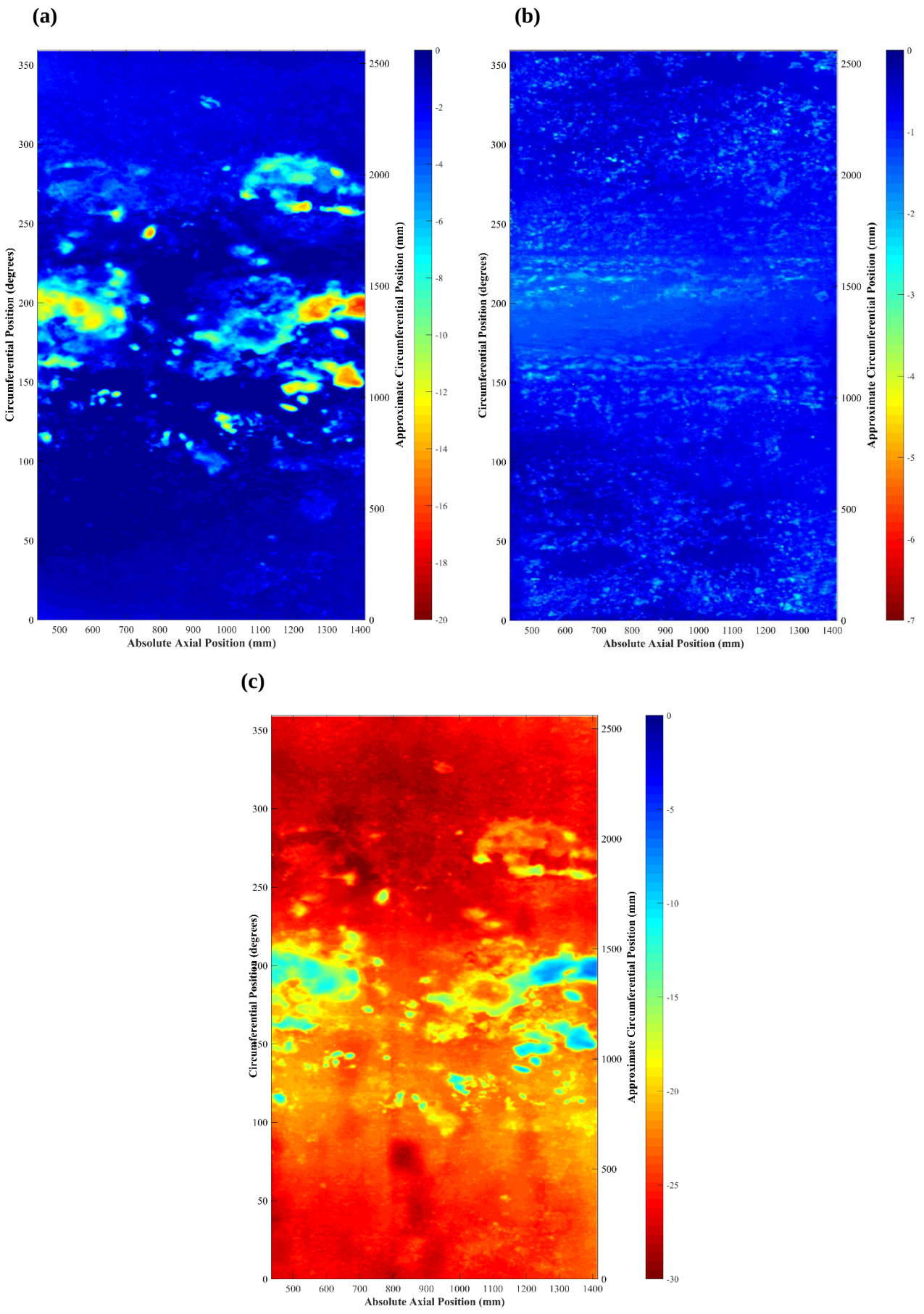

Figure 8.6 - Contour plots showing the condition of Pipe 1, as measured by the 3D scanner: (a) External corrosion, (b) Internal corrosion and (c) Remaining wall thickness.

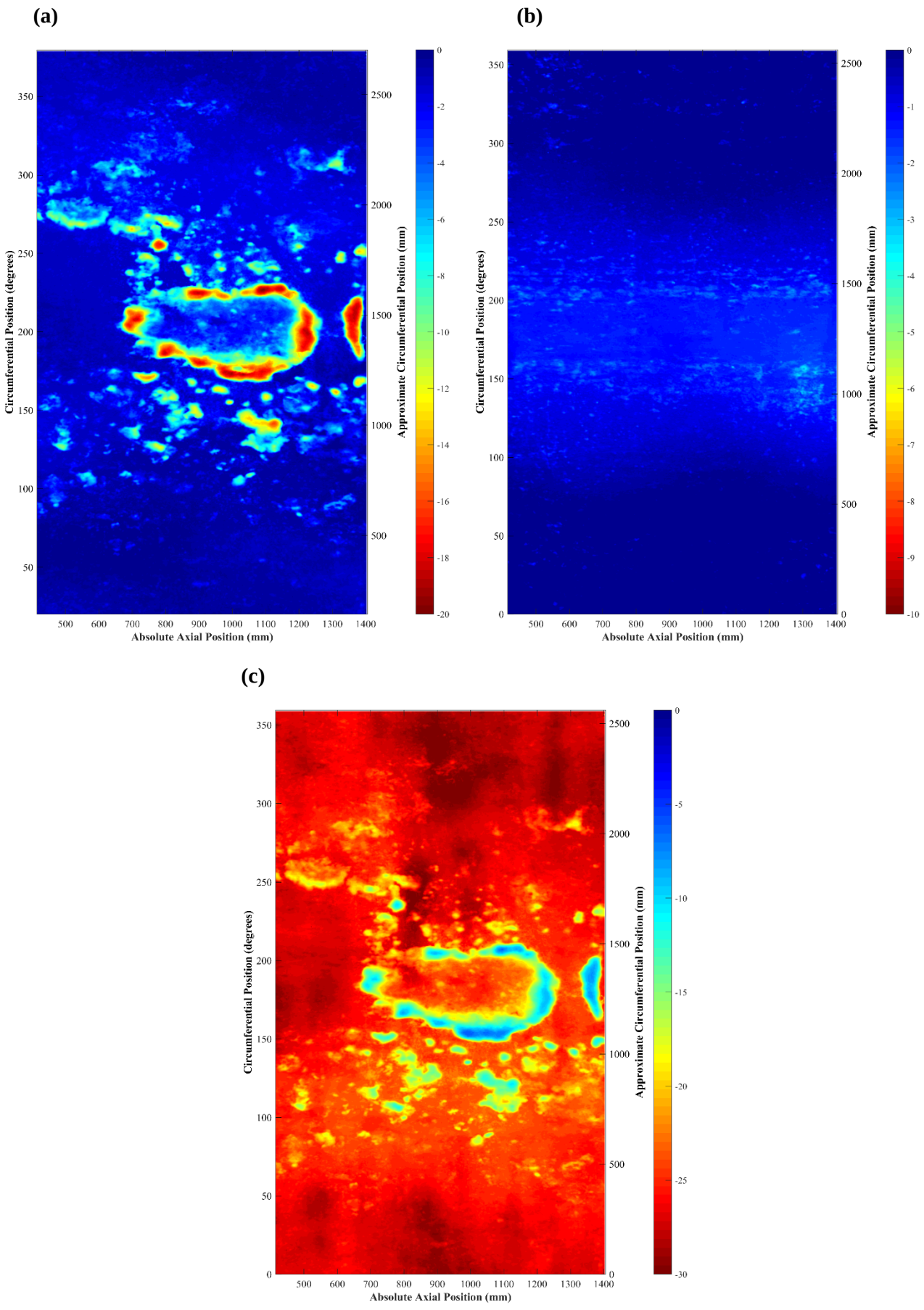

Figure 8.7 - Contour plots showing the condition of Pipe 2, as measured by the 3D scanner: (a) External corrosion, (b) Internal corrosion and (c) Remaining wall thickness.

On examination of the results reported, it was found that the contractor did not take all measurements from the origin specified. Consequently, the results had to be manually corrected such that the axial measurements were in keeping with the values measured by the 3D scanner. Overall the contractor appeared to be helpful and carried out a thorough inspection of both pipe sections.

8.5.2 Contractor A Results and Discussion

Figure 8.8 shows a contour plot illustrating the thickness and position of any material that was removed during the surface preparation of Pipe 1 conducted by Contractor A, as determined using the 3D scanner. Here it can be seen that very little surface material has been removed across the majority of the inspected pipe surface. However, there are five locations where material greater than 5 mm in thickness has been removed. This is due to the surface encrustation being sufficiently well bonded to the graphitic corrosion such that the graphitic corrosion was removed along with the surface encrustation. This illustrates the tenacity of the bond between the encrustation and the underlying surface. Fortunately, the removal of material has only happened in several isolated locations. Across the remainder of the surface, it can be seen that the surface preparation conducted was minimal, if any.

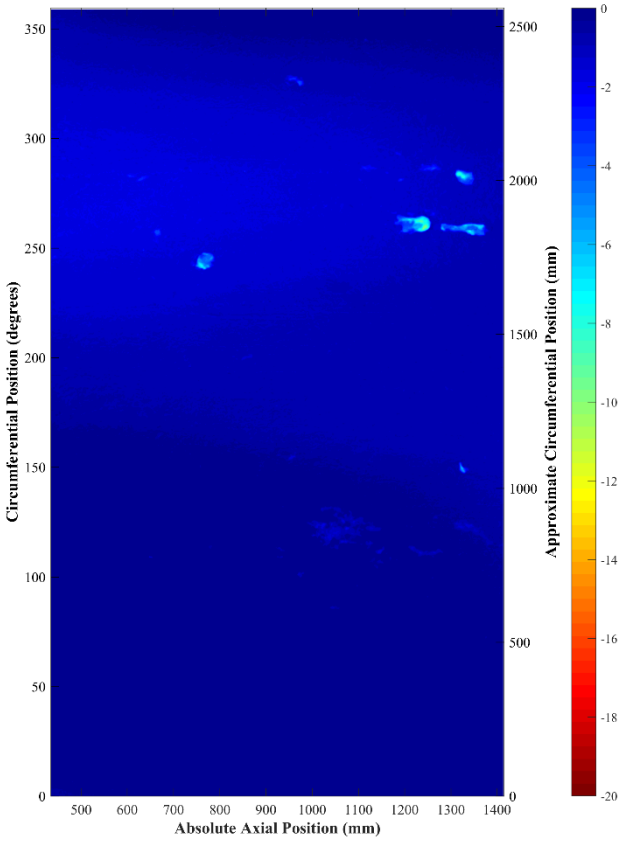

Figure 8.8 - Contour plot detailing the position and level of material removed during the surface preparation of Pipe 1 conducted by Contractor A.

Contractor A provided the data for the inspection as a contour plot showing the remaining pipe wall thickness. Here the average pipe wall thickness has been measured using an ultrasonic thickness probe. The corrosion defects have been found and their size determined using their MFL tool. These corrosion defects have been

subtracted from the average wall thickness measured by ultrasound to derive a remaining wall thickness. The plots for Pipes 1 and 2 are shown in Figure 8.9(a) and Figure 8.9(b) respectively.

Inspection of these results against a visual inspection of the shot-blasted pipe geometry raises questions as to the accuracy of these results. This is most notable as they do not display the approximately hemispherical pit shapes seen on the shot-blasted pipe sections. Instead it appears that all the corrosion pits are flat bottomed cylindrical holes of varying depths. This is clearly not the case. Contractor A has advised that their determination of pit depth is derived from previous results captured for machined cylindrical pits in calibration samples of typical cast iron. These results have then been used to identify corrosion defects present on real samples. The results do show some corrosion distribution expected from real pits including some pit nucleation. This is most prominent in Figure 8.9(b) where one could be convinced that the results outline the large ring of nucleated pits seen on the shot-blasted pipe section. However, its significance is not demonstrated particularly well through these results.

These findings are further supported by the results obtained from the 3D scanning, Figure 8.6 and Figure 8.7. It can be seen that the wall thicknesses reported by the Contractor A are not representative of the real pipe geometry. As shown in Chapter 5, the speed of sound in cast iron varies dependent on the graphite flake structure. This also needs to be considered when processing such results.

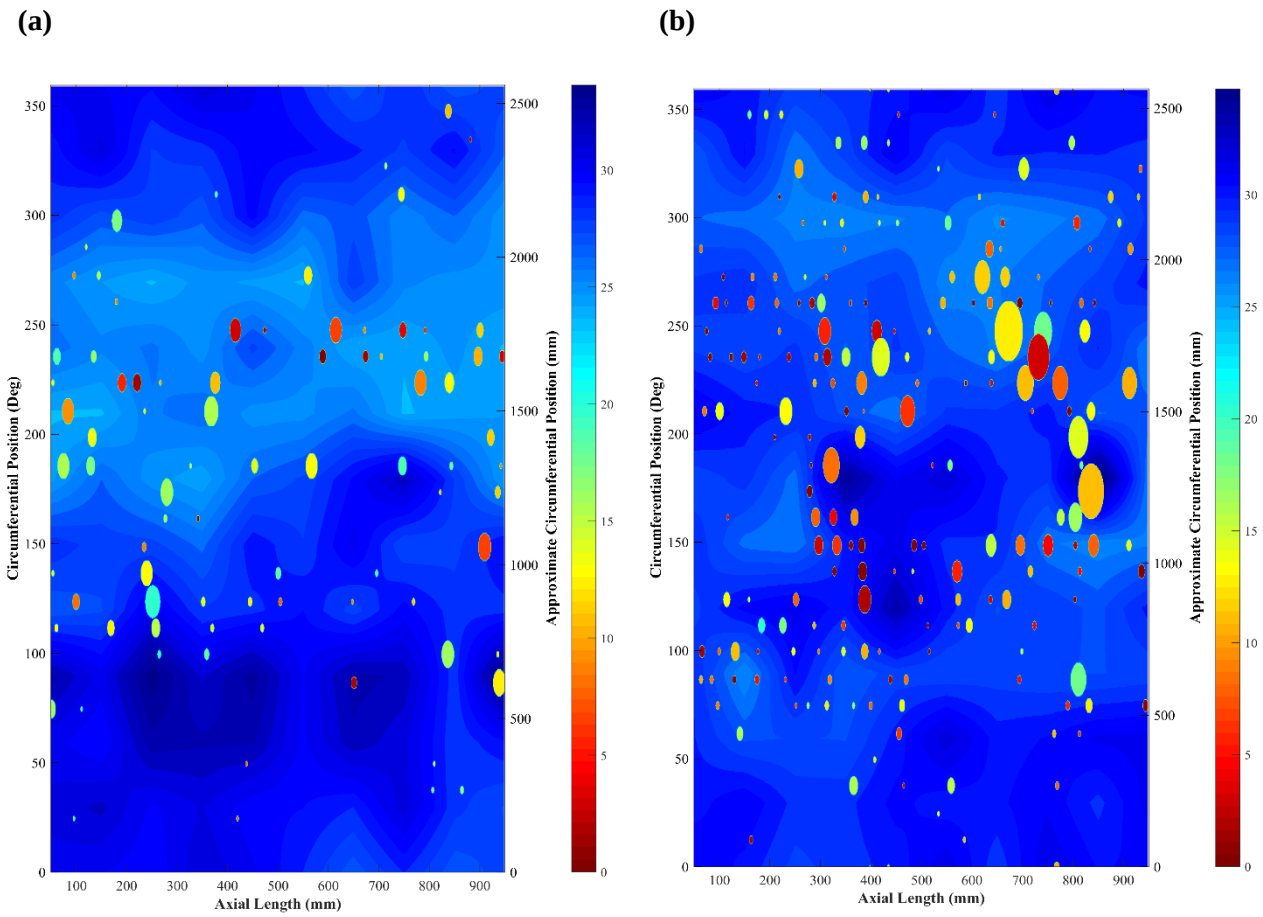

Figure 8.9 - Contour plots detailing the remaining wall thickness for each pipe sample as reported by Contractor A: (a) Pipe 1 and (b) Pipe 2.

The results reported by Contractor A appear to show minimal correlation with the real pipe condition derived by 3D scanning of the same sample following the protocol developed in Chapter 7. In some places, the reported depth of corrosion is excessive with pits that penetrate the pipe wall being reported. This is clearly not the case as the pipe walls are both shown to have several millimetres remaining even at the site of the thickest corrosion. The data displayed in Figure 8.9 has been post-processed according to the Contractor A's own in-house algorithms. As part of the comparison exercise, the raw data captured during the scanning was also requested. Contractor A was able to provide the raw magnetic signals that were captured during each scan. The raw scans were provided as text files which would normally be interpreted by the in-house post-processing software. Each text file details the magnetic measurements made over a 90 mm wide axial strip along the 1 m inspection length. The MFL tool has a moving sensor head containing eight Hall sensors that are equally spaced across the 90 mm scan width. The scanner head is moved along the length of the pipe and its axial position is recorded by a built-in position-encoder. After each pass is complete, the tool is moved around the pipe circumference a further 90 mm and another pass is made. As a result, the data for each pipe scan was contained in some 29 text files. Each text file contains the eight columns that detail the Hall sensor measurement recorded every 3 mm along the scan length. In addition to the raw magnetic signals captured during the scan, the MFL tool also measures its proximity to the surface. The method in which these signals are combined to process the data is unknown, however, it is believed that the proximity sensor seeks to ensure that the Hall sensors are as closely coupled to the pipe wall as possible and when a gap is detected, the separation can be measured and the loss at the Hall sensor is subject to some form of compensation.

Figure 8.10 shows contour plots of the raw magnetic signals measured during the scanning of Pipe 1 and Pipe 2. Both of the figures both show horizontal banding which is due to the contour plot being made up of individual passes. A further set of black lines have been plotted over the contour maps to show the outline of any corrosion pits that were greater than 4 mm in depth. Examination of each figure shows that the magnetic measurements where flux leakage was detected demonstrate a reasonable correlation with the external corrosion as measured by the 3D scanner.

The exact meaning behind each of the Hall sensor readings is unclear as no calibration standards were provided to suggest what readings indicate little or no corrosion and which readings would indicate significant external corrosion. However, the principles behind MFL show that the magnetic flux, normally contained within the pipe wall, leaks out of the pipe wall across the air gap in the presence of graphitic corrosion. Consequently, the increased magnetic readings indicate corrosion, although its thickness is unknown. In order to give a representative scale, the readings for each pipe have been normalised against the largest magnetic flux measurement captured.

It should be remembered that the surface preparation carried out by Contractor A was very minor even when allowed to do so. Figure 8.10(b) shows the contour plot of the magnetic signal measured for Pipe 2 where surface preparation was prohibited. Consequently, the fit in Figure 8.10(b) shows that the MFL tool is capable of recognising external corrosion without significant surface preparation being carried out. The results presented earlier for the MFL contractor were shown to be unrepresentative of the real pipe geometry. These

results suggest that the MFL tool is capable of identifying the locations of the external corrosion, however, the results are being modified by the post-processing algorithms such that they are no longer in keeping with the true geometry.

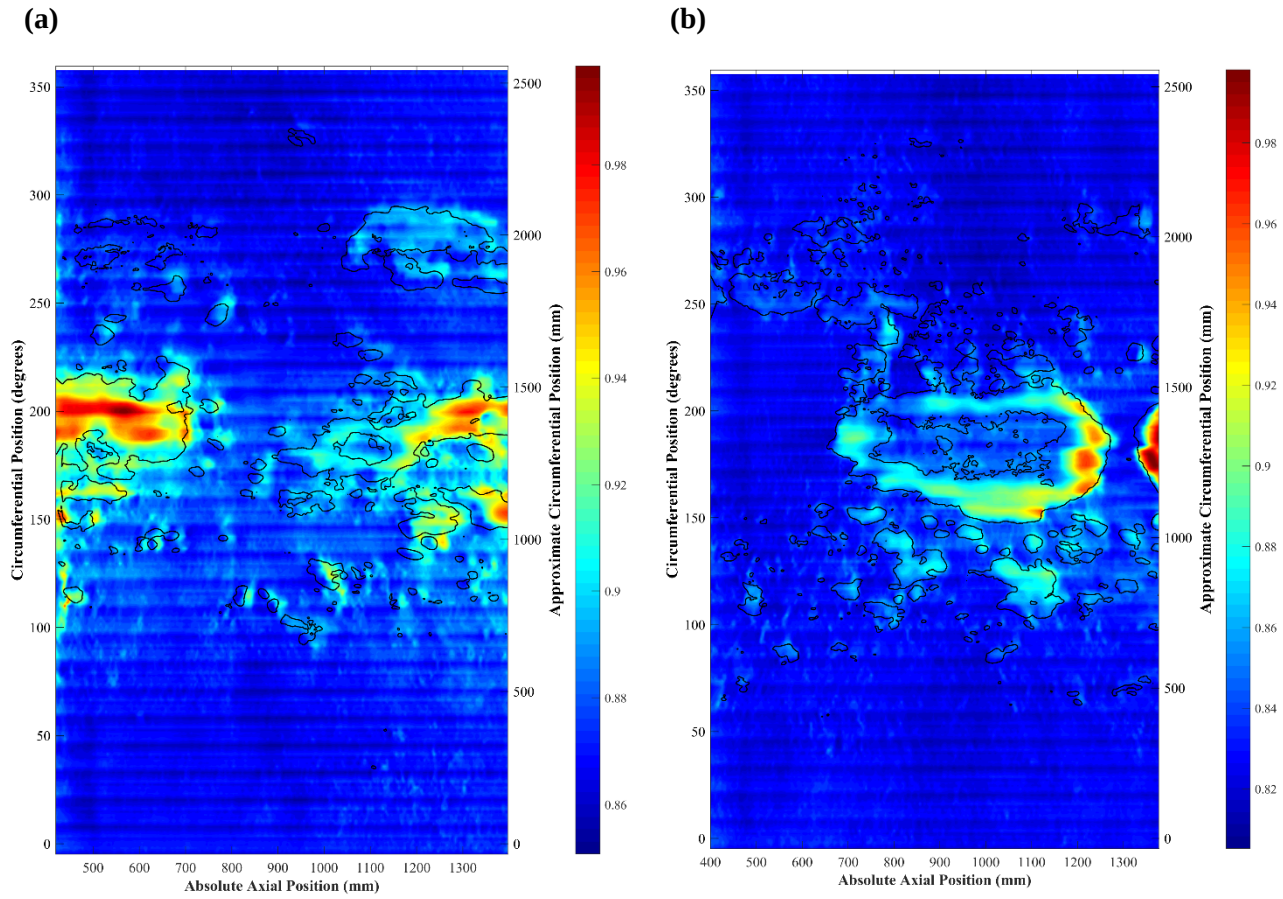

Figure 8.10 - Contour plots detailing the raw magnetic signals captured for each pipe by Contractor A: (a) Pipe 1 and (b) Pipe 2. The black lines indicate the outline of any corrosion pits that were greater than 4 mm in depth.

8.6 Contractor B (Ultrasonics) Analysis

8.6.1 Description of their experience

Contractor B followed the methodology described in section 8.3.2 to conduct their inspection. Significant surface preparation was undertaken before any NDE was undertaken. The analysis was carried out using a twin crystal probe that had its position tracked by an overhead camera strapped to the pipe. The camera was limited to examining small sections consequently the pipe was examined in patches that were put together during the post-processing to give the overall data set for the pipe.

When examining the data supplied by the contractor, it was apparent that they had not followed the measurement directions marked on the pipe. After several messages to and from the contractor, the correct alignment for the data was sorted out. Contractor 2 had also not made their axial measurements from the origin marked on the pipe. Consequently, these results were also adjusted manually to fit with the coordinate system.

8.6.2 Contractor B Results and Discussion

Past experiences of Contractor B have raised concerns with TWUL about the level of surface preparation that they carry out. In some cases, it has appeared to be extremely aggressive. The ultrasonic contractor undertook their inspection after Contractor A had completed their inspection. Their surface preparation was carried out using a poly-abrasive wheel fitted to an angle grinder. This technique has been shown to remove graphitic corrosion easily, section 7.6.8. The level of material removed during their surface preparation of Pipe 1 is given in Figure 8.11(a). When compared to the level of material removed by the Contractor A, Figure 8.8, it is seen to be considerably more aggressive with a maximum of 17.0 mm removed across the pipe surface. This equates to 68% of the pipe wall being removed by the surface preparation process. This level of surface preparation could be considered extreme and it is possible to see other patches across the pipe surface where 10 mm or more of material has been removed during the cleaning. Given that graphitic corrosion is a key feature to be measured during inspection, removal of this features raises questions as to what condition data is being measured by Contractor B.

Figure 8.11(b) is a duplicate of the contour plot presented in Figure 8.11(a) except that a black line tracing the areas of surface preparation deeper than 4 mm has been overlaid. It is clear, when looking at this figure, that the surface preparation has been applied across the whole surface of the pipe and focuses heavily on the graphitic corrosion where significant material was removed. This significant removal of material is not isolated to a handful of pits where the operator may have initially been overzealous but it appears across the whole pipe and each pit has been abraded in a similar fashion. Only the small isolated patches have avoided abrasion. In such cases, it is likely that it was not possible to excavate any corrosion from these patches as they were not large enough to be able to get the abrasive wheel into.

When tasked with inspecting the pipe section where surface preparation was prohibited, Contractor B was unable to conduct a full inspection and was only capable of collecting corrosion thickness measurements across 12% of the pipe section. Within this data, the maximum corrosion pit was found to be 1.9 mm This is clearly too low when compared with the large pit structure seen during visual inspection of the shot-blasted pipe sections let alone when compared to the 3D data captured by the 3D scanner. This is clearly too low when compared with the true pipe condition gathered by the 3D scanner. The contractor fared better in establishing the remaining wall thickness measurements of approximately 48% of the pipe section. However, this is still a small level of surface coverage when compared to Contractor A. The internal corrosion thicknesses were not supplied as they were unable to be determined for either pipe from the data they had gathered. Consequently, the results discussed further for Contractor B are only for Pipe 1.

The available results provided by Contractor B have been plotted as contour maps. In Figure 8.12(a), the external corrosion is plotted. It can be seen that the ultrasonic contractor was able to find several substantial patches of corrosion across the surface of the Pipe 1. These results are in keeping with those expected from visual inspection with several large patches of corrosion being identified by the contractor. These results detail corrosion with the rough shape and size expected of the corrosion pits seen after shot-blasting. However, under closer inspection, these measured patches of corrosion appear to be limited to the areas abraded during the

surface preparation. A maximum corrosion thickness measured by the contractor was determined to be 16.4 mm. Given that the surface preparation was shown to have removed 17.0 mm of corrosion, the maximum corrosion reported appears low. Further the maximum corrosion reported by the 3D scanner was 17.2 mm deep. Consequently, the surface preparation at this patch appears to have removed all of the corrosion product very little to be found by NDE. However, the contractor has reported finding 16.4 mm of corrosion. Figure 8.12(b) shows a contour plot detailing the remaining corrosion thickness after the pipe has undergone surface preparation by Contractor B. It clearly shows little external corrosion remains, particularly at sites where large patches of corrosion were present. The majority of corrosion that remains is linked to small isolated pits which may have proved challenging to abrade. Consequently, given the lack of corrosion present after surface preparation, it appears that the NDE results are obtained through destructive analysis. It is difficult to understand whether the NDE contractor is accounting for the material that is removed during the surface preparation in their results.

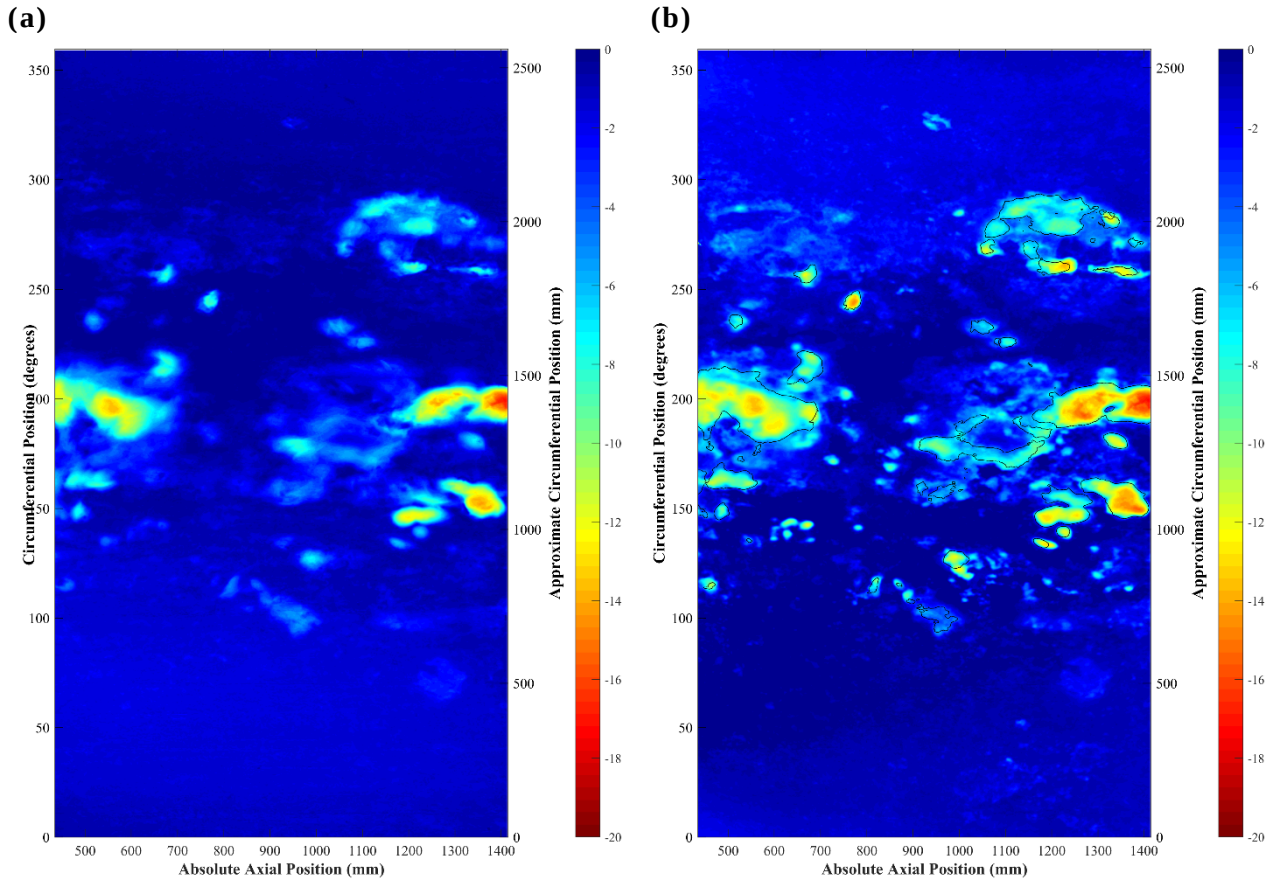

Figure 8.11 - Contour plots detailing the position and level of material removed during the surface preparation conducted by Contractor B: (a) Pipe 1 and (b) The external corrosion present on Pipe 1 with the outline of the areas where over 4 mm of material has been removed during the surface preparation.

Further, when examining the remaining wall thickness measurements given in Figure 8.12(c) it is seen not to be in keeping with the measurements captured for the external corrosion as there are no sites of reduced wall thickness reported at similar positions to the external corrosion. Clearly for a pipe with a fixed wall thickness, an increase in the corrosion thickness would result in a decrease in the remaining cast iron thickness. However, the results show no reductions in wall thickness at the sites of corrosion patches, as would be expected for such extensive corrosion.

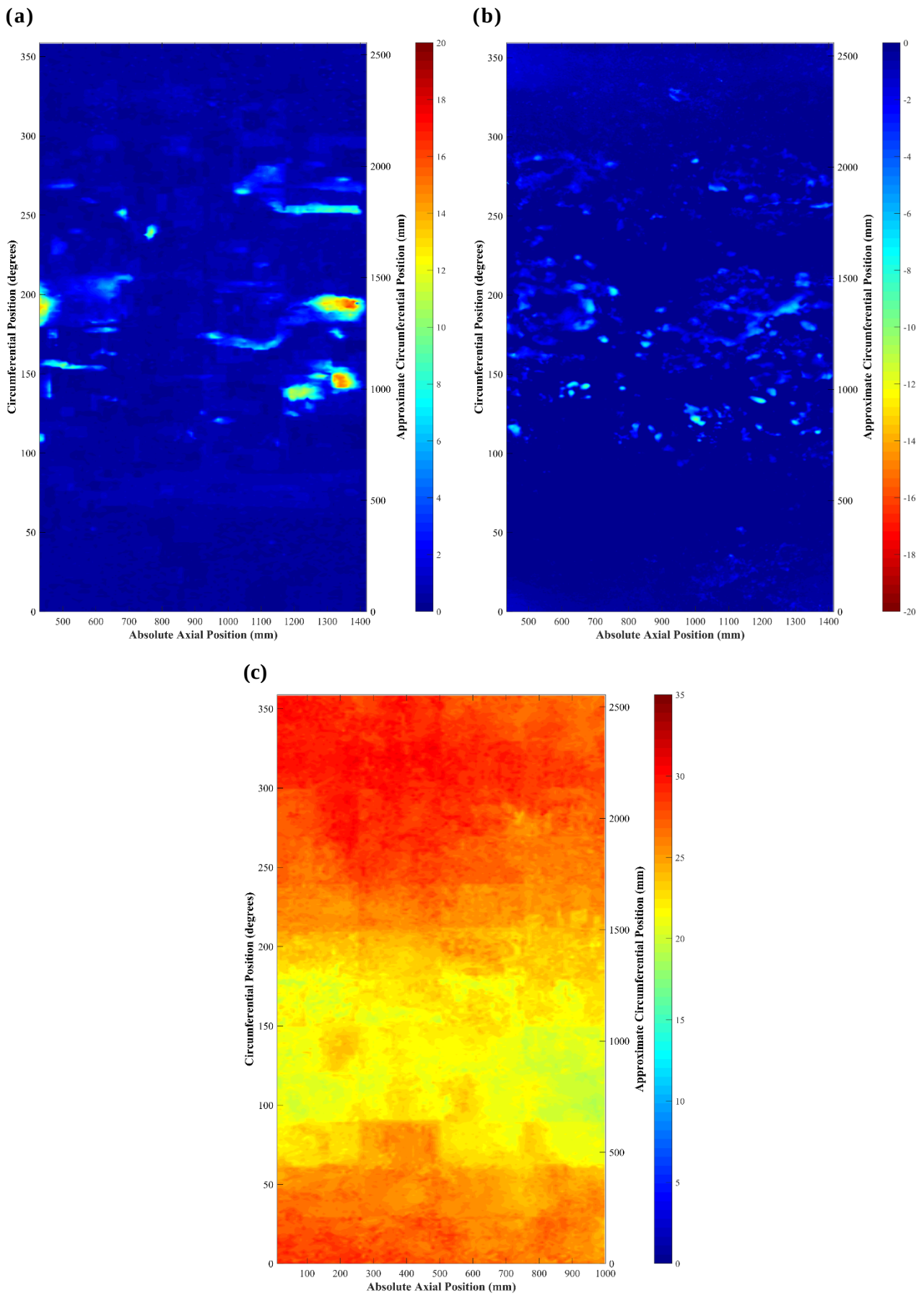

Figure 8.12 - Contour plots detailing the condition reported by Contractor B for Pipe 1: (a) External corrosion, (b) External corrosion left after surface preparation conducted by contractor B (as measured by the 3D scanner) and (c) Remaining wall thickness.

Further, the wall thicknesses provided range up to 30 mm in thickness. This is evidently incorrect as the maximum pipe wall thickness reported from the 3D scanner measurements was 25 mm. The contractor was asked for further details on their methodology, however, they were not happy to provide further details on the way their technique worked. Given the current findings, the NDE looks to be based on pit depth measurements conducted by destructive angle grinding of the graphitic corrosion.

8.7 Further Discussion

8.7.1 Contractor Data Presentation

Both contractors have presented their results in different fashions and neither followed the measurement directions as specified by TWUL. Consequently, it has been necessary to interpret the data to align the results with the coordinate system created by the 3D scanner. This has been successful but it is possible that some extra error could be induced into the process. This problem has occurred in previous comparison exercises. In this comparison, it has been possible to implement some reasonably robust standards but more rigour is still needed to ensure that contractors report data in an acceptable and appropriate format.

8.7.2 MFL Calibration

Contractor A has shown that their current post-processing of the MFL data does not yield results that are representative of the condition of the pipe. However, their raw MFL data sets show that there is a verifiable connection with the measured condition data captured using the 3D scanning methodology. This area should be further investigated as it may be possible to develop a much better calibration which produces results that are in keeping with the pipe condition. It is especially important as the technique has shown that it is capable of working when no surface preparation is undertaken. This is impressive as the contractor conducts little preparation at present, yet the technique can still identify the main pits and remaining wall thickness. This is hugely different from the ultrasonic contractor who has proven that their technique is unable to gather any meaningful data unless the surface of the pipe is heavily abraded.

8.7.3 Ultrasonic Calibration

Despite using different methods to measure external corrosion, both contractors are reliant on ultrasonic wall thickness measurements to provide the remaining wall thickness and put the external corrosion measurements into context. In this comparison exercise, both contractors have over-estimated the wall thickness. Values of 35 mm are significantly over-estimating the total wall thickness. Since these thickness values are calculated using a constant value for the speed of sound in iron, which has already been shown to vary between pipes of the same vintage, it is likely that the wrong value is being used. It is likely that the wall thickness measurements could be made more accurate simply by gathering better values for the speeds of sound in the iron being inspected. Both contractors have advised that they use 4700 ms^{-1} as a value for the speed of sound in cast iron. Values between 4100 and 4580 ms^{-1} have been suggested. Recalculating these wall thicknesses with the lower speed suggests a wall thickness closer to 30 mm which, whilst not directly in-keeping with the measurements made by the 3D scanner, it is progressing closer.

8.8 Encrustation and Tuberculation Links to Corrosion

In Chapter 7, while the methodology was under development, it was used to determine whether the 3D scanner could measure the position and thickness of the encrustation layer present on the test pipe section. The results showed that the technique could identify the areas of encrustation. However, due to the limited encrustation coverage, it was not possible to draw any conclusions from the results regarding any links between the encrustation and the external corrosion.

The results obtained during this comparison exercise have undergone the same scrutiny to ascertain if any links can be determined. Figure 8.13(a) and (b) show the external encrustation layer measured by the 3D scanner for Pipe 1 and 2 respectively. In these graphs, it is possible to see several large patches of encrustation with thicknesses of 10 mm. At local points within these patches the thickness can increase significantly up to approximately 40 mm in thickness. This holds constant with observations of the surface where the encrustation became thicker due to the large stones that were embedded in the encrustation. When compared to the external corrosion thicknesses captured for Pipe 1 and Pipe 2 in Figure 8.6(a) and Figure 8.7(a) respectively it can be seen that the majority of corrosion areas are located in sections of the pipe that were not covered by encrustation, or very thick encrustation. This is not true for all pits as some were located under the encrustation. Different formations of encrustation were found ranging from very soft to very hard. This may also have a bearing on the corrosion protection level offered by the encrustation layer.

As part of the work the internal tuberculation was also compared to the internal corrosion thicknesses present. This adaptation to the methodology has proven to be successful and has allowed two further sets of condition data to be gleaned from the experiment. Figure 8.13(c) and (d) show the tuberculation present on Pipes 1and 2 respectively. When compared to their corresponding internal corrosion thickness maps in Figure 8.6(b) and Figure 8.7(b), it can be seen that there is no obvious link between the presence of tuberculation and internal corrosion. In a similar fashion to that of the external encrustation, it appears that some tuberculation and internal corrosion coincide. Here different formations of tuberculation can be found and it is possible that the corrosion may be linked to the tuberculation formation, however, further experimentation would be needed to determine this.

8.9 Trunk Main NDE Contractor Comparison Exercise Summary

In this chapter, a methodology developed in-house (as discussed in the previous chapter) to use a 3D scanner to determine the “ground truth” pipe condition was deployed to assess the extent of corrosion around the circumference and along the length of a section of cast iron trunk main. In doing so, two sections of nominally identical cast iron trunk main section have been inspected by the two main contractors used to conduct NDE on cast iron pipe sections. One of the sections was restricted from having its surface prepared to understand how effective each NDE methodology was on a plain pipe surface. Where surface preparation has been carried out, the level and coverage has been recorded by the 3D scanner.

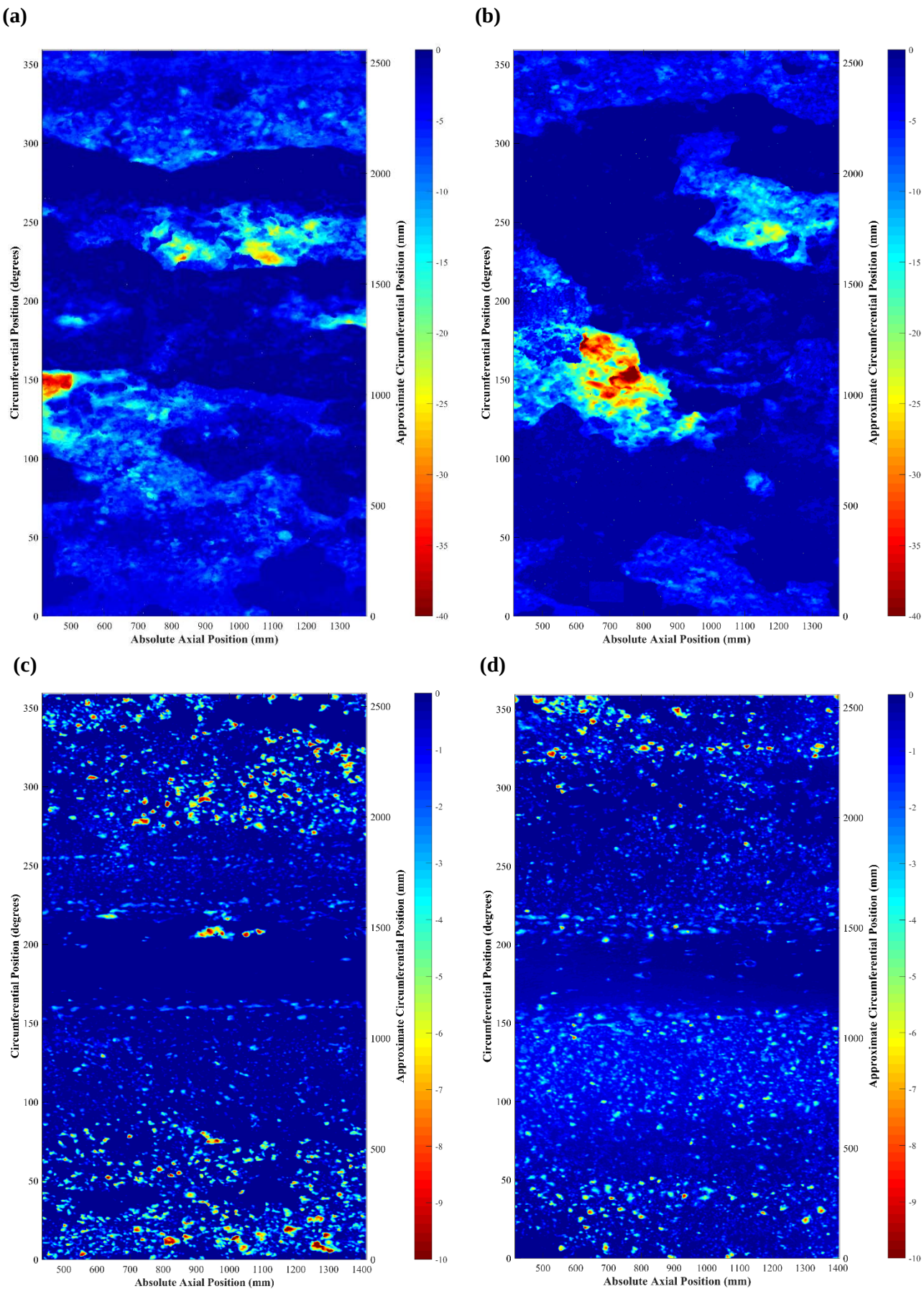

Figure 8.13 - Contour plots detailing the external encrustation and tuberculation for Pipe 1 and 2 as captured by the 3D scanner: a) Pipe 1 encrustation, (b) Pipe 2 encrustation, (c) Pipe 1 tuberculation and (d) Pipe 2 tuberculation.

All of the data supplied by the contractors had undergone a series of post-processing steps before the data was released. In the case of the MFL contractor, their processed results were not representative of the real geometry that was present on the pipe. Consequently, the current methods of post-processing the data do not necessarily add any value to it. In fact, it could be detracting from its value. Fortunately, the MFL contractor was able to provide the raw data captured during the NDE survey. Although, the data could not be interpreted/calibrated to give a quantification of the corrosion thickness present, a normalised plot of the data has shown that the MFL tool is certainly capable of accurately measuring the position of corrosion present on the surface of the pipe, even with little, if any, surface preparation. However, further work is needed to calibrate the raw data to give an accurate corrosion depth. This is a far cry from the ultrasonic contractor who has shown that their technique is heavily reliant on the surface preparation that is carried out and when it is not, no meaningful corrosion could be determined. After which the technique could be considered to be destructive. Further, it is unclear how the measurements are made.

Both contractors need to check the calibration that is needed for the ultrasonic technique as both contractors have overestimated the remaining wall thickness. It has been shown that this is likely to be due to the nominal speed of sound in iron that is used and, as shown in this value is likely to be too great such that thickness values made using this constant are over estimated.

Finally, the 3D scanner methodology developed in Chapter 7 has been shown to be a useful research tool and has allowed thickness and position data for the corrosion mechanisms to be captured and compared to defects on the inner and outer layers. Although this work was unable to prove or disprove a direct link between encrustation or tuberculation and corrosion, it has laid the foundations for further development of the approach and has provided a methodology that could be used to evaluate this questionable link further.

9 Concluding Remarks

9.1 Summary of Work

The UK water infrastructure comprises many thousands of miles of pipes of varying sizes and geometry, and are manufactured from a range of materials. A significant proportion of this network is grey cast iron which, in some areas, was laid over 150 years ago. The network is aging at different rates and is subject to both ongoing leakage and occasional failure in some locations. This causes inconvenience to customers and members of the public through loss of supply, burst related flooding and disruption to travel, and adds significant costs to the operation and management of the network. Failure events can be costly to remedy especially if it is a trunk main failure. TWUL have approximately 6,000 km of grey cast iron trunk main currently in use and are keen to ensure that failure risk is mitigated through proactive replacement of pipes that are near the end of their service life. However, the remaining service life can only be determined accurately if reliable condition assessment data can be obtained for each pipe in the network.

This thesis has detailed three streams of work investigating the possibilities of applying NDE to grey cast iron trunk main. Firstly, a literature review has established the main factors responsible for pipe failure and identified defects, the presence of which suggest an increased potential for failure. The data found in the literature review has enabled an analysis to be carried out to determine the size of defects likely to initiate failure and so provide limits on the size of defects which must be detected by NDE methods. The literature review also established the challenges which must be addressed to enable the application of NDE to cast iron mains. These findings have been drawn together to determine the inspection requirements for any current or future technique for NDE of a cast iron main.

The literature review has also shown that the number of technologies available for use on cast iron is relatively small. Ultrasonic inspection techniques are generally considered to have the potential to identify the defects of interest within sections of cast iron. Laboratory testing using a typical contractor ultrasonic NDE setup has built on the current literature to give experimental results showing the challenges experienced in several inspection scenarios but also the areas where it can be successfully applied. Magnetic techniques were also thought to be a possible choice for application to cast iron pipes. As such, a simple technique, using a permanent magnet to identify sites of graphitic corrosion, has been trialled as a first pass option for water contractors wishing to identify degraded pipes in need of further investigation. It has shown success at characterising corrosion thicknesses of interest and is suggested for development further.

Finally, the findings from these studies highlighted the need to understand better the techniques and processes being used by current water NDE contractors. This led to the development of an improved methodology using a 3D scanner to capture the “ground truth” pipe condition during a destructive analysis for comparison with the reported contractors data. This improved methodology was applied in a contractor comparison exercise to ascertain the abilities of two current TWUL NDE contractors and their techniques for assessing the condition of cast iron trunk main.

The results of these studies have equipped TWUL with an advanced knowledge of the NDE techniques available for cast iron water mains and the inspection requirements. Further, it has identified areas where magnetic tools could be exploited to gather further condition data. Lastly, it has provided the company with a methodology to verify the capabilities any NDE contractor to ensure the data reported will yield results that are representative of the real pipe geometry. Adoption of these points will ensure that TWUL's NDE procedures continues to advance.

9.2 Key Conclusions

The key conclusions for this work are:

- Investigation of pipe failure modes in service suggests that graphitic corrosion is a significant factor responsible for pipe failure, although the presence of inherent defects, such as inclusions, porosity and graphite flakes, also play a role. Acting individually or together they reduce the load carrying area of the metal or promote the formation of cracks which grow and, initiate catastrophic failure under normal service loads. A simple analysis indicates that defects of the order 9 – 16 mm in size can be sufficient to promote pipe failure. Therefore, it is important that all NDE techniques employed to assess pipe condition must be capable of detecting defects of the order of 4 – 5 mm.
- A review of commercially available NDE technologies has demonstrated that variable surface condition, and the presence of corrosion products, need to be overcome in order to accurately assess the condition of trunk mains. It has been shown that ultrasonic inspection, and some magnetic methods, may be adapted for the inspection of grey cast iron trunk mains. Some magnetic methods can only be used for internal inspection which has been shown to be difficult on trunk mains and cannot be used.
- Investigation of ultrasonic inspection has verified that it is possible to use low frequency ultrasound, of the order 1 – 2 MHz, to measure the wall thickness of uncorroded cast iron main. However, an accurate value for the speed of sound in the cast iron must be known, in order to calculate the wall thickness. Further, ultrasonic investigation over a range of samples has shown that the speed of sound in iron can vary by approximately 500 m s^{-1}, which can lead to an error of up to 17% in the thickness calculated. Testing has shown that ultrasound can penetrate graphitic corrosion, termed 'graphitisation', and has a speed of 2700 m s^{-1}. However, it is unable to pass through a multi-layer sample of graphitisation and iron.
- A magnetic technique has been tested on sections of cast iron main to determine the graphitisation thickness. The technique was trialled on a machined cast iron sample with an air gap instead of graphitisation and suggested that it may be possible to detect graphitic corrosion layers 6 mm thick whilst maintaining a spatial resolution of 20 mm. The results have shown that the product of graphitic corrosion possesses weak ferromagnetic properties as opposed to the diamagnetic properties previously believed.
- A 3D scanner methodology for capturing the "ground truth" pipe condition during a destructive analysis has been developed and showed that the external corrosion measurements captured are in-keeping with those currently measured by manual pit depth measurements. However, the 3D

scanner methodology is not subject to the same impairments on corrosion thickness measurements as the hand pit depth measurements and has shown that it can capture measurements across the whole pipe section under investigation regardless of the corrosion geometry. Furthermore, this methodology has enabled the internal corrosion and wall thickness to be measured as well as detailing the level of surface preparation carried out by the NDE contractor during the inspection.

- Finally, when used in a live comparison exercise, the 3D scanner methodology has evaluated two NDE contractors used by TWUL and found that the results provided using the magnetic contractor's algorithm are subject to significant error. However, the raw signals are in-keeping with that of the external corrosion measured by the 3D scanner. These signals have shown that corrosion can be measured even when the surface preparation conducted is restricted to the removal of external encrustation only. The ultrasonic contractor has succeeded in providing some external corrosion results that are in-keeping with those measured by the 3D scanner. However, the analysis has shown that these results have been obtained by the destructive removal of the graphitic corrosion during surface preparation. Further, their technique has been shown to be reliant on significant surface preparation being conducted, particularly at sites of corrosion.

9.3 Further Work

The work carried out here has advanced TWUL's knowledge of the capabilities of NDE technologies currently used in the water industry. In doing so, it has concluded the objectives to measure NDE performance. However, it has also opened further lines of inquiry. Consequently, several streams of further work should be undertaken to continue improving the understanding of NDE in the water industry:

- Whilst ultrasound has proved difficult to apply to a corroded main, it is a potentially useful technique for conducting wall thickness measurements. However, the accuracy of the measurements made is dependent on the correct speed of sound being used for the iron being inspected. A further study should seek to understand the variation in speeds across cohorts of pipes manufactured by horizontal, vertical and spin casting. This should help provide the basis for the selection of suitable calibration standards and methods by which NDE methods and contractor competency can be judged.
- The magnetic testing has shown a capability of detecting corrosion over 4 mm thick, however, even with the strongest magnet available for testing, it was unable to reliably determine the thickness of corrosion thicker than 6 mm. The development of the magnetic testing should be taken further as it could provide a tool that can be applied by untrained operatives to harvest condition data across the network at opportune excavations. To do this, a larger magnet should be investigated to allow deeper corrosion thicknesses to be identified as well as given greater tolerance to variation in spacing between the magnet and the pipe surface due to the surface condition. Magnetic modelling should be employed to investigate other magnetic configurations to enable a magnet with greater strength, and hence the ability to measure the thickness of thicker corrosion, without significant compromise to the spatial resolution of the technique.

- In the live comparison exercise, it was clear that the MFL tool was of benefit, however, the current post-processing applied to the data produces results that are not representative of the real pipe condition. A study should be conducted to evaluate and develop the algorithms used to convert the raw magnetic signals to NDE data to give results that are more in line with the ground truth. This may be a joint project between TWUL and the contractor to provide a tool with enhanced detection capabilities.
- The magnetic contractor used a combination of ultrasonic inspection and MFL to conduct an assessment of the pipe. Both techniques can be seen to be more suited to identifying specific defect types. It is likely that the optimum inspection for a pipe can be gained from inspection with several techniques. Further, NDE contractors of interest should be investigated using the new methodology to understand their capabilities and whether they can improve the inspection currently undertaken. Further, methods of data fusion should be investigated to understand how datasets from different techniques of interest can be brought together to give a more complete dataset showing the condition of a cast iron main.
- The new methodology using 3D scanning to support an NDE comparison exercise is not only about determining the capability of the NDE technique but also the capabilities of the contractor to capture and report accurately the condition of the pipe. This methodology should be further developed to support comparison exercises conducted in a pipe excavation to understand how a contractor performs when exposed to real life conditions rather than on a section of exhumed main where the contractor is provided with good accessibility to the majority of the external surface of the pipe. Further, the shot-blasting process should be reviewed to understand if a full-length section can be shot-blasted satisfactorily. Doing so would reduce the number of 3D scans required, and hence the time taken to run a comparison exercise.
- Finally, the 3D scanner methodology has proven its ability to record the size and position of tuberculation and encrustation as well as the ground truth pipe condition. This methodology should be used to conduct further research to understand if a link between encrustation, tuberculation and corrosion exists.

References

ADDIS, W. (2016) *Structural and Civil Engineering Design.* Routledge.

ADVANCED CONDITION ASSESSMENT AND PIPE FAILURE PREDICTION PROJECT. (2015) *Advanced Condition Assessment and Pipe Failure Prediction Project.* Available from: http://www.criticalpipes.com/ [Accessed on: 26/03/ 2017].

Advanced Engineering Solutions Ltd. (2016) *Advanced Engineering Solutions Limited.* Available from: http://www.aesengs.co.uk/water.php?p=SMFLT [Accessed on: 5th March 2017].

ALLARD, P.H. (2012) 'Pipeline External Corrosion Analysis Using a 3D Laser Scanner'. *Corrosion and Materials,* **37**(2), pp. 50-53.

ALLARD, P.H. and FRASER, J.S. (2013) 'Application of 3D laser method for corrosion assessment on a spherical pressure vessel' *(from the Proceedings of 52nd Annual Conference of the British Institute of Non-Destructive Testing 2013, NDT 2013)* pp.384-392.

ALLEN, R. (2009) *The British Industrial Revolution in Global Perspective.* Cambridge: Cambridge University Press.

ANGUS, H.T. (1976) *Cast iron : physical and engineering properties.* 2nd ed. London: Butterworths.

ARTEC, 3.D. (2016) *3D Scanner Artec Eva | Best Structured-light Scanning Device.* Available from: https://www.artec3d.com/3d-scanner/artec-eva [Accessed on: Dec 30 2016].

ASHBY, M.F. and JONES, D.R.H. (2005) *Engineering materials 1: an introduction to properties, applications and design.* 3rd ed. Boston: Elsevier Butterworth-Heinemann. ISBN 0750663804 9780750663809.

ASTM International. (2016) *ASTM 247-16a: Test method for evaluating the microstructure of graphite in iron castings.* U.S.A.: ASTM

ASTM International. (2014) *ASTM B499 - 09: Standard Test Method for Measurement of Coating Thicknesses by the Magnetic Method: Nonmagnetic Coatings on Magnetic Basis Metals.* U.S.A.: ASTM

ATKINSON, K., WHITER, J.T., SMITH, P.A. and MULHERON, M. (2002) 'Failure of small diameter cast iron pipes'. *Urban Water,* **4**(3), pp. 263-271.

BELMONTE, H.M.S., MULHERON, M.J. and SMITH, P.A. (2007) 'Weibull analysis, extrapolations and implications for condition assessment of cast iron water mains'. *Fatigue and Fracture of Engineering Materials and Structures,* **30**(10), pp. 964-990.

BELMONTE, H.M.S., MULHERON, M.J., SMITH, P.A., HAM, A., WESCOMBE, K. and WHITER, J.T. (2008) 'Weibull-based methodology for condition assessment of cast iron water mains and its application'. *Fatigue and Fracture of Engineering Materials and Structures,* **31**(5), pp. 370-385.

BELMONTE, H.M.S., MULHERON, M.J. and SMITH, P.A. (2009) 'Some observations on the strength and fatigue properties of samples extracted from cast iron water mains'. *Fatigue and Fracture of Engineering Materials and Structures,* **32**(11), pp. 916-925.

BERENS, A.P. (1989) *Metals Handbook, Vol. 17, Nondestructive Evaluation and Quality Control.* Ohio: ASM International.

BISWAS, S., MONROE, C. and PRUCHA, T. (2015) 'Analysis of published cast iron experimental data' *(from the Proceedings of Proceedings of the 3rd World Congress on Integrated Computational Materials Engineering, ICME 2015)* pp.293-303.

BOND, A., MERGELAS, B. and JONES, C. (2004) 'Pinpointing leaks in water transmission mains' *(from the Proceedings of Proceedings of the ASCE Pipeline Division Specialty Congress - Pipeline Engineering and Construction)* pp.955-964.

BRITISH STANDARDS INSTITUTE. (1917) *BS 78:1917 - Cast iron pipes (vertically cast) for water, gas and sewage and special castings for use therewith.* UK: British Standards Institute.

BRUCE, W.A., YAPP, D., BARBORAK, D.M., FINGERHUT, M.P. and KANIA, R. (1997) 'Simple laser-based pipeline corrosion assessment system'. *Pipeline and Gas Journal,* **224**(3), pp. 28.

CARTZ, L. (1995) *Nondestructive testing radiography, ultrasonics, liquid penetrant, magnetic particle, eddy current.* 1st ed. Ohio: ASM International

Cast Iron Pipe Research Association. (1952) *Handbook of cast iron pipe for water, gas, sewerage, and industrial service.* Chicago: Cast iron pipe research Association

CONLIN, R.M. and BAKER, T.J. (1991) *Application of fracture mechanics to the failure behaviour of buried cast iron.* UK: Transport Research Laboratory

COSTELLO, S.B., CHAPMAN, D.N., ROGERS, C.D.F. and METJE, N. (2007) 'Underground asset location and condition assessment technologies'. *Tunnelling and Underground Space Technology,* **22**(5–6), pp. 524-542.

CRUZ, J. (2014) *Discussion on current capability of pit depth measurements.*

DAFTER, M. and PETERSEN, R. (2013) 'Advanced condition assessment of hunter water's cast iron watermains'. *Corrosion and Materials,* **38**(3), pp. 46-49.

DE SILVA, D., DAVIS, P., BURN, S., FERGUSON, P., MASSIE, D., CULL, J., EISWIRTH, M. and HESKE, C. (2002) 'Condition assessment of cast iron and asbestos cement pipes by in-pipe probes and selective sampling for estimation of remaining life' *(from the Proceedings of 20th International No-Dig Conference).*

DEMPSEY, P. and MANOOK, B. (1986) 'Assessing the condition of cast iron pipes'. *Water Research Centre.Swindon, Source Document no.9 for the Water Mains Rehabilitation Manual,(SW/2687),* pp. 41.

DINGUS, M., HAVEN, J. and AUSTIN, R. (2002) *Nondestructive, noninvasive assessment of underground pipelines.* U.S.A.: AWWA Research Foundation and American Water Works Association

DORN, R., HOWSAM, P., HYDE, R.A. and JARVIS, M.G. (1996) *Water Mains:Guidance on Assessment and Inspection Techniques.* London: Construction Industry Research and Information Association.

EVANS, T. (2017) *Discussion on the "Super-pig".*

EVANS, T. (2014) *Discussion on previous comparison exercises.*

FAHIMI, A. (2017) *Mitigating risk associated with the management of trunk mains network.* University of Surrey.

FAHIMI, A., EVANS, T.S., FARROW, J., JESSON, D.A., MULHERON, M.J. and SMITH, P.A. (2016) 'On the residual strength of aging cast iron trunk mains: Physically-based models for asset failure'. *Materials Science and Engineering: A*, **663**, pp. 204-212.

FALQUE, R., VIDAL-CALLEJA, T. and MIRO, J.V. (2015) 'Kidnapped laser-scanner for evaluation of RFEC tool' *(from the Proceedings of IEEE International Conference on Intelligent Robots and Systems)* pp.313-318.

FALQUE, R., VIDAL-CALLEJA, T., MIRO, J.V., LINGNAU, D.C. and RUSSEL, D.E. (2014) 'Background Segmentation to Enhance Remote Field Eddy Current Signals' *(from the Proceedings of Australasian Conference on Robotics and Automation).*

FITZGERALD, J.H. (2007) 'Longevity of a graphitized cast iron water main'. *Materials Performance*, **46**(5).

GERKE, T.L., MAYNARD, J.B., SCHOCK, M.R. and LYTLE, D.L. (2008) 'Physiochemical characterization of five iron tubercles from a single drinking water distribution system: Possible new insights on their formation and growth'. *Corrosion Science*, **50**(7), pp. 2030-2039.

HALMSHAW, R. (1991) *Non-destructive testing.* 2nd ed. London: E. Arnold.

HAO, T., ROGERS, C.D.F., METJE, N., CHAPMAN, D.N., MUGGLETON, J.M., FOO, K.Y., WANG, P., PENNOCK, S.R., ATKINS, P.R., SWINGLER, S.G., PARKER, J., COSTELLO, S.B., BURROW, M.P.N., ANSPACH, J.H., ARMITAGE, R.J., COHN, A.G., GODDARD, K., LEWIN, P.L., ORLANDO, G., REDFERN, M.A., ROYAL, A.C.D. and SAUL, A.J. (2012) 'Condition assessment of the buried utility service infrastructure'. *Tunnelling and Underground Space Technology*, **28**(1), pp. 331-344.

HARRIS, C.M. (2005) *Dictionary of architecture & construction.* New York: McGraw-Hill

HERTZBERG, R.W. (1996) *Deformation and fracture mechanics of engineering materials.* 4th ed. New York: Wiley.

HYDROSAVE. (2017) *Non-Destructive Testing.* Available from: http://www.hydrosave.co.uk/services/pipeline-condition-inspections/non-destructive-testing/ [Accessed on: Mar 5, 2017].

JACKSON, R., PITT, C.and SKABO, R. , 1992. *Nondestructive testing of water mains for physical integrity.* U.S.A: AWWA Research Foundation and American Water Works Association [viewed 9/30/2013 11:52:01 AM].

JD7. (2017) *JD7 :: Pipescan+*. Available from: http://www.jd7.co.uk/water/products/pipescan [Accessed on: 5th March 2017].

JESSON, D.A., LE PAGE, B.H., MULHERON, M.J., SMITH, P.A., WALLEN, A., COCKS, R., FARROW, J. and WHITER, J.T. (2010) 'Thermally induced strains and stresses in cast iron water distribution pipes: An experimental investigation'. *Journal of Water Supply: Research and Technology - AQUA*, **59**(4), pp. 221-229.

JESSON, D.A., MOHEBBI, H., FARROW, J., MULHERON, M.J. and SMITH, P.A. (2013) 'On the condition assessment of cast iron trunk main: The effect of microstructure and in-service graphitisation on mechanical properties in flexure'. *Materials Science and Engineering: A*, **576**(0), pp. 192-201.

JOHNSTON, C. (2016) Stoke Newington flood: 150 north London homes under water. *The Guardian*

KAMIGAKI, K. (1957) 'Ultrasonic attenuation in steel and cast iron', pp. 48-77.

KAYE AND LABY. (2015) *The speed and attenuation of sound 2.4.1 * Available from: http://www.kayelaby.npl.co.uk/general_physics/2_4/2_4_1.html [Accessed on: 19/03/ 2017].

KLEINER, Y. and RAJANI, B. (2013) 'Performance of ductile iron pipes. II: Sampling scheme and inferring the pipe condition'. *Journal of Infrastructure Systems,* **19**(1), pp. 120-128.

KLEINER, Y. and RAJANI, B. (2011) 'Sampling and condition assessment of ductile iron pipes' *(from the Proceedings of World Environmental and Water Resources Congress 2011: Bearing Knowledge for Sustainability - Proceedings of the 2011 World Environmental and Water Resources Congress)* pp.30-41.

KLEINER, Y., RAJANI, B. and KRYS, D. (2013) 'Performance of ductile iron pipes. I: Characterization of external corrosion patterns'. *Journal of Infrastructure Systems,* **19**(1), pp. 108-119.

KLEINER, Y., RAJANI, B. and KRYS, D. (2012) 'Impact of soil properties on pipe corrosion: Re-examination of traditional conventions' *(from the Proceedings of Water Distribution Systems Analysis 2010 - Proceedings of the 12th International Conference, WDSA 2010)* pp.968-982.

KMPFER, W. and ZIEHL, W. (1996) 'Optical pipe-scanning system for sewers: RODIAS' *(from the Proceedings of Proceedings of SPIE - The International Society for Optical Engineering)* **2947** pp.148-156.

KRAUTKRAMER, J. and KRAUTKRAMER, H. (1977) *Ultrasonic testing of materials.* 2nd ed. Berlin: Springer-Verlag.

LARTER, G. and DUFFELL, B. (2017) *Homes flooded as 15-inch water main bursts in Horsell.* Available from: http://www.getsurrey.co.uk/news/surrey-news/littlewick-road-burst-water-main-12563941 [Accessed on: Feb 26, 2017].

LEINOV, E., LOWE, M.J.S. and CAWLEY, P. (2015) 'Investigation of guided wave propagation and attenuation in pipe buried in sand'. *Journal of Sound and Vibration,* **347**, pp. 96-114.

LIU, Z., KLEINER, Y., RAJANI, B., WANG, L. and CONDIT, W. (2012) *Condition Assessment Technologies for Water Transmission and Distribution Systems.* U.S.A: United States Environmental Protection Agency.

LIU, Z., KRYS, D., RAJANI, B. and NAJJARAN, H. (2008) 'Processing laser range image for the investigation on the long-term performance of ductile iron pipe'. *Nondestructive Testing and Evaluation,* **23**(1), pp. 65-75.

LIU, Z. and KLEINER, Y. (2013) 'State of the art review of inspection technologies for condition assessment of water pipes'. *Measurement: Journal of the International Measurement Confederation,* **46**(1), pp. 1-15.

LOGAN, R., MULHERON, M.J., JESSON, D.A., SMITH, P.A., EVANS, T.S., CLAY-MICHAEL, N. and WHITER, J.T. (2014) 'Graphitic corrosion of a cast iron trunk main: Implications for asset management' *(from the Proceedings of WIT Transactions on the Built Environment)* **139** pp.411-422.

LOGAN, R.G. (2016) *The graphitic corrosion of cast iron: aspects on the deterioration of trunk main.* University of Surrey.

MAKAR, J. and CHAGNON, N. (1999) 'Inspecting systems for leaks, pits, and corrosion'. *Journal (American Water Works Association),* **91**(7), pp. 36-46.

MAKAR, J.M. (2000) 'A preliminary analysis of failures in grey cast iron water pipes'. *Engineering Failure Analysis,* **7**(1), pp. 43-53.

MAKAR, J.M., DESNOYERS, R. and MCDONALD, S.E. (2001) 'Failure modes and mechanisms in grey cast iron pipe'. *Underground Infrastructure Research: Municipal, Industrial, and Environmental Applications,*.

MAKAR, J.M. and RAJANI, B. (2000) 'Gray cast-iron water pipe metallurgy'. *Journal of Materials in Civil Engineering*, **12**(3), pp. 245-253.

MARSHALL, P. (2001) *The Residual Structural Properties of Cast Iron Pipe - Structural and Design Criteria for Linings for Water Mains.* UK: UK WIR.

MIRO, J.V., RAJALINGAM, J., VIDAL-CALLEJA, T., DE BRUIJN, F., WOOD, R., VITANAGE, D., ULAPANE, N., WIJERATHNA, B. and SU, D. (2013) 'A live test-bed for the advancement of condition assessment and failure prediction research on critical pipes' *(from the Proceedings of Proceedings of the Leading-Edge Strategic Asset Management Conference (LESAM13)).*

MOHEBBI, H. and LI, C. (2011) 'Experimental Investigation on Corrosion of Cast Iron Pipes'. *International Journal of Corrosion,*.

MOHEBBI, H., JESSON, D.A., MULHERON, M.J. and SMITH, P.A. (2010) 'The fracture and fatigue properties of cast irons used for trunk mains in the water industry'. *Materials Science and Engineering A*, **527**(21-22), pp. 5915-5923.

MOHEBBI, H., JESSON, D.A., MULHERON, M.J. and SMITH, P.A. (2009) 'Characterisation of the fatigue properties of cast irons used in the water industry and the effect on pipe strength and performance'. *Journal of Physics: Conference Series*, **181**(1), pp. -.

MONCHALIN, J., NÉRON, C., BUSSIÈRE, J.F., BOUCHARD, P., PADIOLEAU, C., HÉON, R., CHOQUET, M., AUSSEL, J., DUROU, G. and NILSON, J.A. (1998) 'Laser-Ultrasonics: From the Laboratory to the Shop Floor'. *Advanced Performance Materials*, **5**(1), pp. 7-23.

NACE International (2013) 'Material matters: Handheld laser scanner generates computer images to assess external pipeline corrosion'. *Materials Performance*, **52**(8)

OLYMPUS CORPORATION. (2013) *Material Sound Velocities / Olympus.* Available from: http://www.olympus-ims.com/en/ndt-tutorials/thickness-gage/appendices-velocities/ [Accessed on: January 20th, 2017].

OSKOUIE, P., BECERIK-GERBER, B. and SOIBELMAN, L. (2016) 'Automated measurement of highway retaining wall displacements using terrestrial laser scanners'. *Automation in Construction*, **65**, pp. 86-101.

PETERSEN, R.B., DAFTER, M. and MELCHERS, R.E. (2013) 'Long-term corrosion of buried cast iron water mains: field data collection and model calibration.'. *Water Asset Management International*, **9**, pp. 13-17.

PETERSEN, R.B. and MELCHERS, R.E. (2012) 'Long-term corrosion of cast iron cement lined pipes' *(from the Proceedings of Annual Conference of the Australasian Corrosion Association 2012)* pp.146-157.

PREWITT, T.J. (2016) 'Application of 3D metrology technology in inspection, corrosion mapping, and failure analysis' *(from the Proceedings of NACE Corrosion Conference 2016)*

PRINSLOO, K., WRIGGLESWORTH, M. and WEBB, M. (2011) 'Advancement of condition assessment techniques for large diameter pipelines'. *Civil Engineering*, **19**(9), pp. 20-25.

RAINER, A., CAPELL, T.F., CLAY-MICHAEL, N., DEMETRIOU, M., EVANS, T.S., JESSON, D., MULHERON, M.J., SCUDDER, L. and SMITH, P.A. (2017) 'What does NDE need to achieve for cast iron pipe networks?'. *Infrastructure Asset Management*, **42**(2). pp. 68-82.

RAJ, B. (2001) 'Nondestructive Testing and Evaluation: Overview' *Encyclopedia of Materials: Science and Technology (Second Edition)* Oxford: Elsevier, pp. 6177-6184.

RAJANI, B. and ABDEL-AKHER, A. (2013a) 'Behaviour and response of lead-caulked bell–spigot joints in cast iron water mains'. *Engineering Structures*, **56**, pp. 2005-2013.

RAJANI, B. and ABDEL-AKHER, A. (2013b) 'Performance of Cast-Iron-Pipe Bell-Spigot Joints Subjected to Overburden Pressure and Ground Movement'. *Journal of Pipeline Systems Engineering and Practice*, **4**(2), pp. 98-114.

RAJANI, B. and ABDEL-AKHER, A. (2012) 'Re-assessment of resistance of cast iron pipes subjected to vertical loads and internal pressure'. *Engineering Structures*, **45**, pp. 192-212.

RAJANI, B. and MAKAR, J. (2000) 'A methodology to estimate remaining service life of grey cast iron water mains'. *Canadian Journal of Civil Engineering*, **27**(6), pp. 1259-1272.

RAJANI, B., ZHAN, C. and KURAOKA, S. (1996) 'Pipe-soil interaction analysis of jointed water mains'. *Canadian Geotechnical Journal*, **33**(3), pp. 393-404.

RAJANI, B. and KLEINER, Y. (2011) 'Fatigue Failure of Large-Diameter Cast Iron Mains'. *Water Distribution Systems Analysis 2010*, pp. 1146-1159.

REICHERT, C.T., HUANG, T. and YAPP, D. (2001) 'Laser-based external corrosion mapping of pipelines' *(from the Proceedings of SPIE)* **4189** pp.90.

REID, E.F. (1934) 'Failures in steel and cast-iron mains and provisions for their protection'. *ICE Selected Engineering Papers*, **1**(154).

RIZZO, P. (2010) 'Water and Wastewater Pipe Nondestructive Evaluation and Health Monitoring: A Review'. *Advances in Civil Engineering*, **2010**.

ROBERGE, P.R. (2007) *Corrosion inspection and monitoring.* Hoboken: Wiley-Interscience

SARIN, P., SNOEYINK, V.L., BEBEE, J., JIM, K.K., BECKETT, M.A., KRIVEN, W.M.and CLEMENT, J.A. (2004) 'Iron release from corroded iron pipes in drinking water distribution systems: effect of dissolved oxygen'. *Water Research*, ***38***(5), pp.1259-1269.

SCUDDER, L. (2014) *Discussion on data processing used during NDE comparison exercises.*

SCUDDER, L. (2013) *Discussion on replacement of several London trunk mains.*

SEICA, M.V. and PACKER, J.A. (2004) 'Mechanical properties and strength of aged cast iron water pipes'. *Journal of Materials in Civil Engineering*, **16**(1), pp. 69-77.

SHANNON, B., RATHNAYAKA, S., ZHANG, C. and KODIKARA, J. (2016) 'Lessons learnt on pipe failure mechanisms from observation of exhumed cast iron pipes' *(from the Proceedings of OzWater 2016).*

SHARP, J. (1914) *Some considerations regarding cast iron & steel pipes.* London: Longmans

SHELL BITUMEN. (1995) *The Shell Bitumen industrial handbook.* Chertsey: Shell Bitumen.

SHEPHERD, M. (2014) *Discussion on the Critical Pipes Project Progress.*

SKINNER, B., VIDAL-CALLEJA, T., MIRO, J.V., DE BRUIJN, F. and FALQUE, R. (2014) '3D point cloud upsampling for accurate reconstruction of dense 2.5D thickness maps' *(from the Proceedings of Australas. Conf. Robot. Autom.(ACRA)).*

SUN, G.X. and WANG, Y.M. (1990) 'The role of dendrites and eutectics in the fracture of grey iron, physical metallurgy of cast iron IV'. *Proc., 4th Int.Symp.on the Phys.Metallurgy of Cast Iron,*.

ŚWIETLIK, J., RACZYK-STANISŁAWIAK, U., PISZORA, P.and NAWROCKI, J. (2012) 'Corrosion in drinking water pipes: The importance of green rusts'. *Water Research*, **46**(1), pp. 1-10.

SYRINIX. (2017) *TrunkMinder*. Available from: http://www.syrinix.com/solutions/trunk-minder/ [Accessed on: Mar 5, 2017].

SZILARD, J. (1982) *Ultrasonic testing : non-conventional testing techniques.* New York ; Chichester: New York ; Chichester : Wiley.

TALBOT, A.N. (1926) "'Strength properties of cast iron pipe made by different processes as found by tests"'. *J.Am.Water Works Assoc.*, **16**, pp. 1-44.

THE STANTON IRONWORKS COMPANY LIMITED. (1936) *Cast iron pipe: its life and service.* Nottingham: The Stanton Ironworks Company Limited

THOMSON, J. and WANG, L. (2009). *State of technology review report on condition assessment of ferrous water transmission and distribution systems.* U.S.A: US Environmental Protection Agency

TRAVERS, F.A. (1997) 'Acoustic monitoring of prestressed concrete pipe'. *Construction and Building Materials*, **11**(3), pp. 175-187.

UK GOVERNMENT. (2016) *The Water Supply (Water Quality) Regulations 2016.* Available from: http://www.legislation.gov.uk/uksi/2016/614/contents/made [Accessed on: 5th March 2017].

ULAPANE, N., ALEMPIJEVIC, A., VIDAL-CALLEJA, T., MIRO, J.V., RUDD, J. and ROUBAL, M. (2014) 'Gaussian process for interpreting pulsed eddy current signals for ferromagnetic pipe profiling' *(from the Proceedings of 9th IEEE Conference on Industrial Electronics and Applications, ICIEA 2014)* pp.1762-1767.

VICKRIDGE, I. and LAU, T. (2000) *Lessons Learnt from Pipeline Condition Assessment in Hong Kong*. Hong Kong: Black and Veatch.

VIDAL-CALLEJA, T., SU, D., DE BRUIJN, F. and MIRO, J.V. (2014) 'Learning spatial correlations for Bayesian fusion in pipe thickness mapping' *(from the Proceedings of IEEE International Conference on Robotics and Automation)* pp.683-690.

VIENS, M., LÉVESQUE, D., JEN, C.K. and HÉBERT, H. (1996) 'In-situ ultrasonic thickness measurement of underground water mains'. *Proceedings of SPIE - the International Society for Optical Engineering*, **2947**, pp. 157-164.

WALFORD, C. (2012) *Hundreds of passengers forced to escape on tracks as Tube line is flooded with TWO MILLION litres of water by blundering workmen near Olympic station.* Available from: http://www.dailymail.co.uk/news/article-2155978/Tube-line-flooded-TWO-MILLION-litres-water-blundering-workmen-near-Olympic-station.html [Accessed on: Feb 26, 2017].

WU, W., LIU, Z. and KRYS, D. (2012) 'Improving laser image resolution for pitting corrosion measurement using Markov random field method'. *Automation in Construction*, **21**(1), pp. 172-183.

YAMAMOTO, K., MIZOGUTI, S., YOSHIMITSU, K. and KAWASAKI, J. (1983) 'Relation between graphitic corrosion and strength-degredation of cast iron pipe'. *Boshoku Gijutsu*, **32**(3), pp. 157-162.

Appendix A Journal Paper

Infrastructure Asset Management
Volume XXXX Issue XXXX

What does NDE need to achieve for cast iron pipe networks?
Rainer, Capell, Clay-Michael *et al.*

Infrastructure Asset Management, **XXXX**(XXXX), 1–XX
http://dx.doi.org/10.1680/jinam.16.00020
Paper 1600020
Received 07/12/2016; accepted 03/03/2017
Keywords: materials technology/rehabilitation, reclamation & renovation/water supply

ice
Institution of Civil Engineers
publishing

What does NDE need to achieve for cast iron pipe networks?

Alexander Rainer MEng
Faculty of Engineering and Physical Sciences, University of Surrey, Guildford, UK

Tobias F. Capell PhD
Faculty of Engineering and Physical Sciences, University of Surrey, Guildford, UK

Nic Clay-Michael
Clay-Michael Ltd, Reading, UK

Michael Demetriou MEng
Faculty of Engineering and Physical Sciences, University of Surrey, Guildford, UK

Timothy S. Evans PhD
Innovation, Thames Water Utilities Ltd, Reading, UK

David A. Jesson PhD, CEng, CSci, FIMMM
Centre for Engineering Materials, Department of Mechanical Engineering Sciences, Faculty of Engineering and Physical Sciences, University of Surrey, Guildford, UK (corresponding author: d.jesson@surrey.ac.uk)
(Orcid:0000-0003-1045-6194)

Michael J. Mulheron PhD
Faculty of Engineering and Physical Sciences, University of Surrey, Guildford, UK

Lawrence Scudder PhD
Innovation, Thames Water Utilities Ltd, Reading, UK

Paul A. Smith PhD, CEng, FIMMM
Faculty of Engineering and Physical Sciences, University of Surrey, Guildford, UK

Grey cast iron water pipe networks have been installed around the world, often 100–180 years ago. Cohorts (which can be defined by age, size, casting technology and geographical location, to specify but a few groups) degrade at different rates due to environmental and in-service issues, which can lead to a significant loss in mechanical performance. Hence, the management of these assets can be extremely problematic in terms of identifying priorities. The current paper considers the causes of such degradation, the consequences for defining accurate and up-to-date condition assessment protocols and hence the type and urgency of rehabilitation strategies. It follows that understanding the integrity/life expectancy of water networks requires non-destructive evaluation (NDE) of large-diameter cast iron trunk mains, with particular reference to the kinds of defects that are likely to be present and the issues that make assessment difficult. From this, recommendations for asset managers required to specify NDE protocols, based on an understanding of the nature of the material and conditions in the field, are outlined.

Notation

a	crack length
K	stress intensity factor
K_c	critical stress intensity factor; also referred to as fracture toughness
t_g	depth of external graphitic corrosion
t_i	remaining thickness of cast iron
t_w	total wall thickness
t_z	depth of transition zone
Y	a crack geometry-dependent, dimensionless constant
σ	stress

Introduction

Large-diameter trunk mains, with diameters on the order of 12–60 in. (300–1500 mm), are vital components of water networks around the world, conveying large volumes of water over long distances. Cast iron was considered to be the wonder material of the Victorian era (Gagg and Lewis, 2011). Stilgoe considered this to still be the case in the early part of the twentieth century: 'I can always say of the Cast-iron Water Main that it is a well-tried, faithful, and honest servant of the Water Engineer' (Stanton Iron Works Company, 1936). Hence, many trunk main made of grey cast iron and installed 100–150 years ago are still in service today.

This ageing cast iron infrastructure is deteriorating at different rates (Atkinson *et al.*, 2002; Rajani and Makar, 2000): when sufficiently degraded, it can burst, leading to flooding, property damage and disruption of supply and local transport. Such issues have multiple impacts, raise concerns over public safety and lead to customer dissatisfaction. The risk of a burst can be reduced by replacement programmes, but rehabilitation or renewal can cost millions of pound per kilometre. Therefore, asset managers need models, fed with accurate data from the field, to target replacements strategically.

Non-destructive evaluation (NDE) has been routinely carried out on ferrous oil and gas pipelines for many years (Roberge, 2007), and it is perhaps not surprising that discussion on the NDE of water networks either begins with or rapidly turns to methods deployed in the oil and gas industry. However, what is often overlooked is that many of the challenges facing water networks have not been present in the oil and gas industry or are more easily overcome. Compared with cast iron water trunk mains, these pipelines are straight, well protected against corrosion and constructed from thinner steel (of a consistent microstructure), with facilities for their future inspection. In contrast, water pipes were constructed from thicker sections of cast iron (of heterogeneous microstructure and varying quality), with little protection against corrosion, buried without thought for their future inspection and in the urban context are connected to many smaller pipe networks which directly supply customers.

Water quality is a significant, and legislative, issue placing further constraints on the application of NDE techniques: the taste and odour, not to mention the potability (in terms of acceptable bacterial, particulate and chemical concentrations), must not be compromised by internal or external assessment. With regard to internal assessment, discolouration is also a risk that must be mitigated (HMG, 2000). Further, any NDE used must not damage the pipe such that its remaining life is shortened. Consequently, conducting NDE is significantly more challenging than just finding cracks and other defects.

Starting with a detailed review of the nature of defects and their effect on the strength of pipes, this paper provides context for the various defects that require characterisation in order for asset management models to be informed suitably. The difficulties in collecting such data in the field are also considered and the requirements for data collection by NDE in 'real-world' situations determined.

The nature of defects and their effect on the strength of pipes

What is a defect?

A trunk main can be idealised as a cylinder of consistent diameter, uniform thickness and homogeneous microstructure in which failure occurs when the stresses in the main exceed the strength of the material. However, old cast iron trunk mains contain myriad defects, which may act as stress concentrators, reducing the loads that the main can withstand. These defects can be split into three categories: defects produced during manufacture (defects formed beforehand), defects induced during installation (defects formed at the beginning) and defects arising throughout service (defects *per cultum vitae*).

Manufacturing defects

The properties of cast iron are controlled by the graphite flake structure (Angus, 1976). The use of this material spans several technological advances; hence, cohorts of pipes have been manufactured using successively improved processes, leading to products of greater reliability. Initial production used horizontal pit casting and then moved to vertical pit casting before arriving at spin (or centrifugal) casting. These developments led to a greater uniformity of wall thickness and a more refined microstructure with smaller graphite flakes and improved mechanical properties (Stanton Iron Works Company, 1936). A significant problem with characterising any network that has developed over a significant period is that the stock is extremely variable in terms of manufacturing technique and quality. Variation in wall thickness was reduced, and defects arising from misalignment of internal and external moulds were reduced by the move from one technology to another and indeed by improvements in each technique, where adopted by reputable manufacturers. However, it is not unusual to see variations in the wall thickness of pipes. Figure 1 presents a contour map based on physical measurement of a vertically pit cast pipe dating from the 1920s and produced by the renowned Stanton

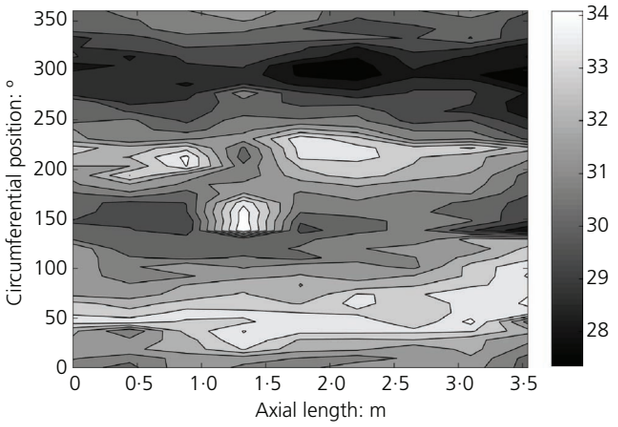

Figure 1. A wall thickness map showing the variation in wall thickness in millimetres from manual point measurements, taken with a calliper, around the circumference of a 3·54 m long, 42 in. (1·07 m) dia. vertical pit cast trunk main sectioned into rings and each ring sectioned into quarters. The darkest point represents the thinnest point and the lightest the thickest. The wall thickness varies by ±4 mm around a mean of 31 mm

Iron Works Company. The pipe, which can be considered to be of the highest quality available at the time, still shows some ±10% variation around a nominal average thickness.

Other possible casting defects, which also diminished because of advances in manufacturing techniques, include porosity, slag inclusions and so-called cold shuts, where two fronts of molten iron fail to fuse properly due to premature cooling.

Installation defects

Following manufacture, the cast iron pipes were transported to site for installation on trucks and trailers and would either be rolled down planks of wood from the edge of the truck or be lifted with a crane. It has been suggested that pipes handled this way were susceptible to damage from collisions between the pipes and other external bodies. Not all impacts would produce a visible crack: an internal crack in the bell or spigot (Rajani and Kleiner, 2010) would not necessarily be detected by on-site hammer testing typical of the time. Additionally, the use of chains for pipe handling rather than canvas slings is known to have damaged the protective outer coal tar or bitumen coating, leaving areas of bare metal.

Once the pipes were in situ, the joint would be packed with hemp to form a seal, filled with molten lead and finally caulked by hammering the solidified lead into the joint (Rajani and Abdel-Akher, 2013; Stanton Iron Works Company, 1936). If the caulking was carried out incorrectly, the lead would be hammered too far into the joint, leading to an increase in stress around the joint, potentially causing a crack to initiate. A worst-case scenario would see poor caulking practice growing a crack created during the siting of the pipe. This could result in a structurally flawed pipe with a reduced service life.

Service-induced defects

Once in service, mains are subject to further mechanisms that can cause defects to form and grow until the defects are too large for the pipe to sustain. In places where the bitumen or tar coating is compromised (often as a result of the installation process as mentioned earlier), corrosion processes are initiated which can further undercut the coating, causing it to spall, expose bare metal and continue to corrode. Of particular concern is 'graphitisation', which should properly be termed 'graphitic corrosion' (Logan *et al*., 2014a, 2014b). Despite anecdotal assertion, it is generally not possible to identify graphitic corrosion by visual inspection in exposed pipes since the corroded region does not change in volume (although the density decreases) and the pipe appears unaffected to the naked eye. This may reduce the residual strength capacity of the pipe (Figure 2).

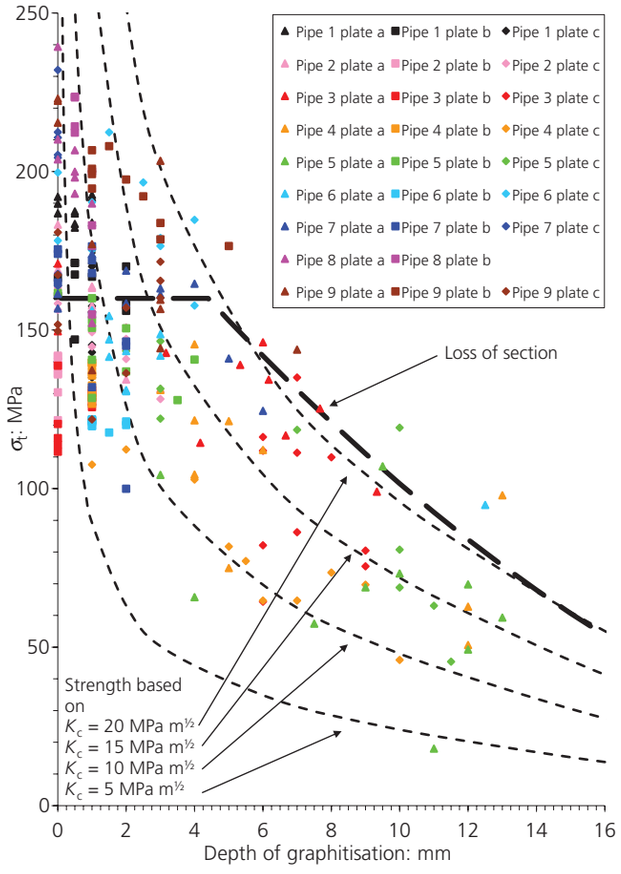

Q4 **Figure 2.** The strength of cast iron samples against the maximum depth of graphitic corrosion measured on the fracture surface of that sample. Ten samples were taken from a plate, and three plates were taken cut from each of the nine pipes studied. The plates were taken from random locations along and around the barrel of the pipe. It is worth noting that in a number of cases, the plates taken from a specific pipe exhibit very different properties. Models for strength based on loss of section and fracture mechanics approaches (values of fracture toughness K_c ranging from 5 to 20 MPa m$^{1/2}$) have also been superimposed (reproduced from Jesson *et al*. (2013) with permission from Elsevier)

Graphitic corrosion is identified by two distinct areas: a passive grey brittle corrosion product and an active transition zone, typically 1–2 mm deep, bounded by the corrosion product on one side and the virgin iron on the other, where the corrosion process occurs (Logan *et al*., 2014a, 2014b). The corrosion product has been seen to occur in two broadly defined topologies (Figure 3): a uniform thickness over large areas or more localised pits with both diameter and depth on the order of 10 mm. It is the more localised corrosion that is potentially more damaging as it provides a stress concentration at its root, which in the worst case can be thought of as a crack.

In smaller-diameter distribution mains, graphitic corrosion has been shown to have a significant impact on the strength of the pipe and to be in competition with defects that have originated during manufacture (formed beforehand) and installation (formed at the beginning). Further, because of the combination of the size of the pipe and its interaction with the local environment, it is possible to comment on the behaviour of the main a significant distance (multiple casting lengths or 'sticks' of pipe, typically 3–5 m long) either side of a sampling point (Belmonte *et al*., 2007, 2008, 2009). The size and spread of graphitic corrosion in distribution mains can be seen in Figure 4.

Q5

In larger-diameter trunk mains, however, the size of the pipe and hence the volume of ground that it interacts with mean that similarly sized samples taken from different parts of the same stick can give very different results (Jesson *et al*., 2013). As part of the present work, the distribution of the depth of graphitic corrosion over single sticks, from each of the mains for which strength data are shown in Figure 2, was assessed and observed to vary greatly across the stick. Figure 5 shows an example of the

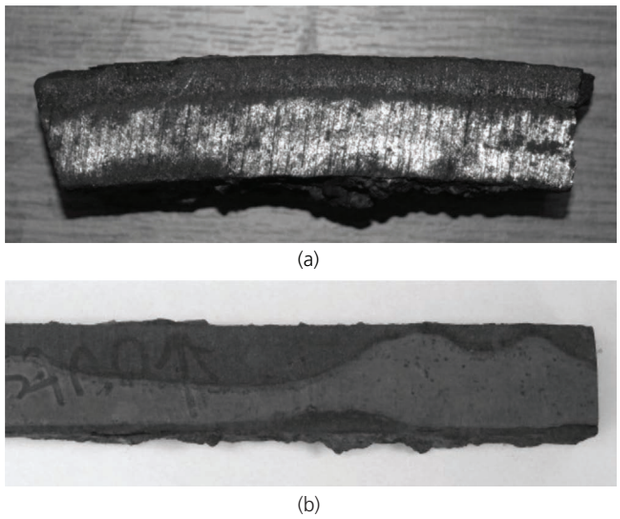

(a)

(b)

Figure 3. Full wall thickness specimens (~30 mm thick) indicating the variation in graphitic corrosion morphology: (a) uniform and (b) more localised, pitting corrosion

(a)

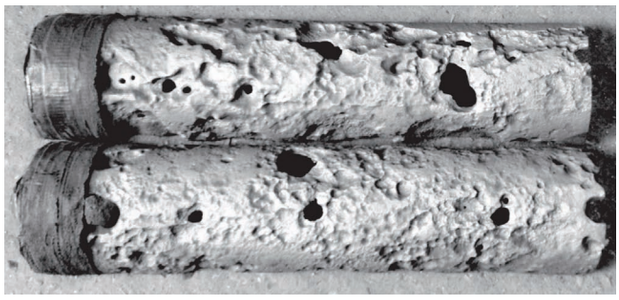

(b)

Figure 4. Digital photographs of a split section of 4 in. (102 mm) dia. distribution main illustrating the spread of corrosion and the amount of metal that can be lost to the graphitic corrosion process: (a) before shot blasting and (b) after shot blasting

data observed for one stick. The variability means that any evaluation technique must consider the whole surface of the pipe (albeit ignoring the difficult geometry of the bell and spigot) in order to provide a meaningful assessment of a pipe. In conjunction with the variation in the depth of graphitisation from point to point within the trunk main pipe, it should be noted that the stress, arising from a combination of vertical load (due for instance to soil and traffic) and water pressure, will vary with position around the pipe. These effects were considered in a recent paper by Fahimi *et al*. (2016).

Finally, in terms of service-induced defects, it is worth noting that fatigue, potentially induced by operational pressure variations and traffic loading, has been cited as a problem, particularly in connection with the growth of installation defects (Rajani and Kleiner, 2010). This assertion is predicated on the presence of a substantial initial crack (on the order of 20 mm) which needs to grow by only a small amount (1–2 mm) to cause catastrophic failure. Experimental work on the fatigue properties of cast iron presents a somewhat mixed view. It perhaps seems more likely that fatigue may be a contributory factor when taken in conjunction with corrosion: these two may combine to cause premature failure (Belmonte *et al*., 2009). Cast iron is known to undergo mechanical fatigue (Angus, 1976; Belmonte *et al*., 2009; Mohebbi *et al*., 2010), although it should be noted that a specific mechanism which combines both fatigue and corrosion has not been established.

Assessing condition in the field

Overview of NDE techniques

Every NDE technique has strengths and weaknesses: there are several excellent reviews on such techniques and their specific capabilities (Costello *et al*., 2007; Dingus *et al*., 2002; Dorn *et al*., 1996; Hao *et al*., 2012; Jackson *et al*., 1992; Liu and Kleiner, 2013; Prinsloo *et al*., 2011; Thomson *et al*., 2009); key features of these reviews are summarised in Table 1. All of these papers review the literature regarding NDE and explain the operation of each technique. In some cases, the results of field tests that evaluate each NDE technique's efficacy on cast iron main are given. However, such reviews, while providing an insight into potential NDE techniques that may be applicable to cast iron, rarely consider the different *types* of defect and the challenges in *finding* such defects in a buried pipe in service ('live') in the field. Where field results have been obtained, the results consider only inspection carried out internally on small-diameter pipes. Little consideration has been shown for techniques that can be applied to the outside of the pipe, nor on the techniques that could be used to inspect much larger trunk main. Ultimately, many of the reviews identify very similar tools for potential use on cast iron pipes, rather than describing how their methodology may be applied to the pipe or locating specific defects.

What does NDE need to do?

The risk of a trunk main burst and the need for proactive NDE to inform targeted rehabilitation and replacement to avoid these bursts are clear. The suitability of a technique for this application must be determined, particularly when it is borne in mind that corrosion processes may occur at both external and internal surfaces and that other defects (such as cracks, voids, cold shuts and inclusions) may exist throughout the section. The application of NDE to a cast iron trunk main is further complicated by the challenging environment in which inspection must be carried out.

In this section, the type and size of defects which must be sought to prevent failure in a worst-case scenario are considered further and an order of priority advised. This is important as certain defects may be more detrimental than others to the remaining service life of the main since they can continue to grow until failure ensues. Finally, the logistics of conducting an inspection on a trunk main and other issues for NDE of a cast iron trunk main are also described.

Which type of defect is the most important to locate?

Determining what the NDE is trying to find requires a good understanding of what indicates a poor condition. While the defects mentioned previously could all contribute to failure, some are more likely to cause failure than others are. Corrosion has been shown to reduce severely the structural performance of cast

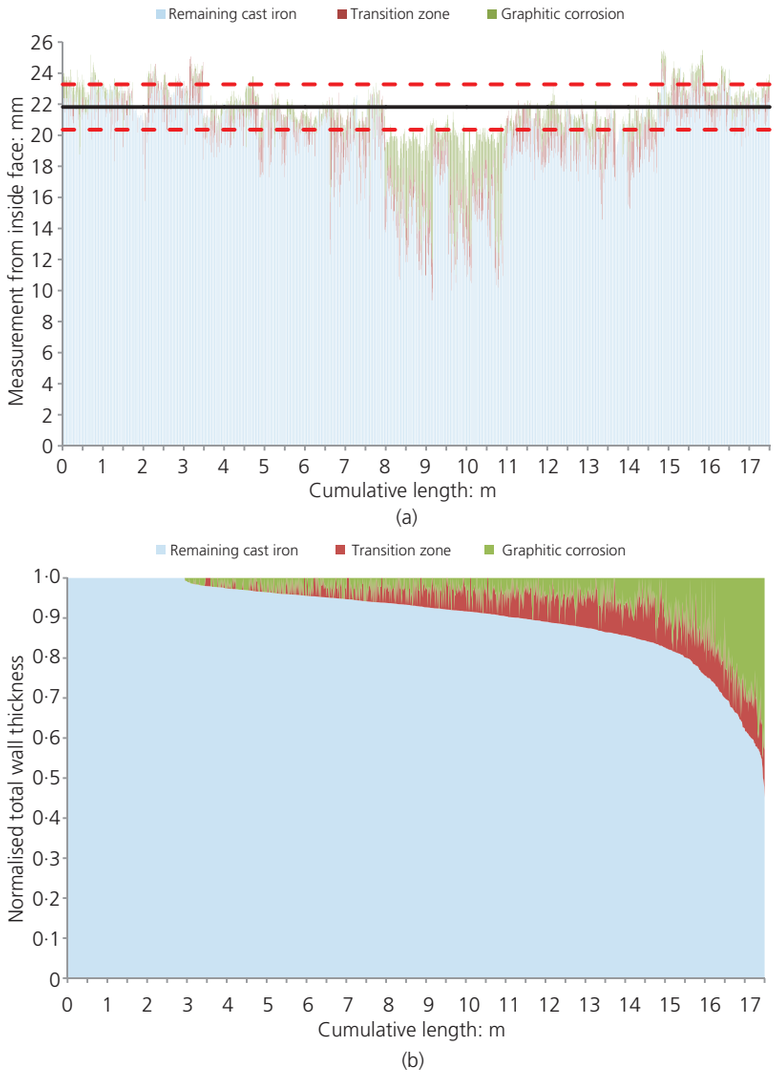

Figure 5. Stacked bar chart of measured values of total wall thickness t_w measured at 10 mm intervals along the sides of a series of (N = 23) test samples (350–400 mm × 30 mm × wall thickness t_w) cut from pipe 4 (see Jesson *et al*. (2013)). The total length of pipe edge examined was 17·4 m. The values were obtained from direct inspection of the cut face by using optical microscopy. Note: The (assumed) total wall thickness t_w (= t_i + t_z + t_g) at any position is given by the sum of the remaining thickness of cast iron t_i, depth of transition zone t_z and depth of external graphitic corrosion t_g. (a) Data obtained from each sample are presented in sequence running from left to right. As a consequence, the position along the cumulative length has no physical meaning in relation to the original pipe, or to the plate from which each sample was cut. The solid black line shows the mean total thickness t_{wa} of all the samples examined, while the dashed lines are positioned at one standard deviation from t_{wa}. (b) Data from (a) have been replotted by normalising the value of t_w at each position (i.e. removing the absolute variation in total wall thickness) and then ranking the values of the remaining thickness of cast iron t_i in decreasing value from left to right. The resulting figure provides a measure of the distribution of wall thickness within all of the samples examined. It can be seen that of the 17·4 m of the total sample length examined, some 3 m showed no signs of corrosion loss, while there are positions where the loss of metal section exceeds 40%

iron (Jesson *et al*., 2013; Yamamoto *et al*., 1983) and must be a priority for inspection. It is also important to establish the level of sound metal remaining in the pipe, particularly as geometric disparities such as wall thickness variations, not necessarily known about beforehand, can further concentrate the stress around the corrosion and further weaken the pipe.

Following on from corrosion, cracks also present a significant risk to the structural performance of the pipe as they have the potential to grow until failure. It would be beneficial to be able to identify the location and dimensions of any cracks, particularly if there is a potential for them to intensify further the stress due to an interaction with another defect present. However, finding small

Table 1. A summary of the literature comparing NDE on cast iron water pipes in chronological order (continued on next pages)

Reference	Format	Pipe				NDE techniques discussed	Defects considered	Comments
		Materials considered	Diameter	Length	Wall thickness	Field conditions		
Jackson *et al.* (1992)	Physical study (laboratory testing)	Cast iron, ductile iron	4·5–6 in. (114–152 mm)	Up to 5·49 m	3·175–8·76 mm	Sections of jointed pipe	Acoustic emission, magnetic phase shift, RFEC, ultrasonic	Wall thinning, man-made defects (10–40% of the wall thickness)	This review shows the start of NDE of cast iron pipes and comprises a literature review and a physical study split between the laboratory and the field. Potential NDE techniques were identified from the literature of well-established techniques present in the oil and gas industry. These techniques were then applied to laboratory pipe samples and buried pipelines. Here the RFEC test shows potential for inspection; however, this study was limited to internal inspection of small 4·5–7 in. (114–152 mm) dia. mains, which is not reflective of the true sizes of pipe present.
	Physical study (field testing)	Cast iron	7 in. (188 mm) 6 in. (152 mm)	80 m 65 m	~8 mm N/S	Abandoned pipeline	Magnetic phase shift, RFEC, ultrasonic	Wall thinning, graphitic Corrosion	
	Literature study	Steel, ductile iron, cast iron	Up to 36 in. (914 mm)	N/S	N/S	N/A	Visual, penetrant flaw detection, radiology, ultrasonic, MFL, eddy current testing, potential drop inspection, acoustic emission, thermography, holography	Cracking, breaks in lining, pitting, wall thinning	
Dorn *et al.* (1996)	Literature study	Ferrous materials, cementitious materials	>150 mm	N/S	N/S	N/A	Eddy current, radiographic, ultrasonic, visual	Graphitic corrosion, wall thickness	The paper reviews techniques for assessing a pipe's condition and then suggests methods of inspecting this condition by using NDE. The review recognises the many defects that can cause pipe deterioration, but the size and importance of detection are not given. It then suggests which NDE techniques could work on cast iron. The paper goes on to suggest indirect identifiers that can be used to identify pipes that may be susceptible to failure based on other data that can be gathered non-destructively, such as soil corrosivity.
Dingus *et al.* (2002)	Literature study	Metallic pipes	N/S	N/S	N/S	N/A	Impact echo, RFEC, ultrasonic, visual	Cracking, graphitic corrosion, pitting, wall thinning	This paper is split into two parts and initially reviews the current literature to identify NDE that could be useful for cast iron mains. The paper continues by showing the results of field trials which used NDE selected based on the information provided in the literature review. All cast iron pipe inspection was conducted using internal inspection pigs. RFEC was shown to be the best at inspecting metallic pipe for thinning but could not find any cracks or voids. While the results show
	Physical study (field testing)	Cast iron	6 in. (152 mm)	50 feet (ft) (15·2 m) 800 ft (244 m)	N/S	Abandoned pipeline	RFEC	Cracking, graphitic corrosion, man-made grooves, wall thinning	

Table 1. Continued

Reference	Format	Pipe				NDE techniques discussed	Defects considered	Comments
		Materials considered	Diameter	Length	Wall thickness	Field conditions			
			10 in. (254 mm) 16 in. (406 mm)	1080 ft (329 m) 1000 ft (305 m)		In-supply pipeline	Electromagnetic		potential for inspecting cast iron, they are limited as only two different techniques were tested on cast iron pipes, covering only a small range of diameters compared to the 60 in. (1·52 m) cast iron mains that are present in the UK. Further, the paper does not explain the sizes of defects that are important to detect.
Costello *et al.* (2007)	Literature study	N/S	N/S	N/S	N/S	N/A	Eddy current, impact echo, laser profiling, MFL, RFEC, sonar, ultrasound, visual	Cracking, pitting	The review covers methods of NDE that could be used to locate buried utilities or to conduct condition assessment of known utilities. The mode of operation is explained for each technique, and some known potential problems with each technique are given. Many of the techniques listed are for use in sewers. However, as the focus of the paper is not specifically on buried cast iron water pipes but buried utilities in general, the review of each technique does not suggest how each technique would cope when applied to an ageing cast iron pipe and tasked with finding the specific deterioration mechanisms present in cast iron. Further, there is no mention of the size of the utilities these techniques is applied on.
Thomson *et al.* (2009)	Literature study	Ferrous pipes	<6 to >48 in. (<0·152 to >1·21 m)	N/S	N/S	N/A	Visual, ultrasonic, eddy current, MFL, RFEC, radiographic	Corrosion, pitting, cracking, remaining wall thickness	This paper reviews the published literature on cast iron mains failures and methods of conducting condition assessment on them. It recognises the different types of cast iron manufacturing and the defects that each pipe suffers, before going on to describe the possible failure modes and detailing the indicators that should be detected to prevent a failure. The capabilities of some techniques are suggested but not for all. Further, the practicalities of conducting this inspection are not considered.

Table 1. Continued

Reference	Format	Pipe				NDE techniques discussed	Defects considered	Comments
		Materials considered	Diameter	Length	Wall thickness	Field conditions			
Prinsloo *et al.* (2011)	Literature study	Metallic pipes	>100 mm	N/S	N/S	N/A	Acoustic emission, visual, MFL, RFEC	Corrosion	The paper reviews the current techniques available for internal inspection of large-diameter mains but not specifically to water. The defects that cause deterioration to cast iron water mains, and the NDE ability to detect these types of defects, are not mentioned.
Hao *et al.* (2012)	Literature study	N/S	N/S	N/S	N/S	N/A	Eddy current, impact echo, MFL, rapid magnetic permeability, RFEC, sonar, laser profiling, visual	Cracking, pitting	This paper provides an updated review of the techniques mentioned by Costello *et al.* (2007). However, the focus of the paper is still on the tools that can be applied to the buried utilities in general, and while some areas have been updated as new technologies have become available, the fundamental defects affecting deterioration in cast iron pipe and their chances of being detected are not discussed.
Liu and Kleiner (2013)	Literature study	Metallic pipes, prestressed concrete pipes, polymeric pipes	N/S	N/S	N/S	N/A	Eddy current, impact echo, MFL, laser profilometry, radiography, RFEC, sonar, thermography, ultrasonic, visual	Corrosion, pitting	The paper reviews the latest NDE technologies that can be used to conduct NDE. It covers many more techniques than those that are mentioned in previous papers. While the paper covers the techniques that could be applied to all buried pipes, it does not suggest the specific defects of interest in cast iron and the capabilities of the NDE for assessing these. Further, the paper does not consider the difficulties of implementing any of the methods suggested on a buried cast iron main.

Although each paper may describe NDE for more than one material, any technique which is not applicable to cast iron, or which is used only to evaluate the environment around a pipe, is not considered in the table
RFEC, remote field eddy current; MFL, magnetic flux leakage; N/S, not specified; N/A, not applicable

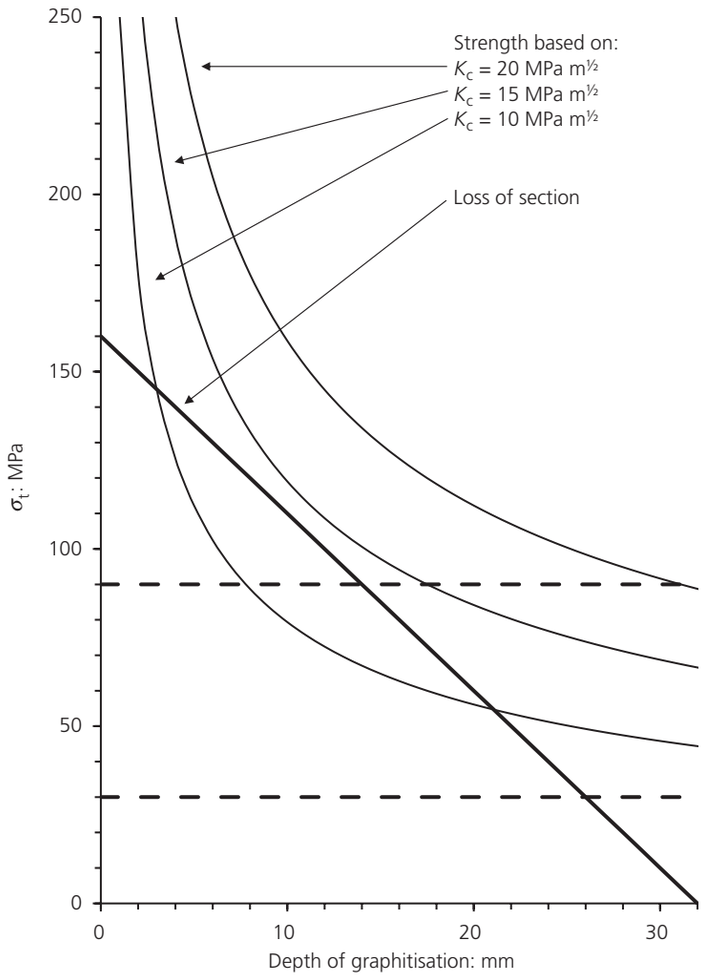

Figure 6. Tensile strength as a function of pit depth for progressive graphitic corrosion of a trunk main of wall thickness of 32 mm. The straight line is the prediction based on loss of section, while the curves are based on fracture mechanics analysis for cast irons with fracture toughness values of 10, 15 and 20 MPa $m^{1/2}$ and with a 'thumbnail' crack. The horizontal lines at 90 and 30 MPa represent two different levels of operating stress (see text)

cracks is likely to be the most demanding requirement to meet: it must be remembered that it is more important to find a subcritical crack with the potential to grow than it is to find a critical crack. (This is discussed further in the section headed 'What is the required resolution of the NDE technique(s)?') In addition, such defects may be hidden under corrosion and/or accretions of location material, further obfuscating NDE assessments of cracking.

Finally, it would also be beneficial for asset management if the presence and location of porosity, inclusions, cold shuts and other such defects could be determined, to characterise the condition of a pipe fully. However, if the defect populations introduced at manufacture have not led to early failure, they are likely to be in a stable state and may not lead to failure in the near future, unless combined with newer defects. Hence, the detection of cracks and corrosion, both of which tend to worsen over time, is of much greater importance.

What is the required resolution of the NDE technique(s)?

Treating, for the moment, all defects in the same manner – that is, as cracks – their size informs the resolution and accuracy required of the NDE methods. Conlin and Baker (1991) demonstrated the use of fracture mechanics on cast iron to determine the size of the critical defects that would cause catastrophic failure. Fracture mechanics gives a relationship between the applied stress σ; the crack 'length' a (in this case the depth of penetration into the wall) and the resulting intensified stress at the crack root, termed the 'stress intensity factor', K (where Y is a crack geometry-dependent, dimensionless constant)

$$1. \quad K = Y\sigma\sqrt{\pi a}$$

The critical stress intensity factor K_c, which may also be referred to as fracture toughness, is a material property. As noted in

Figure 7. An exposed 20 in. (0·508 m) trunk main in situ at Regent Street in central London with several other pipes and services crossing it, showing the restricted space available around a main

Figure 2, two cases can be considered – that is, loss of section and fracture mechanics – with these two models providing an envelope capturing the majority of failures. For illustrative purposes, a thumbnail crack geometry is assumed (for which $K = 1{\cdot}26\sigma a^{1/2}$); the relationship between tensile strength for catastrophic failure and crack size is shown graphically in Figure 6 for a range of fracture toughness values for cast iron taken from the literature (Ashby and Jones, 2005). A value of 90 MPa was suggested by Marshall (2001) as the maximum value of stress that a pipe would experience in service. This stress would mean that crack lengths greater than 8 mm in a material with a fracture toughness K_c of 10 MPa $m^{1/2}$ would cause fast fracture. Conversely, for cast irons with K_c greater than or equal to 14 MPa $m^{1/2}$, failure would occur by loss of section when the crack becomes 14 mm long, if the original wall thickness is 32 mm. More recent work by Rajani and Abdel-Akher (2013) suggests that this value of operating stress is higher than what is routinely seen in practice; based on this, a value of 30 MPa is used as a more 'realistic' estimate. In this situation, longer defects could be tolerated before catastrophic fracture.

The fracture mechanics predictions allow some tentative observations to be made on the possibility of a leak-before-break in cast iron water mains. In simple terms, the leak-before-break condition requires the critical crack length at the operating stress to exceed the pipe wall thickness. Based on the analysis used to make the fracture mechanics predictions in Figure 6, this condition is met; hence, a leak-before-break may occur in this example. This requires additional investigation because of the uncertainties regarding the level of working stress and details of possible defect shape, which would modify the stress intensity factor. Further, for a given working stress, a leak-before-break becomes more likely in pipes with a smaller wall thickness. Leakage from permeable through-wall graphitic corrosion has been observed previously in distribution mains (Jesson *et al.*, 2010). Anecdotally this phenomenon has also been observed in trunk mains.

The implication of the data presented in Figure 2 and the analysis in this section is that in order to be truly useful, an NDE technique must be able to detect reliably graphitic corrosion depths on the order of 4 mm and greater, to a resolution of ±1 mm. The surface resolution would ideally be comparable to this, but in practice may be constrained by the physics of the NDE technique itself, by practicalities associated with data storage or by the time needed for scanning.

What are the challenges posed by the field environment?

It is an aspiration that the condition of a buried asset could be assessed above ground without the need to excavate the pipe, thus saving time and expense. The Engineering and Physical Sciences Research Council (EPSRC)-funded UK research programmes Mapping the Underworld and, more recently, Assessing the Underworld, have been working to determine what underground assets can be successfully inspected without being exposed. While progress on identifying the location of a buried asset has been made, no methods of NDE have shown the ability to detect the defects discussed here either above ground or by using point assets, such as valves or hydrants, as access points (Hao *et al.*, 2012).

Consequently, whatever the optimum NDE technique is found to be for the collection of condition data, the ideal deployment would be through an inspection system which can pass along the inside of an in-service main. The device could have an umbilical cord or a winch cable, but to enable greater survey lengths, it would ideally be propelled by the flow of water (such a tool often being referred to as an intelligent pig, a smart pig or an inspection pig). In principle, this would allow large portions of the network to be inspected without disruption to supply. However, in practice, this is problematic as the implications for water quality cannot be ignored and must be considered in the ultimate deployment methodology of the NDE sensor/instrumentation package. Here the physical contact of the sensor and/or the carrier with the pipe wall is likely to cause surface deposits to be dislodged or in the worst case may damage corrosion prevention measures (e.g. bitumastic coatings). In a worst-case scenario, protruding corrosion features (known as tubercles) can be damaged by internal NDE, leading to chronic water quality issues and accelerated internal corrosion due to the removal of the passivated layer. Lining a main can reduce problems with water quality during internal NDE, but this is costly and further impedes NDE. Hence, the use of an inspection pig is likely to require the main to be taken out of service during inspection and subsequently flushed. The use of this technology would also require a significant amount of network modification to enable a pig to be inserted and retrieved from the network, and a device or a collection of devices that could cope with the range of mains diameters in use (12–60 in. (0·305–1·52 m)). It must be capable of both recording its own position and being located from the

surface. Lastly, the pig must be capable of traversing a trunk main which may change direction or depth along its length and could have offtakes: some pipes are not always easily accessible if the device should become stuck (Dingus *et al*., 2002; Vickridge and Lau, 2000). Further, if 'pigging' is to become an industry standard, it must be capable of assessing corrosion (and ideally the other defects discussed in this paper) reliably, through the full wall section.

Hence, conducting NDE from the outer surface of the pipe is currently preferable, even if it means that the pipe must be excavated for NDE to be conducted. Very often mains are exposed for routine work, which may present sufficient opportunity to assess the mains condition while the excavation is still open. However, this is still not without challenge. An excavation creates a muddy trench and may expose only a small section of main (approximately 1 m long), which is not significantly longer than the pipe's diameter. This can leave limited access to the surface of the pipe, particularly underneath the pipe (Figure 7). Any NDE method will need to be capable of operating within the clearance around the pipe afforded by the excavation and the neighbouring utilities.

Following on, the NDE method must be capable of dealing with an outer surface which is often hidden by a well-adhered layer of surface encrustation which is formed from the soil and aggregates around the pipe, and in some circumstances, iron leached from the pipe may react with the soil and the aggregates to form a binder, increasing the tenacity of the encrustation to cling to the surface. This can be removed but it must be done carefully so that the pipe is not compromised or the degradation accelerated. Even once removed, the surface can be seen to be heavily pitted. This is a long way from the smooth surfaces seen in the aerospace industry, where NDE techniques are routinely used. Finally, NDE must be capable of penetrating thick sections of cast iron, on the order of 35 mm.

Specifying NDE protocols in support of asset management

Fundamentally, then, what does NDE need to achieve for cast iron infrastructure? It needs to (*a*) collect meaningful data about the condition of specific assets and (*b*) provide these data in a form that can be used by asset managers to improve their decision-making processes. In the context of the present paper on pipes, the condition data collected should be able to locate accurately a number of key features

- section thickness
- manufacturing defects, such as porosity (where possible)
- the extent of internal and external corrosion
- the presence of internal and external cracks.

Of course, this list can be applied generically and forms a useful starting point for dealing with any cast iron asset. Further, it must be recalled that the collection of these data must take place in difficult circumstances. This places an onus on asset managers in that they must be careful to specify the data to be collected, the form that it is to be collected in and any preliminary steps that must (or must not) be taken. However, there is also an onus on contractors to specify the necessary conditions required for successful collection of NDE data. On this basis then, the key steps in an NDE process are

(*a*) preparing the surface with minimal destruction to the pipe (or other assets)
(*b*) conducting NDE in an agreed space around the pipe, which is likely to be limited
(*c*) reporting the data in the format defined by the network operator.

Some form of validation testing, that is to say a piece of cast iron which is assessed through NDE and then dissected to match observed defects, is a useful step in assessing any given NDE technique offered for use on cast iron infrastructure.

In the Appendix, a number of techniques are considered for application. These are taken from the review papers discussed earlier and then reviewed in the light of a potential field test, or with respect to other issues such as legislation or risk to the public perception of a network operator. From this it can be seen that while a plethora of NDE tools exist, and could potentially be applied, there remain difficulties in actually using the majority of these options. A very few NDE techniques can be applied to cast iron, but the resolution of defects remains poor and requires much calibration and development if they are to be viewed positively by asset managers.

Concluding remarks

Networks of ageing cast iron mains supply drinking water to millions of consumers around the world, and any interruption in supply associated with pipe failure, catastrophic or otherwise, is both undesirable and problematic. As a consequence, network operators seek to reduce the occurrence of failure by proactively targeting and replacing high-risk mains. The failure of cast iron mains has been linked to a range of defects present in the pipes, including those present at manufacture and those created during installation or induced through degradation during extended periods in service. This last group of defects is primarily associated with graphitic corrosion, which is known to contribute, both directly or indirectly, to a significant proportion of cast iron water main failures. Graphitic corrosion has significant implications for the remaining load capacity of a pipe. Hence, the extent of corrosion, its conformation and the remaining wall thickness must be assessed and quantified in order to predict reliably the remaining life in service.

The methods used to perform NDE on materials and engineered systems are diverse, and various physical properties are used to assess the 'health' of cast iron infrastructure. These include methods based on the magnetic and electrical properties of the cast

iron, as well as the speed of elastic waves – for example, ultrasound – through the material, or the absorption of X-rays. Such methods rely on the detection of some level of change in the properties associated with the presence of an unexpected secondary phase, the degradation due to the presence of corrosion or cracking. Other methods for checking pipe integrity include those that 'listen' for leaks or the use of a solution that bubbles when it comes into contact with, usually, leaking air. Many of these techniques are routinely deployed in a number of industries, and their effectiveness is well documented and standardised. With respect to the use of NDE in the water industry, there have been a number of detailed reviews that consider NDE as a whole, specific branches of NDE or NDE in a particular context. However, they focused less on applying the filters of the field environment and the working practices of the industry. A number of well-established techniques are limited to the laboratory, as they are unlikely to be practical in the field, are regulated against or do not take into account the inherent variation in microstructure (and properties) of cast iron. For example, while ultrasonic inspection is routine in the aerospace sector, a few millimetres of aluminium is a very different prospect from tens of millimetres of cast iron, particularly when the cast iron is corroded. The graphite flake structure of the metal acts to dissipate the ultrasonic signal, and the transition zone of active corrosion is strongly attenuative rather than giving rise to a clean reflection.

Q7 A significant problem for any NDE technique is accessing the structure to be assessed: with buried assets, inspection must rely on either exhumation or, if possible, an internal assessment. Both scenarios present significant issues, particularly in the context of a water main. Further, in either case, once access has been achieved, surface preparation is often required to ensure adequate measurement quality, and that process can lead to the asset being damaged. Such damage may or may not be immediately apparent, but will reduce the residual life of the asset being assessed.

These comments notwithstanding, ultrasonic inspection, although facing the hurdle of poor surface condition, would appear to have the best opportunity of finding all of the defects discussed in this paper, but significant work is required to overcome the issues that the presence of graphitic corrosion presents to meaningful data collection and interpretation. It may be best to pair ultrasonic inspection with another technique (such as eddy current testing, or magnetic flux leakage (MFL)) to provide complementary results that can be combined together to give a complete, composite picture.

Given the potential length of water networks and the range of soil environments in which they are situated, external NDE conducted in small excavations can only give a snapshot of the local pipe condition. Statistical analysis can allow these data to predict the condition of nearby pipes, and asset managers can use further analysis to consider cohorts of similar pipes by using data from across the network to make a decision about a specific pipe. However, greater (contiguous) lengths of the network must be inspected to understand its condition more fully. At present, a device capable of characterising the range of defects typically present in cast iron main at the physical resolution suggested does not exist. Further developments in this area must be made if any certainty on the condition of the trunk main networks is to be obtained.

Acknowledgements

The authors gratefully acknowledge the funding provided for this research by the EPSRC (grant EP/G037388/1, through the Micro- and Nanomaterials and Technologies Centre for Doctoral Training, University of Surrey) and by Thames Water Utilities Limited. The authors would particularly like to thank Dr S. A. Adegbite, formerly of the University of Surrey, for useful suggestions to this paper and for his contribution to the larger project of which this paper is a part.

The opinions expressed in this paper are those of the authors and not necessarily endorsed by the University of Surrey or Thames Water Utilities Limited.

Appendix: Application of NDE techniques

Introduction

A plethora of NDE techniques are available to determine the condition of large structures. While the spectrum of techniques is broad and difficult to compare, the principle of NDE may be summarised as the exploitation of a physical material property in order to assess condition against some empirical or notional base line. For the fundamentals of a specific technique, the reader is referred to the reviews mentioned earlier in this paper (or to a suitable textbook such as that by Halmshaw (1991) or Cartz (1995)). It is not the purpose of this paper to critique the operation of one technique compared with another: rather, it is to identify the physical practicalities which affect a technique's ability to be applied to cast iron trunk main. In particular, the ability of the techniques to identify each category of defect outlined earlier from the outer surface of the pipe is discussed. Other considerations such as the safety implications, space requirements and practicalities are also considered and used to eliminate techniques which are unlikely to be feasible for inspection of a live main.

A reasonably comprehensive list of NDE techniques might be expected to include ultrasonic, MFL, eddy current, acoustic, radiographic, dye penetration, visual and pit depth measurements. However, in practice many of these techniques are unsuitable.

Unsuitable methods

Constrained by safety

- Dye penetration testing requires the use of a fluid dye which must not enter the water supply but could be drawn in through a through-wall crack.
- Radiographic inspection with gamma rays or X-rays carries immediate health risks and would require an extremely

powerful source and lengthy exposure time to penetrate the thick cast iron. Given the small exposure area, this process would need to be repeated several times to build up a complete image of the pipe successively. Furthermore, the inspection would have access only to the outer surface of the pipe, which would mean that the radiation source and detector would be sited either side of the pipe, effectively doubling the material that the rays would need to penetrate. Hence more powerful X-rays with longer exposure times would be needed, which increase the health and safety risks. Finally, there is a public perception issue regarding the deployment of radiographic equipment, and associated shielding, barriers and signage, in urban areas.

Constrained by working space

- Remote field eddy current techniques have been shown to assess the level of corrosion on a main well, but it would be impeded by the available space in the excavation (Dingus *et al*., 2002). Hence, the technique is suited to an inspection pig application since it requires a substantial separation, on the order of two pipe diameters (Hao *et al*., 2012), between the exciter and the detector. This is unlikely to be possible in an excavation where space may be limited.

Constrained by damage to the asset

- It is feasible to gather visual condition data on the level of external corrosion by mechanically removing corrosion products and measuring with more or less accuracy the pits which are revealed. However, this is a partially destructive method which, while providing a useful measure of corrosion, could lead to problematic situations for an in-service main. If through-wall corrosion is present, disturbing it may lead to a leak or, worse, failure of the pipe.

Constrained for other reasons

- Passive acoustics are used in water mains to detect leaks but can also be employed to listen for mechanical deterioration in a structure, such as the wires breaking inside a prestressed concrete pipe (Travers, 1997). This method can be applied only to situations requiring continual monitoring and not inspection as it can only measure the deterioration since it was installed rather than providing a complete instantaneous picture of condition (Makar and Chagnon, 1999). It is questionable whether such an approach is relevant in the context of the subcritical growth of a crack. Presupposing that such a crack has been identified and a sensor placed at an appropriate location to monitor ongoing crack growth, such a detector would need to be capable of detecting the energies associated with crack growth at the scale on the order of 1 μm per cycle (Mohebbi *et al*., 2010) while also being subjected to a range of other events found in live main, in particular those under busy roads.
- Active acoustic methods such as modal analysis, where the frequencies at which an object resonates are monitored and compared to a known reference, as in the traditional tapping test of a train wheel for identifying a flaw, have also been suggested. For a buried water pipe, the different volumes and types of earth which surround it, and the large volumes of water within it, can affect greatly the resonances of the pipe wall (Leinov *et al*., 2015). Such environmental variations may be very difficult to factor in to the reference; hence, the results obtained may be negated. At higher acoustic frequencies, shorter-range guided waves might be used to inspect trunk mains. This technique is often used to inspect long lengths of welded pipes where the waves can progress between lengths of pipes. However, the bell and spigot joint between sticks on trunk mains would limit the wave progression between sticks.
- Non-contact strain measurements which use interference optical methods such as holography and shearography may be challenged by the environment in which to perform measurements on a large pipe. Preparing the surface sufficiently well to use precision optical equipment in such a context would be very demanding, and it is doubtful that an excavation on trunk main could provide a suitable environment for such optically based NDE methods to function.
- Visual inspection may not be sufficient on its own but would be a precursor to any other technique, allowing information, such as casting marks, the environment in which the pipe sits and the presence of other utilities or traffic loadings, to be assessed. All this information can contribute to a 'health check' of a pipe. If the pipe is badly deteriorated to the naked eye, then this may negate the need to proceed with further inspection.

Potentially suitable techniques

MFL shows some potential for the inspection of cast iron and is already commercially available as an inspection technique (Liu *et al*., 2012). However, there are some questions over the efficacy of the method in characterising defects in the pipe wall. In particular, the often poor surface condition present on an exhumed trunk main can make it challenging to ensure that the tool is in full contact with the pipe wall. Failure to maintain full wall contact does not ensure that the magnetic field generated by the magnets is coupled to the pipe wall consistently and can lead to difficulties with accurately determining the size and shape of the defect as the tool's capacity to capture the flux leakage around a defect is linked to the spacing between the tool and the pipe wall. Further, the sensitivity of the tool is reduced for greater wall thicknesses as it becomes progressively harder to detect magnetic flux leaking from the distant wall with a system stationed at the proximate wall (De Silva *et al*., 2002). Given the operating principles of MFL, it seems very unlikely that narrow cracks will be detected because it is debateable whether the crack will provide a sufficient discontinuity for the flux to leak out of the pipe.

Eddy current technology, using low-frequency alternating electromagnetic fields, is another possible method for corrosion

detection in a trunk main. Conventionally, alternating current (AC) fields, in the 5–60 MHz range, are applied to find surface-breaking cracks in metallic objects with good surface finishes. However, the inspection of thick sections with this technique is limited by the depth to which the eddy currents can penetrate. This is dependent on the induced frequency (Rizzo, 2010) – for example, skin depth of 3 mm in a steel pipe exposed to a 50 Hz AC field (Hao *et al*., 2012). Reducing the frequency to the order of 10–100 Hz can enable the skin depth penetration to be increased (Jackson *et al*., 1992); however, full coverage of a 35 mm wall still may not be possible. The challenge for a field-deployable system will be to achieve the required resolution of cracks and other defects, although this will be aided by the technique's tolerance of a variety of surface conditions.

Finally, ultrasonic inspection may prove to be of great use as, in principle, it can be applied in different ways to search for different defect populations from one surface of the trunk main (Liu *et al*., 2012). Configured in its simplest pulse-echo mode, with ultrasonic signals travelling normal to the pipe wall, it can measure the degree of corrosion thinning in a wall. It can also be arranged for the ultrasonic pulses to travel into the pipe wall at an angle to search for cracks in more remote locations within the bulk of the wall material. As with most NDE methods, raw waveforms from these tests must be post-processed to ascertain the condition of the pipe, and this requires a good understanding of the propagation of ultrasound within corroded iron to arrive at a robust determination of pipe condition. A key factor in accurately determining defect sizes is how fast the ultrasound travels in corroded and uncorroded areas of the pipe wall. In uncorroded cast iron, the speed might range from 3500 to 5600 m/s (AIH Committee, 1989). This large velocity range covers all types of cast iron, but for the types of cast iron in trunk main, the range is likely to be narrower as a result of the relationship between velocity and modulus. For the trunk mains investigated by Jesson *et al*. (2013), the variation in modulus between the ten different pipes was less than a factor of 2, which would give a much more narrow velocity range. Ideally, the speed of sound should be determined for the particular pipe being inspected, but having access to only one surface of the pipe provides little opportunity to make speed measurements on a section of known thickness, unless a calibration coupon is available. There is then the added complication that the speed of sound may vary through the pipe wall due to earlier formed variations in microstructure. Improved accuracy could be achieved if the date and place at which the pipe was cast are known, thus allowing pipes of a similar provenance with known properties to provide a closer estimate for use in an inspection. Also, the graphitic corrosion products of cast iron have been shown to be very attenuative and greatly impede the ultrasonic wave (Dorn *et al*., 1996); there remain issues with respect to the compensation for this in the post-processing of field data. In principle, as with many techniques, a good surface finish is required for reliable contact between the sensors and the pipe, and this may necessitate cleaning the pipe surface (Thomson *et al*., 2009). However, this may be mitigated through the use of ultrasonic immersion testing: in such systems, a thick layer or column of water is used between the sensor and the pipe wall to couple the ultrasound to the pipe.

Q12

Despite these potential issues, tools using ultrasound have been developed to inspect cast iron trunk main and it is commonly offered as a method for characterising a pipe's condition. Finally, ultrasound has the potential to detect the defects discussed previously, and as progress on its performance is made, it may be capable of giving sufficient corrosion data for both internal and external corrosion. The possibility of operating NDE techniques in tandem, so that one may fill in the gaps where another technique struggled, could be beneficial in providing a better overview of a pipe's condition. However, it is worth noting that it is highly unlikely that a true NDE of a pipe can be carried out, as in most situations, some surface cleaning to facilitate an inspection will be required, and this will inevitably have an impact on the remaining life of the pipe.

REFERENCES

Q13

AIH Committee (ASM International Handbook Committee) (1989) *Nondestructive Evaluation and Quality Control*, 9th edn. Metals Handbook. ASM International, Materials Park, OH, USA, vol. 17.

Angus HT (1976) *Cast Iron: Physical and Engineering Properties*, 2nd edn. Butterworth, London, UK.

Ashby MF and Jones DRH (2005) *Engineering Materials 1: an Introduction to Properties, Applications and Design*, 3rd edn. Butterworth-Heinemann, Oxford, UK.

Atkinson K, Whiter JT, Smith PA and Mulheron M (2002) Failure of small diameter cast iron pipes. *Urban Water* **4**: 263–271, http://dx.doi.org/10.1016/S1462-0758(02)00004-3.

Q14

Belmonte HMS, Mulheron M and Smith PA (2007) Weibull analysis, extrapolations and implications for condition assessment of cast iron water mains. *Fatigue and Fracture of Engineering Materials and Structures* **30**: 964–990, http://dx.doi.org/10.1111/j.1460-2695.2007.01167.x.

Belmonte HMS, Mulheron M, Smith PA *et al.* (2008) Weibull-based methodology for condition assessment of cast iron water mains and its application. *Fatigue and Fracture of Engineering Materials and Structures* **31**: 370–385, http://dx.doi.org/10.1111/j.1460-2695.2008.01233.x.

Belmonte HMS, Mulheron MJ and Smith PA (2009) Some observations on the strength and fatigue properties of samples extracted from cast iron water mains. *Fatigue and Fracture of Engineering Materials and Structures* **32**: 916–925, http://dx.doi.org/10.1111/j.1460-2695.2009.01395.x.

Cartz L (1995) *Nondestructive Testing: Radiography, Ultrasonics, Liquid Penetrant, Magnetic Particle, Eddy Current*. ASM International, Materials Park, OH, USA.

Conlin RM and Baker TJ (1991) *Application of Fracture Mechanics to the Failure Behavior of Buried Cast Iron Mains*. Transport Research Laboratory, Wokingham, UK, Contract Rep. No. 266.

Costello SB, Chapman DN, Rogers CDF and Metje N (2007) Underground asset location and condition assessment technologies. *Tunnelling and Underground Space Technology* **22**: 524–542, http://dx.doi.org/10.1016/j.tust.2007.06.001.

De Silva D, Davis P, Burn S *et al.* (2002) Condition assessment of cast iron and asbestos cement pipes by in-pipe probes and selective sampling for estimation of remaining life. In *20th International No-dig Conference and Exhibition* (Fischer G (ed.)).

International Society for Trenchless Technology, Copenhagen, Denmark, pp. 1–13.

Dingus M, Haven J and Austin R (2002) *Nondestructive, Noninvasive Assessment of Underground Pipelines*. American Water Works Association Research Foundation, Denver, CO, USA.

Dorn R, Howsam P, Hyde RA and Jarvis MG (1996) *Water Mains: Guidance on Assessment and Inspection Techniques*. Construction Industry Research and Information Association, London, UK, Ciria Report 162, vol. 162.

Fahimi A, Evans TS, Farrow J *et al.* (2016) On the residual strength of aging cast iron trunk mains: physically-based models for asset failure. *Materials Science and Engineering: A* **663**: 204–212.

Gagg CR and Lewis PR (2011) The rise and fall of cast iron in Victorian structures – a case study review. *Engineering Failure Analysis* **18**: 1963–1980, http://dx.doi.org/10.1016/j.engfailanal.2011.07.013.

Halmshaw R (1991) *Non-destructive Testing*, 2nd edn. Edward Arnold, London, UK.

Hao T, Rogers CDF, Metje N *et al.* (2012) Condition assessment of the buried utility service infrastructure. *Tunnelling and Underground Space Technology* **28**: 331–344, http://dx.doi.org/10.1016/j.tust.2011.10.011.

HMG (Her Majesty's Government) (2000) The Water Supply (Water Quality) Regulations (2000). The Stationery Office, London, UK, Statutory Instrument 2000 No. 3184.

Jackson R, Pitt C and Skabo R (1992) *Nondestructive Testing of Water Mains for Physical Integrity*. American Water Works Association Research Foundation, Denver, CO, USA.

Jesson DA, Le Page BH, Mulheron MJ *et al.* (2010) Thermally induced strains and stresses in cast iron water distribution pipes: an experimental investigation. *Journal of Water Supply: Research and Technology – Aqua* **59(4)**: 221–229, http://dx.doi.org/10.2166/aqua.2010.078.

Jesson DA, Mohebbi H, Farrow J, Mulheron MJ and Smith PA (2013) On the condition assessment of cast iron trunk main: the effect of microstructure and in-service graphitisation on mechanical properties in flexure. *Materials Science and Engineering: A* **576**: 192–201, http://dx.doi.org/10.1016/j.msea.2013.03.061.

Leinov E, Lowe MJ and Cawley P (2015) Investigation of guided wave propagation and attenuation in pipe buried in sand. *Journal of Sound and Vibration* **347**: 96–114, http://dx.doi.org/10.1016/j.jsv.2015.02.036.

Liu Z and Kleiner Y (2013) State of the art review of inspection technologies for condition assessment of water pipes. *Measurement: Journal of the International Measurement Confederation* **46**: 1–15, http://dx.doi.org/10.1016/j.measurement.2012.05.032.

Liu Z, Kleiner Y, Rajani B, Wang L and Condit W (2012) *Condition Assessment Technologies for Water Transmission and Distribution Systems*. US Environmental Protection Agency, Washington, DC, USA.

Logan R, Mulheron MJ, Jesson DA *et al.* (2014a) Graphitic corrosion of a cast iron trunk main: Implications for asset management. *2nd International Conference on the Design, Construction, Maintenance, Monitoring and Control of Urban Water Systems, Algarve, Portugal.*

Logan R, Mulheron MJ, Jesson DA *et al.* (2014b) Observations on the graphitic corrosion of cast iron trunk main: mechanisms and implications. *Eurocorr 2014: European Corrosion Congress, Pisa, Italy.*

Makar J and Chagnon N (1999) Inspecting systems for leaks, pits, and corrosion. *Journal American Water Works Association* **91**: 36–46. **Q15**

Marshall P (2001) *The Residual Structural Properties of Cast Iron Pipes – Structural and Design Criteria for Linings for Water Mains*. UK Water Industry Research Limited, London, UK.

Mohebbi H, Jesson DA, Mulheron MJ and Smith PA (2010) The fracture and fatigue properties of cast irons used for trunk mains in the water industry. *Materials Science and Engineering: A* **527**: 5915–5923, http://dx.doi.org/10.1016/j.msea.2010.05.071.

Prinsloo K, Wrigglesworth M and Webb M (2011) Advancement of condition assessment techniques for large diameter pipelines. *Civil Engineering* **19**: 20–25. **Q16**

Rajani B and Abdel-Akher A (2013) Performance of cast-iron-pipe bell-spigot joints subjected to overburden pressure and ground movement. *Journal of Pipeline Systems Engineering and Practice* **4**: 98–114, http://dx.doi.org/10.1061/(ASCE)PS.1949-1204.0000125.

Rajani B and Kleiner Y (2010) Fatigue failure of large-diameter cast iron mains. In *Water Distribution Systems Analysis 2010* (Lansey KE, Choi CY, Ostfeld A and Pepper IL (eds)). American Society of Civil Engineers, Reston, VA, USA, pp. 1146–1159.

Rajani B and Makar J (2000) A methodology to estimate remaining service life of grey cast iron water mains. *Canadian Journal of Civil Engineering* **27**: 1259–1272, http://dx.doi.org/10.1139/cjce-27-6-1259.

Rizzo P (2010) Water and wastewater pipe nondestructive evaluation and health monitoring: a review. *Advances in Civil Engineering* **2010**: 818597, http://dx.doi.org/10.1155/2010/818597.

Roberge PR (2007) *Corrosion Inspection and Monitoring*. Wiley-Interscience, Hoboken, NJ, USA.

Stanton Iron Works Company (1936) *Cast Iron Pipe: Its Life and Service*. Stanton Iron Works Company, Nottingham, UK.

Thomson J, Wang L and Royer M (2009) *State of Technology Review Report on Condition Assessment of Ferrous Water Transmission and Distribution Systems*. US Environmental Protection Agency, Washington, DC, USA.

Travers FA (1997) Acoustic monitoring of prestressed concrete pipe. *Construction and Building Materials* **11**: 175–187. **Q17**

Vickridge I and Lau T (2000) *Lessons Learnt from Pipeline Condition Assessment in Hong Kong*. Black & Veatch, Hong Kong, China.

Yamamoto K, Mizoguti S, Yoshimitsu K and Kawasaki J (1983) Relation between graphitic corrosion and strength-degradation of cast iron pipe. *Boshoku Gijutsu* **32**: 157–162. **Q18**

How can you contribute?

To discuss this paper, please submit up to 500 words to the editor at journals@ice.org.uk. Your contribution will be forwarded to the author(s) for a reply and, if considered appropriate by the editorial board, it will be published as a discussion in a future issue of the journal.